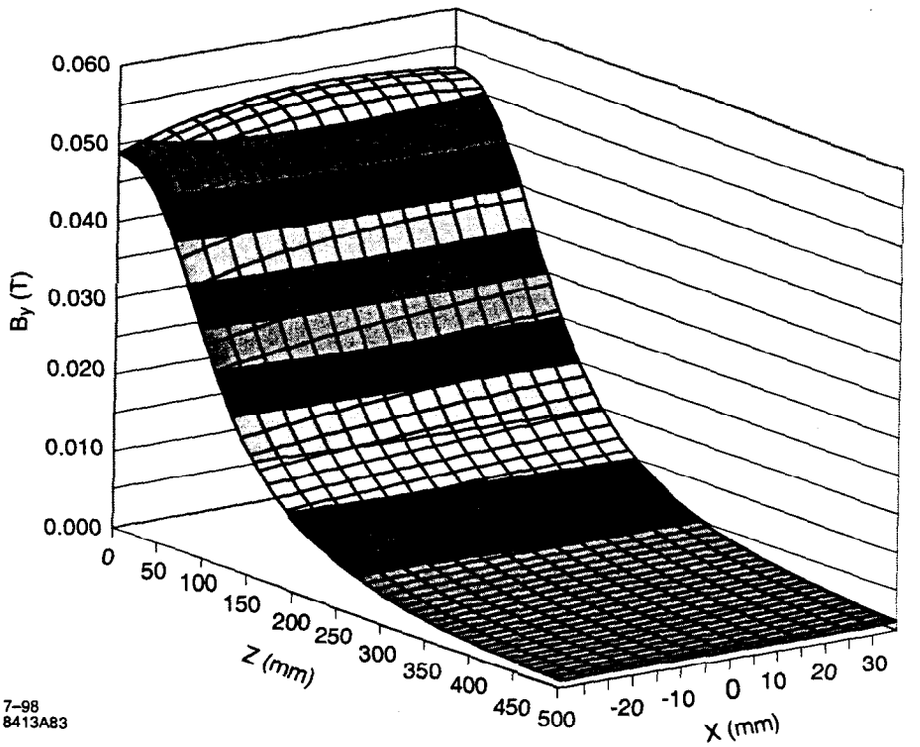

Figure 4.35 Horizontal steering field vs. x and z in the H/V corrector at I_n = 2656 A-T. The end effects are very important because of the magnet's low length/gap ratio.

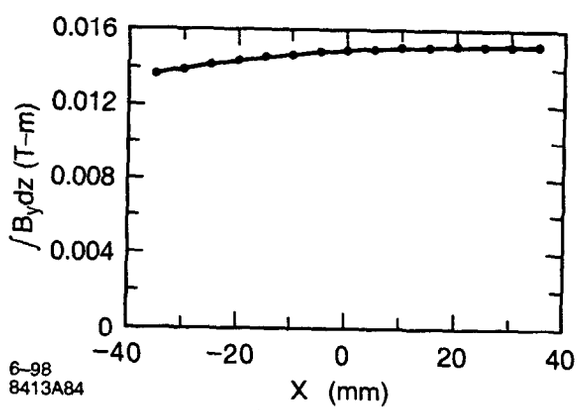

Figure 4.36 Integral of horizontal steering field vs. X in the H/V corrector at I_n=2656 A-T. The quadrupole and sextupole components can be minimized by shaping the gap. Although the horizontal steering magnet exhibits some field non-linearity at large beam displacement, we do not anticipate problems in the ± 1-2 mm region where the fast orbit feedback system operates.

Table 4.23 Integrated multipoles of horizontal steering field in the H/V corrector at I_n = 2656 A-T (also Figure 4.39).

n	$\int b_n dz$ (T-m/cm$^{(n-1)}$)	$\int B_n dz$ @ r = 35 mm (T-m)	$\int B_n dz / \int B_1 dz$ @ r = 35 mm
1	1.5000E-02	0.01500032	1
2	1.8608E-04	0.00065127	4.34E-02
3	-4.3241E-05	-0.0005297	-3.53E-02
4	2.6316E-06	0.00011283	7.52E-03
5	-9.7160E-08	-1.458E-05	-9.72E-04
6	6.1150E-09	3.2117E-06	2.14E-04

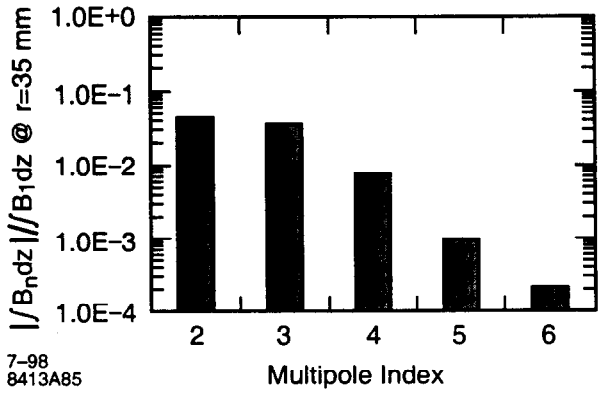

Figure 4.37 Integrated multipoles of horizontal steering field in the H/V corrector.

4.1.6.2 Horizontal Correctors

The horizontal correctors magnets are identical to the combined horizontal/vertical correctors except for the vertical correction coils which are not installed. The magnet location is shown in Figure 4.78.

4.1.6.3 Vertical Correctors

The vertical correctors magnets are identical to the combined horizontal/vertical correctors except for the horizontal correction coil which is not installed. The magnet location is shown in Figure 4.78.

4.1.7 Septum Magnet

In Figure 4.116 it is shown part of the injection line from the booster to SPEAR 3 and the vertical Lambertson septum magnet. The injection line terminates with the horizontal bend magnet B7H, the quadrupoles Q8 and Q9, the vertical bend magnet B8V and the vertical bending septum magnet B9V. During injection the stored beam is moved 3 mm towards the septum by a horizontal corrector and then a further 17 mm by a AC kicker (Figure 4.40). A new d.c. injection septum magnet is required in SPEAR 3 to accommodate the reduced distance between the stored and injected beam (from 53 mm to 33 mm, see Figure 4.40) and the increased injection energy (from 2.7 GeV to 3.0 GeV).

The cross section of the septum magnet is shown in Figure 4.41 and the main parameters are listed in Table 4.25. The septum magnet has a vertical bend of 8.79° to match the existing transport line

magnet B8V. The function of the septum magnet is to bend the injected beam close to the stored beam without perturbing it. It is important to minimize the leakage field at the stored beam central orbit location when the septum magnet is turned on but there is no injected beam. This is accomplished by a Lambertson septum configuration similar to the PLS design [10] that provides a uniform dipole field to the injected beam and a low field region to the stored beam. The horizontal separation between the two beams inside the septum is reduced to 13 mm by inserting the stored beam vacuum chamber into a yoke V-notch. The leakage field from the V-notch into the stored beam area is minimized using an insert made of high permeability 2.5% silicon steel (Carpenter Silicon Core Iron B-FM annealed at 1066 °C [11]) inside the 1010 steel yoke (Section 4.22).

Figures 4.41 and 4.42 show the flux lines inside the yoke and the leakage flux. Figure 4.42 shows the flux density in the yoke. Since the field at the V-notch is 1.5 T (1.31 T is the horizontal component) and the permeability of 1010 steel at that field is very low, a high permeability 2.5% silicon steel insert was placed in the area. Figure 4.123 shows the stray field in the V-notch at the stored beam location. The integrated dipole field at the center of the stored beam is 0.34 mT×m (no end effects) and causes a bending of only 34 μrad. The flux leakage at the ends, not yet computed with a 3D magnetic code, is minimized by extending the yoke beyond the coils. The integrated dipole field could be further reduced machining a tapered slot to increase the yoke gap and reduce the leakage at the front end of the magnet where the two beams have a larger vertical separation. The multipole coefficients of the magnetic field at the stored and injected beam locations are shown in Tables 4.25 and 4.26. The maximum $\Delta B/B_1$ for the injected beam is 2.7×10^{-3} at 90 mm from the midplane (Figure 4.124).

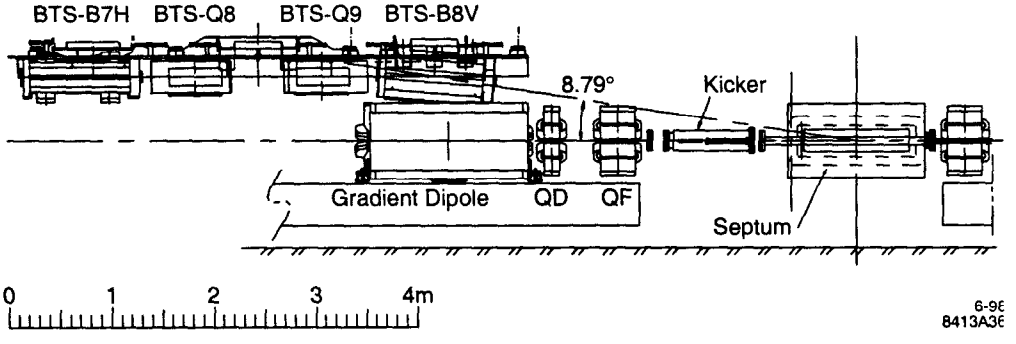

Figure 4.38 SPEAR 3 injection line and septum

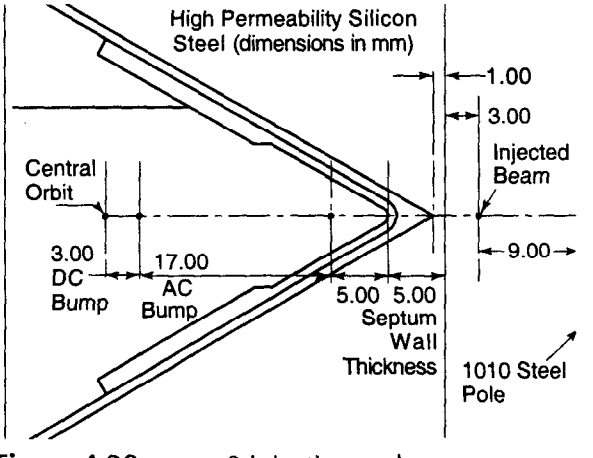

Figure 4.39 SPEAR 3 injection and septum magnet

Table 4.24 Septum magnet parameters.

	B9V
Nominal Energy (GeV)	3.00
Number of Magnets	1
Bending Angle (deg)	8.790
Magnetic Length (m)	1.168
Field (T)	1.313
Bending Radius (m)	7.616
Integrated Field (Tm)	1.534
Sagitta (m)	0.089
Pole Width (m)	0.230
Gap Height (m)	0.012
Core Length (m)	1.168
Lamination Height (m)	0.184
Lamination Width (m)	0.762
Core Weight (kg)	2344
Septum thickness (includes chamber) (mm)	5.0
Ampere-Turns per Pole	12538.5
Turns per Pole	64
Pancakes per Pole	4
Conductor Width (mm)	6.35
Conductor Height (mm)	6.35
Cooling Hole Diameter (mm)	4.75
Conductor Cross-Sectional Area (mm^2)	22.60
Conductor Length/Pole (m)	213.674
Current (A)	195.91
Current Density (A/mm^2)	8.67
Inductance (H)	0.115
Total Coils Weight (kg)	42.5
Magnet Resistance @ 40 C (mΩ)	163.7
Power/Magnet (kW)	6.28
Power/String (kW)	6.28
Voltage Drop/Magnet (V)	32.1
Water Circuits	4
Water Flow Rate/Magnet (gpm)	1.84
Water Pressure Drop (psi)	150
Water Temperature Rise (°C)	12.9
Reynold's Number	7941
Water Velocity (m/s)	1.64
Friction Factor	0.0343

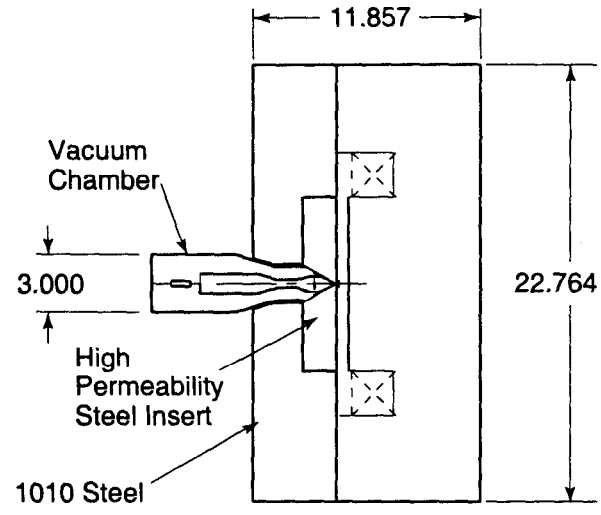

Figure 4.40 Cross-section of the septum magnet.

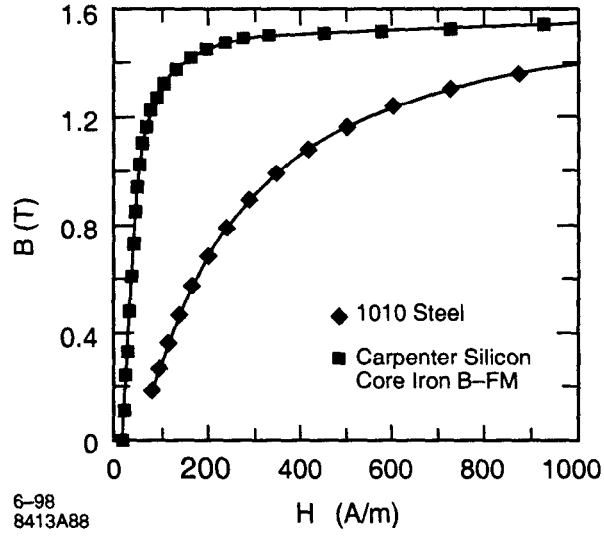

Figure 4.41 Induction vs. magnetizing force for 1010 steel and Carpenter Silicon Core Iron B-FM annealed at 1066°C. The high permeability material is used to reduce the flux leakage into the stored beam.

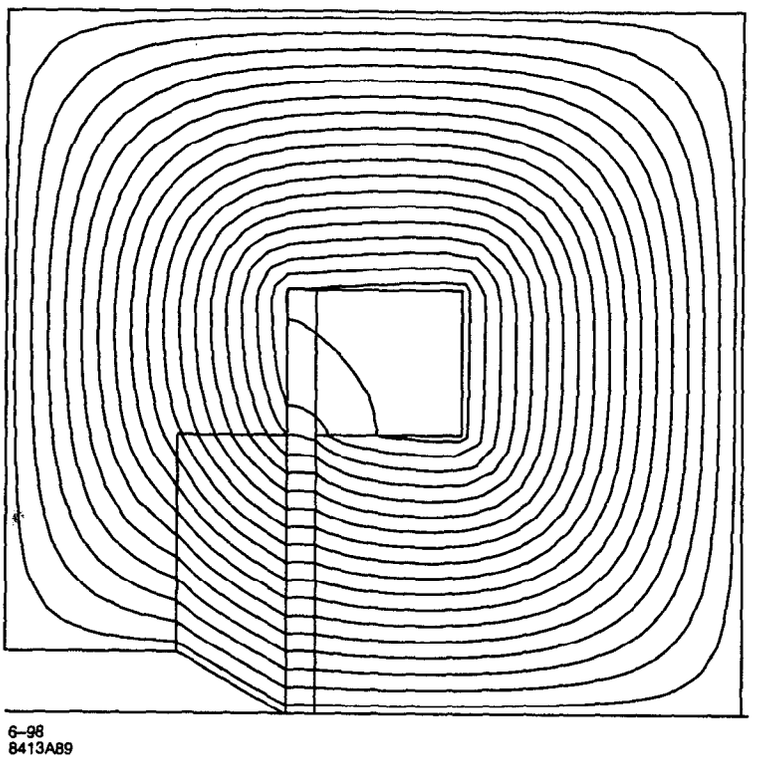

Figure 4.42 Septum flux plot (the vector potential values are in T-m). As flux lines at the V-notch are bent of 30° the field increases from 1.3 T to 1.5 T.

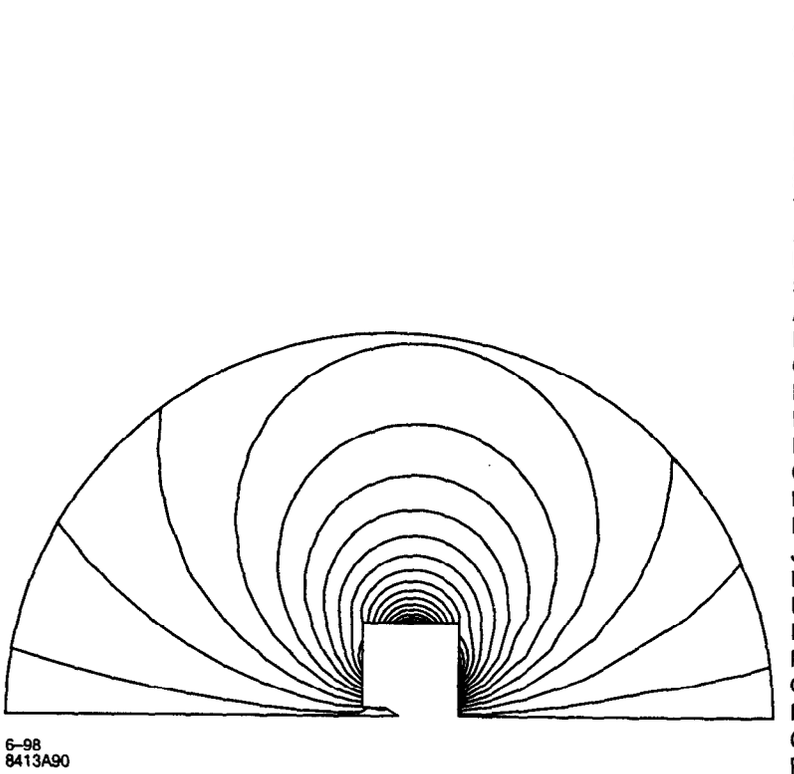

Figure 4.43 Septum stray flux lines (the vector potential values are in Tm). The stray field has been computed using infinite boundary elements at the outer radius. The stray field inside the V-notch is shown in Figure 4.46.

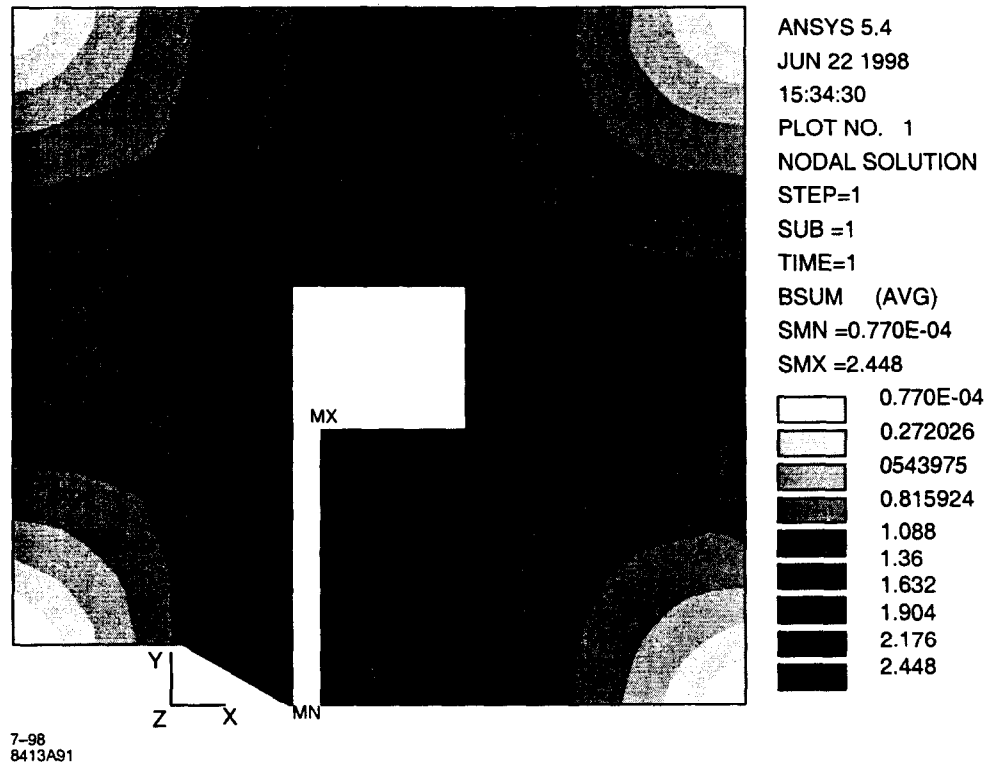

Figure 4.44 Septum magnetic induction plot (the values are in Tesla). The field at the V-notch inside the high permeability insert is 1.5 T.

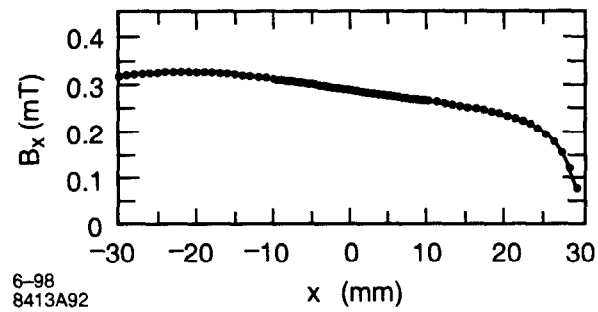

Figure 4.45 Septum stray field into the stored beam area. The origin is at the stored beam location and the x-axis is horizontal. The integrated dipole field at the center of the stored beam is 0.34 mT–m.

Table 4.25 Septum multipole coefficients ($T/cm^{(n-1)}$) at the stored beam location

a_1	2.8784E-04	a_{10}	-5.0762E-09
a_2	-2.3791E-05	a_{11}	-1.2675E-09
a_3	1.4328E-06	a_{12}	-2.6528E-09
a_4	4.2758E-07	a_{13}	-6.3035E-09
a_5	-8.4596E-07	a_{14}	5.6012E-09
a_6	6.3473E-08	a_{15}	-1.0487E-08
a_7	9.2237E-09	a_{16}	-6.2772E-09
a_8	-2.8503E-08	a_{17}	-6.9875E-10
a_9	-7.1820E-10	a_{18}	7.8320E-09

Table 4.26 Septum multipole coefficients ($T/cm^{(n-1)}$) at the injected beam location (even skew multipoles not shown)

a_1	1.25725E+00
a_3	-2.23240E-05
a_5	-4.20286E-06
a_7	-3.54981E-07
a_9	-1.90148E-08
a_{11}	-6.20382E-10
a_{13}	-1.23115E-11
a_{15}	-1.44574E-13
a_{17}	-9.24959E-16
a_{19}	-2.48456E-18

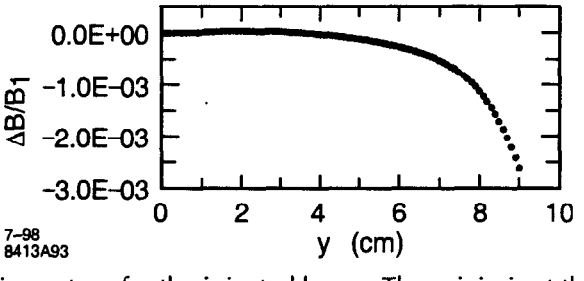

Figure 4.46 $\Delta B/B_1$ in septum for the injected beam. The origin is at the magnet midplane and the y-axis is vertical. The injected beam sagitta is 89 mm.

4.1.8 Magnetic Measurements

Magnetic measurements will be done on all SPEAR 3 magnets to evaluate integrated field strength and field quality to a few parts in 10^{-4} and verify compliance with the specifications. The position of the magnetic axis and the roll angle will be measured with respect to the six alignment balls located on the top and on the side of the magnets. The tolerances on these items are 200 μm and 500 μrad, respectively. Measurements will be required for all the prototypes to determine the

parameters of the magnet pole end chamfer required to compensate for the field distortion due to the three dimensional end effects.

Gradient magnets. Extensive magnetic measurements will be performed in order to qualify the prototype magnet (and determine the required end chamfer) as well as provide magnetic measurements for the quality control of the production quantity. The translating wire technique has been used at SLAC to characterize the transfer functions and the line integral field quality of the production PEP-II High Energy Ring (HER) magnets. The same technique can be applied for characterizing the transfer function and the line integral field quality for the SPEAR 3 gradient magnets. The integrated field strength will be measured at different excitation currents and a Hall probe will be used for calibration and to detail the end field shape. The magnet center will be located by measuring the dipole and quadrupole components.

Quadrupole magnets. The present Collins quadrupoles are made from two core segments. Since this geometry is symmetric about its vertical center plane, it is expected that the magnetic center will coincide with the mechanical center of the structure. It is further expected that, since precise mechanical assembly tolerances can be achieved, a low unallowed multipole spectrum will result. Dimensional measurements will also be performed to assure adherence to mechanical fabrication and assembly tolerance specifications.

The SPEAR field quality specifications call for integrated multipole errors of the order of a few parts in 10^{-4}. Since the electrical sensitivity required to measure these small errors is at the limit of what can be achieved with uncompensated rotating coils, it is expected that quadrupole and sextupole measurements will need to use compensated coils and a data acquisition system which includes a digital integrator. The compensated coil is designed and fabricated with nearly zero sensitivity to the fundamental so that the error multipole amplitudes can be more easily measured with the fundamental signal rejected. The integrator makes the measurement insensitive to variations in the rotational velocity of the measurement coil.

Sextupole magnets. Despite the mechanical constraints forced by the clearance requirements for the photon beam lines, it has been devised a sextupole design which is rotationally symmetric. Because of this symmetry, it is expected that the magnetic center will coincide fairly closely with the mechanical center. The field quality will be dominated by the multipoles "allowed" by the magnet rotational symmetry. However, since the yoke is assembled from 6 segments (3 core segments and 3 spacers), some level of unallowed multipole errors will be present. Thus, it is expected that up to 100% of the sextupole magnets will need to be measured. Again, it is expected that a compensated coil/integrator system will be used because this method will provide higher measurement precision.

The skew quadrupole trim coils will be assembled on the sextupole yoke. It is expected that the field quality for this trim configuration will be poor and multipole errors will produce a large electrical signal. The multipole spectrum for the sextupole excited as a skew quadrupole can be measured using any rotating coil connected in an uncompensated mode.

Trim magnets. The field quality requirements for the trim magnets are modest and can be easily measured using a line integral coil on a pair of translating stages. The multipole field spectrum can be closely approximated by computing the least square fit coefficients to a polynomial using the data gathered from the line integral coil translated along the horizontal central plane.

Assembly reproducibility. The quadrupole and sextupole magnets will be disassembled prior to installation in the SPEAR 3 ring and reassembled around the vacuum chambers after the chambers are installed. Procedures must be developed and tested to assure that the field quality for these magnets does not suffer because of mechanical errors in reassembly. During the prototype stage of

magnet manufacture, in order to test reassembly procedures and to assure the reproducibility of the multipole spectrum, both the quadrupole and sextupole will be measured repeatedly prior to dissassembly and after reassembly. Measurements are not required to determine the assembly reproducibility of the gradient and trim magnets because they are made from one piece yokes.

Fiducialization and magnet alignment for gradient magnets. Small manufacturing variations of the length of the gradient magnet cores will affect the integrated field and thus the bending angle of the gradient magnet on the nominal central axis at a prescribed power supply current. The wire technique used at SLAC for the PEP-II HER magnets can identify these small variations quite accurately. Since the field integral varies linearly transversally across the aperture, one can compensate for small variations of the integrated field for individual magnets at the nominal central axis by making a small transverse translation of the measurement coil to find the position where the field integral is precisely equal to the required value. The fiducial coordinates can then be adjusted to relate their values to this offset axis rather than the nominal mechanical axis. The gradient magnet can then be aligned to the axis which provides the required bend. Each magnet can be also individually corrected by using the trim coils.

Fiducialization and magnet alignment for quadrupoles and sextupoles. Transverse and vertical magnet alignment tolerances of <200 μm have been specified. These specifications apply to a "locally smooth curve" through the ideal lattice orbit. Larger global errors are allowed as long as the local orbit is smooth. A "roll" tolerance of 500 μrad has also been specified. These specifications challenge not only the capabilities of the alignment group, but require that any errors in the measured locations of external fiducials and any deviation of the magnetic axis with respect to the mechanical magnet center datum use only a small fraction of the tolerance.

Magnetic measurement techniques can identify the transverse and vertical locations of the magnetic axes for quadrupoles and sextupoles by measuring the "spilldown" multipole errors due to offset of the magnet measurement coil axis from the magnetic center axis. It will be important to provide means for identifying the location of the magnetic measurement coil axis. Thus, it is planned to assemble fiducial balls on the measurement coil axis. The location of these fiducial balls can be measured and related to the magnet fiducials. Present plans call for the use of laser interferometer theodolites which can locate the three dimensional coordinates of numerous objects and relate them to any arbitrary datum coordinate system. Prior to the measurements, magnet mechanical measurements using the interferometer system will be made to identify and define the magnet mechanical datum coordinate. This interferometer system technique is far simpler than fiducializing magnets using a large coordinate measuring machines.

The PEP-II LER quadrupoles were magnetically symmetric about the vertical central axes. Measurements of the magnetic center offsets for 320 quadrupoles showed that the magnetic axes coincided with the mechanical axes within a standard deviation value smaller than 50 μm. This is a small fraction of the alignment budget. The present SPEAR 3 quadrupole and sextupole designs are magnetically symmetric about their vertical central axes. Therefore, it is expected that magnetic center offset measurements will reproduce the PEP-II LER results and can be "sampled" for a small percentage (say 20%) of the production magnets.

Roll magnetic measurements are difficult and tedious for quadrupoles and sextupoles. The quadrupole and sextupole mechanical designs are magnetically symmetric about their horizontal axes. It is difficult to hypothesize a means of introducing a roll in the magnetic axes. A small number of magnets will be measured using a method similar to that used for the APS magnet. This involves turning the measurement coil, whose central plane is carefully identified, end for end and taking the average of the phase angle from the central plane as the rotational offset of the magnetic field.

References

[1] Halbach, Tanabe - Conformal Mapping + Pole overhang

[2] Halbach, Tanabe - Spilldown multipoles

[3] Helmut Wiedeman, Particle Accelerator Physics (Springer Verlag, Berlin, 1993).

[4] Halbach, Tanabe - ALS gradient dipole

[5] J. K. Cobb, R.A. Early, The New SLAC Permeameter, SLAC-TN-89-04, December 1989.

[6] Collins quadrupole

[7] Shanghai Synchrotron Radiation Facility, Conceptual Design Report (Draft), SSRF Report-01, September 1996.

[8] BESSY Laboratory, Berlin, The Bessy II Parameter List, version 1, (1993)

[9] Argonne National Laboratory, 7 GeV Advanced Photon Source - Conceptual Design Report, ANL-87-15, (1987).

[10] J.E. Milburn, S.H. Hong, et al., Injection System for the PLS Storage Ring, Pohang Accelerator Laboratory.

[11] Electronic Alloys Catalog, Carpenter Technology Corporation.

4.1.9 Magnet Girders

The existing 18 concrete SPEAR 2 magnet girders will be replaced with new steel girders (14 long girders for the standard cells and 12 short girders for the matching cells) to support SPEAR 3 magnets.

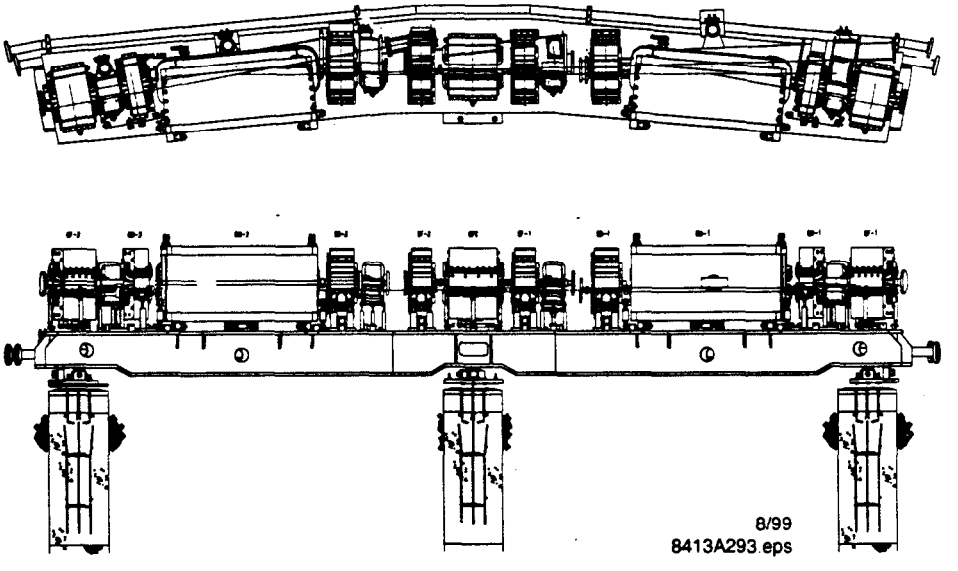

Figure 4.47 New Steel Girder

Each of the 9 m-long steel girders will be supported on three existing 1.5 m long piers, embedded into sandstone beneath the asphalt floor of the ring, and on one new support Figure 4.47. Concrete ring shielding blocks rest on the asphalt floor and do not directly affect girder alignment. The new support will be added for SPEAR 3 to attenuate the present girder vibrational modes at ~5 Hz and 12.5 Hz as well as to help accommodate the increased magnet weight and altered weight distribution.

4.1.9.1 Steel Girder

Each new steel girder (0.47 m deep, 0.96 m wide, 9 m long) is mounted rigidly on 3 concrete piers, 0.61 m in diameter, which are embedded 1.5 m deep in stable sandstone (Figure 4.50). Connections between girders and piers are made with pinned and bolted steel I-beams. The new fourth support is being designed.

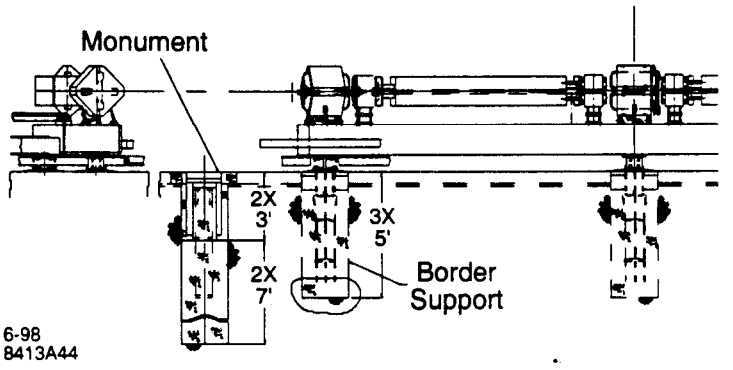

Figure 4.48 SPEAR magnet girder mounting arrangement.

Each girder weighs 11,000 lbs and will support a SPEAR 3 magnet and vacuum chamber load of 42,500 lbs for Standard Cells and 24,500 lbs for Matching Cells. This load is 13,000 lbs more than that for SPEAR 2 magnets. Engineering analysis of the steel girders has been done to ensure their strength is adequate for the additional load. With the present 4-point supports, the girder will deflect and twist approximately 0.16 mm under the SPEAR 3 magnet load. The design for the girder supports will be optimized using a mockup of the fully loaded girder

4.1.9.2 Girder Stability

The girders are subject to thermally induced and vibrational motion which will affect magnet alignment and cause beam motion. These effects will be reduced to tolerable levels by controlling ring tunnel temperature, damping girder vibrational modes with additional girder supports, and employing an active orbit feedback system as discussed in Section 4.7.1.

With a coefficient of thermal expansion of 10.8×10^{-6} for the steel girder and magnet supports, the ±1°C expected diurnal temperature fluctuation in the ring tunnel will cause the center of the magnet, 1.06 m from the floor, to change elevation by ±12 μm. The effects of this motion on beam stability are discussed in Section 3.4.1.

Figure 4.50 shows the dominant vibrational modes for the existing concrete girders with three supports. Figure 4.51 shows the power spectral density and integrated amplitudes for these modes. The new steel girder with four supports has two principal oscillation modes with frequency of 20.4 Hz and 23.8 Hz. The natural microseismic ground vibrations at SPEAR, with an amplitude of ~40 nm rms (integrated between 1 Hz and 1 kHz as measured at midday) (Figs. 3.4.1.2-3 and -4) will not be amplified due to the high natural frequencies of the steel girder. The expected motion is ~20 nm rms.

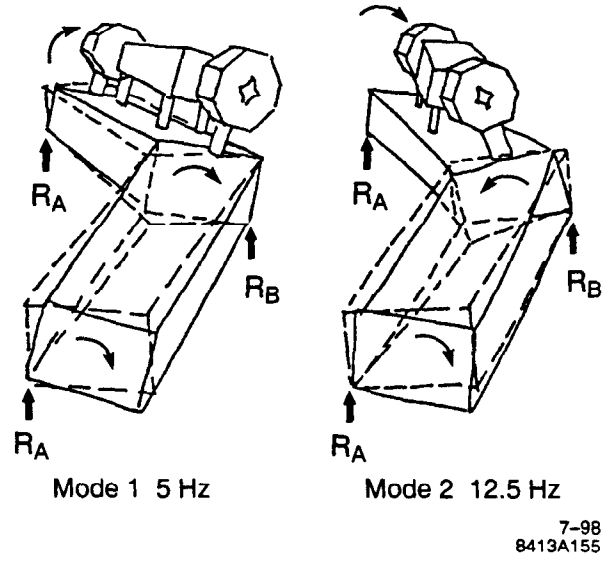

Figure 4.49 Dominant vibration modes for SPEAR2 magnet girders having 3-point support.

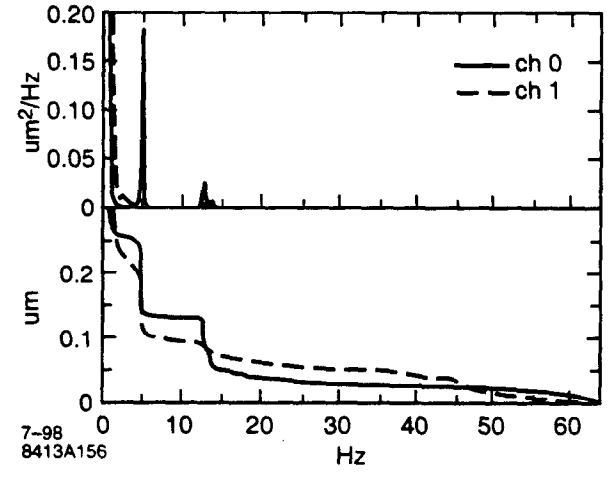

Figure 4.50 Power spectral density and integrated rms motion for SPEAR 2 magnet girders.

References

[1] D. Kaul, internal memo, October 1997

[2] G. Bowden; internal memo, June 4, 1997.

4.1.9.3 Matching Cell Magnet Stands

Twelve new support stands will be installed flanking the East and West pits to carry portions of the Matching Cell magnet and vacuum hardware that are well separated from the existing nearby concrete girders (Figure 4.56). Each stand will span a small gap between the edge of the pit and the new concrete platform poured in the pit (Sec. 6.1.1-1).

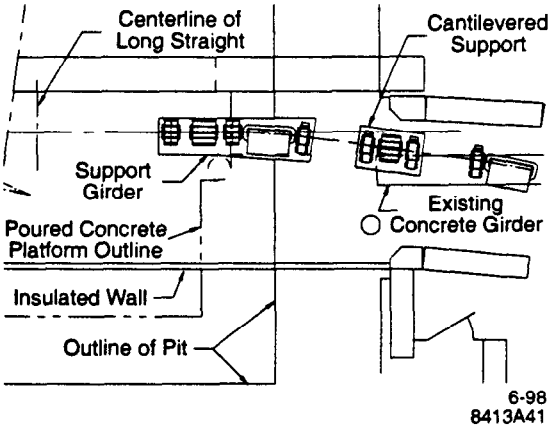

Figure 4.51 Matching Cell supports adjacent to the East and West pits.

4.1.10 Magnet Supports

SPEAR 3 magnets require 3-D position adjustments having ±50 μm tolerances. Since the support girders themselves are not adjustable, each magnet must have its own adjustment system. A 6-strut, 3-point kinematic support system capable of attaining the 50 μm alignment tolerances will be used for each of the dipole, quadrupole and sextupole magnets. Similar to those used for the ALS and the B-Factory, the support system consists of 3 vertical Y-axis struts, 2 horizontal X-axis struts, and 1 longitudinal Z-axis strut (Figure 4.52).

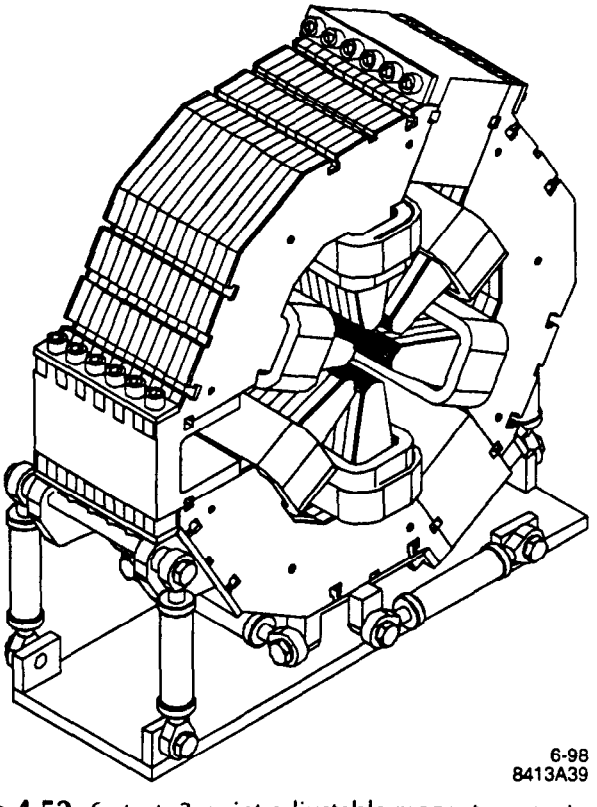

Figure 4.52 6-strut, 3-point adjustable magnet support system.

4.2 Vacuum System

The SPEAR 3 ring is a racetrack oval 243 m in circumference, consisting of two arcs and two 7.5 m "long" straight sections. The arcs consist of two 11 m matching girder chambers adjacent to the 4.5 m matching straight sections, and seven 9 m standard magnet girders joined by six 3.1 m straight sections (see figure 4.2-1). Standard magnet cells bend the beam by 21.1 degrees and the matching cells bend the beam 15.9 degrees.

SPEAR 3 incorporates an antechamber design with discrete pumping and crotch absorbers. The vacuum chambers are designed to reach 500 mA at 3 GeV. The new ring fits in the existing straight section lengths and maintains the nominal beam line alignment currently operating in SPEAR 2. All new vacuum chambers are required to achieve the goals of a third generation light source. The majority of the insertion device (ID) chambers will remain, but transition mask modules will increase their design limits to 500 mA. Currently, at least one of the ID chambers and magnet will be replaced.

4.2.1 General Requirements

Included here are the major requirements, physics related and mechanical, that need to be balanced to produce a suitable vacuum system for a electron storage ring. Additional requirements exist for SPEAR 3 which are inherited from the existing SPEAR 2 machine, such as tunnel space, existing beam lines and IDs.

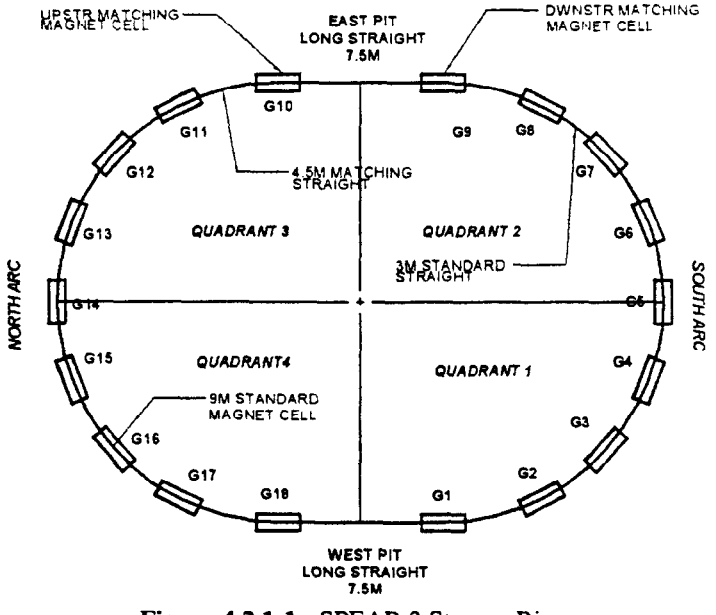

Figure 4.2.1-1: SPEAR 3 Storage Ring

- **Base Pressure:** It is essential for users to have consistent beam time, therefore beam lifetime is one of the most crucial requirements for the vacuum system. An ~20 hour lifetime at 500 mA is desired. In order to achieve this lifetime it has been shown that an average pressure of 1.8 nTorr is required (see Section 3.7). Since, the error bar for the calculated average pressure and liftetime is large, an average pressure requirement of 0.8 nTorr N_2-equivalent was set to ensure that this lifetime goal is achieved. The average pressure in the existing beam line IDs are pre-determined by their original design and limit the vacuum performance of the ring (see Section 4.2.5.1).

- **Chamber Impedance/HOMs:** Minimizing beam impedance and higher-order-mode (HOM) power dissipation aids in increasing beam lifetime. Therefore, it is necessary to reduce changes in the vacuum chamber cross-section. Transitions between existing and new IDs need to have 1:5 tapers in the vertical direction, to reduce their impedance. Also, absorbers and pump ports should be located outside of the the beam passage where possible or be designed with an RF shield. Bellows will be designed to provide smooth RF continuity using RF liners and seals. Minimizing the number and physical size of transverse gaps is required. Transverse gaps must be less than 1 mm wide by 3 mm deep (see section 3.5).

- **Beam-Stay-Clear (BSC):** The chamber cross section including manufacturing tolerances and alignment can not violate the BSCas described in section 3.1.12.

- **Beam Mis-steer:** The vacuum chamber must be able to survive under spurious beam operation conditions. The possibility of mis-steering the photon beams, especially during comisioning and machine conditioning could be large. Beam trajectory analysis finds that without interlocks a vertical mis-steer of +/- 12 mm is achievable (see section 3.1.13). In fact, the limiting effect is the aperture of the ID vacuum chambers, otherwise these mis-steers could as large as 17 mm. A horizontal mis-steer of 30 mm is also possible and will be limited physically by vacuum chamber apertures or by globally interlocking the ID BPMs.

  During off-axis operation, the largest source of thermal loading is from ID SR striking the vacuum chamber wall. Above 50 mA, vacuum chamber failure could result and therefore the vertical motion of the beam will be interlocked for the ID power required (see section 3.1.1.3). However, the dipole synchrotron radiation is lower and at 500 mA, a SR strike would not damage the vacuum system, thus interlocks are only required when ID magnets are in their closed position. The following table summarizes the mis-steer scenarios with interlocks on and off and IDs closed and opened.

Table 4.2.1-1: Mis-steer scenarios

Interlocks	Current (mA)	BL Moveable Masks	Insertion Devices	Girder Chambers		Insertion Device	
				x_{max} offset (mm)	y_{max} offset (mm)	x_{max} offset (mm)	y_{max} offset (mm)
off	0-500	closed	open	±21	±17	±30	±9
off	0-50	closed	closed	±21	±17	±30	±9
on	0-500	open	open or closed	±5	±5	±5	±5

- **Beam Stability:** It is necessary that the stability of the beam be less than 5 microns vertically and 15 microns horizontally during normal operation. Discrete absorbers are required to mask synchrotron radiation from striking the chamber walls that would otherwise cause thermal motion of the chambers. Also, the BPMs need to achieve high resolution and precision requirements and need to be supported to prevent motion. The beam stability requirement also lends itself to require a fast correction scheme. In order to achieve fast feedback to 100 Hz, the vacuum chambers are designed to minimize the eddy currents that could adversely affect the performance of the fast correctors.

- **Beam lines:** Maintain existing photon beam alignments and allow for 24 mrad of bend radiation and 18 mrad of ID radiation at pre-determined source locations.
- **Existing Insertion Device Chambers:** Incorporate existing IDs and increase their safe operating current to 500 mA.
- **Cooling:** Sufficient cooling to safely dissipate head loads associated with synchrotron radiation.
- **Installation, Cost & Schedule:** Design must be consistent with cost and schedule.

4.2.2 Defining Vacuum Aperture

The vacuum chamber aperture is dependent on the beam-stay-clear (BSC), magnet geometry, manufacturing tolerances and alignment. The BSC is dependent on the beam emittance, the energy spread and the optical functions of the lattice (see section 3.12). The vacuum chamber must accommodate the BSC to ensure adequate beam lifetime. Table 4.2.2-1 summarizes the maximum BSC (in half apertures) at different locations around the ring.

Table 4.2.2-1: Beam Stay Clears

Locations	BSC x (mm)	BSC y (mm)
Standard Magnet Cell	±30	±15
Matching Magnet Cell	±30	±15
Straight Section	±30	±6
Injection (Girder 15)	±40	±15

The BSCs were calculated using the following, beam parameters, plus addition tolerance (see figures 3.25 and 3.26)

Table 4.2.2-2: Aperture Defining Requirements

	Xcod	$\varepsilon_{x/eff}$	Ycod	$\varepsilon_{y/eff}$
Injection	±10.0mm	22 mm-mrad	±3.1mm	2.2 mm-mrad
Stored	±3.0mm	47 mm-mrad	±2.0mm	3.4 mm-mrad

The vacuum aperture in the standard and matching cell vacuum chambers accommodates the largest BSC which occurs only in girder 15 (where the injected beam first enters the storage ring). The vacuum chamber cross section is a 34 mm high by 84 mm wide octagon with a 12 mm tall slot leading into the antechamber. The four angled walls are sloped at 30 from horizontal. This cross section allows a minimum of 2 mm to the magnet poles and 3 mm to the magnet coils. The clearance to the prescribed BSC is 2 mm both vertically and horizontally. The clearance accommodates manufacturing and alignment tolerances, as well as the deflection of the chamber due to vacuum loading. The height of the slot is the most critical dimension of the vacuum chamber profile. The straight section chambers, excluding the ID chamber, RF straight sections and some diagnostic equipment will maintain a similar vacuum chamber aperture.

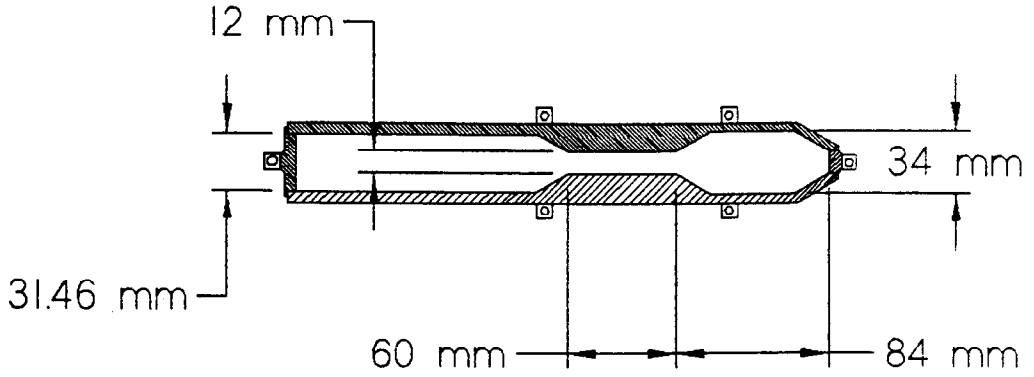

Figure 4.2.2-3: Typical vacuum chamber cross section and BSC (except in IDs)

The slot geometry is dependent on beam impedance and beam mis-steering. Impedance calculations found that a maximum slot height of 15 mm is acceptable [section 3.5]. Also a 1:5 ratio between slot height and depth is required to reduce field leakage. Vertical interlock trip levels are also dependent on slot height. Therefore, the slot height was set at 12 mm to allow for a trip level of 1mm and minimize the impact on field leakage slot length. However, due to imaging requirements, the synchrotron light monitor slot height was increased to 15 mm.

4.2.3 Steady State and Transient Thermal Loads

The primary sources of thermal loading on the vacuum system are

- Synchrotron Radiation,
- Resistive wall losses,
- HOM losses,
- Scattered synchrotron radiation.

4.2.3.1 Synchrotron Radiation

The linear synchrotron radiation power density produced from the bend magnets can be estimated by the following equation

$$P_L = \frac{885E^4 I}{2\pi\rho^2} \quad \text{(W/cm)} \qquad (4.2.2\text{-}1)$$

where E is the total energy (GeV), I is the total beam current (A) and ρ is the bend radius (meters). In SPEAR 3 the linear power density along the circumferential path of the dipoles is 92.4 W/cm at 500 mA and 3GeV.

Dipole Radiation

The 36 bend magnets emit a total of 456 kW with each standard cell emitting 27 kW. Of this, 25 kW are absorbed in the cell's seven photon masks and absorbers and approximately 2 kW is handled in the straight section chambers under nominal operating conditions.

Insertion Device Radiation

There are presently seven ID chambers in SPEAR 2. The synchrotron radiation emitted by these magnets is powerful. The power densities for the IDs are shown in Figure 4.2.3.2-1. No practical amount of water cooling close to the strike can protect the chamber from a direct strike of ID power at 500 mA. The absorbers can handle a small portion of the synchrotron radiation fan for a few cycles.

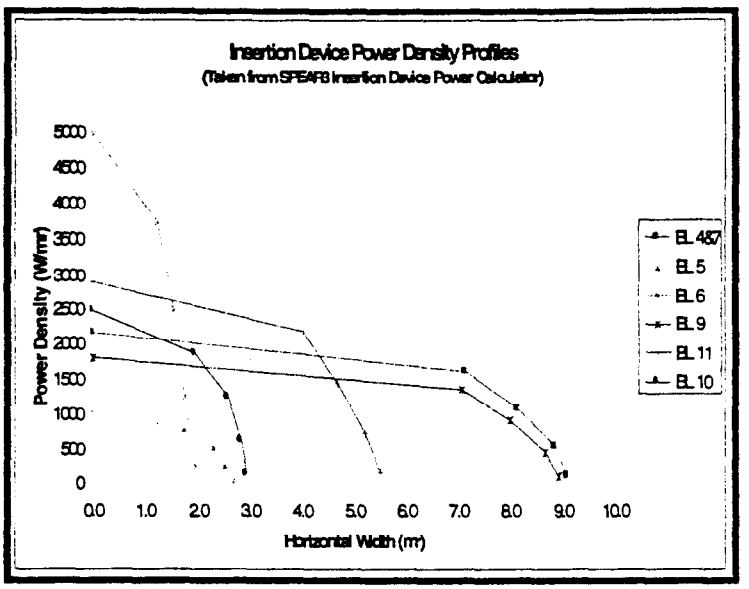

Figure 4.2.3.2-1: Insertion device power densities

4.2.3.2 Beam Mis-Steer

The beam mis-steer scenarios discussed in Sections 4.2.1 and 3.1.1.3 indicate that at low current (0-50 mA) with the interlock system deactivated and the IDs closed the chambers can see impinging SR on the chamber walls. When the electron beam is mis-steered more than ±6 mm vertically, SR will strike the vacuum chamber walls above or below the chamber slot. The largest source of thermal loading is from ID SR impinging on the chamber walls. The maximum heat flux of 140 W/mm^2 is produced from the BL 6 wiggler at 500 mA. Clearly, at this power level, the chamber cannot last long before the chamber wall melts. Again, no practical amount of water cooling close to the strike can protect the chamber. At full power, the time-to-melt for copper (MP = 1085°C) exceeds 500 ms while the time-to-melt for stainless steel (MP = 1397°C) is less than 100 ms. For comparison, at 100 mA operation the time-to-melt for both materials is increased to well above 500 ms. The time increase is due to the decrease in input power relative to the heat conduction paths along the chamber walls and the convective cooling power provided by water flow. The horizontal and vertical mis-steering of the beam and limited by interlocks when the current is above 50 mA and IDs are closed.

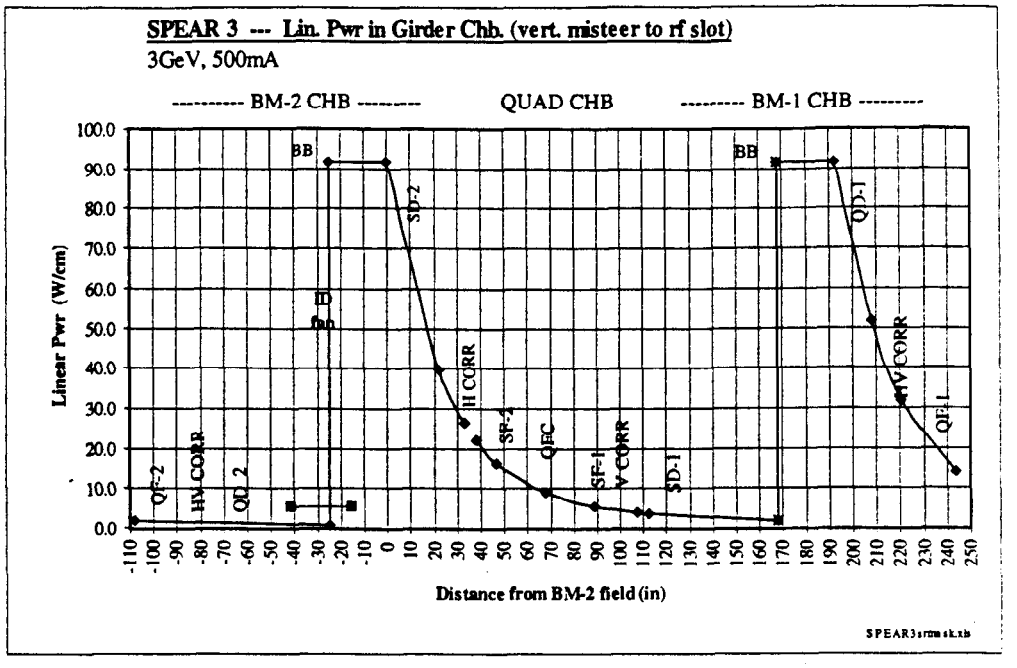

Figure 4.2.3-3: Heat Loads at 500 mA on chamber walls during off-axis operation

An off-axis operation at high currents (0-500mA) could occur with the IDs open. Thus the chambers would only intercept SR emitted from the dipoles, approximately 20% of the maximum ID power. The secondary source is SR emitted from the dipoles is 10 W/mm at 3 GeV and 500 mA. The worst case considered is where the heat load from the impinging bend fan strikes the chamber at the top of the slot. The peak temperature in the girder chamber with and without pole pockets is 196°C and 148°C, respectively, and 115°C in the straight drift chambers. Copper cooling tubes, attached by EB welding to the exterior surface of the chamber, with 1.0 gpm of water flow, provide adequate cooling capacity.

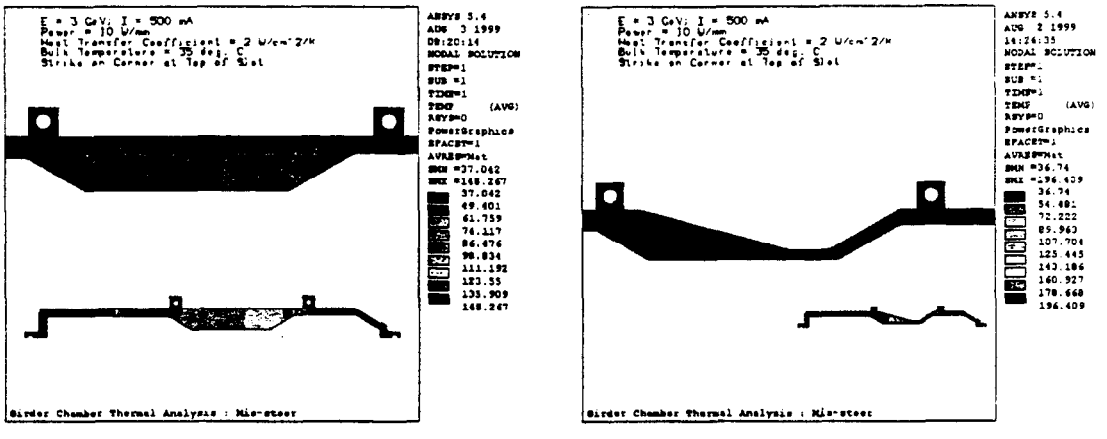

Figure 4.2.3-4 Thermal analysis of the girder chamber : 10 w/mm lineal heat flux above slot

Additional, masking is necessary for the seven existing IDs to protect the un-cooled chambers from a dipole SR strike during off-axis operation.

4.2.3.3 Resistive Wall Heating, Higher Order Mode Heating and Scattered SR

There are three additional sources of heat: 0.005 W/cm^2 scattered SR, 0.005 W/cm^2 from ohmic losses and 0.005 W/cm^2 from HOM heating, (preliminary estimates). The total uniform heat flux applied to the vacuum system is 0.015 w/cm^2. Thermal calculations produce less than a 10°C rise in the peak chamber temperature.

4.2.3.4 Gas Desorption

There are two main source of gas desorption in the girder chambers. The primary source is gas evolution from the surfaces of the absorbers and masks caused by photon stimulated desorption (PSD) due to impinging SR fans. Secondary sources are thermal desorption as well as scattered and fluoresced photons from the absorbers that bombard the surrounding surfaces of the vacuum chamber liberating adsorbed gas molecules. PSD accounts for the majority of the gas pumped from the system.

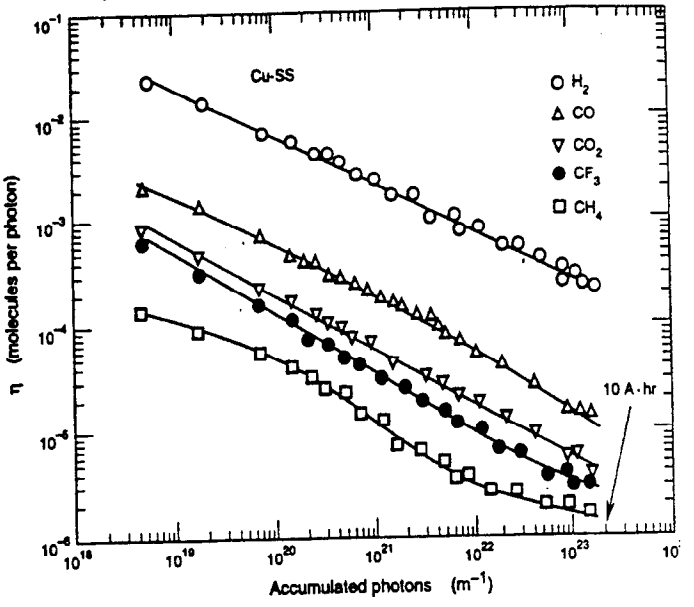

Figure 4.2.3.4-1: Variation of Photodesorption coefficient versus accuumulated photon dose

The gas load contribution from PSD is dynamic and directly related to the machine current. Also, the dynamic pressure rise due to PSD is reduced with increasing integrated photon dose (A-h) on the incident surface. This phenomena is known as scrubbing. The PSD gas loads for SPEAR 3 are calculated using a minimum photo-desorption coefficient of $2x10^{-6}$ molecules per photon [1]. The material chosen for the absorbers is GlidCop, an alumina dispersion strengthened copper. Since this material is more than 99% copper by weight, it is assumed that PSD rates for copper and this material do not vary significantly.

PSD rates in photons per second are calculated from the incident photon flux as follows:

$$N_\gamma = \frac{P_{SR}[W] * 6.242x10^{15}[keV/Joule]}{E_{average}[keV/photon]} \qquad (4.2\text{-}2)$$

For the H-3 Absorber, the incident power at 3 GeV and 500 mA is approximately 9 kW, yielding a photon dose of

$$N_\gamma = 2.37x10^{19}\,photon/sec \qquad (4.2\text{-}3)$$

Knowing the photon flux and the PSD coefficient, the gas evolution rate is:

$$Q_{PSD} = \eta_{PSD}[\text{molecules/photon}] * N_{\gamma}[\text{photon/sec}] * 2.83\text{x}10^{-20}\,\text{Torr}\cdot\ell/\text{molecule} \quad (4.2\text{-}4)$$

$$Q_{PSD} = 1.34\text{x}10^{-6}\,\text{Torr}\cdot\ell/\text{molecule} \quad (4.2\text{-}5)$$

Gas loads for each of the power absorbing components are summarized in Section 4.2.5.1.

BLs 4,5 and 7 contain aluminum chambers that intercept SR power along the outer wall. Initial PSD outgassing rates for aluminum are a factor of ten greater than for either copper or stainless steel [2]. The difference decreases with total photon dose; at 10^{21} photons/meter, the aluminum is only a factor of three higher. Thermal desorption rates for aluminum are about a factor of ten higher when compared with copper for the same pumping time and operating conditions, and little change in the ratio occurs during thermal "clean-up".

The background outgassing rate attributed to thermal desorption tends to decrease more slowly than PSD rates. This is mainly because the majority of the chamber surface intercepts little or no direct SR. Thermal desorption decreases with increased time at low pressure as the molecules are slowly removed from the large surface area in the antechamber and beam passage. Outgassing rates as low as $1\text{x}10^{-12}$ Torr*l/s/cm^2 can be achieved with proper clean fabrication and vacuum processing techniques.

4.2.4 Choice of Material

Copper has excellent thermal properties that enable a more robust design when considering safe operating current with IDs, safe operating current without IDs and transient thermal response. Copper also offers greater thermal stability and increases the beam stability threshold, reducing the need for feedback. The vacuum performance of copper is nearly identical to stainless steel for both thermal outgassing rates and photon stimulated desorption. Also, copper chambers have been constructed for other machines at SLAC with excellent operational results. The mechanical properties are more than adequate to achieve acceptable slot deflections and react vacuum loads as well as other loading conditions due to assembly.

4.2.5 Vacuum Analysis

4.2.5.1 Pressure Profiles

The vacuum system must be sized to handle the large gas loads produced by synchrotron radiation at the photon absorbers as well as provide the desired pressure at the beam passage to achieve an acceptable beam lifetime. Once the gas loads due to PSD and thermal sources have been determined, the pumping system configuration can be specified.

The pumping system is comprised of Noble Diode Ion Pumps, Titanium Sublimation Pumps (TSPs) and Non-Evaporable Getters (NEGs). The TSPs and NEGs are located at the major photon absorbers and the Sputter Ion Pumps are located in the girder and straight sections where space allows. The TSPs and NEGs have been chosen because they can provide very high pumping speeds for most gases while fitting in confined locations. The noble diode style of sputter ion pump has been selected to extend the pumping capacity and speed down to 10^{-10} Torr when compared with Triode style ion pumps. The sputter ion pumps will pump noble gases in addition to maintaining the pressure in the ring while processing TSPs and NEGs.

Table 4.2.5.1-1: Photodesorbed gas loads for standard girder chamber masks and absorbers

For 3 GeV, 500 mA, $2x10^{-6}$ molecule/photon	V-1 Mask	V-2 Mask	H-1 Absorber	H-2 Absorber	V-3 Mask	H-3 Absorber	V-4 Mask
PSD Gas Load (Torr*l/s)	$6.3 x10^{-8}$	$7.9 x10^{-8}$	$7.2 x10^{-7}$	$5.9 x10^{-7}$	$8.4 x10^{-8}$	$1.2 x10^{-6}$	$2.9 x10^{-7}$

Table 4.2.5.1-2: Photodesorbed gas loads for bl masks and standard straight drifts

For 3 GeV, 500 mA, $2x10^{-6}$ molecule/photon	BL5	BL6	BL9	BL10	BL11	Standard Straight
M1 PSD Gas Load (Torr*l/s)	$6.8 x 10^{-13}$	$3.6 x 10^{-13}$	$4.5 x 10^{-13}$	$3.3 x 10^{-13}$	$2.3 x 10^{-13}$	$3.0 x 10^{-13}$
M2 PSD Gas Load (Torr*l/s)	$5.6 x 10^{-13}$	$2.7 x 10^{-13}$	$2.4 x 10^{-13}$	$3.1 x 10^{-13}$	$2.0 x 10^{-13}$	$3.0 x 10^{-13}$
M3 PSD Gas Load (Torr*l/s)	0	0	0	0	$2.1 x 10^{-13}$	0

The antechamber construction has several benefits. First, the beam passage is more efficiently pumped along the entire length of the slotted portion of the chamber. Second, the overall chamber conductance is increased by the addition of the antechamber. Finally, and most importantly, the high gas loads produced from PSD are located close to the high-speed pumps. One drawback of this type of design is the increase in surface area due to the flared chamber construction; as a result, the total thermal gas load is increased.

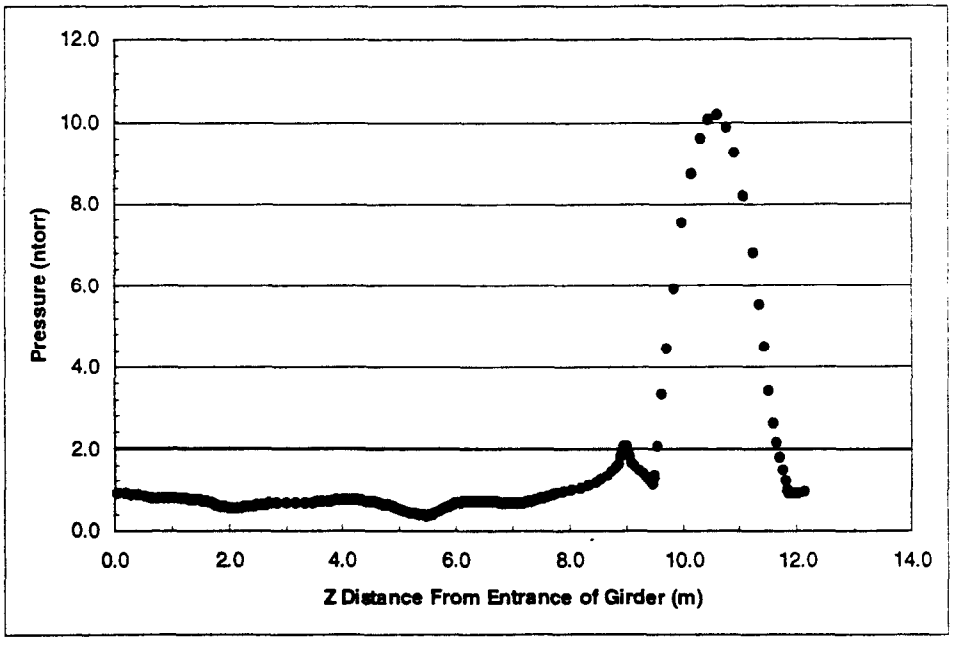

Figure 4.2.5.1-1 : Pressure Profile Girder 13 and BL 10

A N_2-equivalent gas pressure profile for a standard girder and straight section is shown in Figure 4.2.5.1-1. The gas loads produced at each power absorbing component correspond to 3 GeV and 500 mA conditions with a PSD outgassing rate of $2x10^{-6}$ molecules per photon and a thermal

outgassing rate of $5x10^{-12}$ Torr*l/s/cm^2. These conditions exists after approximately 150 Amp*hours of operation. The new ion pumps were sized at 220 l/s with a net speed of 165 l/s each. The three TSPs were sized at 1500 l/s and the NEG pump was sized at 600 l/s with a net speed of 140 liter per second. The total gas pumped from a girder section is almost $3.0x10^{-6}$ Torr*l/sond. The resulting average pressure predicted for SPEAR 3 vacuum system is 0.8 nTorr with a peak pressure of 2.2 nTorr occurring at the V4 Absorber. Based on these numbers, the beam lifetime (dominated by inelastic gas scattering) is acceptable (see Section 3.7).

The TSPs and NEG modules must be processed periodically during operation in order to renew their effective pumping speed and capacity. The TSP is regenerated by flashing fresh titanium onto the extended surface using a 50 Amp power supply. The NEG module is regenerated by heating the getter material to 400°C to diffuse the captured gas into the bulk of the pump. Regeneration schemes and durations are discussed in the design description sections for each type of pump.

4.2.6 Vacuum System Design Overview

This section describes the SPEAR 3 vacuum system for the standard and matching cell girder chambers and straight sections. The discussion includes a description of the manufacturing processes, absorbers and masks, eddy current breaks for fast corrector field penetration, TSP and NEG modules. Special components, beam lines, bellows modules diagnostics and injection elements, are also covered.

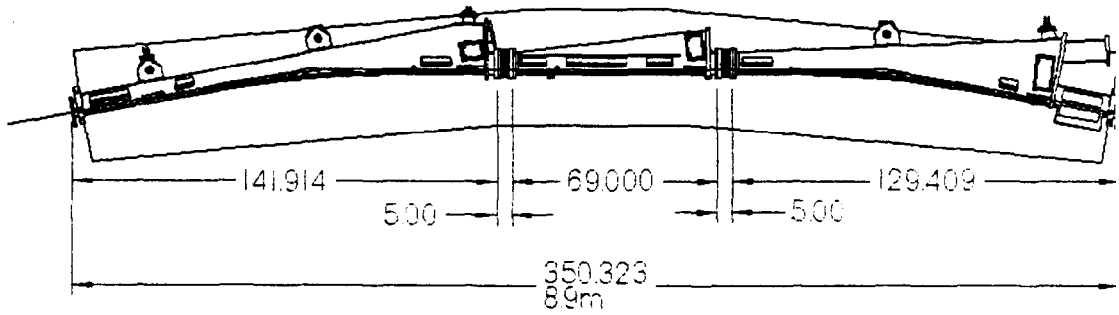

Figure 4.2.6-1: Standard Girder Section Chamber Layout

4.2.6.1 Girder Chambers

There are fourteen sets of standard cell chambers and four sets of matching cell chambers located around the ring that comprise the girder chambers. These chambers employ a saw-tooth antechamber design with discrete photon absorbers to that minimize the chamber wall exposure to synchrotron radiation. Except in cases of extreme beam mis-steering, all radiation that does not exit through beam line ports is intercepted on masks and absorbers.

The magnet designs drive the size of the vacuum chamber. Clearance requirements to the magnets are: 2 mm spacing from the chamber outer wall to the pole, and 3 mm clearance from the chamber outer wall to the coil. Pole pockets cut in the outer portion of the upper and lower chamber halves provide clearance for the magnet poles. The same cuts are employed for all quadrupole and sextupole magnet locations. The gradient dipole magnet does not require additional cuts in the chamber.

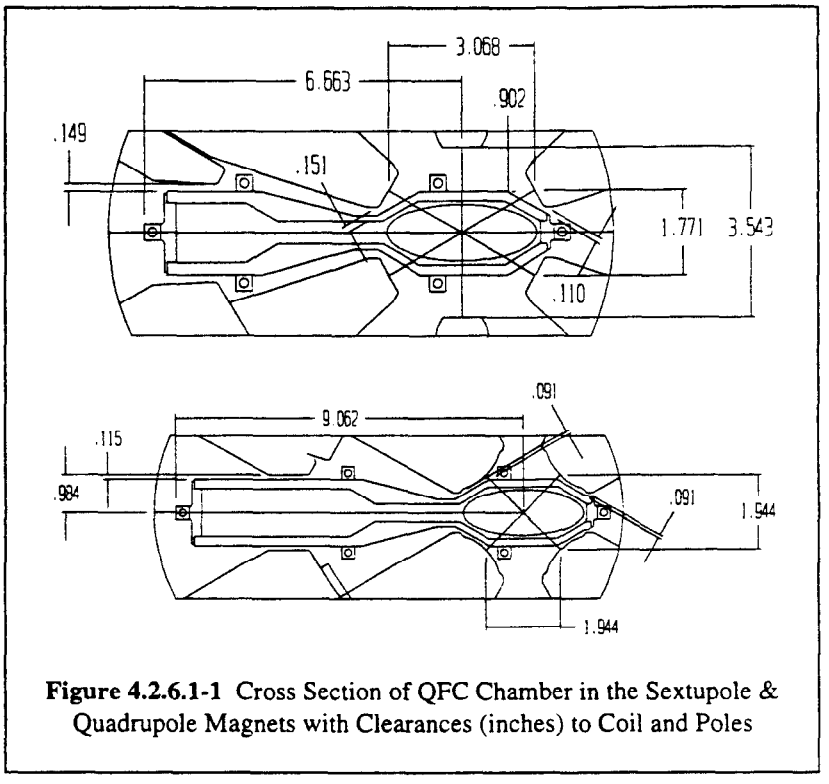

Figure 4.2.6.1-1 Cross Section of QFC Chamber in the Sextupole & Quadrupole Magnets with Clearances (inches) to Coil and Poles

4.2.6.1.1 Analysis

The requirement for slot deflection under vacuum loading is < 0.25 mm. Structural analysis of the BM-2 chamber indicates that deflection for the chamber wall in the area of the slot is between 0.1 and 0.2 mm. It is expected that both the QFC and BM-1 chambers will exhibit similar deflections under vacuum loading. The chamber wall thickness in the antechamber, combined with the additional material in the areas without pole pockets significantly increase the chamber stiffness. This eliminates the need for reinforcing ribs as in other light source chamber designs.

4.2.6.2 Design & Manufacturing

Each cell is composed of a set of three separate chambers, BM-2, QFC, and BM-1, interconnected by bellows. The chambers, each named according to the largest magnet that it passes through, are water-cooled throughout their length to withstand heating in the event of beam mis-steer. The BM-1 and BM-2 chamber have curved segments that follow the beam trajectory along the 7.8575 m bend radius and have flanged exit ports for ID radiation and bend magnet radiation fans. Any unused exit ports will be sealed with a water-cooled blank flange. The central QFC chamber is much shorter and contains no radiation exit ports. The matching cells are also divided into three separate chambers connected by bellows.

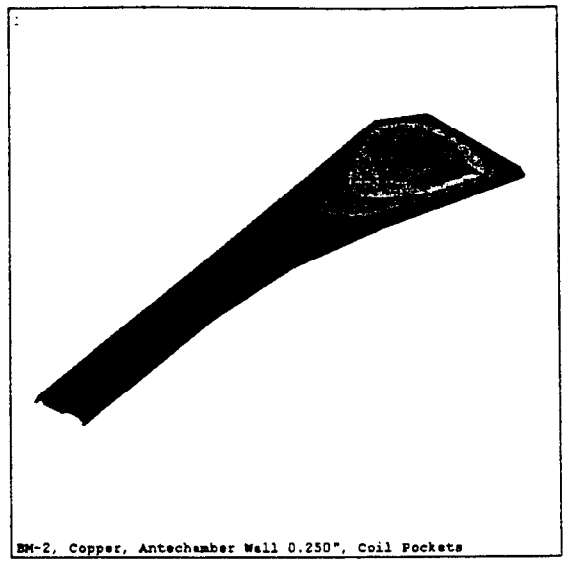

Figure 4.2.6.1-2: Structural Analysis of the BM-2 Vacuum Chamber

Six water lines are attached to each chamber: one each on the inner and outer chamber walls and two each on the top and bottom chamber halves that straddle the slot. A flow rate of 1 gpm is required to provide adequate cooling. During accidental off-axis operation when nearly all of the 13kW dipole fan strikes the three chambers above the slot, the bulk temperature in each of the two cooling lines rises by only ~12°C.

Alignment at flange pairs is accomplished by using the outer diameter of the Conflat gasket to position one flange relative to the next. A tapered dowel pin 2.5" above the flange center provides angular alignment across the flange pairs between the bellows module and any of the chambers. The position and size of the pin is chosen to reduce steps across a flange pair to less than 0.020". This method reduces transverse steps or discontinuities along the beam passage wall. Also, axial discontinuities are minimized by employing an RF seal attached to the bellows module that register on the flange face.

Copper chamber construction is divided into three major portions:

- Machining of mating, mirror-image halves, and ancillary ports and flange preps,
- Electron Beam (EB) welding and assembly,
- Vacuum processing.

The upper and lower halves of each of the girder chambers are machined from single pieces of copper plate, UNS C10100 or C10200. For the quantities required in SPEAR 3, this approach falls within existing budgetary constraints. Pockets are cut in the outer surfaces of the machined halves to allow pole clearances. Holes for the BPM buttons and cut-outs for the CuproNickel (Section 4.2.6.4) breaks are added.

Next, the majority of the assembly will occur in the SLAC electron beam (EB) welder. This machine produced all of the copper chambers for the PEP-II B-Factory. First, the halves are

clamped using tooling and EB-welded, then beam position monitors (BPMs), cooling lines and the CuproNickel breaks are added, followed by pumping port Cu/SS transitions and lastly the crotch absorbers are welded in. Some additional TIG welding is required to attach Conflat® flanges and pump housings for Ion Pump ports, Titanium Sublimation Pumps (TSPs), instrumentation and chamber interconnects

Finally, the welded chamber is required to be leak tight to 2 x 10-10 std cc/sec using Helium gas. The option for glo-discharge (GDC) processing the beam passage with a 5%Oxygen/95%Argon gas mixture prior to bake-out is being considered to help reduce overall PSD rates. The chambers are then placed in vacuum ovens and processed at 200°C until outgassing rates and partial pressures are below acceptable limits.

4.2.6.3 Absorbers and Masks

Table 4.2.6.3-1 : Girder chamber mask and absorber power loads

Mask or Absorber	Ave. Fan Height (mm)	Power (kW)	Heat Flux (W/mm^2)
Mask V-1	1.56	0.42	5.7
Mask V-2	2.42	0.53	2.4
Absorber H-1	0.48	4.76	21.5
Absorber H-2	0.94	3.92	5.5
Mask V-3	1.95	0.56	3.7
Absorber H-3	0.56	8.11	15.4
Mask V-4	0.43	1.95	19.3

The primary function of the discrete masks and absorbers is to shadow the chamber from dipole radiation. A distinction is made between masks and absorbers; absorbers are located in crotch areas between chambers, masks are not. The power intercepted on the components ranges from ~0.5 kW up to slightly more than 8 kW for normal operating conditions.

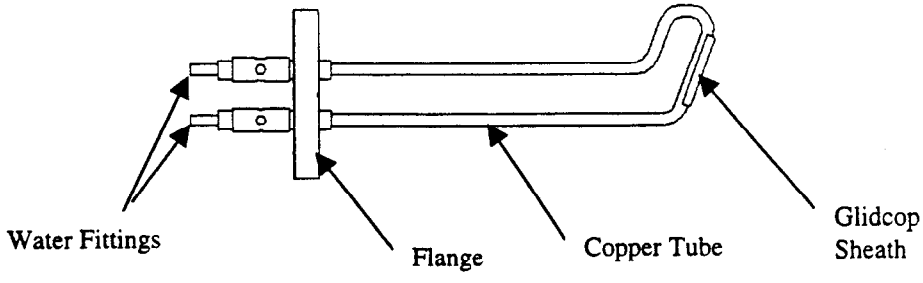

Figure 4.2.6.3-1 : Plan view of mask assembly with glidcop™ on intercepting face on 2-3/4" flange

Three of the four masks are located along the outside of the chamber to intercept SR power emitted from the dipoles. The total power incident on these mask is relatively low, only about 0.5 kW. The surface that intercepts the power is a planar face on a sheath of GlidCop® brazed to a copper cooling tube. The planar face on the sheath is oriented vertically and sloped at 30° to grazing. The

resulting temperatures and induced compressive stresses are modest, about 74°C and 7.4 ksi respectively.

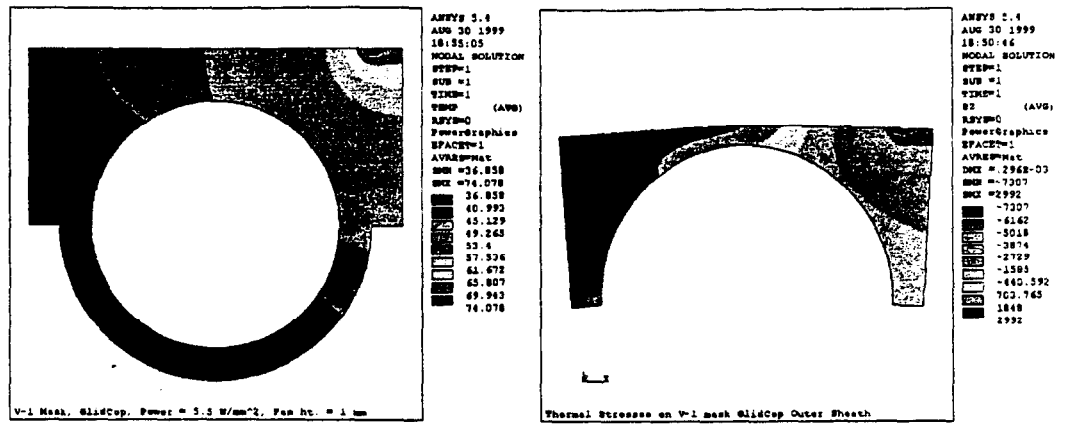

Figure 4.2.6.3-2 : Thermal and structural results for the v-1 mask

The fourth mask, V-4, located behind crotch absorber H-3, provides special protection for the downstream surface and intercepts a heat flux of 193 W/cm. Water cooling is located directly behind this incident surface. Due to space constraints, the mask is welded in to the chamber.

The three H-style absorbers consist of a GlidCop® power absorbing surface, a stainless steel water passage cover and a copper outer flange. The grated surface that intercepts power is sloped at 10°-to-grazing relative to the horizontal plane. Grating the surface helps to reduce the peak compressive thermal stress by allowing expansion. The peak heat flux is 21.5 W/mm^2 yielding a peak temperature of 191°C on the H-1 absorber with thermally induced stresses estimated at ~26 ksi. GlidCop® can easily withstand these types of cyclic thermal stress conditions, possessing yield strength well over 50 ksi. Water cooling is provided on the backside of the incident surface. The copper outer flange brazed to the GlidCop® allows the sub-assembly to be welded directly in to the chamber as part of the final assembly process.

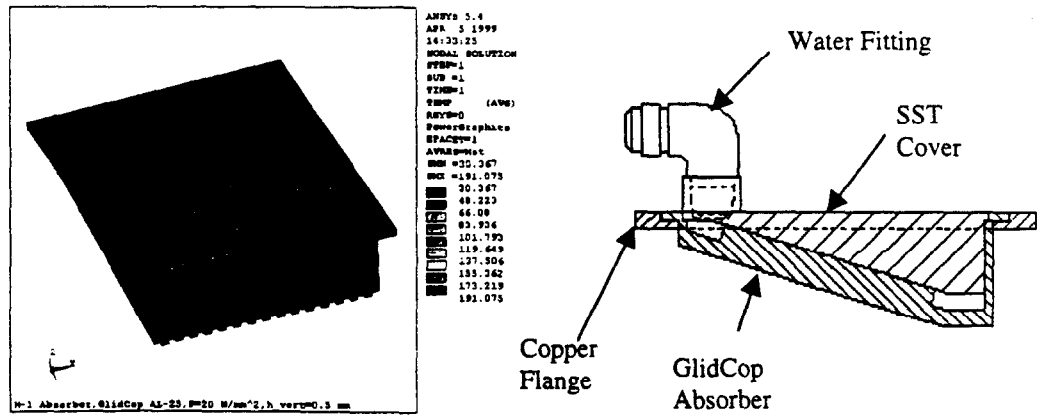

Figure 4.2.6.3-3 : H-2 absorber thermal analysis and assembly cross section

Water flow rates are sufficiently high to provide adequate heat transfer for removal of deposited heat. The nominal flow rates in the masks and absorbers are 1.0 gpm and 2.0 gpm respectively. The corresponding heat transfer coefficients are approximately 2.0 W/cm^2/K. Bulk temperature rises are within acceptable limits for all devices. For 2.0 gpm flow, the peak bulk temperature rise of 16°C occurs in the H-3 Absorber.

4.2.6.4 Eddy Current Break

Fast orbit feedback is required for SPEAR 3 to stabilize the beam orbit to less that 5 μm [sections 3.3, 4.7.1). Four corrector magnets on each girder are modulated as part of the orbit feedback scheme. The fast modulation can creates eddy currents within the vacuum chamber walls, which in turn induce bucking fields that reduce the amplitude and shift the phase of the correction field. Primarily, the vertically modulated fields that provide horizontal orbit control.

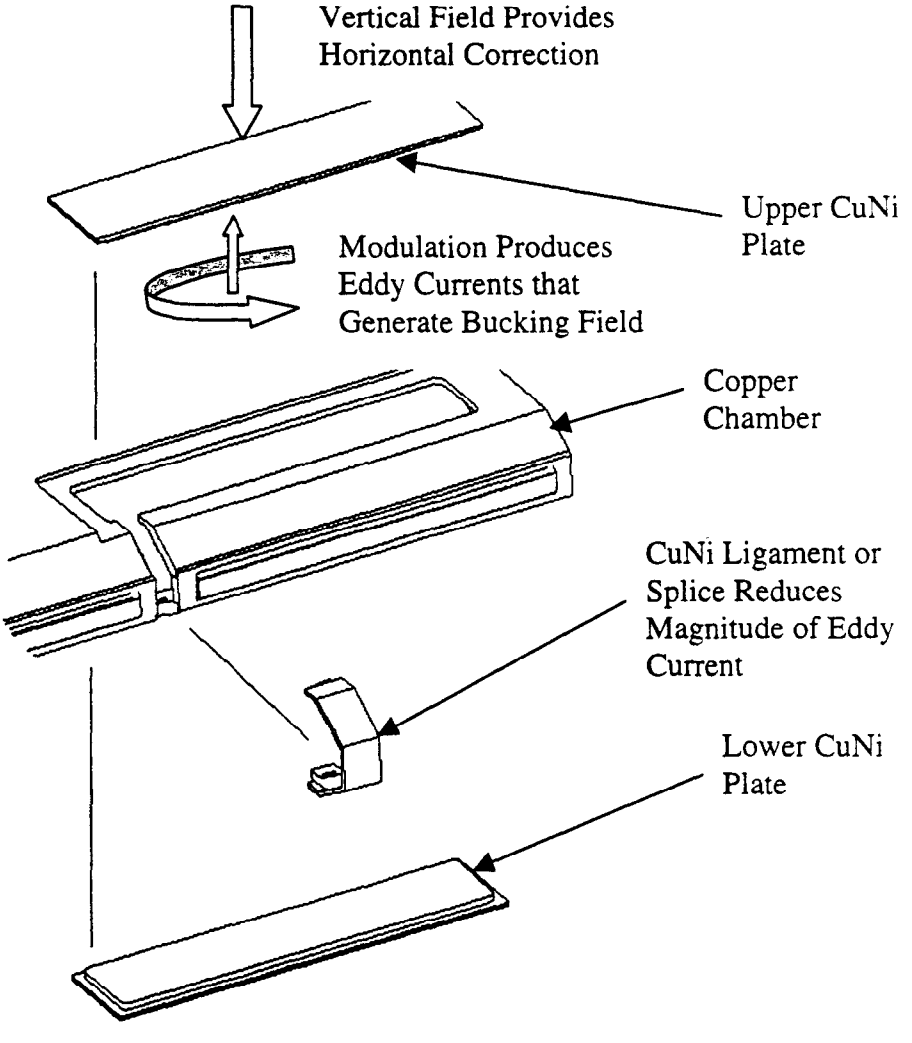

Figure 4.2.6.4-1. Exploded end view of qfc chamber with cupronickel™ (70/30) eddy current break

Induced eddy currents can be significant in copper and aluminum vacuum chambers due to their

relatively high electrical conductivity. For these types of materials, one approach is to break the circulating eddy current loop geometry by inserting short pieces of low electrical conductivity materials. By inserting a high resistance in the loop, the effective circulating eddy current is reduced. One such material is CuproNickel™ (CuNi), a copper-nickel alloy with electrical conductivity about 1/20th of OFE Copper. It can be joined reliably to OFE Copper with electron beam welding techniques.

Initial electro-magnetic calculations using MAFIA have verified this approach analytically. The most effective method to reduce the magnitude of the circulating eddy current is to place the CuNi splice in the loop. Lengthening the CuNi plates on the top and bottom of the chamber help to increase field penetration, but not as effectively. As an example, by doubling the plate length, the amplitude and phase change at 50 Hz from -9.4 dB and 54° to -6.7 dB and 45° respectively.

Magnetic measurements have also been conducted on a steering magnet provided by ALS and a copper test chamber bearing the proper beam passage cross section. The field measurements (Fig. 4.2.6.4-2) agree well with MAFIA calculations and show that the longitudinally integrated field contains more phase shift than hall probe data taken at several points within the magnet gap. This increased phase shift is attributed to fringe field curvature at the ends of the magnet.

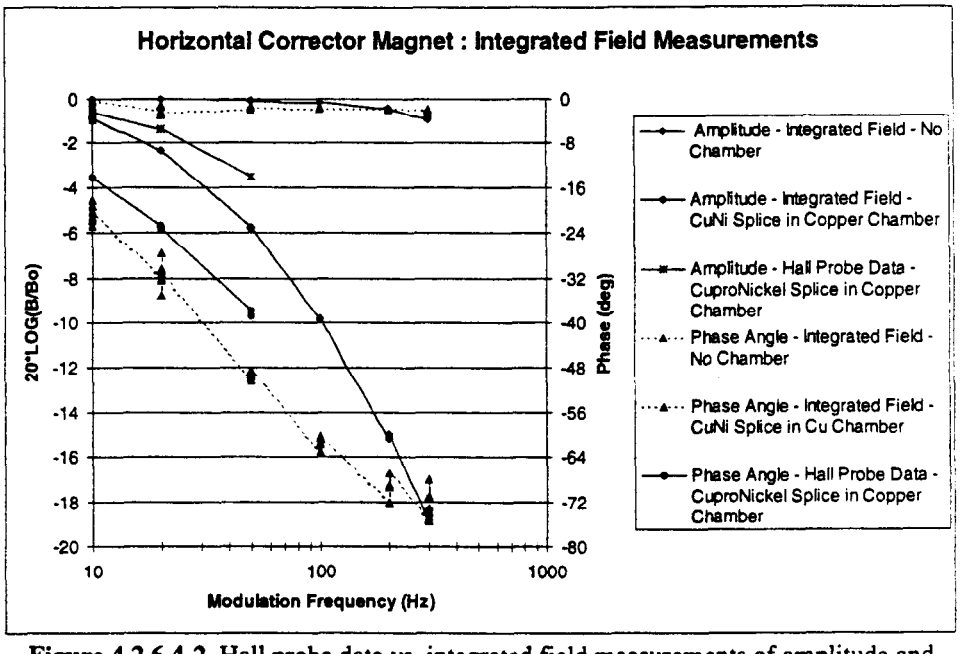

Figure 4.2.6.4-2 Hall probe data vs. integrated field measurements of amplitude and phase measurements

Based on the information obtained from both analysis and measurement, it can be concluded that lengthening the axial dimension of the CuNi splice is the most effective method for reducing eddy currents in the vacuum chamber. Lengthening the CuNi plates also serves to reduce the eddy currents but not as effectively. It should be noted that metallic cooling lines (or other conductive connections) must not bridge this eddy current break.

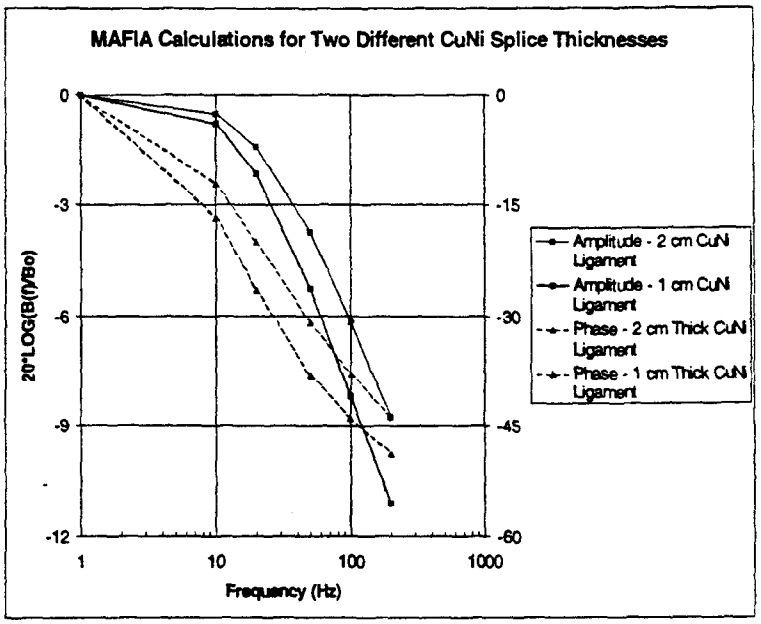

Figure 4.2.6.4-3 : MAFIA calculations indicate improvements by increasing the axial thickness of the cuni ligament

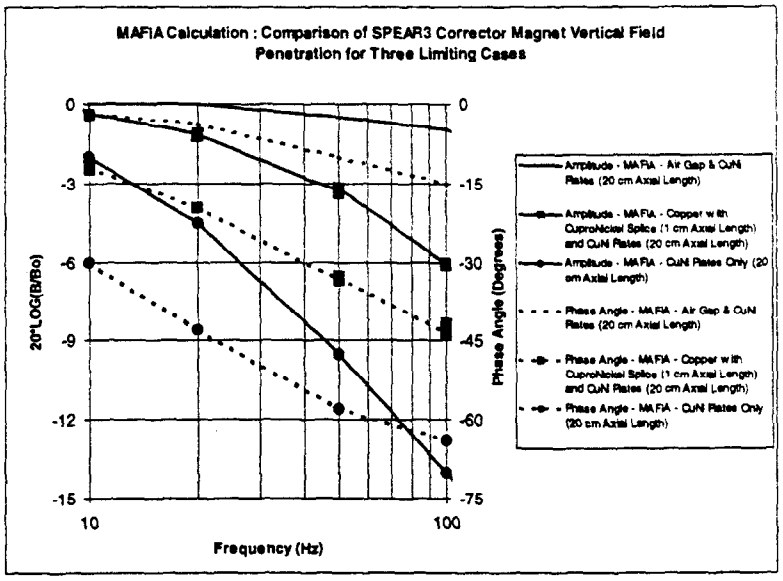

Figure 4.2.6.4-4 : MAFIA calculations for several axial gaps

4.2.6.5 Titanium Sublimation Pump

Titanium Sublimation Pumps (TSPs) remove the large photodesorbed gas loads produced by the absorbers by reactive chemisorption creating Titanium compounds trapped on the extended surface. Their very high pumping speed is an advantage in vacuum systems where large steady gas loads are present, although noble gases are not effectively removed.

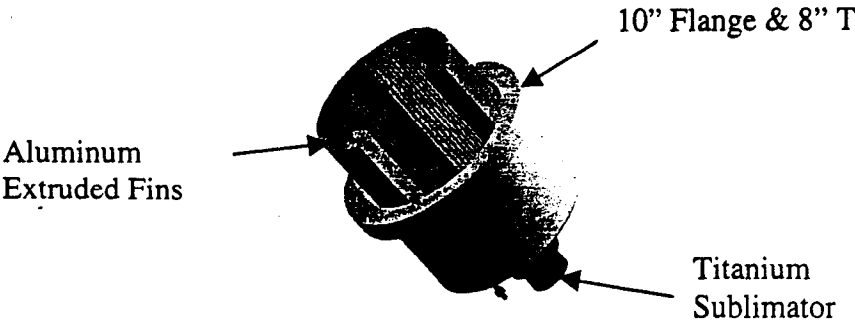

Figure 4.2.6.5-1 : TSP isometric view

The design of the TSP is based on the PEP-II B Factory Low Energy Ring Arc TSP. A sublimator with Titanium filaments periodically deposits several monolayers of atomic titanium on a large surface area. The extended surface employs fins to increase the total surface area for coating Titanium to more than 10,000 cm^2. The large surface area is important to obtain the required pumping capacity; capacity is nearly directly proportional to surface area. The pump is housed in an 8" diameter stainless tube with a flanged sublimator that supplies 3.6 grams of Titanium over the life of the pump. Water cooling is required to remove power deposited on the fins by electron scattering and photon fluorescence. A heat load of ~900 Watts is estimated to be as much as 10% of the power incident on the absorber.

Gas	Sticking Coefficient	Gas Velocity (m/s)	Intrinsic Speed (liter/sec)	Aperture Conductance (liter/sec)	Effective Speed (liter/sec)	Throughput (Torr*Liter/sec)
H2	0.06	1687	21158	7439	5504	5.50E-06
CO	0.7	453	66284	1998	1939	1.94E-06
N2	0.3	453	28407	1998	1866	1.87E-06
O2	0.8	424	70904	1870	1822	1.82E-06
CO2	0.5	361	37730	1592	1527	1.53E-06

Table 4.2.6.5-2: Pumping characteristics for various gases

The pumping speed is primarily limited by the geometry of the fins surrounding the sublimator and filaments. The fins create an aperture 5.5" in diameter. While the intrinsic speed of the freshly coated film is tens of thousands of liters per second, the fin aperture limits the pumping speed to values between ~1400 and ~5000 l/s depending on the gas species pumped.

Each pump is capable of chemisorbing more than 1 Torr*liter of gas before a new layer of Titanium must be flashed onto the extended pumping surface. The capacity of the TSP depends on the internal surface area of the pump, and to some extent the thickness of the Titanium. The pumping speed remains fairly constant as the capacity of the pump is consumed.

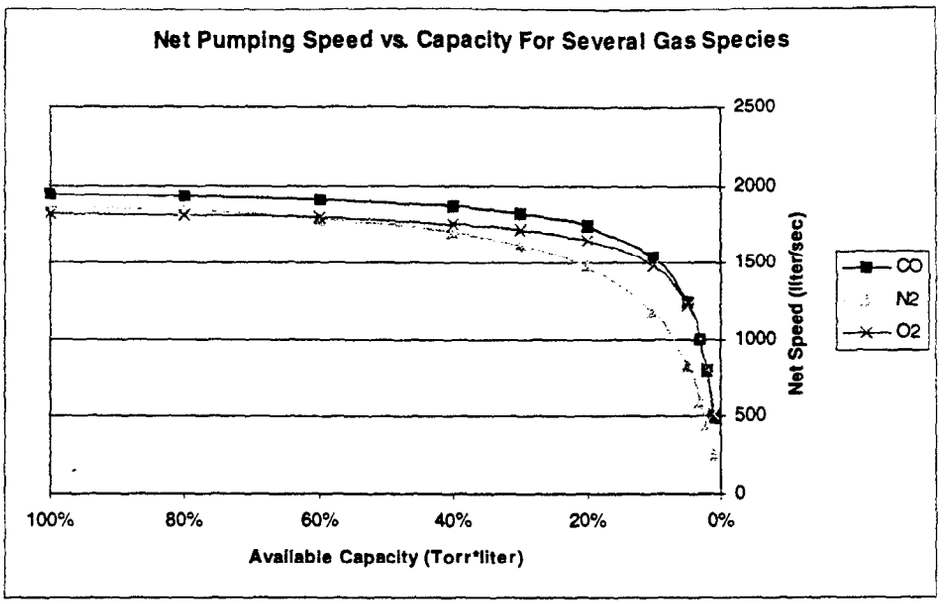

Figure 4.2.6.5-3 : TSP speed and capacity comparison for carbon dioxide, nitrogen and oxygen

During initial commissioning, the pumps may be flashed often due to the relatively high, initial dynamic gas load. Estimates show flashing will be required after approximately an A-hr of operation for the pump positioned under the H-3 Absorber. Cables connected to remote power supplies will permit flashing as required during operation. As scrubbing continues, the photodesorption rates drop from $2x10^{-3}$ molecules per photon to $2x10^{-6}$ molecules per photon in approximately 150 A-hr. The filaments on the sublimator will allow more than 600 flashes before depleting the supply of titanium and requiring replacement.

4.2.6.6 Non-Evaporable Getter (NEG) Pump

The NEG pump is a compact module that provides over 600 l/s pumping while fitting inside a 4cm x 4 cm x 30 cm antechamber adjacent to the beam passage. The downstream end of the BM-1 chamber contains a single NEG module directly opposite the V4 mask which is linked to the beam passage by a 1.2 cm tall x 30 cm long x 6 cm deep slot. The proximity is required to effectively pump the PSD gas load generated at the V4 mask.

The design is based on a NEG pump module developed for the PEP-II B-Factory at SLAC that uses a getter material, ST-707, developed by SAES Getters. The porous material is prepared by sintering a mixture of Zirconium, Vanadium and Iron. A series of 3 cm square strips of the material are alternately stacked with 3mm spacers on a ¼" diameter stainless steel tube. The stacked construction allows a large quantity of material in a small volume. This serves to increase both the speed and capacity of the pump.

Similar pumps designed for the PEP-II B-Factory possess gross pumping speeds of 2000 l/s/m. The 30 cm long module has a gross speed of 600 l/s. The slot conductance reduces the effective pumping speed at the beam passage to 140 l/s.

The total gas load generated at 3 GeV and 500 mA is 2.9x10-7 Torr-l/s. The capacity estimated for this pump is approximately 0.5 Torr-liter, with an interval between regeneration cycles of 479 hours for a scrubbed absorber surface. During initial commissioning, the interval will be much shorter due to the relatively high PSD gas loads. Because the duration between regeneration cycles is long, the process will be conducted manually, as required, in order to maintain acceptable ring operations.

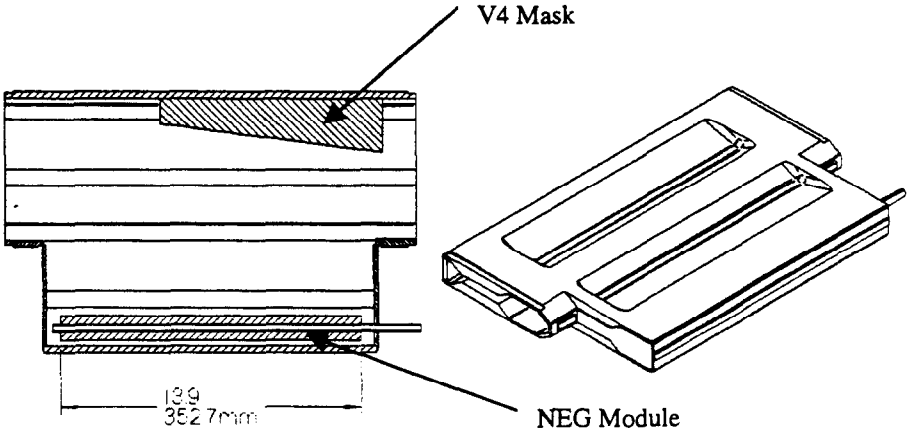

Figure 4.2.6.6-1 V4 with NEG module in downstream end of bm-1 chamber

Regeneration of the NEG modules require periodic processing at 400°C to clean the gettering surfaces by diffusing the captured molecules into the bulk of the material. A heater rod inserted into the stainless steel tube provides the required power. Laboratory tests are planned to determine the required voltage and current to attain the optimum processing temperature.

4.2.7 Straight Section Chambers

The straight sections comprise of RF cavities, ID, diagnostic and injection chambers. The component layout and specific vacuum chamber designs for the injection and beam diagnostics are discussed in the following sections. Also the integration and design overview of the existing SPEAR 2 beam lines is reviewed.

4.2.7.1 Component Layout

SPEAR 3 contains 14 standard cell straight sections having ~3.1 m length, 4 matching cell straight sections having ~4.7 m length, and 2 racetrack straights of ~7.5 m length. All components will be replaced except for the IDs chambers for BL 5, 6, 9, 10, and 11. BL 4 will be replaced for FY 2002 and BL 7 will be replaced soon after. With the exception of the ID chambers, the SPEAR 3 straight section chambers will be redesigned for 500 mA operation. The overall layout for SPEAR 3 and its straight section components is shown in figure 4.2.7.1-1 and Table 4.2.7.2-1.

The 7.5 m long straights, located in the West Pit, will house the RF system. The other long 7.5m straight (East Pit) is reserved for a future beam line. Two of the four 4.7 m straight sections are reserved for future beam lines while the remaining two house the diagnostic equipment. The injection components are located in straight sections 13S14, 14S15 and 15S16. There are two 3.1 m straight sections reserved for future beam lines.

As stated earlier, the vacuum system is divided into six sections, East Pit, West Pit and Quadrants 1, 2, 3 and 4 (figure 4.2.7.1-1). Each of these sections are isolated by valves. These isolation valves will also have the octagonal profile with a slot and RF seals to maintain electrical continuity.

Bridging the gap between the girder and straight section are the bellows modules which also allow for the thermal expansion and manufacturing and alignment tolerances. The bellows modules will preserve the octagon beam passage and slot geometry to provide a smooth chamber aperture. The ID chambers have unique chamber apertures (as described in Section 4.2.1.3) and require transition modules to provide smooth tapers between existing and new vacuum chambers.

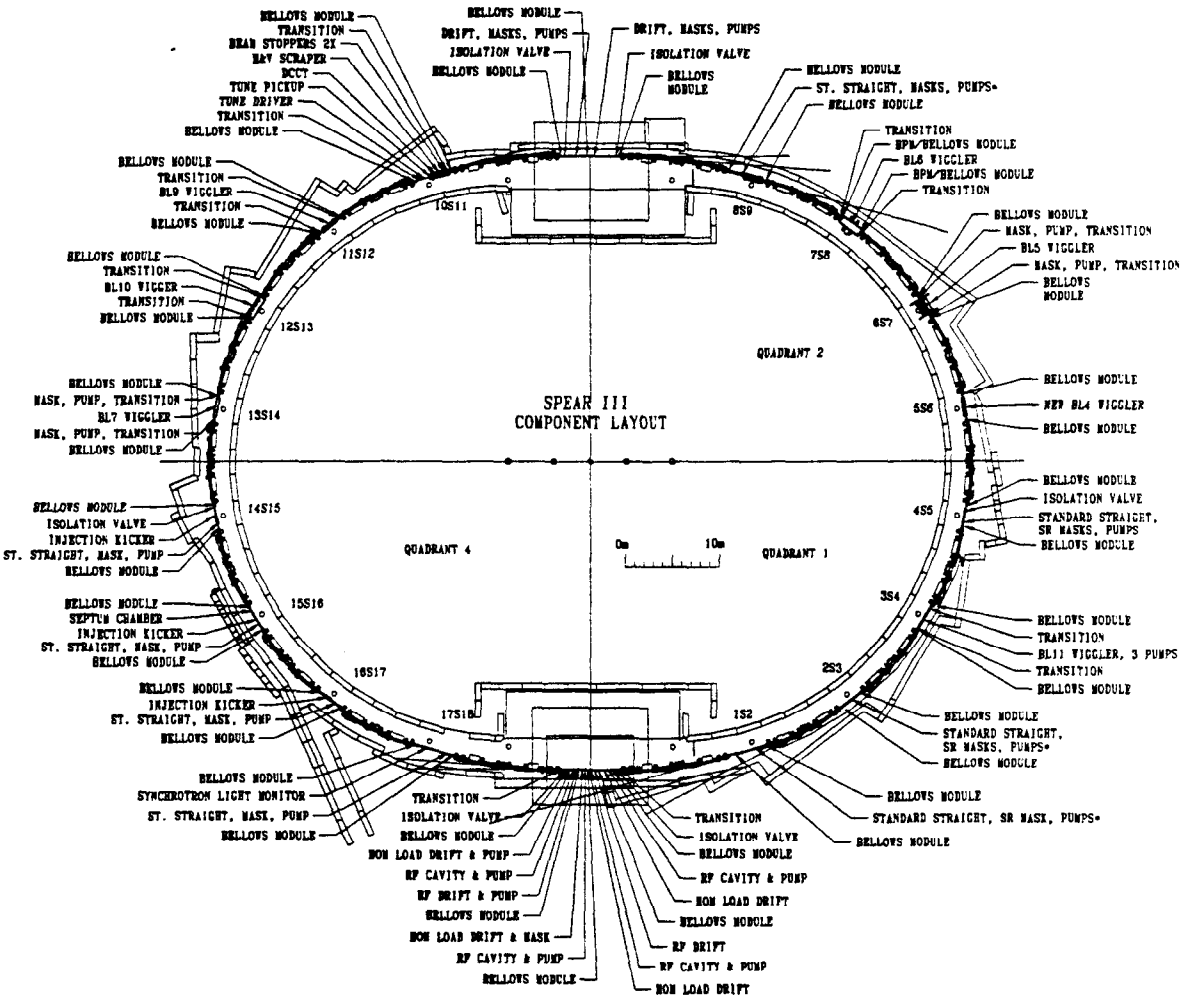

Figure 4.2.7.1-1: Component layout for SPEAR 3 straight sections

Table: 4.2.7.1-1: Straight section component list

Component Description	Profiles	new
Quadrant 1		
1S2 (Future BL)		
Bellows Module		yes
Standard Drift, Masks, 3 pumps		yes
Bellows Module		yes
2S3 (Future BL)		
Bellows Module		yes
Standard Drift, Masks, 3 pumps		yes
Bellows Module		yes
3S4 (BL11)		
Trans Bellows Module		yes
BL11 Wiggler, 3 pumps		no
Trans Bellows Module		yes
4S5 (Future BL)		
Bellows Module		yes
Isolation Valve		yes
Standard Drift, Masks, 3 pumps		yes
Bellows Module		yes
Quadrant 2		
5S6 (New BL 4)		
Bellows Module		yes
BL4 Wiggler, 3 Pumps		yes
Bellows Module		yes
6S7 (BL5)		
Bellows Module		yes
Transition, Pump		yes
BL5 Wiggler		no
Transition, Pump		yes
Bellows Module		yes
7S8 (BL6)		
Bellows Module		yes
Transition		yes
BL6 Wiggler, 4 Pumps		no
Transition		yes
Bellows Module		yes
8S9 (Future BL)		
Bellows Module		yes
Standard Drift, Masks, 3 pumps		yes
Bellows Module		yes
East Pit Long Straight		
East Pit (Future BL)		
Bellows Module		yes
Isolation Valve		yes
Standard Drift, Masks, Pumps		yes
Bellows Module		yes
Standard Drift, Masks, Pumps		yes
Isolation Valve		yes
Bellows Module		yes
Quadrant 3		
10S11		
Bellows Module		yes
Transition		yes
Standard Drift, Masks, Pumps		yes
Tune Driver (Tr Kicker 0.3m)		yes
Tune Pickup		yes
DCCT (3 in diameter)		yes
H&V Scraper		yes
Beam Stoppers (2)		yes
Transition		yes
Bellows Module		yes

Component Description	Profiles	new
Quadrant 3 (continued)		
11S12 (BL9)		
Bellows Modue		yes
Transition		yes
BL9 Wiggler, Masks, 3 pumps		no
Transition		yes
Bellows Modue		yes
12S13 (BL10)		
Bellows Module		yes
Transition		yes
BL10 Wiggler, Masks, 4 Pumps		no
Transition		yes
Bellows Module		yes
13S14 (New BL7)		yes
Bellows Module		yes
BL7 Wiggler, 3 Pumps		no
Bellows Module		yes
Quadrant 4		
14S15		
Bellows Module		yes
Standard Drift, Masks, 3 pumps		yes
Injection Kicker		yes
Isolation Valve		yes
Bellows Module		yes
15S16		
Bellows Module		yes
Standard Drift, Masks, Pumps		yes
Injection Kicker		yes
Septum		yes
Bellows Module		yes
16S17		
Bellows Module		yes
Standard Drift, Masks, 3 Pumps		yes
Injection Kicker		yes
Bellows Module		yes
17S18		
Bellows Module		yes
Standard Drift, Masks, 3 pumps		yes
Synchrotron Light Monitor		yes
Bellows Module		yes
West Pit, Long Straight		
West Pit (center at 0,0,0)		
Transition		yes
Isolation Valve		yes
4" Bellows Module		yes
RF Cavity, Pump		yes
HOM Load Drift, SR Mask		yes
4" Bellows Module		yes
RF Drift & Pump		yes
RF Cavity, Pump		yes
HOM Load Drift		yes
4" Bellows Module		yes
RF Drift & Pump		yes
RF Cavity, Pump		yes
HOM Load Drift, SR Mask		yes
4" Bellows Module		yes
RF Drift & Pump		yes
RF Cavity, Pump		yes
HOM Load Drift, SR Mask		yes
4" Bellows Module		yes
Isolation Valve		yes
Transition		yes

4.2.7.2 Straight Section Masking

Existing Beam line Insertion Device Chambers

The SR ray traces for both the nominal beam orbit and for a horizontal offset of 30 mm were performed on the existing beam line ID chambers. The SR rays show that masks must be added in the transition modules to prevent SR impinging on uncooled chamber sections. The power densities at 500mA for the existing ID masks are summarized in Table 4.2.7.2-1. Initial estimates show that the new SPEAR 3 power loadings are acceptable. However, detailed analyses need to be performed on all existing mask designs. A replacement design employing the GlidCop sheath mask has been shown to handle a linear power density up to 200 W/mm. Thus, if further analysis shows that existing masks need to be upgraded they can be replaced on all the ID chambers except BL 5 and 7. The design and analysis of BL 5 and 7 is discussed further in section 4.2.7.3.

Table 4.2.7.2-1: Insertion device masks power densities, nominal beam orbit, 500 mA

BL	Mask 1		Mask 2		Mask 3	
	Q (W)	q" (w/cm)	Q (W)	q" (w/cm)	Q (W)	q" (w/cm)
4,7*	1136	61	937	197	-	-
5	1136	61	937	197	-	-
6	1192	tbd	897	tbd	-	-
9	1457	150	792	87	-	-
10	1085	124	1044	195	-	-
11	774	154	679	109	711	146

Straight Section SR Ray Traces

There are two masks required to prevent a direct strike on the back wall of the antechamber, on the downstream bellows and on the downstream flange pair. The masks are designed for a 30 mm horizontal beam orbit distortion. The masks intercept approximately 1kW each with a linear densitiy of 74 W/cm. Calculations have shown that the GlidCop sheath mask have acceptable thermal stresses for this power loading.

A vertical beam displacement larger than ± 6 mm produces a direct synchrotron radiation strike on the walls of the vacuum chamber. As discussed in section 4.2.3 the peak temperature of the straight section chambers during a large offset in the beam orbit can reach 115° C.

4.2.7.3 Existing Beam lines

Beam lines 5 and 7 are constructed of Aluminum alloy 6061-T6 plates. The vacuum chamber is designed to have distributed radiation power along the chamber walls. Over 1 kW strikes the 16.6 cm sloped mask surface and an additional 900 watts strikes the chamber wall. The peak temperature of this chamber with 8 gpm of water flow is 129°C with an equivalent thermal stress of 22 ksi. This is above the yield strength of Al 6061-T6, however fatigue curves for aluminum indicates that a stress of 22 ksi is acceptable for 1 x 10^6 cycles. Also, BLs 5/7 are constructed of aluminum its PSD and thermal outgassing rates are higher than copper and stainless steel, and there are no pump ports along the chamber. One 220 l/s noble diode ion pump will be located on each of the transition modules at either end of the ID. Pressure calculations show that these chambers contribute to the largest peak pressure in the ring.

The other remaining IDs are a stainless steel construction and do not have chamber cooling, except

for the SR masks. A brief summary of the different ID chamber apertures, pumping and masking design is presented in table 4.2.7.3-1.

Table 4.2.7.3-1: BL 4 and 7 will be replaced with new vacuum chambers and magnets.

BL	Material	Power Absorbers	Aperture (mm)	Ion Pumps
4,7*	Al	Distributed	16 x147 Rectangle	0
5	Al	Distributed	16 x147 Rectangle	0
6	SS	2 Discrete Masks	12 (min) x 202 Rectangle, inside vacuum tank	2-220 l/s
9	SS	2 Discrete Masks	16 x178 Rectangle, with Ø51 antechamber	2-220 l/s
10	SS	2 Discrete Masks	13 x142 Rectangle, with 51 x 51 antechamber	4-220 l/s
11	SS	3 Discrete Masks	18 x165 Rectangle, with 51 x 70 antechamber	3-150 l/s

* Chambers and magnets will be replaced.

The majority of these chambers were designed for a maximum of 200 mA operation and minimal beam impedance requirements. The existing ID chambers have large step discontinuites. Some of the newer beam line chambers, for example BL 11, considered chamber discontinuites. BL 11 has a transition to the SPEAR 2 cross section which is larger than the SPEAR 3 cross sections. This chamber allows less than two inches to transition to the SPEAR 3 chamber aperture. Therefore, a small cavity is produced by the multiple vacuum chamber aperture changes so further studies using MAFIA are in progress.

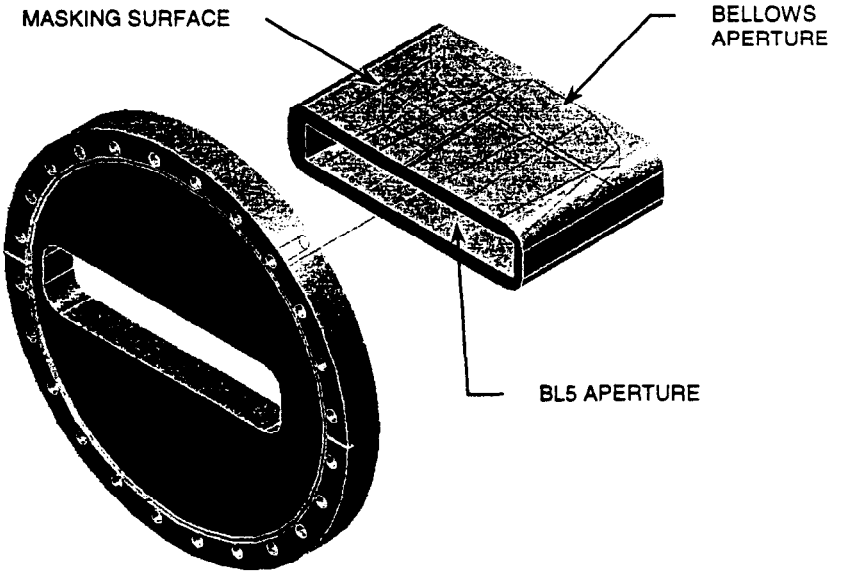

Figure 4.2.1.3-1: Transition module, cooling tubes not shown

As stated earlier transition modules are required to provide smooth transitions between the existing ID chambers and the new vacuum chamber aperture. The new vacuum chambers and existing ID set the lengths of the transitions. Each transition module is unique due to the varying vacuum

apertures and lengths. A transition with a 1:5 slope is achievable in the vertical direction, but not in the horizontal direction. Calculations have shown that steep transition in the horizontal direction has little impact on the overall impedance budget of the machine.

The transition modules also need to provide additional masking necessary to prevent SR impinging on un-cooled vacuum chamber walls. A transition module is shown in figure 4.2.7.3-1. The masking surface can be seen on the back wall of the slot. Transition modules will be used at every ID, except for BL 11 due to space constraints. BL11 will employ a special bellows/transition module. Instead of building unique bellows/transition modules at every existing ID, separate transition modules will be built. This provides maximum flexibility for future upgrades.

4.2.7.4 Straight Section Vacuum Chamber Design

The straight section drift chambers will be similar in design to the QFC chamber in the girder section. The chambers will be made of machined copper plates and assembled using the EB welder. The antechamber provides additional conductance. Three pump ports and two discrete masks will be located in the antechamber/slot area.

The standard cell straight section vacuum chambers will be supported on strong backs which are connected to the end of the girder rafts. The East and West pit chambers will be supported directly to the floor of the ring.

4.2.8 Bellows Module

The primary function of the bellows module is to allow for thermal expansion of the chambers and for lateral, longitudinal and angular offsets due to tolerances and alignment, while providing RF continuity between adjoining chambers. The SPEAR 3 bellows will use the "double finger" mechanism developed for PEP-II. This design keeps the high heat areas away from high stress areas, because the RF shield does not provide the spring force and is kept relatively stress free during operation.

4.2.8.1 Design Description

The design employs a silver-plated high conductivity GlidCop® Al-25 RF shield finger which slides and makes electrical contact on the outside wall of a Rhodium-plated GlidCop®Al-15 stub (Fig. 4.2.8.1-1). This assembly preserves the chamber profile to create a uniform beam pipe. A welded bellows maintains vacuum and allows for travel along the beam axis with a lateral offset. The bellows module will be masked upstream from synchrotron radiation.

The bellows module is designed to satisfy several key requirements. First, it allows for thermal expansion of the arc and straight section vacuum chambers. In addition, capabilities for a lateral offset of ±2 mm and 25 mrad of angular misalignment are required for fabrication and chamber alignment tolerances. The lateral offset is limited by the welded bellows and not the RF shield.

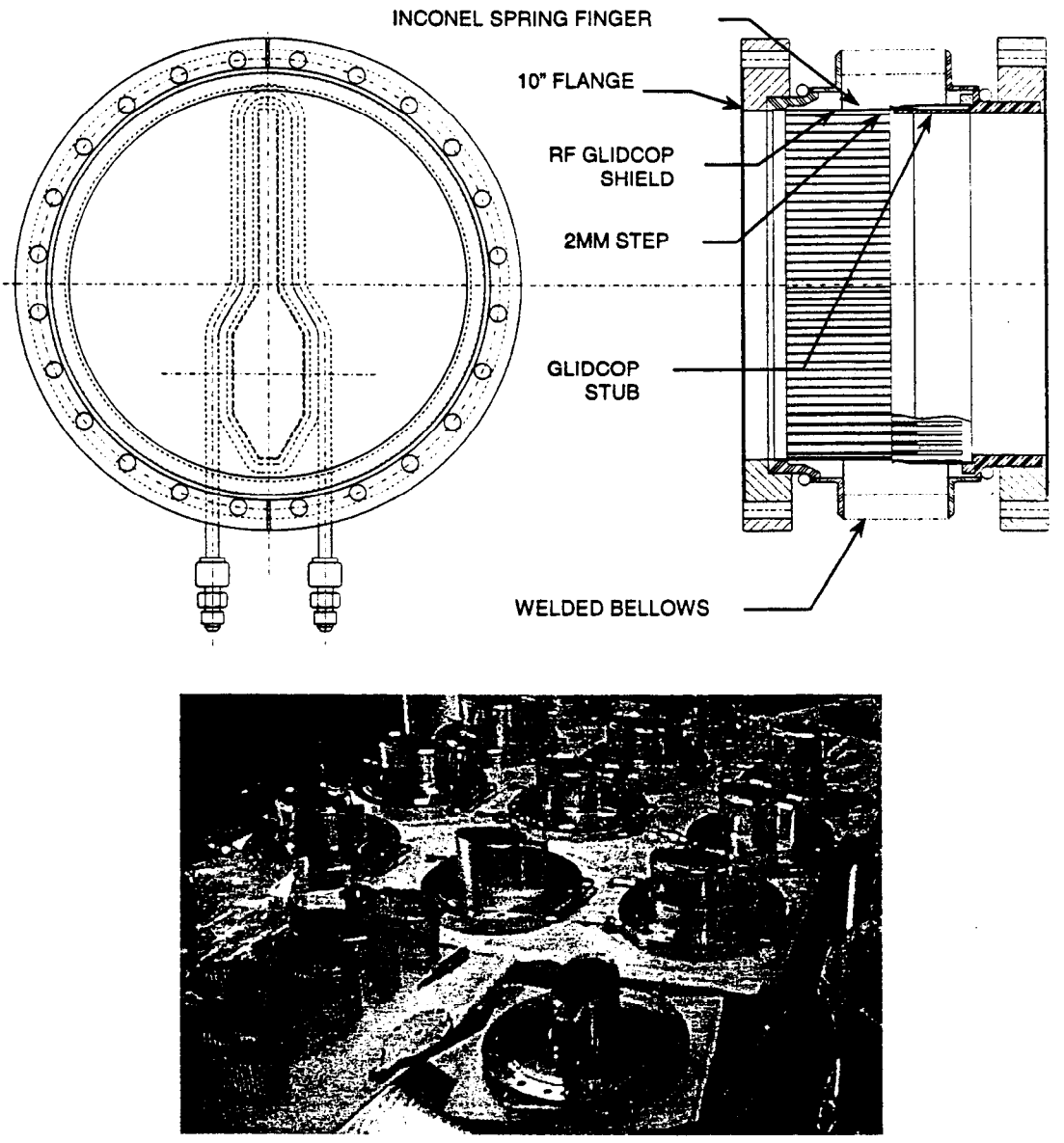

Figure 4.2.8.1-1. Bellows module

A second function of the bellows module is to maintain a continuous electrical conduction path for beam image currents to minimize impedance and beam instability. Module failure could result if a cavity is created that produces a trapped RF field mode. The RF shield bridges the gap between the vacuum chambers to avoid this. It has the octagonal cross section of the typical chamber and slides on the outside wall of the GlidCop®stub. This ensures that potential failure will not result in the RF shield falling into the beam tube, and produces a 2 mm step toward the beam centerline. This constriction eliminates the potential for mode trapping. The size of the step is driven by two features: the mechanical stability of the stub wall and the rounded contact surface at the tip, which ensures that the shield finger will not make a secondary contact on the stub.

For every RF shield finger there is a mating Inconel® 718 spring finger, which applies an average of 170g of force to provide sufficient electrical contact. Previous RF shield designs had dual

purpose fingers which served as both the spring and the shield. However, this is extremely difficult to implement successfully, since conductive materials do not exhibit the mechanical properties of high temperature springs.

The conductivity of the materials used for the electrical contact joint is a key parameter in its current carrying capacity. Numerous designs in the past utilized beryllium-copper (BeCu) for the RF shield. The thermal conductivity of GlidCop® Al-25 is 90% of copper and a factor of two higher than BeCu. Also, the mechanical properties of BeCu are extremely sensitive to the precipitation age hardening process conducted after forming. Due to the hardening process, BeCu is also susceptible to overaging, which significantly lowers the strength properties at slightly elevated temperatures. The yield strength of GlidCop® is slightly reduced to 448 Mpa at 1000°C [1], which is the braze temperature for the RF shield sub-assembly. This decrease in yield strength is not sufficient to cause permanent distortion due to lateral offsets across the fingers. Stress relaxation at elevated temperatures does occur in GlidCop®, but does not affect the contact force.

4.2.8.2 RF Shield/Spring Finger

GlidCop® was used for the stub and shield for its high thermal and electrical conductivity, its mechanical stability at high temperatures, and manufacturability. The temperature at the tip of the shield finger is balanced against structural loading. Thin shield fingers are stressed by the lateral and angular offsets across the module. Required finger length is determined by the total travel of the module. The thickness and width of the RF shield is optimized to decrease tip temperature, keep the bending stress at the base below yield, maintain the force due to operational bending stress below 28 g and prevent buckling. The maximum finger temperature will be designed to be below 100°C. Test data indicates minimal stress relaxation in GlidCop® at 300°C [4]. The consequences of a high tip temperature are reduced by the independent Inconel® spring fingers. These isolate the high-temperature region at the ends of the shield fingers from the high-stress area at the base of the spring fingers.

During normal operation a 2 mm offset produces a low stress at the root and less than 10 g of force. This bending stress does not significantly affect the contact force because the spring fingers are 15 times stiffer.

Inconel® also has a mu of less than 1.005 as required for all components of the vacuum system. The pre-deflection on the Inconel® spring applies 85 to 200 g on the shield finger and is relatively insensitive to manufacturing tolerances. The bending stress at the root is nominally 60 percent of yield. Inconel® 718 was selected for the spring because of its high strength, high temperature capabilities and ease to manufacture.

During off-axis beam operation the RF shield fingers are masked by the GlidCop stub from a direct SR strike.

4.2.9 Beam Position Monitor

The BPMs are located in 5 locations in each standard girder. They are positioned downstream of QF-2, SD-2, SD-1 and QF1 and upstream of SF-2. The BPMs consist of four button-style pick-ups welded symmetricaly on the beam passage. The individual button pickups are 2.4 cm apart to equalize the x and y position sensitivities.

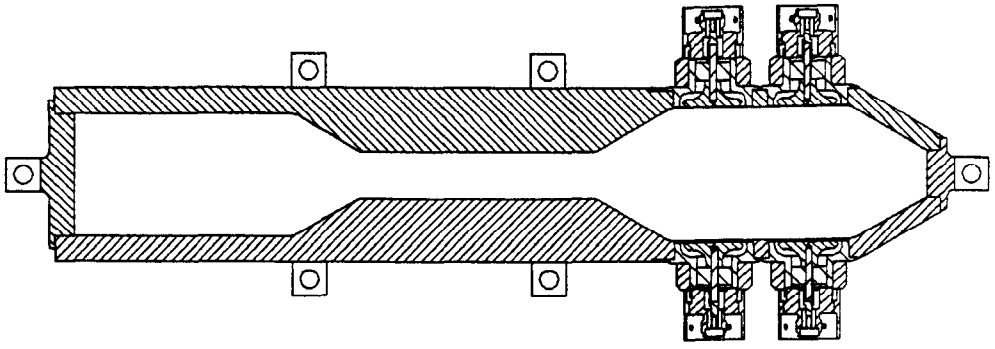

Figure 4.2.9-1: Cross-section of BPMs in chamber

The BPM is designed to achieve precision resolution requirements, to handle high power due to the bunch and current requirements of the machine, to minimize large discontinuities and subsequent impedances developed from resonances or trapped modes and to serve as a reliable vacuum feedthru. The design is a compromise between electrical performance and vacuum reliability. Numerical modeling with MAFIA and ANSYS were used to optimize the design for PEP-II.

The feedthru is compatible with an ultra-high vacuum environment. It is designed for a minimum of 50 vacuum bakeouts at 200°C and 80,000 cycles from 15°C to 100°C. The design is compact with a low profile and a protective shroud to prevent vacuum failures from damaged or broken feedthrus.

BPM Design Details

Button and Center Conductor

The BPMs consist of four button style UHV feedthrus. The buttons are 1.5 cm in diameter to provide 1mm of position resolution at 5 x 10^8 e- (single injector pulse). The button is joined to the molybdenum center conductor. The diameter was optimized using MAFIA to increase sensitivity and decrease the Q of trapped modes. The gap between the button and the housing is 1 mm to minimize the HOM effects without adding excessive capacitance.

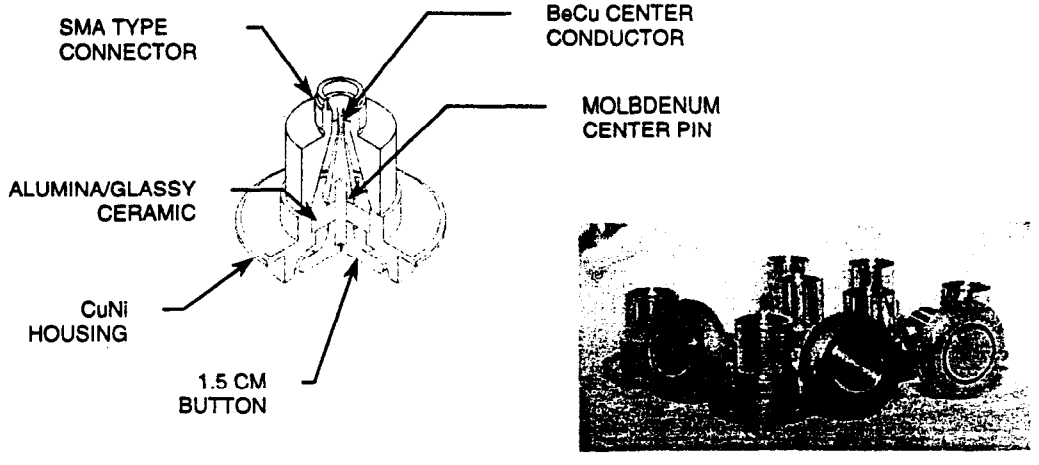

Figure 4.2.9-2: Beam Position Monitor

Vacuum Seal-Dielectric Material

The dielectric material for the SPEAR 3 BPMs will be alumina or borosilicate glass. A minimum of 98% alumina is required for its thermal conductivity. The PEP-II design was an improved design by using a pin seal configuration instead of a compressive T-joint for the ceramic-to metal seal. The latter seal has many discontinuities that can adversely affect the electrical performance or create trapped modes. The pin seal produces an outer diameter compression seal due to the mismatch of the thermal expansion coefficients of the materials. The pin seal joint is not as robust as the compressive T-joint, but has been proven in the PEP-II prototype to have sufficient strength to handle the vacuum loads and thermal stresses.

Alumina borosilcate glass or "glassy ceramic: has been shown to be an exceptional alternative dielectric material. The glassy ceramic is an alumina-strengthened glass and has a lower dielectric constant. This improves the electrical performance by decreasing the impedance mismatch. The design also eliminates brazing and simplifies the manufacturing process. The vacuum seals are a compressive pin seal between the metal housing and the glassy ceramic and a chemical bond between the galssy ceramic and the molybdenum pin. This design has provided exceptional electrical and vacuum performance in PEP-II. A flaw in the initial design created a stress riser in the molybdenum pin which lead to a fracture in the pin at the button interface. The design of the pin was modified and no pin failures occurred on the revised design. Thousands of feedthrus were welded into the vacuum chambers and there were no vacuum failures in the ceramic to metal seals.

Vacuum seal-Welding Feedthru to chamber

The pick-ups are EB welded into the chamber. Instead of being mated to the chamber with flanges, the EB joint reduces the overall profile of the feedthru, decreases manufacturing tolerances, and fits easily into the chamber space. An electron beam weld minimizes the heat affected zone and increases the control and accuracy of the weld.

For precise and stable beam orbit control, the BPMs must be mounted with sufficient mechanical rigidity and thermal stability to meet beam specifications outlined in Sections 3.3 and 4.7.1 ($\pm$ 5 μm vertical and $\pm$ 15 μm horizontal).

4.2.10 Diagnostic components

The 4.5 m matching straight in 10S11 will house several of the specialty diagnostic components. This section will contain the tune driver, tune pickup, DCCT, horizontal and vertical scrapers, and two beam stoppers. A 70 mm diameter vacuum aperture will be used in this section to simplify the designs of these components. This aperture provides adequate clearance around the BSC and is acceptable for beam impedance. A full layout of this section, together with SR masking and pressure profiles are in progress. The designs of the diagnostic components are discussed.

4.2.10.1 Synchrotron light monitor

The Synchrotron Light Monitor (Sec. 4.8.2.7) images visible and near ultraviolet light. One of the most difficult problems with imaging systems like this is the thermal distortion of the first mirror, located within the vacuum chamber, that can be caused by the high heat load from the x-ray light. The x-rays are concentrated in the vertical mid-plane of the radiation pattern, while the visible and UV light have much larger vertical opening angles and do not produce a significant amount of power.

The design for the SPEAR 3 Synchrotron Light Monitor places a "cold finger" mask in front of the imaging surface to shadow the high power x-rays. This design is ideal for SPEAR 3 if the

synchrotron light mirror is located inside the antechamber, because then the "cold finger" mask would not pose as either a rf antenna or an impedance perturbation. Since the synchrotron light mirror is located in the 4.5 m matching straight section 17S18, it can be placed at least 5 m away from its synchrotron radiation source, which greatly reduces the impinging power density. However, increasing the distance from the source also increases the vertical aperture needed to accommodate diverging light beam. Since a vertical angular acceptance of $\pm 2\sigma$ of the UV beam divergence (σ = ~1 mrad) is required in the chamber to image the beam properly, the aperture at 5 m will be larger than the antechamber height. More study is needed the optimize the geometry and locations of the "cold finger", mirror and mirror chamber.

4.2.10.2 Tune Driver

One tune driver device will perform both the vertical and horizontal driver functions. The tune driver is comprised of four 32 cm stripline electrodes, two electrodes drive the beam in the horizontal direction and the other two in the vertical direction. All four electrodes have the same z location and is fabricated into quarter sections of the circular vacuum chamber cross section. The electrodes maintain the the 70mm diameter circular profile of the other chambers located in straight section 10S11 (see figure 4.2.9.3-1).

The stripline electrodes are housed in a round stainless steel vacuum chamber and are supported by Inconel® flex supports connected to a 50 ohm feedthru. The flex supports allow for differential thermal expansion of the electrodes due to image current heating. Bending and shear stresses in the Inconel® members and ceramics are well below acceptable limits. Since standard 50 ohm feedthrus are not designed to conduct heat other than from signal tranmission losses a special feedthru fabricated with a high thermal conductivity boron nitride ceramic and an outer water cooled jacket is being investigated. Initial thermal analysis demonstrates that the power generated from resistive wall loses and HOM in the electrodes can be sufficiently handled by the high conductivity feedthru. The detail design of this chamber is dependent on MAFIA simulations to determine the width of the electrodes and the spacing of the outer vacuum chamber. MAFIA simulations will also provide a more accurate heat density to determine if additional cooling is necessary. A high emissivity copper oxide coating can be applied to the electrodes to provide additional cooling via radiation. An emissivity of 0.9 was achieved by applying a copper-oxide coating using an arc deposition process developed at the Lawrence Berkley Labs for PEP-II.

The electrode cannot withstand a direct SR strike from the upstream bend magnet. Two methods for masking the SR fan are being investigated. The first would employ an upbeam mask protruding into the 70 mm diameter aperture, but well outside of the 25 mm BSC. The second method is to offset the tune driver assembly horizontally by 5 mm to shadow the electrode. A mask downstream of the driver would absorb the heat load shadowed from the offset of the tune driver and a transition section would bring the chamber aperture back onto nominal beam centerline.

A detailed layout of the 10S11 straight section geometry and adjacent chambers along with MAFIA simulation of the tune driver for precise electrode geometry and heat loads will be required to determine the most economical masking method.

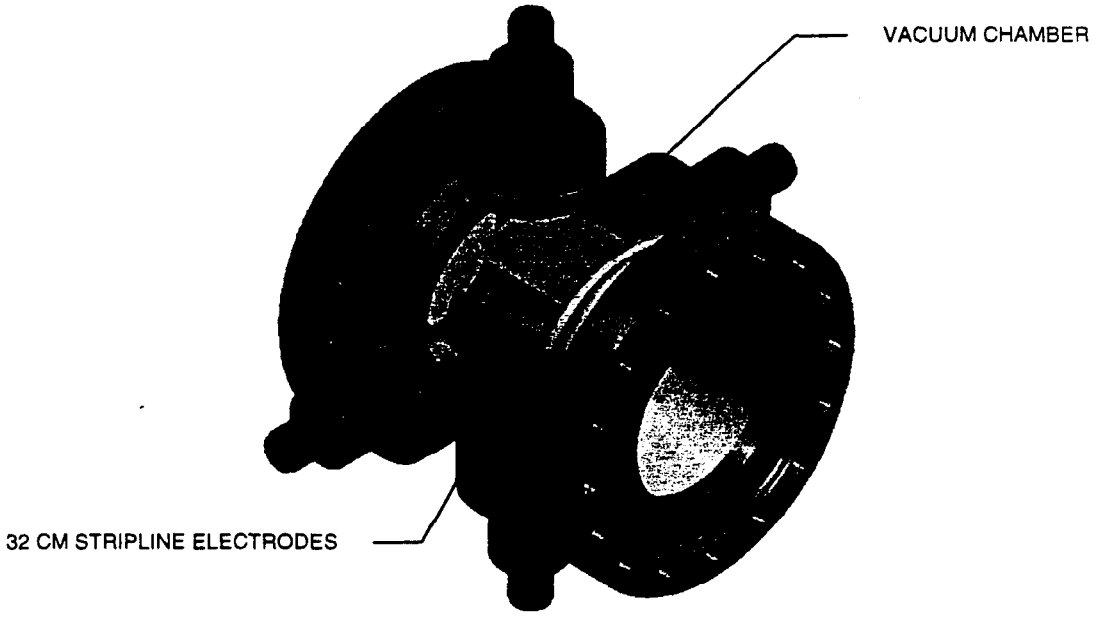

Figure 4.2.9.3-1: Tune driver design

4.2.10.3 Tune Pickup

The tune pickup is used to monitor transverse beam motion and to provide correction signals for the tune drivers. The tune pickup is a conventional four electrode stripline pickup. Each of the four electrodes, two for horizontal and two for vertical, are electrically grounded to the outer vacuum chamber at one end and connected to a 50 ohm type N feedthru at the other end. The stripline electrodes are 52 mm long. The electrodes are fabricated from OFE copper and each electrode is approximately a quarter circle section profile to duplicate the 70 mm diameter beam tube of the adjacent vacuum chambers.

The stripline electrodes are a monolithic fabrication with the outer vacuum enclosure. This provides a direct thermal path to the cooling loop on the outside of the chamber, and minimizes fabrication tolerances. The connection between the feedthrus and the electrodes will employ flexible Inconel® sheet members to allow for differential thermal expansion of the electrodes due to image current heating and a possible synchrotron radiation strike.

The cooling on the vacuum chamber housing provides sufficient cooling for a low power SR strike. In order to keep the SR strike low the tune pickup needs to be located at the downstream end of 10S11. A detailed layout of 10S11 and its associated components is necessary to determine if the tune pickup will see a direct SR strike or if the masking required for the tune driver will also mask the tune pickup.

4.2.11 Injection Components

4.2.11.1 Septum Chamber

The SPEAR 3 injection septum chamber will be fabricated in a method similar to that used for the standard girder cell chambers. However, the septum design requires a higher strength material due

to its thin cross section near the Lambertson side of the beam passage. As a result, the septum chamber will be constructed from stainless steel. The chamber is capable of managing the SR loads from a mis-steered beam.

The septum chamber will be manufactured from four pieces: a top and bottom plate that forms the beam passage and antechamber chamber, an 0.8 mm thick septum side cover on the Lambertson side of the beam passage and an upbeam and downbeam transition / flange adapter.

The septum chamber is adjacent to the Lambertson magnet, immediately downbeam of the second injection kicker. The injection kicker has no antechamber or photon exit slot, therefore when the beam is mis-steered less than 6 mm vertically, the kicker masks the septum chamber from a direct synchrotron radiation strike. However, SR will impinge on the septum chamber when the beam is mis-steered beyond 6 mm vertically producing a peak temperature rise in the chamber of approximately 55°C and related 23 ksi thermal stress.

The septum chamber aperture has a 12.5 mm vertical half height. The antechamber and pump slot match the standard girder cell configuration. The Lambertson side of the beam passage (formed from 0.8 mm SST sheet) is 25 mm from the stored beam centerline. During injection, with a total beam bump (fast plus static) of 22 mm, there is 3mm of chamber clearance to the stored beam and 1 mm minimum clearance to the Lambertson pole. The stresses due to vacuum loading in the 0.8 mm septum wall is negligible. However, the deflection in the top and bottom chamber halves that are cantilevered from the far side of the pumping chamber produces a stress of 20 ksi.

The upbeam chamber transition/flange adapter will transition from the injection kicker vacuum aperture with a maximum slope of 1:5. This transition will also be sufficiently cooled to handle beam mis-steers that exceed the 25 mm half aperture of the septum chamber.

The downbeam flange consists of a transition, injection beam window and a flexible joint. The injected beam window is 0.05mm thick stainless steel and experiences negligible heating during injection.

The standard girder cell chamber (BM2) immediately downbeam of the septum will be located to correctly align the flanges with respect to the Lambertson magnet. A single convolution flex flange will provide for attitude adjustment (pitch and yaw) of the septum chamber. This will allow proper alignment the upbeam flange of the septum. The flex flange will have an RF seal to minimize chamber discontinuities.

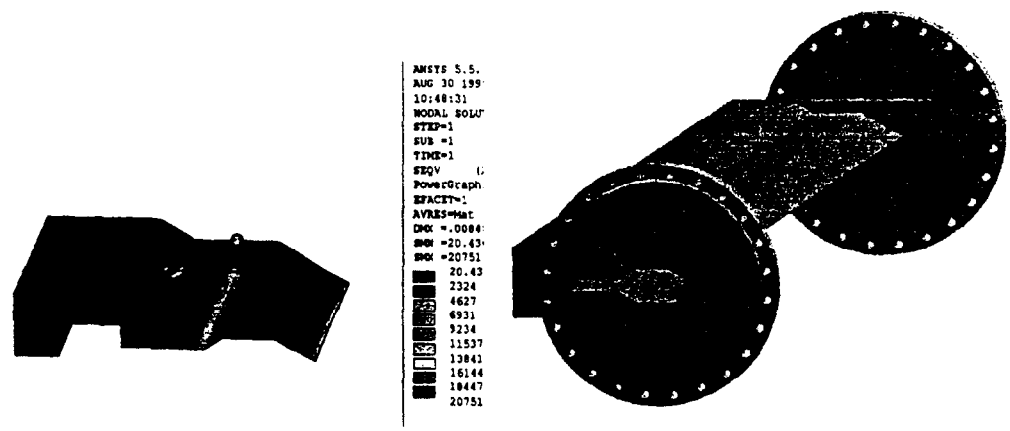

Figure 4.2.11.1-1: Septum chamber & septum analysis

4.2.11.2 Injection Kicker

There will be a total of three injection kickers located in straight section 14S15, 15S16 and 16S17. The injection kickers will be a low impedance design similar to the design slotted beam pipe kickers used at the DESY storage ring.[5] The ~0.6m magnet, composed of two stripline conductors, is housed and supported in an outer vacuum enclosure. The conductors form the beam passage to create a high gain (dB/I) kicker. This approach limits discontinuities, and therefore beams instabilities. Proper placement of formed sheets between the striplines and the outer vacuum enclosure optimize the kicker gain and impedance characteristics.

The conductors are grounded at one end and connected to a 50 ohm high voltage/current feedthru on the other end. The stripline conductors are grounded at opposite ends of the magnet eliminating the need for a bi-directional pulser. The conductors are separated by a grounded flux excluder that eliminates magnet flux coupling.[4]. In addition, the flux excluders form the top and bottom portions of the beam passage, carries the largest beam image currents, supporting and grounding the stripline conductors. Using the flux excluder as the support for the striplines reduces the complexity of the design, which must allow for differential thermal expansion between the strip line/beam passage and the outer vacuum enclosure.

Since there is no exit slot or antechamber, the injection kickers will intercept a SR strike and require cooling on the associated conductor. The injection kicker adjacent to the septum chamber is closer to the bend magnet than the other two kickers and therefore experiences the highest heat load. This kicker's forward location in the straight excludes the possibility of installing an absorber forward of the injection kickers and masking their length. The stripline conductors are copper to manage the SR strike. The copper construction will also serve to lower the current skin depth and flatten the B field slope during the kicker pulse as compared to a stainless steel conductor. [5]

The high voltage (30 kV) feedthru will require approximately 15 A_{RMS} rating. Flexible Inconel® sheet members that join the striplines and the feedthrus allow for differential thermal expansion of the electrodes due to the synchrotron strike and image current heating. Bending and shear stresses in the Inconel® members and ceramics are well below acceptable limits.

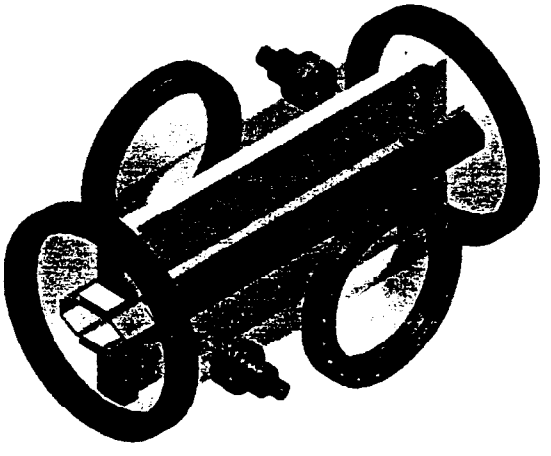

Figure 4.2.11.2-1: Injection kicker design

References:

[1] C. L. Foerster et al, "Photon Stimulated Desorption (PSD) Measurements of Extruded Copper and Welded Copper Beam Chambers for the PEP-II Asymmetric B Factory," July 1994

[2] Mathewson, Grobner et al, 1990

[3] G. Blokesch, et. al., " A Slotted Pipe Kicker For High-Current Storage Rings," Nuclear Instruments and Methods in Physics Reasearch A 338.

[4] SCM Metal Products, Inc., "GlidCop Product Information," North Carolina

[5] Pappas, C and Cassel, R, "Damping Ring Kickers for the Next Linear Collider,",US Particle Accelerator Conference, May 1999.

4.3 Beam Line Front Ends

The higher power density resulting from the increased stored current and bend magnet field strength in SPEAR 3 will place new demands on the front-end components of the existing SPEAR beam lines (BLs). Existing front-end masks for BLs 1 through 10 will be replaced with masks rated for 500 mA stored beam current. The front-end masks for BL 11 are already rated for 500 mA operation.

4.3.1 Beam Power Analysis

Table 4.27 details beam line source characteristics, total power, horizontal peak power density, and areal peak power density for each of the beam lines on SPEAR 3 at 3.0 GeV and 500 mA. The BL9 and BL11 power figures include the effects of reduced field end poles and non-sinusoidal field profiles. Most insertion device (ID) beam lines experience a factor of five power density increase relative to the SPEAR 2 configuration while the power density of BL 4 increases almost 14-fold owing to installation of a new ID. The power density on the bend magnet beam lines increases eight-fold due to the combination of higher bend field and ring current.

Table 4.27 Beam line photon-source magnet and power parameters at 3 GeV and 500 mA

characteristic	BL 1-3, 8	BL 4	BL 5	BL 6	BL 7	BL 9	BL 10	BL 11
B_{max} (T)	1.35	2.1	0.53	1.10	1.78	2.04	1.45	2.0
period or radius (cm)	780.0	26.0	18.3	7.0	45.1	26.0	12.85	17.5
number poles	1	18	20	54	8	16	30	26
total power (W)	n. a.	33700	1450	6560	12800	27700	11500	25500
peak power density (W/mr^2)	280	8280	2310	13000	2980	6930	9550	11200
peak horz power density (W/mr)	72	2150	600	3340	773	1800	2480	2900

4.3.2 Bend Magnet Beam Lines

There are four bend magnet beam lines on SPEAR: BL 1, BL 2, BL 3 and BL 8. These beam lines, which include both VUV and hard x-ray branch lines, are quite varied in their layout and use. There will be significant changes in the bend magnet sources with the SPEAR 3 upgrade, including 1) a reduction in source size, 2) increased current, 3) improved source stability, and 4) a hardening of the photon spectrum.

The bend magnet sources points and the exit ports in the ring vacuum chamber will be moved relative to their present locations, requiring a realignment of the four beam lines. All four beam line front ends will be standardized to provide the same relative source points and fan acceptances. The new standardized source point will be set to minimize the displacement of the beam line components. While the layouts of each of the beam lines is somewhat different, Figure 4.53 summarizes the realignment geometry. In general, the beam lines are rotated about the SPEAR shielding wall (located approximately 11 meters from the source) to accept the tangent from the SPEAR 3 bend magnets about 0.7 meters from the SPEAR 2 source point. Rotating about the SPEAR shielding wall presents the least disruption to the existing beam lines. Moreover, the relocated source points can be accommodated by relatively minor changes of the beam line optics.

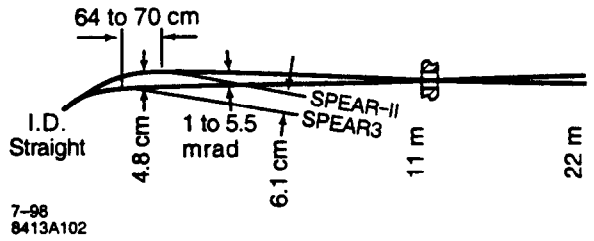

Figure 4.53 Realignment of the bend magnet beam lines necessitated by the SPEAR 3 bend source point relocation. The layout captures the range of realignments required to accommodate the differing SPEAR 2 bend magnet beam line geometries.

The relocation of beam line source points, coupled with the higher beam current and critical energy, necessitates new fixed and movable masks for the front ends. Additionally, the relocation of the exit ports approximately 1.3m downstream from the current location requires the reconfiguration of the in-alcove systems on all the branch lines and interferes with three existing branch lines: 1-1, 1-2 and 3-4.

Using standardized source point locations and front-end components for all four bend magnet lines will minimize the design and fabrication costs for the front ends. Given the relatively low power density of the bend magnet beams, simplified versions of the fixed and movable mask designs employed for BL 11 (Section 4.3.3.7) should provide adequate thermal performance while simultaneously conserving longitudinal ("z") space to facilitate the relocation of exit ports discussed above.

4.3.2.1 Beam Line 1

BL 1 is the oldest beam line at SSRL. It has gone through a number of significant reconfigurations over the years. At present, the BL 1 front end includes components, such as sweeping magnets, no longer required for SPEAR operation. These superfluous components will be removed, providing some of the space required to accommodate the exit port relocation. Nonetheless, in the SPEAR 3 configuration there is a conflict between the front-end components and the BL 1-1/1-2 M0 mirror tank. It is proposed to decommission these two branches as each is currently under-utilized.

4.3.2.2 Beam Line 2

BL 2 has three x-ray branch lines and a diagnostic station. As in the case of BL 1, removal of superfluous components will help accommodate the exit port relocation. It is not anticipated that the modest reconfigurations required for SPEAR 3 will jeopardize any of the branch lines or the diagnostic station.

4.3.2.3 Beam Line 3

Presently there are two branch lines on BL 3 with a third, white light x-ray station in commissioning. The front-end components, moved downstream to accommodate the SPEAR 3 exit port, will interfere with the BL 3-4 M0 system. This interference will hasten the planned decommissioning of this branch line, slated to be retired upon installation of an ID in the straight section adjacent to the BL 3 source point.

4.3.2.4 Beam Line 8

No functional changes are planned for BL 8, which features one VUV and one soft x-ray branch line. It is critical that the relocation of the beam line exit port not necessitate a repositioning of the M0 mirror for branch line 8-1. To this end, the vacuum valves and injection stoppers will be replaced

with more compact components. The fixed and movable masks, however, will maintain commonality with the other SPEAR 3 bend magnet front ends.

4.3.3 Insertion Device Beam Lines

SPEAR currently features six operational insertion devices with a seventh being commissioned. Of the seven IDs, six produce hard x-rays while the seventh is optimized for VUV. One of the hard x-ray beam lines also features a VUV side station.

Unlike the bend magnet beam line source points, the ID beam line source points do not move in the SPEAR 3 lattice. Thus, front-end components for ID beam lines are replaced only for thermal power handling reasons. As shown in Table 4.27, the IDs produce much higher power densities than the bend magnets. While providing some design and engineering challenges, masking these higher power densities is not an insurmountable problem. In particular, thermal designs developed for BL 11 masking provide adequate solutions for all the SPEAR 3 front-end masking applications. For example, typical finite element analyses (FEAs) of the temperature profile and thermal stress in a "crenelated" glidcop mask subjected to a power strike over a large area are depicted in Figures 4.54 and 4.55, respectively [1]. It is anticipated that similar crenelated masks will be employed for ID movable masks. Electro-discharge machined glidcop taper masks will be used for the fixed masks [2].

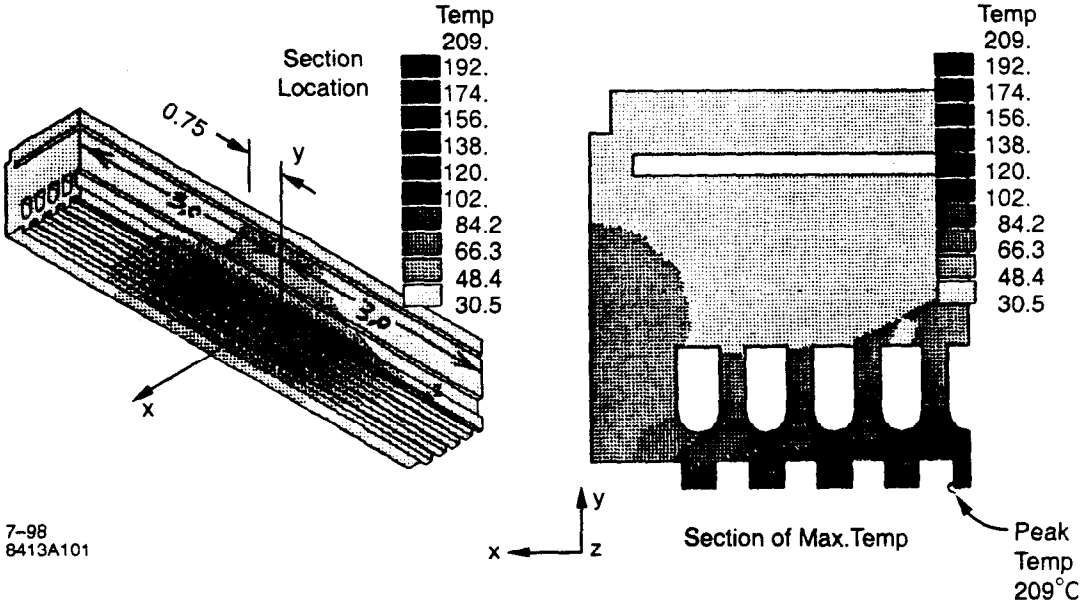

Figure 4.54 Temperature contours determined by finite element analysis of a "crenelated" glidcop mask subjected to a 10W/mm2 peak power density. The power strikes the mask at grazing incidence resulting in a 34-mm displacement of the beam footprint at the top relative to that at the bottom of the crenelations. The footprint is 14 mm (rms) along the crenelations and 41 mm wide. The cooling channels are formed with a 0.125" ball end-mill, plunging 0.25" deep and leaving a 0.125" thick hot wall.

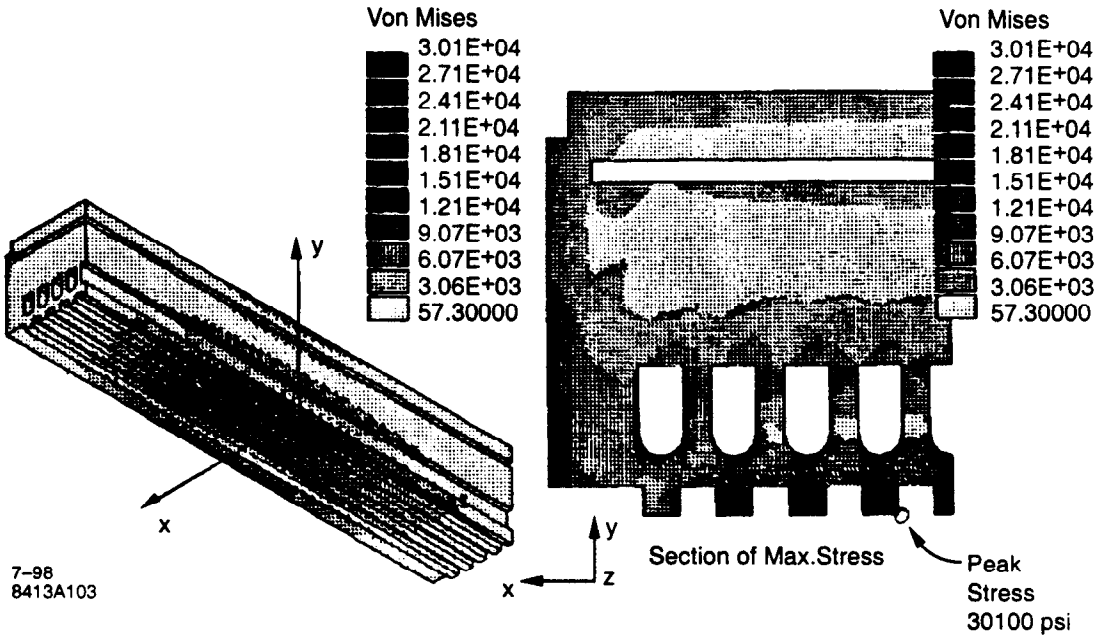

Figure 4.55 Von Mises stress contours associated with the FEA depicted in Figure 4.3.3-1.

4.3.3.1 Beam Line 4

The existing 8-pole electromagnet wiggler for BL 4 has a magnetic deflection parameter of 79 at 3 GeV, producing a wide radiation fan for three x-ray branch lines. This ID is scheduled to be replaced by a modern 18-pole, 2.1 T hybrid wiggler in 2002 [3]. The photon power density from this new ID greatly exceeds the design power density rating of the existing front-end fixed and movable masks, necessitating their replacement. Since the new power density rating requirement is similar to that for BL 11, front-end component designs from BL 11 will be scaled for the BL 4 geometry.

4.3.3.2 Beam Line 5

The synchrotron radiation for BL 5 is generated by one of five selectable undulators covering the energy range from 10 to 1200 eV. One of these IDs is the Elliptically Polarizing Undulator (EPU) which can generate circularly polarized radiation from 500 to 1100 eV. There are two major branches in the beam line: the old Locust monochromator, serving BLs 5-1, 5-2 and 5-3, and the new normal incidence monochromator serving BL 5-4. Because of the narrow horizontal divergence of the undulator radiation, only one monochromator can be used at a time.

The front end fixed and movable masks for BL 5 will be replaced to handle the higher thermal load for SPEAR 3. Given the relatively low power densities produced by BL 5 IDs, no significant mask design problems are envisioned.

4.3.3.3 Beam Line 6

BL 6 is a general purpose x-ray beam line. Since the beam line permits nearly windowless operation, this station is especially well suited for low energy x-ray absorption spectroscopy (E > 2100 eV). The radiation source is a 54-pole, 1.1 T wiggler featuring a variable gap vacuum

chamber located in the southeast quadrant of SPEAR. This ID produces the highest photon power density in SPEAR.

The existing front-end masks, which are rated for 200 mA operation, will be replaced by components rated for 500 mA as part of the beam line upgrade for SPEAR 3. Since the power density of BL 6 exceeds that of BL 11 by only 15%, the existing BL 11 front-end mask concepts can be adapted to the BL 6 requirements.

4.3.3.4 Beam Line 7

The 8-pole electromagnet wiggler for BL 7 has a magnetic deflection parameter of 79 at 3 GeV and produces a wide fan of radiation for three branch lines. Like BL 4, the BL 7 front-end components are only rated for 100 mA operation and must be replaced as part of the SPEAR 3 project. To facilitate the eventual replacement of this ID with an 18-pole, 2.1 T hybrid wiggler identical to that employed on BL 4, the new BL 7 front-end components will be identical to those discussed in section 4.3.3.1 above.

4.3.3.5 Beam Line 9

BL 9 consists of three hard x-ray branch lines designed for Structural Molecular Biology research. The radiation source is a 16-pole, 2 T wiggler in the northeast quadrant of SPEAR. The beam line was nominally designed for 200 mA operation. To permit 500 mA operation, the BL 9 front-end masks will be replaced as part of the beam line upgrade for SPEAR 3. The BL 4 and BL 9 ID and radiation fan requirements are similar, rendering BL 4 mask designs suitable for BL 9.

4.3.3.6 Beam Line 10

BL 10 consists of two branch lines. The end station, 10-2, is a general purpose, hard x-ray beam line capable of focused and white light operation. The side station is designed for VUV studies. The beam line radiation source is a 30-pole, 1.45 T wiggler in the northeast quadrant of SPEAR. The beam line was designed for 200 mA operation and, like BL 9, the BL 10 front-end masks will be replaced as part of the SPEAR 3 beam line upgrade. Given the lower power density of BL 10 relative to BL 11, the technology used for the BL 11 front-end masks will serve adequately for BL 10.

4.3.3.7 Beam Line 11

BL 11 is in the final stages of construction and the initial stages of commissioning. The radiation source is a 26-pole, 2 T wiggler in the southwest quadrant of SPEAR. Once fully commissioned, all components on this beam line will be rated for 500 mA operation.

References

[1] SSRL Engineering Note M289.

[2] SSRL Engineering Note M281. For an example of such a tapered mask, see PF 441-189-52.

[3] SSRL Engineering Note M275.

4.4 Survey and Alignment

Table 4.28 summarizes the alignment tolerances of SPEAR 3's magnet and vacuumchamber components.

Table 4.28 Tolerances for lattice-component alignment

Component	Rotation rms error (mrad)			Displacement rms error (mm)		
	ΘZ	ΘX	ΘY	ΔX	ΔY	ΔZ
	roll	pitch	yaw	Dx	Dy	Ds
Bend magnets	0.50	0.30	0.50	0.20	0.20	1.50
Quadrupoles	0.50	0.50	0.50	0.20	0.20	1.50
Sextupoles	0.50	0.20	1.00	0.20	0.20	1.50
RF cavity	1.00	0.50	0.50	0.20	0.20	1.50
bpm	1.00	0.50	0.50	0.25	0.25	1.50
Vacuum Chamber	--	--	--	0.25	0.25	0.50
Kicker	1.00	0.25	0.25	0.50	0.50	1.50
Insertion Device	0.50	--	--	0.25	0.25	1.50

Optical survey equipment will be used to align components with respect to floor monument locations (Appendix A.2). Currently, twenty of these floor monuments exist near straight sections of the ring. To increase the number of sighting locations–and thereby increase alignment precision–an additional local monument is located at the center of each of the 18 existing girders. Monument line-of-sight is limited primarily to the inside of the tunnel. Only two cross-ring sight lines exist, because buildings obstruct most sight lines within the ring's circumference. (Figure 4.56).

Magnets and vacuum-chamber components can be aligned independently. Each magnet and vacuum-chamber component will have an alignment fiducial based on known coordinates with respect to the center of the component (beam axis). To ensure successful alignment, fiducialization errors will be restricted to <50 μm.

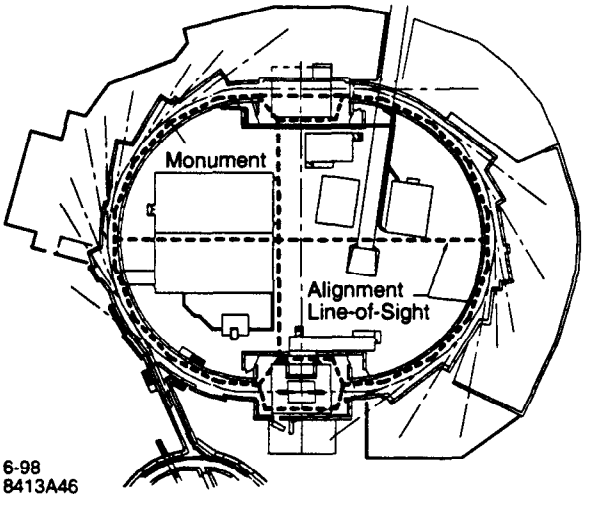

Figure 4.56 SPEAR alignment lines-of-sight.

4.5 RF System

The SPEAR RF system will be upgraded to provide increased power as well as minimize cavity impedances that can induce beam instability. The new system builds upon the PEP-II design for single-cell, mode-damped cavities operating at 476.337 MHz. The four cavities are driven in groups of two by a pair of 650 kW klystrons to produce a gap voltage of up to 3.4 MV. Table 4.29 gives SPEAR 3 parameters and RF system requirements. Figure 4.57 provides a block diagram of a typical station.

The cavities were originally designed for the larger higher order mode (HOM) power of the high-current PEP-II B-Factory (3 amperes) which exceeds that in SPEAR 3 by a factor of approximately 36. Nevertheless, the cavity and HOM absorber designs will be used without modification not just to avoid a costly new development effort, but also to take advantage of this opportunity to share RF component stocks and technical resources with SLAC.

Initially, SPEAR 3 will use the existing high-voltage power supplies currently used by SPEAR 2, thus limiting system performance. With insertion devices (IDs) operating at full strength, klystron output will be 500 kW per tube, and the maximum gap voltage will be 2.75 MV at 500 mA. The Touschek lifetime of the500 mA beam will be approximately 51 h, and the total beam lifetime will be to 17.9 h. These lifetimes should rise to 70 h and 20 h, respectively, once the power supplies are upgraded . A 3.2 MV gap voltage and longer lifetimes can be reached with the SPEAR 2 supplies, but only if the beam current is reduced to 390 mA. The SPEAR 2 HV power supplies can attain a 3.2 MV gap voltage, but the beam current is 390 mA, and the resulting beam lifetime is limited to approximately 25 h. The higher gap voltage and beam lifetimes will be attainable at 500 mA only after upgrades to the high-voltage power supplies provide full klystron power.

Figure 4.57 Block diagram for one of two SPEAR 3 RF stations.

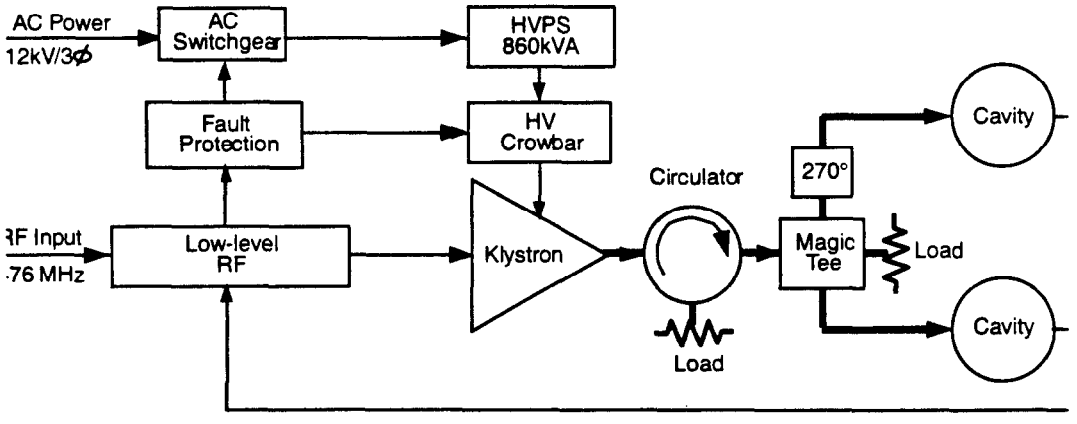

8-9
8413A28

Table 4.29 SPEAR 3 parameters and RF system requirements in 2002.

Parameter	Value (2002)	Comments
Beam energy	3.0 GeV	
Beam current I_b	500 mA	
Bend radius	7.86 m	
Total ID strength	42.4 T^2m	100 T^2m by 2020
Energy loss per turn	1.18 MeV	1.5 MeV/turn by 2020
Ring circumference	234.126 m	same as SPEAR 2
RF frequency	476.337 MHz	Booster RF is 358.533 MHz
Harmonic number	372	
Number of active klystrons	2	
Number of active cavities	4	
Cavity type	1-cell	1-cell cavities are HOM damped
Total shunt impedance	30 MΩ	$R_s=V_g^2/P_{rf}$
Total gap voltage Vg	2.75 MV	3.2MV @ 500mA with upgraded supplies
Overvoltage factor	2.33	2.7 @ V_g = 3.2 MV
Total cavity wall power	252 kW	341 kW @ V_g = 3.2 MV
Synchrotron rad. power	580 kW	increase to 1036 kW with new IDs by 2020
Misc. losses	78 kW	108 kW @ V_g = 3.2 MV
Total RF power loss	910 kW	1030 kW for V_g = 3.2 MV; 1180 MW by 2020
Klystron power requirement	1000 kW	approximately 10% control overhead; 1.13 MW @ V_g=3.2 MV; 1.3 MW in 2020
Available klystron power	1000+ kW	limited by HV supplies; 1.3 MW with upgraded supplies

4.5.1 RF Power Requirements and Performance

The stored electron beam dissipates power in the forms of 1) synchrotron radiation, 2) induced HOMs in the vacuum chamber and RF cavities, and 3) resistive loss from the beam-image current in the walls of the vacuum chamber. This beam-related power loss reduces the electron energy at each turn of the ring, and that energy must be restored by acceleration in the RF cavities. The power loss P for a beam current I_b having energy loss per turn U_0 is

$$P = U_0 I_b \tag{7}$$

Not only does the RF system have provide this beam power, it must also supply power for the gap voltage that produces acceleration within the cavity. Reflected power and losses in the waveguide network add to the total power dissipation. Table 4.30 lists the various contributors to RF power loss, and the resulting total RF power requirement P_{RF}.

Table 4.30 Beam energy and power losses in SPEAR 3 in 2002 (at 500 mA and 3 GeV, with a 2.75 MV gap voltage).

Mechanism	Energy loss/ turn (keV)	Power loss (kW)	Comments
Synchrotron rad. - dipoles	912	456	
Synchrotron rad. - IDs	248	124	550 keV, 275 kW by 2020
Chamber parasitic loss	10	5	280 bunches; 2x more for 140 bunches
Chamber resistive wall loss	1.2	0.6	"
RF cavity HOM loss	< 6	< 3	"
RF cavity wall loss	n/a	252	341 kW @ V_g = 3.2 MV
Reflected power	n/a	4	26 kW @ V_g = 3.2 MV
RF network insertion loss	n/a	65	74 kW @ V_g = 3.2 MV
Total	1.18	910	1030 kW @ V_g = 3.2 MV; 1180 kW by 2020

The cavity overvoltage factor, defined as

$$\text{overvoltage factor} = eV_g / U_0, \tag{8}$$

where e is the electron charge, and V_g is the gap voltage, must exceed two to maintain an adequate beam momentum acceptance [1]. A higher overvoltage factor increases the Touschek lifetime, as discussed in Section 3.7.3. If the available RF power is limited, the overvoltage factor can be reduced to increase the maximum storable beam current (and vice versa)-as long as a reasonable beam lifetime is maintained and the overvoltage factor is at least 2. Since the existing klystron HV power supplies, which will be used for initial SPEAR 3 operation, are power-limited, this trade-off between current and lifetime provides the subject for the following sections.

4.5.1.1 Beam Energy Lost to Synchrotron Radiation

Synchrotron radiation from dipole magnets is the dominant cause of beam energy loss in SPEAR 3. The average energy loss per turn due to dipole radiation is

$$U_{0\text{-bend}}\,(\text{keV/turn}) = 88.5\,E^4\,(\text{GeV})\,/\rho(\text{m}) = 912\ \text{keV at 3 GeV} \tag{9}$$

where ρ is the dipole bend radius.

The energy loss per turn in an ID is

$$U_{0\text{-ID}}\,(\text{keV/turn}) = 0.633\,E^2\,(\text{GeV}) < B^2(T) > L\,(\text{m}) \tag{10}$$

where $< B^2(T) >$ is the average of the square of the ID magnetic field strength, and L is the ID length. This expression also represents the energy loss-per-turn due to all IDs in the ring if the field average is taken over all IDs, and L is the total ID length. Table 4.31 shows the energy loss/turn from individual IDs, and the total energy and power loss from dipoles and IDs is given in Table 4.30.

Figure 4.55 depicts the projected energy loss per turn from synchrotron radiation (and vacuum chamber HOMs) over a period of 20 years as a function of future ID installation.

Table 4.31 Initial and proposed SPEAR 3 insertion devices at 3 GeV and 500 mA†.

ID	Year	# Poles	Period (cm)	L (m)	B_{pk} (T)	Loss/turn (keV)	Beam Power (kW)
BL 4 PM Wiggler	2002	18	26.0	2.34	2.1	67.3	33.7
BL 5 Undulator	2002	20	18.3	1.83	0.53	2.9	1.5
BL 6 Wiggler	2002	54	7.0	1.89	1.1	13.3	6.7
BL 7 EM Wiggler	2002	8	47.5	1.90	1.79	34.7	17.4
BL 9 Wiggler	2002	16	26.0	2.08	2.0	55.4	27.7
BL 10 Wiggler	2002	30	12.85	1.93	1.45	23.0	11.5
BL 11 Wiggler	2002	26	17.5	2.28	2.0	51.0	25.5
4S5 Wiggler	2004	26	17.5	2.28	2.0	51.0	25.5
8S9 Undulator	2006	200	3.5	3.50	0.68	9.2	4.6
East pit Vertical Polar Wiggler	2008	26	17.5	2.28	2.0	51.0	25.5
2S3 Wiggler	2010	26	17.5	2.28	2.0	51.0	25.5
1S2 Undulator	2012	200	3.5	3.50	0.68	9.2	4.6

†. PM = permanent magnet EM = electromagnet

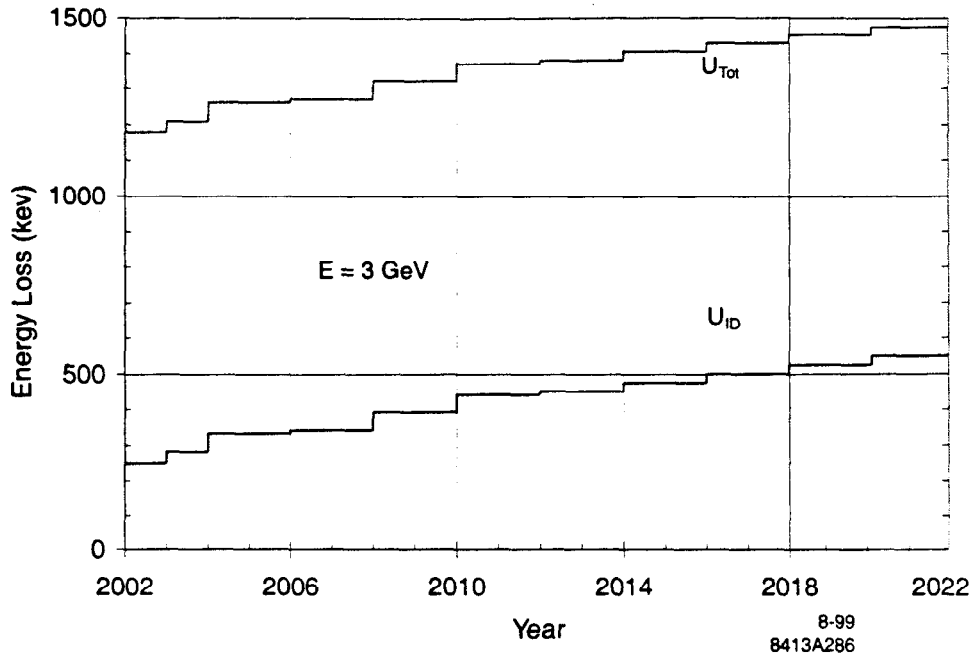

Figure 4.58 Energy loss/turn from synchrotron radiation and vacuum chamber.

4.5.1.2 Beam Energy Lost to Vacuum Chamber

The energy and power loss per turn due to vacuum chamber discontinuities and wall resistance has been estimated inSection 3.5. The loss scales as I_b^2/N, where I_b is the total beam current, and N is the number of bunches. RF-cavity HOM losses also contribute to beam energy loss. Table 4.30 tabulates the beam energy and RF power lost to the vacuum chamber.

4.5.1.3 Miscellaneous RF Power Losses

RF cavity-wall power, power reflected into RF loads, and insertion losses in the RF power transmission network do not affect beam energy.

The RF cavity wall power P_{cav} is determined primarily by the required gap voltage V_g and the cavity shunt impedance R_s:

$$P_{cav} = \frac{V_g^2}{R_s}. \tag{11}$$

For a 30 MΩ total cavity shunt impedance, the wall power dissipated in producing the 2.75 MV total gap voltage in four cavities is 252 kW. A 3.2 MV gap voltage requires 341 kW.

Ideally, the coupling coefficient (β_{cav}) of the cavities is set so that optimal coupling and maximum power transfer occur at full-beam current:

$$\beta_{cav} = 1 + \frac{P_B}{P_{cav}} \tag{12}$$

where P_B is the total power supplied to the beam. The desirable coupling factor for the initial ID configuration—500 mA beam current and a 2.75 MV gap voltage—is $\beta_{cav} = 3.3$ ($\beta_{cav} = 2.7$ for a 3.2 MV gap voltage). The PEP-II cavities are designed with a coupling factor of $\beta_{cav} = 3.8$. With a

3.2 MV gap voltage, more optimal matching at 500 mA will be achieved as IDs are added (e.g. β_{cav} = 3.2 for the projected ID installation in 2020). In any case, the reflected power from mismatched coupling is modest (< 10 kW total for operation in 2020).

Insertion loss in the waveguide network and circulator amounts to 0.35 dB, or 60-80 kW total at 500 mA, depending on gap voltage.

4.5.1.4 Klystron Power Requirements

The klystrons provide the RF power needed to replace the losses discussed above. The klystron power rating must be approximately 10% more than the dissipated power to provide a control margin for the RF feedback system.

Although the klystrons have a 650 kW rating, the power available for initial SPEAR 3 operation is limited to approximately 500 kW per tube by the existing HV power supplies (Section 4.5.4). Using these supplies (with the 10% control overhead), the power available to drive the RF system is 455 kW. When the HV supplies are upgraded, the klystrons will each produce the full 650 kW, with 590 kW available to drive the system.

4.5.1.5 RF System Performance and Limitations

As mentioned previously, the 910 kW total klystron power available using the existing HV power supplies is sufficient to support a 500 mA beam with a 2.75 MV gap voltage. Under these conditions, the Touschek lifetime will be 51 h, and the total lifetime will be 17.9 h. (Section 3.7.3; Figure 3.67)

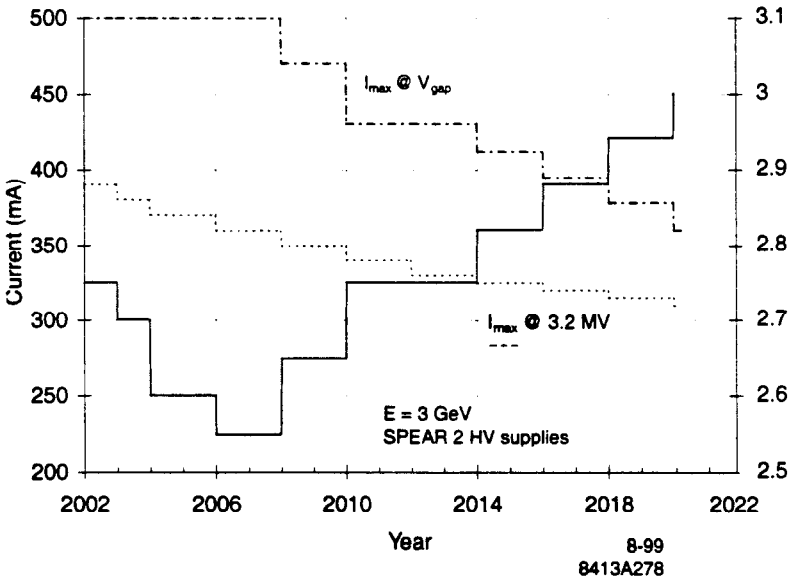

Figure 4.59 Gap voltage and maximum current at 3 GeV using the spear 2 HV power supplies.

To support 500 mA operations with a 2.75 MV gap voltage, the existing HV power supplies will be operating near maximum capacity. Therefore, to sustain 500 mA after new IDs are added, the gap voltage must be reduced—with a consequent reduction in beam lifetime. For example, for 500 mA operation following the proposed ID installation of 2006, the gap voltage will have to be reduced to 2.6 MV. The Touschek lifetime will then be reduced to 45 h, and the total lifetime will become 17 h.

Table 4.59 shows the maximum storable current for the projected ID installation, assuming that the SPEAR 2 HV supplies are still being used, and that the overvoltage factor is at least two.

As an option, the stored beam current can be reduced during the first years following SPEAR 3 commissioning, so as to obtain higher gap voltage and beam lifetime. In 2002, for example, a 3.2 MV gap voltage would be sustained for currents up to 390 mA (with a total lifetime of 25 h). In 2008, the current would drop to 350 mA. Immediately following SPEAR 3 commissioning, this mode is likely to be compatible with the beam current limits temporarily imposed by the power ratings of the beam line components. The maximum current with a 3.2 MV gap voltage using the existing HV supplies for the projected ID installation appears in Figure 4.59.

For full 500 mA operation, it is desirable to increase the gap voltage to 3.2 MV (which yields longer beam lifetime) and to maintain this 3.2 MV gap voltage for subsequent ID installations. The Touschek lifetime for the initial ID installation increases to 70 h at 500 mA, and the total lifetime becomes 20 h. This is possible if the HV power supplies are upgraded to provide the full klystron power. Figure 4.60 depicts the projected klystron power requirements for 500 mA SPEAR 3 operation with a 3.2 MV gap voltage as the number of IDs is increased. The Touschek lifetime at 500 mA in 2020 would be approximately 47 h and the total beam lifetime 17 h. The Touschek lifetime can be increased to a factor of three, (simultaneously, the total beam lifetime will be restored to >20 h), by means of a bunch-lengthening cavity. A more expensive approach can achieve the same results by adding another RF cavity pair.

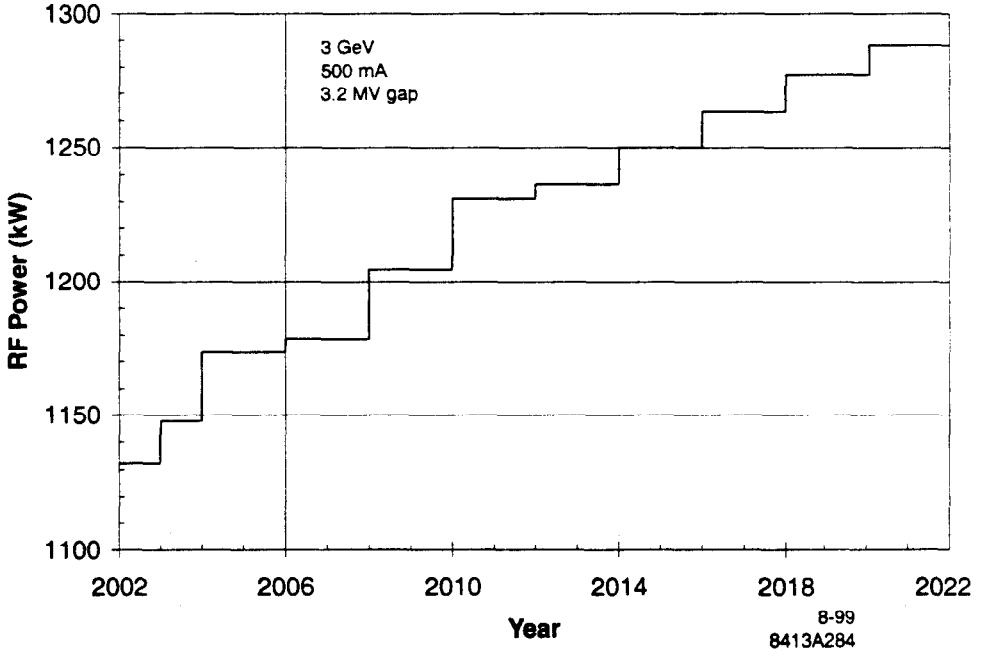

Figure 4.60 The Total RF klystron power for SPEAR 3 at 3 GeV with a 3.2 MV gap voltage.

4.5.1.6 Single Klystron Operation

The RF waveguide system will be designed to permit reconfiguration for driving all four cavities from a single klystron in the event that one klystron station is disabled for an extended period of time (Section 4.5.5). In this mode, it is likely that the gap voltage would be reduced to a minimum tolerable level (≥ 2 the overvoltage factor) to maintain an acceptable beam lifetime and to maximize the stored beam current.

Assuming use of an existing HV power supply, a single klystron will be able to support a 160 mA beam current at 3 GeV in 2002 with a 2.4 MV gap voltage. Figure 4.61 shows the maximum current for the projected ID installation for both the existing and upgraded HV power supplies (assuming an overvoltage factor of two).

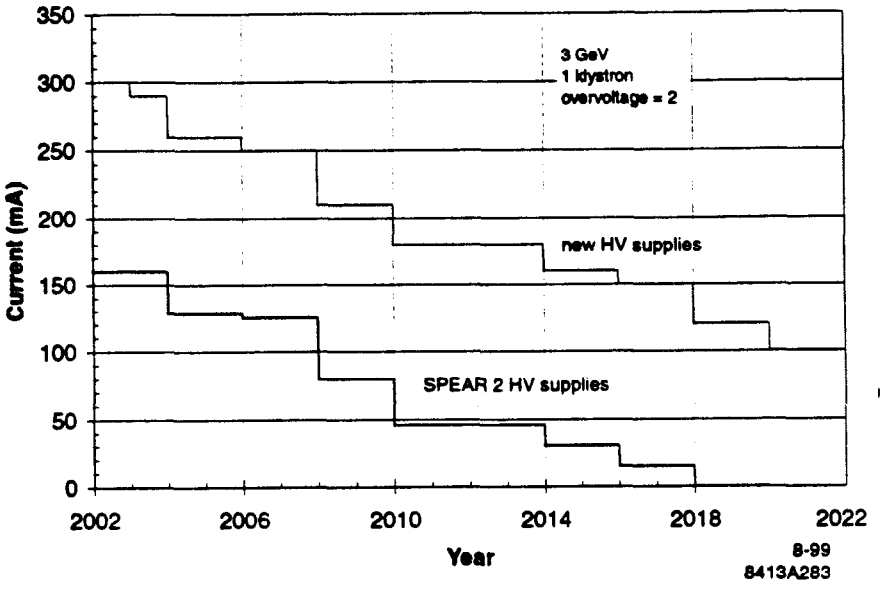

Figure 4.61 Maximum beam current for single-klystron operation at 3 GeV.

4.5.1.7 Higher Energy Operation

Both the energy loss-per-turn (from synchrotron radiation) and the consequent RF power requirement scale rapidly with increasing energy (Equations 9 and 10). Assuming the overvoltage factor should not decrease below approximately 2 to maintain an adequate momentum acceptance, the limit of the energy loss-per-turn is approximately 1.7 MeV for a maximum gap voltage of 3.4 MV. The total energy loss-per-turn for the initial complement of IDs in SPEAR 3 reaches approximately 1.7 MeV at an energy of 3.32 GeV, and at 3.13 GeV for the projected 2020 ID installation. The maximum operating energy as a function of ID installation appears in Figure 4.62.

The maximum beam current at higher energy is limited by the power ratings of photon absorbers, masks and beam line components. The current must be scaled as $1/E^4$ to maintain a constant photon power density from dipoles at a higher energy E. This sets an upper current limit of 330 mA at 3.32 GeV for chamber components rated for 500 mA at 3 GeV. Figure 4.62 shows the current limits for maximum operating energy as a function of ID installation. The maximum current for higher energy operation is limited to 220 mA using the existing HV power supplies.

With another RF cavity pair and klystron added in 2020, total gap voltage will reach 5 MV. The energy available for future ID installations (assuming an overvoltage factor of two) will rise to 3.5

† Assuming an overvoltage factor of two. Current is supply-limited with existing klystron hv power supplies. With new supplies, current is limited by vacuum chamber power ratings.

GeV. If the SPEAR 3 magnets can operate at this energy, the maximum current sustainable by the 6-cavity RF system should be 520 mA, while the current limit based on vacuum chamber and beam line power ratings would be 270 mA. The new cavity pair can be installed in one of the 4.5 m straight sections not currently used for IDs (e.g. 10S11).

References

[4] J. J. Thompson and D.M. Dykes, "Synchrotron Radiation Source–A Primer," Chapter 4, pg. 94. H. Winick, editor. Ward Scientific, Singapore, 1994.

4.5.2 Single-cell Cavities

Four PEP-II-style, HOM-damped RF cavities [1] (Figures 4.63 and 4.64) operating at 476.337 MHz will be installed in SPEAR 3. Table 4.32 gives cavity parameters.

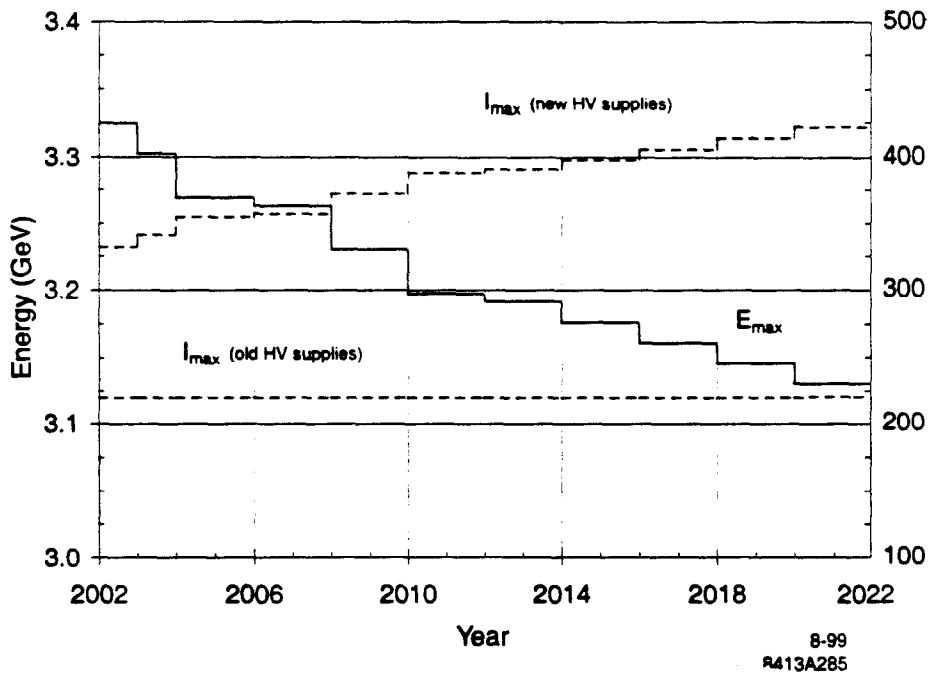

Figure 4.6 2 Maximum operating energy and current with four RF cavities for SPEAR 3.†

Table 4.32 SPEAR RF cavity parameters

Parameter	Unit	Value	Remarks
Frequency	MHz	476.337	+/- 0.5
Q value		33000	unloaded
Shunt impedance	MΩ	7.6	V_g^2/P_{rf}, measured
Max. wall power	kW	100	0.85 MV max
Max. window power	kW	500	
Nominal wall power	kW	84	
Nominal gap voltage	kV	800	at 84 kW
RF coupling		3.8	fixed iris coupling

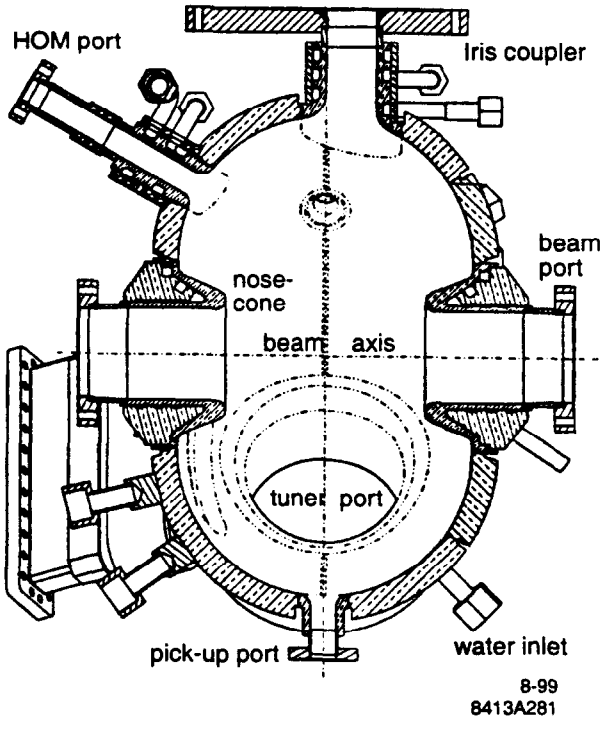

Figure 4.63 A cross-sectional view of the PEP-II HOM loaded cavity.

The PEP-II cavities have been designed for multibunch operation with beam currents up to 3 A in a 2.2 km storage ring. From 600 MHz to 5 GHz and above, the three HOM coupling ports terminate into three loads, reducing the Q of the HOM modes to values as low as 70 [2]. The combined power-handling capacity of the three HOM loads is 30 kW [3]. This design allows for a 3A beam current, and it will easily handle any HOM power the 500 mA SPEAR 3 beam can induce. An additional 3 kW HOM load is provided in the coupling waveguide to damp possible resonances between the coupling iris and the ceramic window and to prevent HOM crosstalk between the two stations.

The ceramic window [4] is designed for a power-handling capability of 500 kW CW. Physically, it has been placed one wavelength from the detuned short position of the cavity (approximately at the

coupling slot) to assure a constant electrical field level across the ceramic. At this location, the field is tied to the field in the cavity and is independent of beam-loading and associated variable standing waves.

A plunger-type tuner provides a tuning range of ±500 kHz [5]. The tuner employs sliding spring fingers to keep fundamental and HOM power from reaching the vacuum bellow. An additional fixed-tuner plunger can be pre-adjusted to rough-tune each cavity within the appropriate tuning range.

A 400 liter/s VacIon pump is part of the assembly providing nanoTorr (and better) vacuum at the cavity and window.

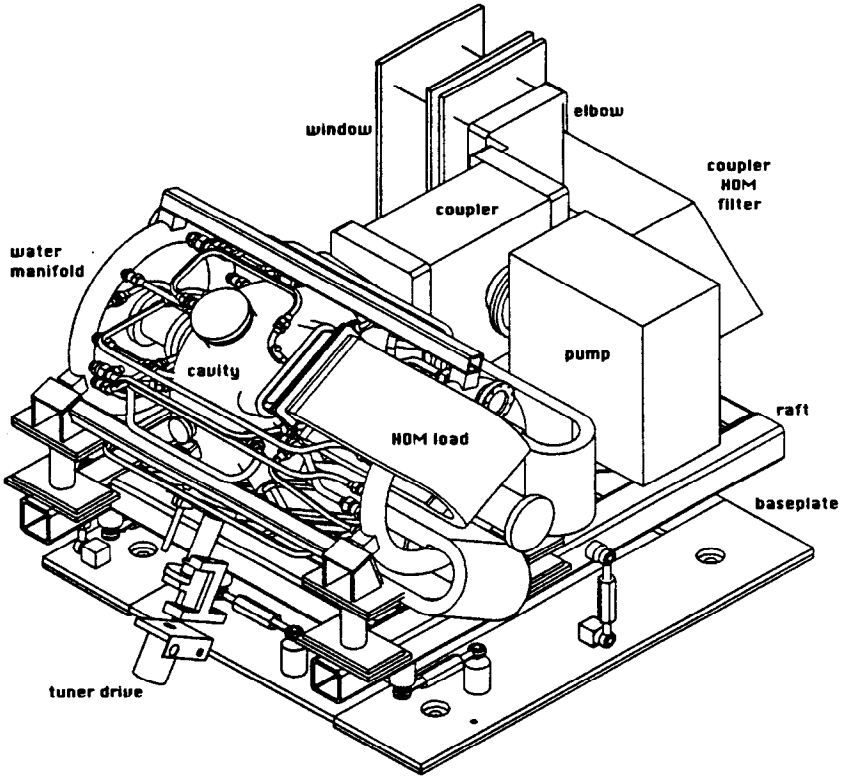

Figure 4.64 PEP-II cavity assembly.

4.5.3 Klystrons

Two 650 kW CW klystrons will be used to provide the RF power to the four cavities, one klystron per cavity pair. These klystrons are similar to the 500 kW, 358 MHz tubes built by SLAC and currently in use at SPEAR. The SLAC tube originally served as the prototype for the so-called super-klystrons developed by industry to produce over a megawatt of CW power at frequencies between 350 and 700 MHz. A 650 kW version, with performance parameters given in Table 4.33, is currently available from industrial sources. The klystrons will be mounted vertically in the location of the existing 358 MHz SPEAR 2 klystrons.

Table 4.33 Typical klystron parameters

Parameter	Value
Frequency	476.337 MHz
Bandwidth	± 0.5 MHz (-1 dB)
Output power	650 kW (saturated)
Cathode voltage V_c	72 kV
Cathode current I_c	15 A
Perveance	0.77×10^{-6}
Efficiency	65%
Gain	43 dB

The klystron perveance P, defined by

$$P = \frac{I_c}{V_c^{3/2}}, \tag{13}$$

where I_c and V_c are the cathode current and voltage, respectively, has been specified to provide an approximate match for the existing HV power supples, which have 66 kV, 13A ratings.

The klystron are designed for 65% efficiency both at the full cathode voltage and 650 kW output level, and also, by virtue of a changeable post in the klystron output waveguide, at the reduced cathode voltage available from the existing HV supplies. An output power of 500 kW will be available with a 63 kV cathode voltage and 12.2 A current. This is well within the limits of the existing power supplies. When more RF power becomes necessary to accommodate new insertion devices, the power supplies will be upgraded.

4.5.4 HV Power Supplies

SPEAR has two high-voltage power supplies to power the two existing klystrons. Each supply has switchgear for the 12 kV, 3-phase input voltage, a variable voltage transformer (VVT), and a HV transformer with rectifier diode stacks followed by a filtering inductor and capacitory (Figure 4.65). A delta-wye series configuration is used for the HV transformer primary to reduce output voltage ripple. Table 4.34 summarizes HV power supply parameters.

Full klystron power can only be reached by upgrading or replacing the HV supplies to provide the 70 kV, 14.2 A input power needed by each klystron to produce 650 kW of output power. The upgraded supplies would be rated for 75 kV and 18 A so that a PEP-II klystron (1.2 MW with 85 kV cathode voltage) could be used in place of a SPEAR 3 klystron as a back-up spare if necessary. The PEP-II klystron output power would be 650 kW with a 75 kV cathode voltage. VVTs might be replaced with SCR controllers [6] in the upgraded supplies.

Table 4.34 SPEAR RF HV power supply specifications.

Parameter	Value	Remarks
Input voltage	12kV	3-phase
Input current	40 A rms	per phase
VVT voltage	308-549 Vrms	line-to-line
VVT current	122-218 Arms	per phase
Output phases	6	wye – delta
PS output voltage	37-66 kVDC	filtered
PS output current	8-13 ADC	load dependent
PS output power	300-860 kW	load dependent
Inductor	8 H	on HV side

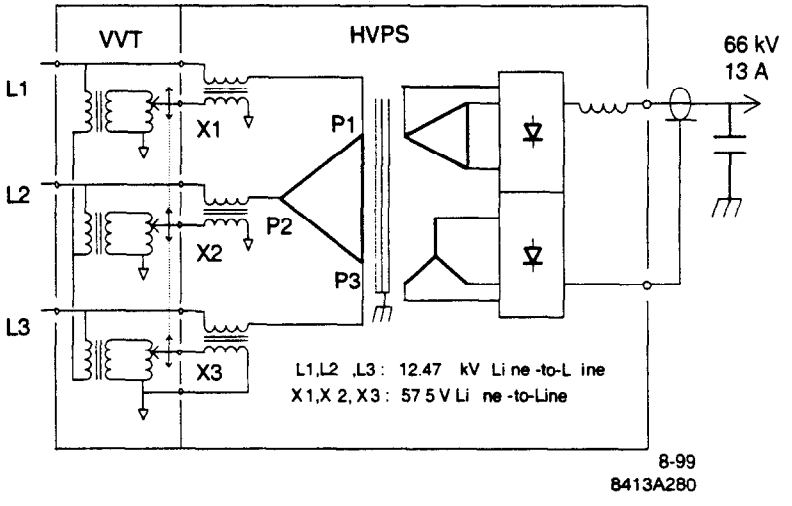

Figure 4.65 Schematic of the SPEAR klystron HVPS.

4.5.5 Waveguide and Circulators

SPEAR 3 will continue to use WR 2100 waveguide, but the layout must be modified to accommodate the new cavities in the West pit location (Figure 4.66), as well as the new klystrons and circulators in the klystron hut (Figure 4.65). A Magic-Tee will serve as power splitter between the two cavities. The cavities will be located in the beam line (11/4 λ_{RF}) and spaced an odd number of 1/4 wavelengths apart. This distance ensures that common-mode reflections will be directed towards the terminated port of the Magic-Tee and provides valuable reflected-power isolation between the cavities and klystron. An additional 12" bellow and 11" delay piece are inserted into the waveguide leg going to one of the cavities for each pair (Figure 4.66) to provide a λ_{RF} path length difference between the two waveguide legs that will equalize beam and RF phases in the two cavities for each station. Small length adjustments of the 12" bellow provide fine-tuning and optimization of the vectorial addition of cavity fields seen by the beam. The load at the fourth port of each Magic-Tee is rated for the full 650 kW klystron power and will absorb large power spikes when the beam is aborted. This and other RF loads are cooled with high conductivity water (Section 4.5.7).

A circulator is required to protect each klystron from reflected power and for increased system stability. The circulator and its load will also have a minimum 650 kW power capability. Klystrons

and circulators for both SPEAR 3 RF stations can be installed in the existing Klystron Hut (Figures 4.65 and 4.68).

In case one klystron or HV power supply should become disabled for an extended time, the other klystron can be connected to drive all four cavities by rearranging the waveguides to connect to another Magic-Tee with RF load and phase-adjusting bellow. This scheme, also supported by the low-level RF control system (Section 4.5.6), will permit ring operation with a current reduced current (Section 4.5.1.6).

For protection against leaking RF radiation, the waveguide system is pressurized to about 1/4 psi and interlocked to shut off a station should a pressure leak occur.

No additional measures are required to suppress beam-induced HOMs in the waveguide system since those modes are well suppressed in the cavities and its HOM load before the window.

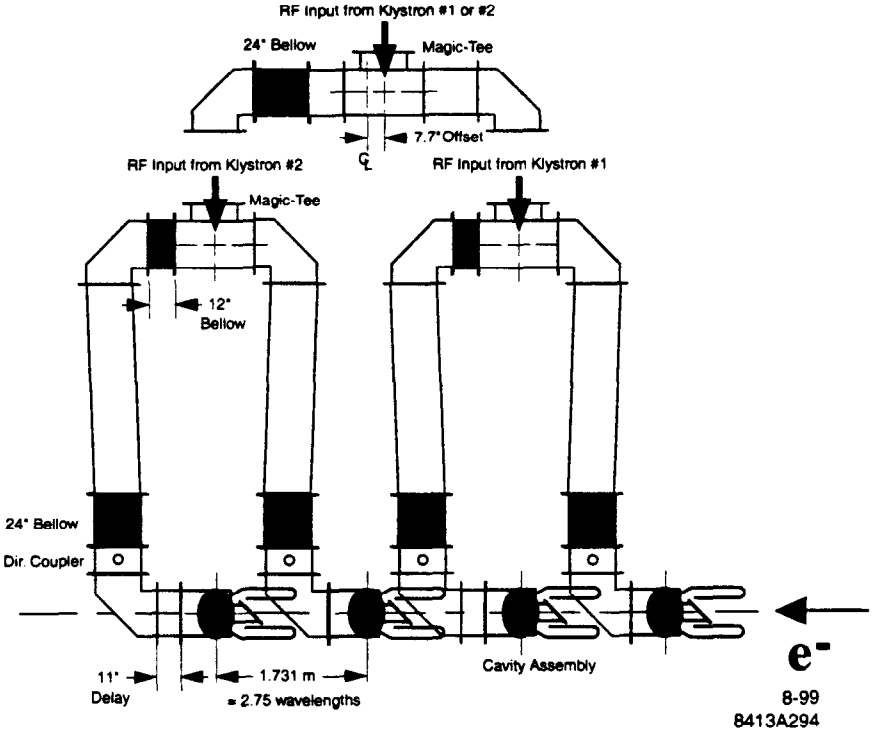

Figure 4.66 Typical waveguide layout with cavities and Magic-Tees in the West pit

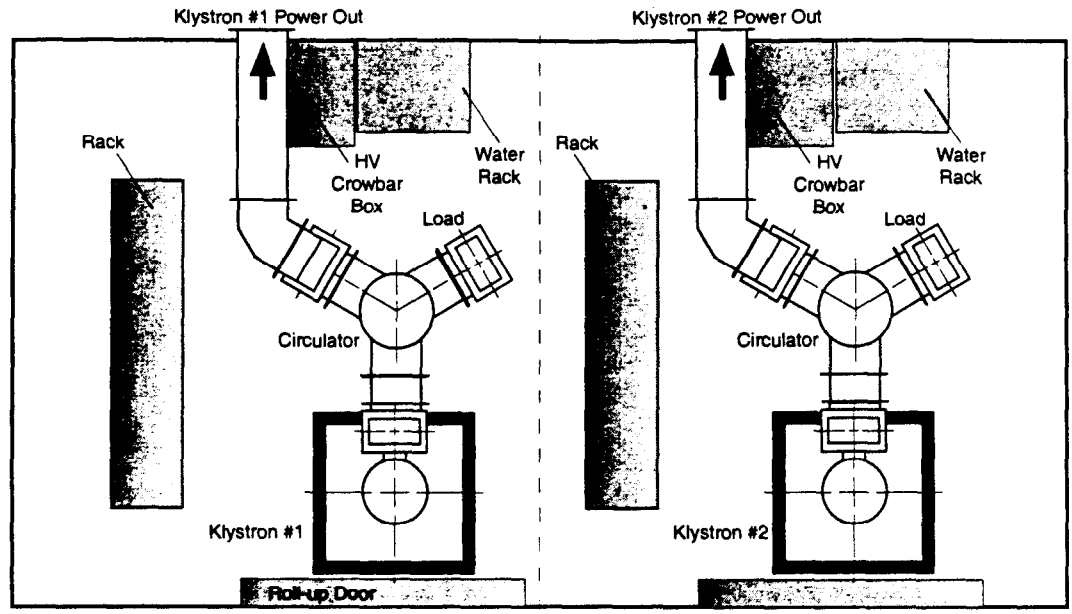

Figure 4.67 Top view of new klystrons and circulators installed in the existing klystron hut.

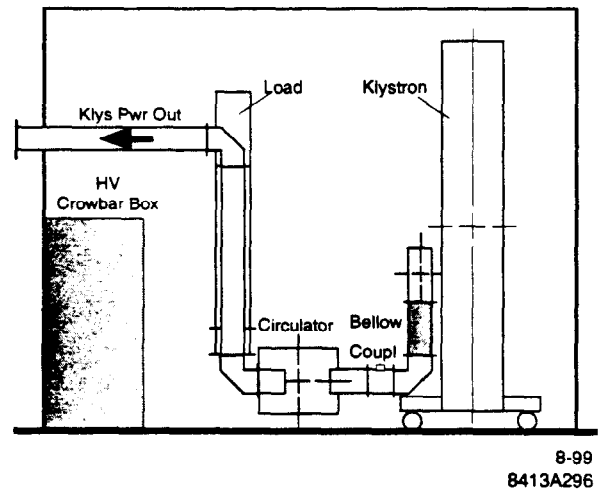

Figure 4.68 Side view of new klystron and circulator.

4.5.6 Low-Level RF Control System

The SPEAR 3 low-level RF (LLRF) system will be upgraded to a fully programmable digital system based on the recent PEP-II design [7] for improved RF control. The system employs EPICS (Section 4.8.1) control software, forming a "turn-key" RF system, requiring minimal operations support.

The LLRF electronics has a modular topology housed in a family of VXI modules. All controls and adjustments are fully programmable through EPICS forming a flexible and user-friendly system. System calibration and configuration is achieved by a collection of MATHLAB/EPICS routines which form an "expert" system, allowing non-experts to set up and monitor the system.

Several RF feedback loops will be supported by the SPEAR system (Figure 4.69). Like the PEP-II system, direct RF feedback will be implemented with baseband processing allowing integral and lead-lag compensation for superior performance. SPEAR 3 does not require direct RF feedback but will become more stable with feedback (Figure 4.69). A fiber optic link to the longitudinal feedback system will allow using the RF system to suppress the lowest few modes of beam motion (Section 4.7.2). Unlike the PEP-II system, an analog feedback loop across the klystron will cancel HV power supply ripple independently of the direct feedback loop.

Feedback loops with approximately 1 Hz sample rates are handled by EPICS program sequences. These include klystron cathode voltage control, gap voltage control, cavity tuners, and direct loop gain/phase tracking. This method has proven to be very flexible and easy to diagnose when problems occur.

The system will be designed to normally operate with two klystrons, each driving two cavities. However the system will be readily switchable to support operation with one klystron driving all four cavities (Section 4.5.1.6) with minimal hardware reconfiguration.

Slow interlocks for temperature, water flow, and solenoid magnet power supplies will be handled by a family of industrial programmable logic controller modules. The state of all interlocks will be passed to the EPICS database in real time and displayed on a local panel by a matrix of LEDs. All fast RF interlocks and arc detectors will be managed by dedicated hardware in VXI. In the event of a fault the first interlock to trip will be tagged in software to assist in diagnosing problems. After a fault, selected RF waveforms are stored in files which can be reviewed at a later time.

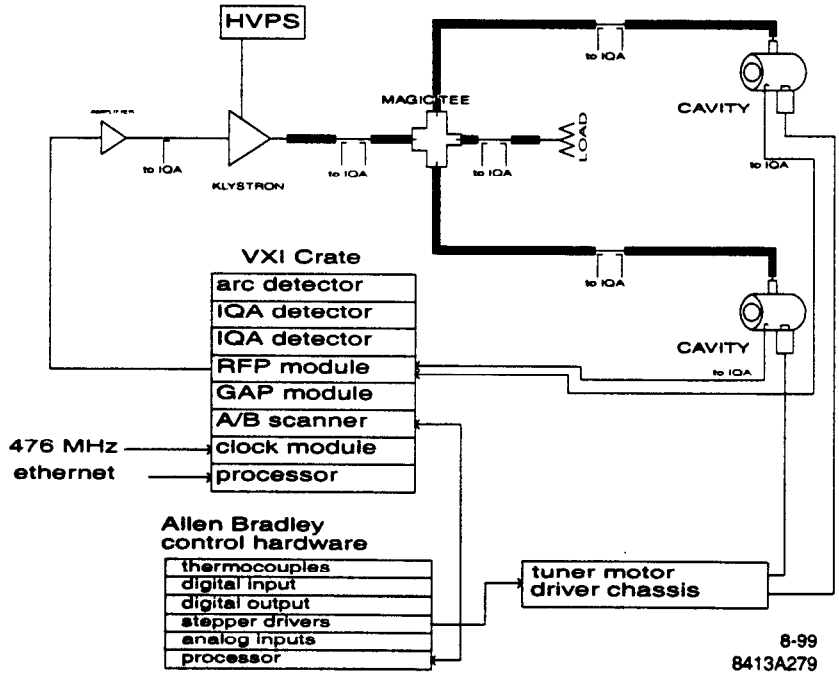

Figure 4.69 low-level RF (LLRF) system.

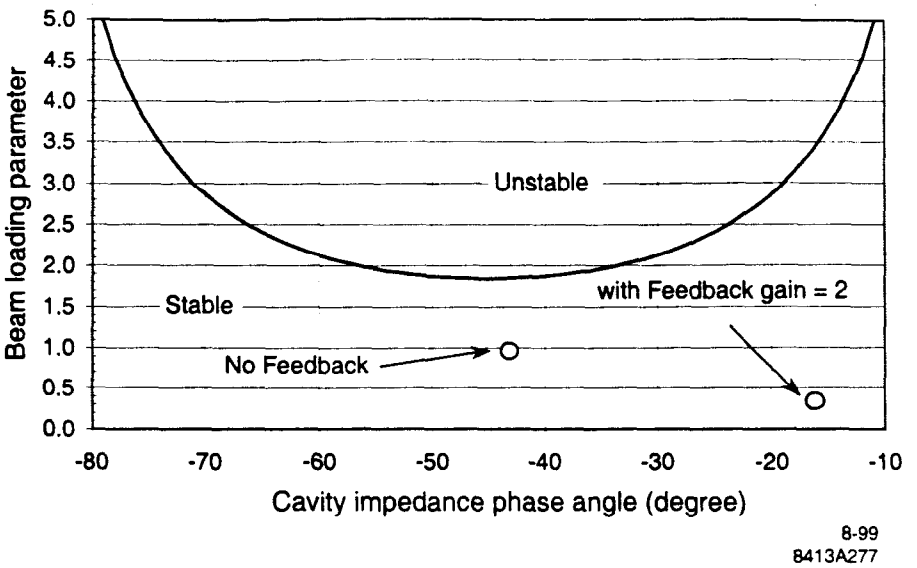

Figure 4.70 LLRF stability beam

Figure 4.70 shows the following stability condition of the beam:

$$\frac{2\cos\psi_\beta}{Y^*} < \sin(2\psi_z) \tag{14}$$

where ψ_B is the beam phase angle, ψ_Z is the cavity impedance phase angle, and

$$Y^* = \frac{Y}{(1+H)} \tag{15}$$

Y is the beam loading parameter given by

$$Y = \frac{I_B}{I_0} \tag{16}$$

where I_B is the beam current, I_o is the cavity generator current, and H is the feedback gain when it is employed. With the SPEAR 3 beam and RF parameters, the beam is stable even without feedback as can be seen in the above figure. In the event that the stored beam is feedback-controlled, the gain is limited by the long delay (approximately 1.3μs) across the klystron, waveguide, and cables.

4.5.7 Water Cooling System

The low conductivity water (LCW) cooling system of SPEAR will be upgraded to provide additional flow for the new cavities, klystrons and circulators (Figure 4.71). Approximately 700 gpm of LCW flow will be needed for the 4 cavities, 2 klystrons and 2 circulators. The incoming LCW temperature stability of ±0.5°C is sufficient for RF system operation and no additional temperature stabilization is planned.

A stand-alone high conductivity water (HCW) system having a capacity of 200 gpm is needed to cool four high-power waveguide loads (Figure 4.71). The conductivity is tightly controlled with a regulating system.

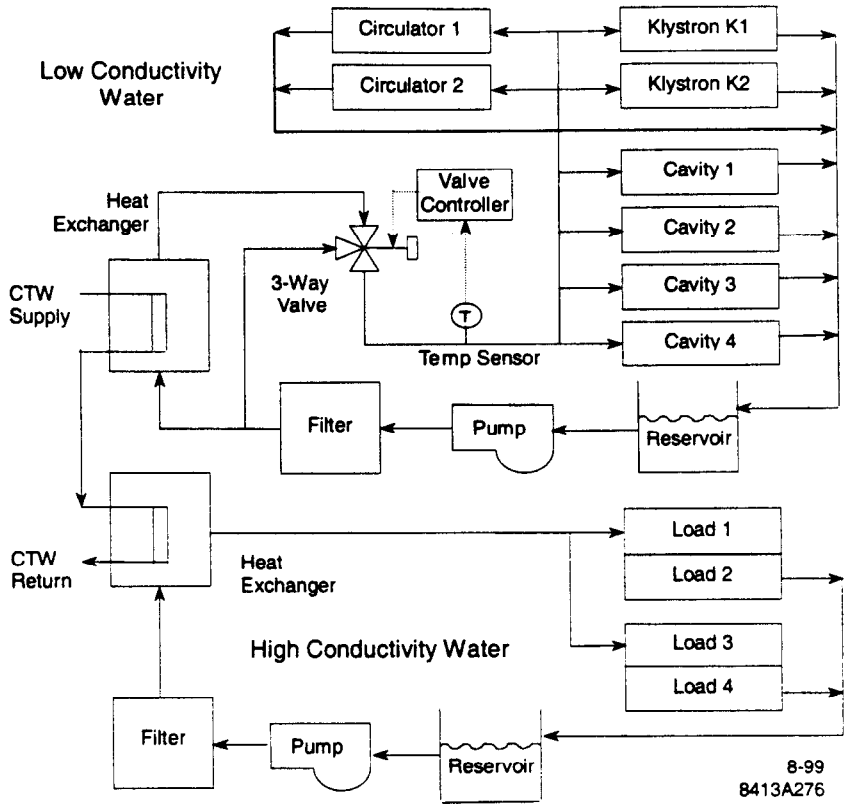

Figure 4.72 LCW and HCW 0.5°C temperature control system.

References

[1] Development of a High-Power RF Cavity for the PEP-II B Factory," R. A. Rimmer et al., PAC95.

[2] "Updated Impedance Estimate of the PEP II RF Cavity," R. A. Rimmer et al., EPAC96.

[3] "PEP-II B-Factory Higher Order Mode Load Design," R. Pendleton et al., PAC95.

[4] "High-Power RF Window and Coupler Development for the PEP-II B-Factory," M. Neubauer et al., PAC95.

[5] "Development of a Movable Plunger Tuner for the High-Power RF Cavity for the PEP-II B-Factory," H. D. Schwarz et al., PAC97.

[6] "A Unique Power Supply for the PEP-II Klystron at SLAC" R. Cassel et al, PAC95

[7] "Low Level RF System Design for the PEP-II B Factory," P. Corredoura et al., PAC95.

4.6 Power Supplies

All power supplies for SPEAR 3 magnets are rated for stable operation at a nominal energy level of 3.0 GeV–with a 10% operating margin and an additional nominal overhead of 10% (bringing the actual rating to 3.3 GeV). The power-supply performance specifications tabulated in this section take into account the allowable tune shifts for the ring as well as the requirements for beam position stability. While ring energy ramping is not a requirement for normal 3 GeV operation with at-energy injection, this capability will be provided for >3 GeV operation and for accelerator studies by implementing power supply controllers whose set points can be synchronously updated.

To handle SPEAR 3's somewhat diverse set of magnet requirements, the power supplies provide three types of output: unipolar DC, bipolar DC and pulsed. All new DC magnet power supplies employ switchmode technology. Some SPEAR 2 power supplies are reused. The new and reused power supplies and their ratings are identified in Table 4.35.

The listed power-supply voltage ratings include the inductive and resistive compliance voltages necessary when the current to the magnets is ramped, and also during sinusoidal current modulation. All power supplies incorporate freewheeling diodes in their output circuits to prevent the chopping of magnet currents, and to dissipate magnet energy when the power supply is turned off. Since a power supply's status is returned to the operators via a computer link, front-panel displays are minimal. They consist of: 1) AC and DC ON lamps, 2) a FAULT lamp, 3) a voltmeter, and 4) an ammeter. The controllers discussed in Sections 4.6.5.1 and 4.6.5.2 provide both remote and local control for the power supplies. All the power supplies conform to both the PEP-II specification for modern technology and the SLAC maintenance standard.

4.6.1 Stability and Regulation

Power supplies act as controlled current sources that endeavor to satisfy the magnet-current stability values given in Table 4.35. Within this table, stability is defined as "correction for the short- and long-term accumulation of all internal and external disturbances" to the power supply. Stability also implies that the maximum-output current error is acceptable over all frequencies at any point in time.

Table 4.35 SPEAR 3 magnet power supplies.

Magnet			Power Supply 3 GeV + 20% Requirements							
Circuit	Stability		Output Rating (each power supply)				AC In Total			
	Resolution	Ripple	Qty	Volts	Amps	kW	kVA In	Output Type	Enclosure	New or Reused
Dipole String	5.00E-05	5.00E-05	1	1200	775	930	1025	Unipolar	Free-standing	New
QD, QF Strings	1.00E-04	1.00E-04	2	750	100	75	118	Unipolar	Free-standing	New
QD, QF Individuals	1.00E-04	1.00E-04	40	100	100	10	339	Unipolar	Rack-mounted	New
Quadrupole QFC	1.00E-04	1.00E-04	2	750	100	75	154	Unipolar	Free-standing	New
QDX, QDY, QDZ	1.00E-04	1.00E-04	3	400	100	40	87	Unipolar	Rack-mounted	New
QFX, QFY, QFZ	1.00E-04	1.00E-04	3	400	100	40	87	Unipolar	Rack-mounted	New
Sextupole SD, SF	5.00E-04	5.00E-04	2	650	250	163	251	Unipolar	Free-standing	New
Sextupole SDI, SFI	5.00E-04	5.00E-04	2	125	150	19	36	Unipolar	Rack-mounted	New
Septum	5.00E-04	5.00E-04	1	65	275	18	19	Unipolar	Rack-mounted	New
Octupole	1.00E-04	1.00E-04	1	70	90	6	7	Unipolar	Rack-mounted	Reused
Wiggler	1.00E-04	1.00E-04	1	133	3000	400	346	Unipolar	Free-standing	Reused
Corrector	5.00E-04	1.00E-04	108	50	30	2	NA	Bipolar	Crate-mounted	New
Corrector Bulk PS	1.00E-03	1.00E-03	14	80	125	10	75	Unipolar	Rack-mounted	New
Insertion Device Trim	5.00E-04	1.00E-04	10	50	30	2	NA	Bipolar	Crate-mounted	New
ID Trim Bulk PS	1.00E-03	1.00E-03	2	80	125	10	21	Unipolar	Rack-mounted	New
Quad Modulation (QMS)	5.00E-04	1.00E-04	1	50	30	2	NA	Bipolar	Crate-mounted	New
Modulation Bulk PS	1.00E-03	1.00E-03	1	80	125	10	4	Unipolar	Rack-mounted	New
Skewquad Trim	5.00E-04	1.00E-04	14	50	30	2	NA	Bipolar	Crate-mounted	New
Skewquad Trim Bulk PS	1.00E-03	1.00E-03	1	80	125	10	23	Unipolar	Rack-mounted	New
Injection/Vertical Kicker	1.00E+00	1.00E+00	4	5000	0.25	1	5	Pulsed	Rack-mounted	New
BTS B7H, B8V	1.00E-01	1.00E-01	2	45	525	2.4	48	Unipolar	Rack-mounted	New
BTS Q8, Q9	1.00E-01	1.00E-01	2	50	40	2	1	Unipolar	Rack-mounted	Reused
				Total Input kVA			2,646	(at 3 GeV +20%)		

The disturbances can be categorized in two broad classes of frequencies—low and high. Low-frequency effects result from changes in the load on the power supply and variations in the ambient temperature. Typically, the ambient temperature equals that of the room or rack containing the power supply. Therefore, power-supply purchase specifications list minimum and maximum ambient temperatures as well as the type of cooling available. Smaller power supplies (i.e., those rated less than 100 kW) are air-cooled. Larger units, including dipole units, must incorporate water-cooling to maintain their temperature fluctuations within practical limits. The cooling water's inlet temperature, quality, pressure, and flow rate are all valid parameters upon which to base power-supply designs. Properly rated components as well as high system efficiency can reduce temperature increases significantly. Since some temperature deviation is unavoidable, components featuring low-temperature coefficients can further reduce the effect of ambient temperature shifts.

Load variations typically arise from changes in 1) the resistance of the power cables, 2) the ambient air temperature, 3) and the magnet-winding resistance, which changes according to the temperature of the water cooling the magnet. The ambient temperatures of the cable and the cooling water are both parameters the power-supply designer must take into account.

DC regulation of the power supply reduces the low-frequency effects described above. This has been reasonably quantified in the reproducibility and tracking error specifications. These effectively define the open-loop gain of the power supply.

Faster or high-frequency effects arise primarily from current ripple and AC line excursions. For an SCR phase-controlled power supply, the frequency range over which the stability specifications applies is on the order of hundreds of hertz. In the case of the modern switcher-type power supplies planned for SPEAR 3, the stability specifications can be maintained over a frequency range spanning many kilohertz.

The rectifiers, filters, and switching circuits always produce unavoidable residual ripple in the DC output of the power supply. Line rectifiers create low-frequency ripple (typically 360 Hz for six-pulse rectifiers and 720 Hz for 12-pulse rectifiers), while the switching elements produce higher frequency ripple (typically 20 kHz or more). The low-frequency ripple also contains sub-harmonic components. These are effectively filtered by passive, multi-pole, low-pass LC filters—and also by the dynamics of the high-frequency control loop. The higher frequency ripple components can be reduced to acceptable levels by multipole LC filters contained within the power supply's output stage. Because the higher-frequency ripples are attenuated by the magnet's inductance, as well as by core and/or vacuum chamber eddy currents, the high-frequency ripple components usually manifest lower amplitudes–and therefore, they prove less bothersome than the low-frequency ripple components.

The design goals for power-supply regulators emphasized suppression of sudden AC line changes. Stability must hold for 5% step-changes in the input-line voltage over 5-cycle periods (at an operating frequency of 60 Hz).

The stability values listed above in Table 4.28 represent the total allowable power-supply (magnet) diurnal errors expressed as fractions of the maximum operating currents ($\Delta I/I_{max}$). The ripple-current values are also expressed as fractions of the maximum operating currents over the DC–to–1 MHz frequency range.

4.6.2 Unipolar DC Power Supplies

The following DC-magnet families use unipolar power supplies:

- Dipole magnets
- Quadrupole magnets

- Sextupole magnets
- Septum magnet
- Octupole magnets
- Wiggler magnets
- BTS B7H, B8V and Q8, Q9 magnets
- Bulk power supplies for the Corrector, Trim and Modulation magnet supplies.

The unipolar DC power supplies designated for SPEAR 3 are typically AC-to-DC converters. Power supplies rated above 35 kW are free-standing, As Figure 4.73 shows, power supplies are rack-mounted when rated 35 kW or less. When a single large power supply of a particular rating is unavailable, two or more small power supplies are used in parallel. The paired power supplies use a "democratic" current sharing scheme; there is no "master" and no "slave". This current-sharing scheme has worked quite well on the PEP-II project. Each unipolar power supply interfaces the global control system via one of the single channel controllers described below.

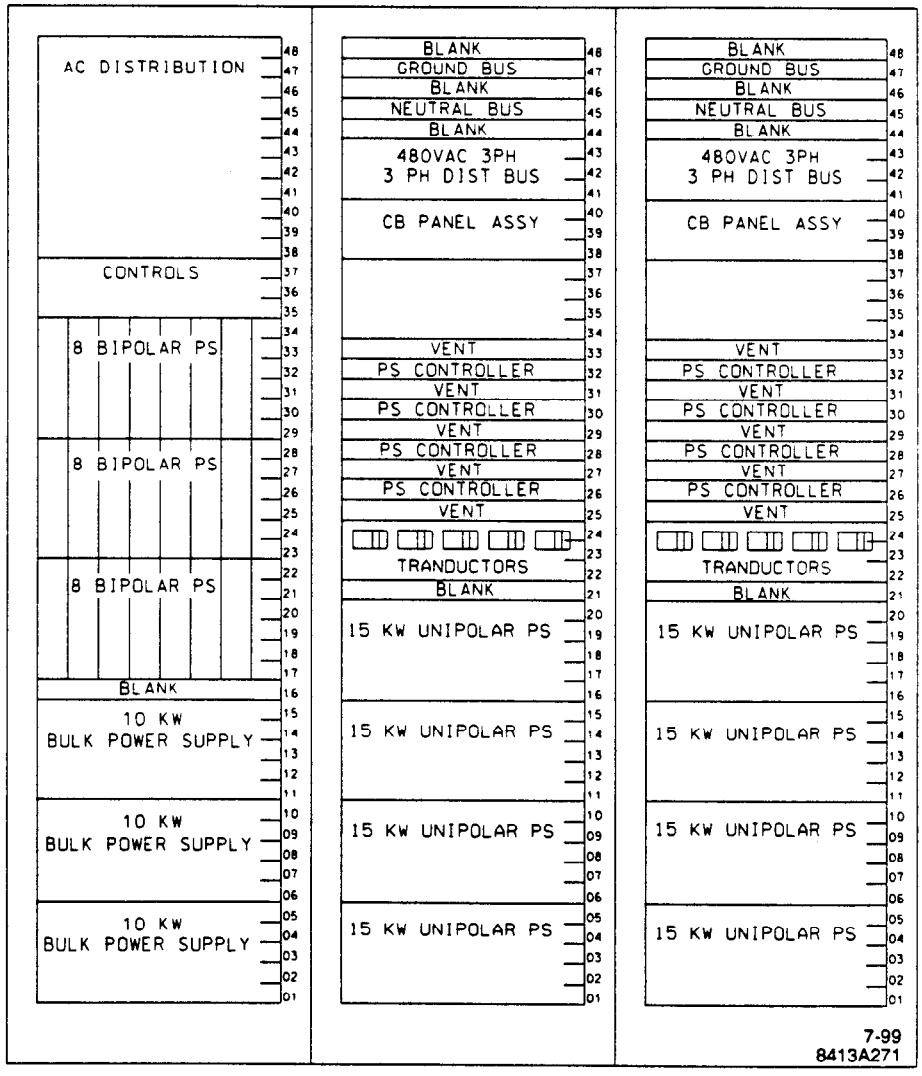

Figure 4.73 Rack-mounted power supplies.

4.6.2.1 Dipole Power Supply

The 36 gradient-bending storage-ring magnets are electrically connected as a single series string powered by a single power supply that delivers about 740 kW (1075 V, 688 A) to the dipole magnets at 3.3 GeV. In terms of both voltage and current, the power supply rating is nominally 10% higher than these specifications. As Figure 4.73 [shows, the power supply consists of 1) a six-phase transformer, 2) a 12-pulse SCR rectifier, 3) a low-frequency LC filter, 4) an IGBT (Insulated-Gate Bipolar Transistor) chopper converter, and 5) a high-frequency output filter. The two series-connected rectifiers are grounded at the center of their connection. This keeps the voltage to ground to a level suitable for 600V-class insulation systems, and it also keeps the string voltage symmetrical with respect to ground.

SCR control minimizes the inrush currents that would occur during initial power supply turn-on due to the charging of the critically damped low frequency filter capacitor. This filter attenuates the 720 Hz voltage ripple to the chopper converter, which regulates and controls the output current. Recently developed 3.3 kV, 1200 A IGBTs make switchmode technology attractive for this application [1]. The 740 A supply-current rating mandates two parallel-connected current-sharing IGBTs.

The chopper operates with a switching frequency of 20 kHz. This frequency is high enough to reduce whatever residual 720 Hz ripple remains after passive filtering. The critically damped high-frequency LC filter attenuates both the 20 kHz fundamental frequency as well as the harmonics produced by the choppers.

As Figure 4.74 shows, three feedback loops achieve the requisite $\Delta I/I$ stability by adjusting the duty cycle of the IGBTs:

- A feed-forward voltage loop to measure the rectified voltage ahead of the low frequency LC filter, so as to compensate for line voltage variations.
- A loop to regulate output voltage.
- The third loop to control external output current.

A pair of independent current transductors monitor the magnet current. One transductor belongs to the external current regulation loop. The other transductor verifies that the magnet current is correct.

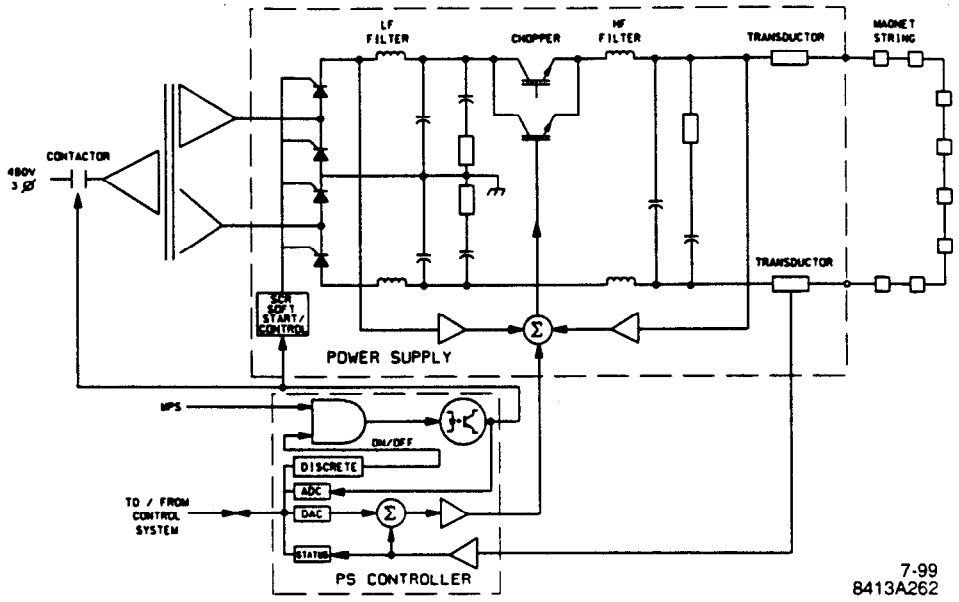

Figure 4.74 Dipole SCR + series chopper regulator power supply.

4.6.2.2 Quadrupole Power Supplies

New unipolar power supplies will also be used for the following magnet systems:

- QF and QD magnets
- QFC magnets
- QDX, QFX, QDY, QFY, QDZ, QFZ magnets

The operating voltages of the magnets listed above do not match the AC input-line voltage. Therefore, power supplies configured as H-bridge converters operating into step-down/isolation transformers are preferred. The topology and regulation loops of a typical quadrupole/sextupole/septum power supply appear in Figure 4.75. Note that the feed-forward loop within the dipole loop is unnecessary since the stability requirements are less severe.

Each of the QD and QF systems is arranged as one string of eight magnets powered by a single power supply and 20 magnets, each powered by a separate power supply. Because the eight QD and eight QF string magnets exist within standard cells that do not contain insertion devices, the magnets will never be used for local optics tuning. Thus, these magnets can share a single, common power supply. On the other hand, the QD and QF magnets (20 of each type) exist in standard cells adjacent to straight sections of the ring that feature insertion devices. Each of these 20 QD and 20 QF are used for local optics tuning.

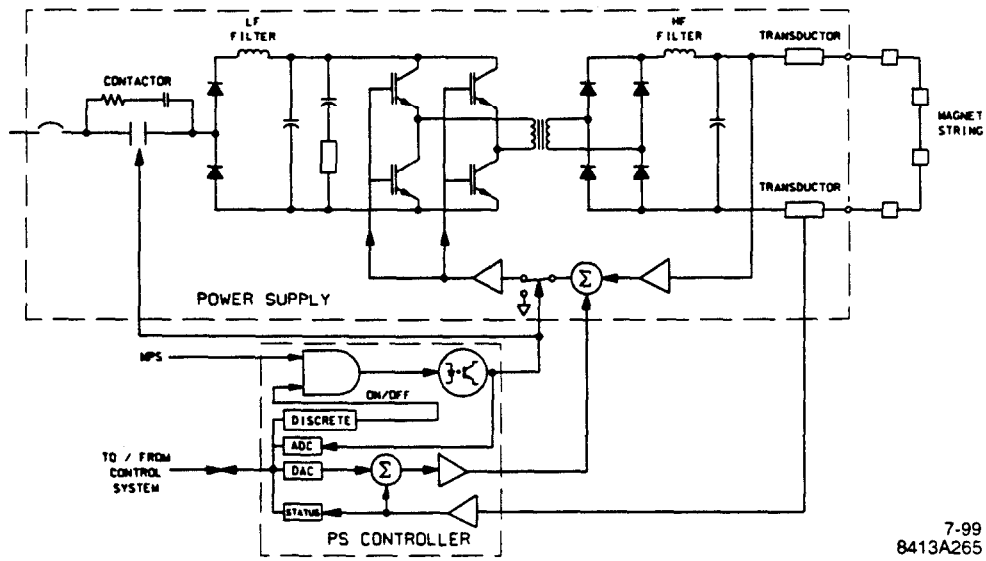

Figure 4.75 Unipolar power supply (500W to 200 kW rating).

The 14 QFC magnets in the 14 standard cells are connected as one string powered by a single power supply. Because of cell symmetry, these magnets do not require individual strength trimming.

The other six families of quadrupoles QDX, QDY, QDZ, QFX, QFY, QFZ each contain 4 magnets located in matching cells. They do not now have insertion devices adjacent to them, so the 4 magnets in each of these families are connected in series powered from a single power supply. However, new insertion devices may be added in the future. Therefore, adjacent quadrupoles now connected to family-based strings might eventually require reconnection to individual power supplies. Furthermore, if, in the future, a higher degree of lattice tuning becomes necessary—i.e., tuning that goes beyond the first-order needs imposed by the insertion devices—individual supplies may be needed for more quadrupoles. Thus, the current design of the quadrupole-magnet power system anticipates a long-term migration towards more individual power supplies. This entails reserving room for additional power supply racks and connections to the AC distribution system.

4.6.2.3 Sextupole and Septum Power Supplies

New unipolar power supplies will also be installed for the following magnet systems:

- SF, SD magnets
- SFI, SDI magnets
- Septum magnets

As holds for the quadrupole families, the operating voltages of the magnets listed above do not match the AC-input line voltage. Therefore, power supplies configured as H-bridge converters operating into step-down/isolation transformers are preferred. Figure 4.75 shows the topology and regulation loops of a typical sextupole/septum power supply.

4.6.2.4 Octupole/Wiggler/BTS B7H, B8V, Q8 & Q9 Power Supplies

The existing octupole magnets and their 60 V, 80 A power supply are reused. An intermediary chassis is used to interface the power supply to the new single channel controllers described in later in this section.

The beam line 7 wiggler magnet and its 133 V, 3000 A power supply will be reused. An intermediary chassis also interfaces the power supply to the new single channel controller.

The BTS, B7H, and B8V magnets are reused. The power supplies for these two magnets are new since it is less expensive to purchase rack-mounted power supplies that conform to the new control system than to move, store, and reinstall the current, physically-large power supplies, which would also need to undergo adaptation to the new control system.

The BTS, Q8, and Q9 magnets and their 50 V, 40 A power supplies are reused. An intermediary chassis is used to interface the power supplies to the new single-channel controllers described later in this g.

4.6.3 Bipolar DC Power Supplies

SPEAR 3 uses more than 130 bipolar converters. Each converter is rated 50 V, 30 A. As Figure 4.76 shows, these are two-quadrant output, high-frequency switch-mode power amplifiers configured as H-bridges. The design and development of these supplies will be completed prior to the SPEAR 3 Project.

The high frequency switch-mode topology yields a small signal bandwidth on the order of hundreds of hertz while maintaining excellent low-frequency regulation. Cross-talk between converters fed from a common bulk power supply is reduced by the use of an input filter in each converter and by synchronization of the converter switching. The converters are crate- and rack-mounted, and they interface to the global control system via multi-channel controllers described later in this section. For redundant current monitoring, each converter uses two, low-temperature coefficient current sensors mounted on its chassis. Typically, 8 DC-DC converters are fed from one bulk power supply.

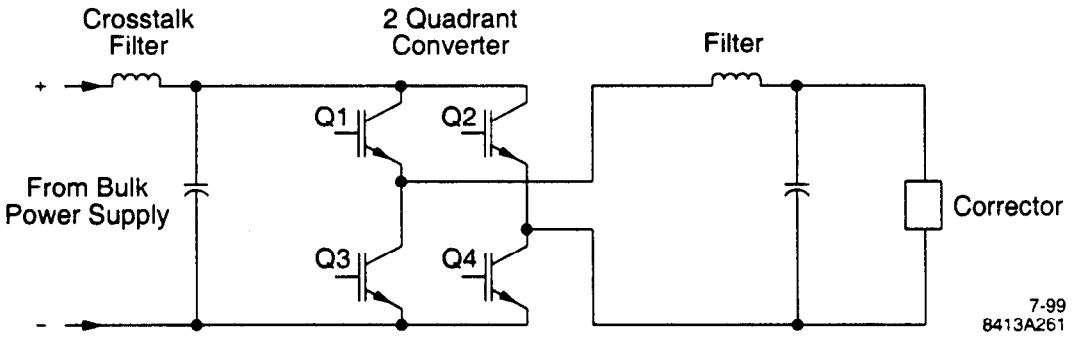

Figure 4.76 Bipolar power supply.

4.6.3.1 Corrector Power Supplies.

The 40 V, 50 A linear bipolar corrector power supplies used for SPEAR 3 will be replaced with 50 V, 30 A converter power supplies in SPEAR 3. The 0.05% stability requirement shown in Table 4.35 for the corrector power supplies depends on the limitation of beam kick-generated supply noise to 0.1μrad rms in amplitude.

The correctors require a power supply with a small signal bandwidth on the order of 500 Hz and high stability at lower frequencies. Specifying the small-signal bandwidth defines the regulator bandwidth. Specifying the maximum allowable tracking error defines the required gain. Specifying the stability indirectly defines the frequency range over which there must be high gain.

Fluctuations in the output current of the correctors contributes to orbit motion. Unlike magnets within a family that are connected in series to a common power supply, each corrector must have its own power supply. It therefore becomes a potential source of motion, independent from the other correctors. Since there are many corrector magnets, a significant fraction of orbit motion (especially vertical perturbation) can originate from the corrector magnet power supplies. Additionally, corrector set-points are continually changed by the orbit feedback systems, thus introducing quantization or tracking errors as potential sources of motion. Another potential area of concern lies in the corrector step responses. The corrector power supplies must not have under-damped step responses, since these introduce oscillatory components in the orbit-motion spectrum.

Limitations exist on how much a corrector should change with each cycle. Under normal conditions, the change-per-cycle is small, since the regulator is essentially an integrator at the highest frequencies, and it has real gain at lower frequencies. In some cases, however, the regulator detects a large glitch, and it therefore tries to apply a large correction. The maximum change-per-cycle should be limited because the glitch might not be real (or is, in any case, too fast to be corrected). For this reason the correction-per-step should be limited to a small fraction of the corrector's full scale.

The corrector supply must have sufficient voltage to drive the corrector magnet inductance for "high"-frequency control from the Orbit Feedback System (Section 4.7.1). The Orbit Feedback System is specified to have a 100 Hz closed-loop bandwidth, indicating a step-response corrector rise time of approximately 3.6 ms. approximately 29 V (= L dI/dt) is the voltage induced in a corrector having inductance L = 47 mH for a current step dI of 10% of the full-scale corrector operating current (2.2 A) in dt = 3.6 ms. This current step corresponds to an orbit displacement of approximately 100 μm, and represents a worst-case performance specification for the Orbit Feedback System. The induced voltage, added to the 17V maximum DC voltage for full 22 A corrector energization (0.77 Ω load, including cable resistance) is 46 V, implying that the 50 V corrector-supply rating is sufficient. Other anticipated AC orbit disturbances, occurring at frequencies corresponding to accelerator girder vibrations (<60 Hz) or power supply regulation and ripple (≥60 Hz), are of small amplitude and will induce voltages that are much less significant than those produced by a 100 μm orbit step.

4.6.3.2 Trim Power Supplies

The ten trim power supplies for insertion devices as well as the 14 skew-quadrupole trim power supplies are listed in Table 4.35. Each trim magnet is fed from a dedicated bipolar power supply and these in turn are powered from bulk power supplies. This setup is identical to the power supply scheme used for the correctors.

4.6.3.3 Modulation Power Supplies

The Quadrupole Modulation System (QMS, Section 4.8.3) employs (at least) one bipolar power supply of the type used for the correctors and the trims described above. The QMS supply provides DC or sinusoidal currents at frequencies up to the order of 10 Hz. The induced voltage at these frequencies is a small fraction of DC voltage.

4.6.4 Pulsed Power Supplies

The injection kicker system will use strip-line, air-core magnets. These will be contained in a vacuum vessel that serves to lower the magnet impedance. Pulsed power supplies will be needed for the three new injection kickers and one vertical kicker that will be installed in SPEAR 3 (Section 4.4). Table 4.36 provides pulsed-magnet and power supply parameters.

Table 4.36 SPEAR 3 injection kicker parameters.

Parameter	Kicker 1	Kicker 2	Kicker 3
Energy	3.3 GeV	3.3 GeV	3.3 GeV
Length	0.6 m	0.4 m	0.6 m
Bend angle	1.7 mrad	0.75 mrad	1.7 mrad
Field	32.5 mT	20.1 mT	32.5 mT
Peak voltage	19.2 kV	7.9 kV	19.2 kV
Peak current	4070 A	2516 A	4070 A
Rise time	200 ns	200 ns	200 ns
dB/dI	8 mT/kA	8 mT/kA	8 mT/kA
Pulse width (at base)	750 ns	750 ns	750 ns
Inductance	0.6 μH	0.4 μH	0.6 μH
Impedance	4.7 ohms	3.1 ohms	4.7 ohms

An IGBT-based pulser furnishes each kicker magnet with a current waveform similar to the idealized version shown in Figure 4.77. When the right-hand IGBT stack is turned on, diodes in a switchmode power supply pre-charge the pulser capacitors in parallel. The response of the power supply is fast enough to charge the capacitors without significant voltage overshoot, thus obviating the need for a conventional de-Q'ing circuit. At the appropriate instant, the left-hand IGBT stack is triggered, placing the charge voltage across the saturable reactors. When the reactors saturate, the right-hand IGBT stack is opened. The current pulse from the capacitors is discharged into the kicker magnet load. To end the pulse, the left-hand IGBT stack is opened. The use of solid-state switches yields greater reliability and longer device life. Parallel charging of the capacitors allows use of a smaller power supply and keeps the IGBT voltage rating reasonable. Series discharge obviates the need for a source-to-load match-pulse transformer.

The pulser, consisting of 1) switchmode power supply, 2) capacitors, 3) diodes, 4) saturable reactors and 5) system controls, is located in Power Supply Building 118, as shown in Figure 4.77.

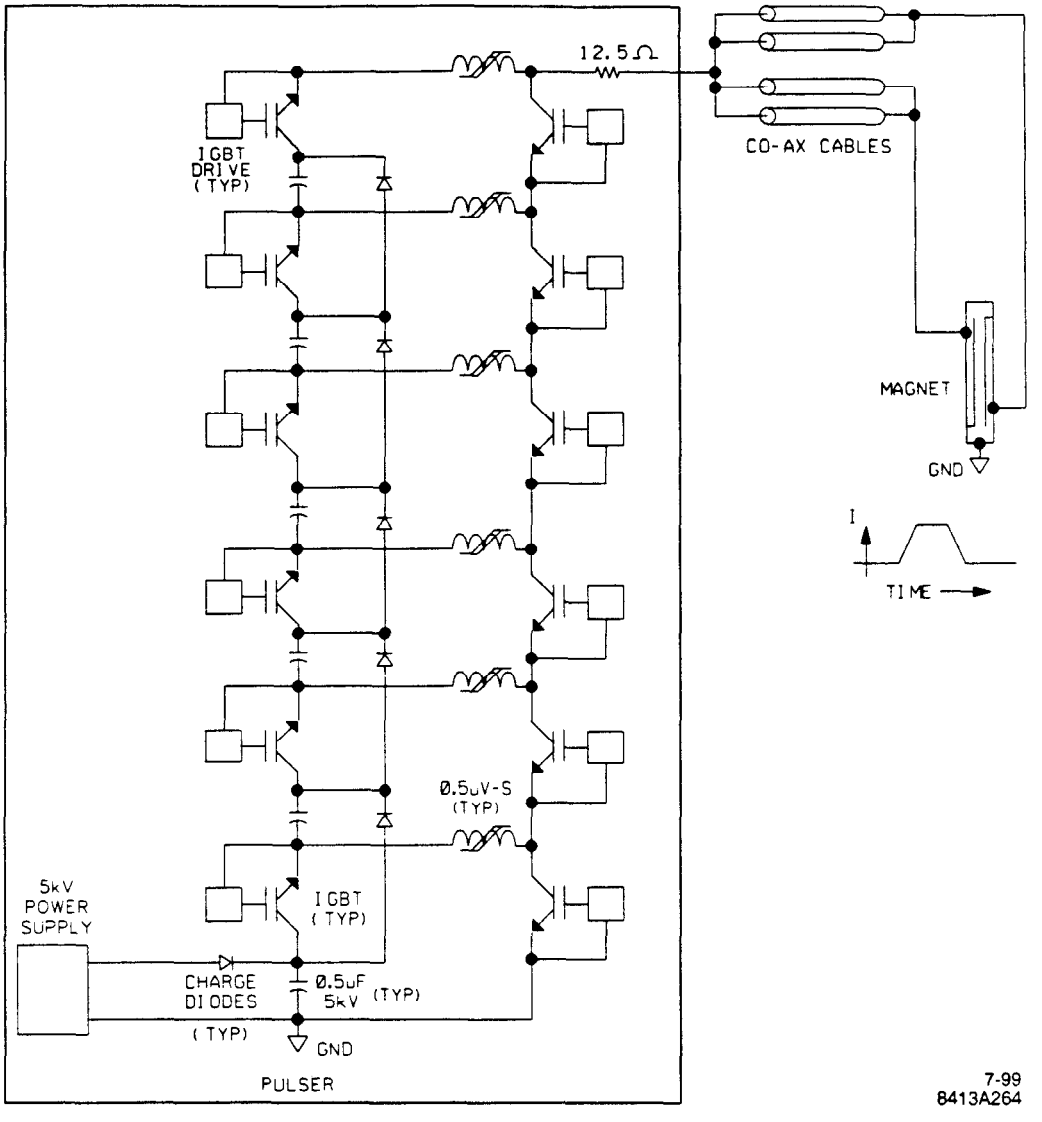

Figure 4.77 Kicker pulser schematic. Baseline pulse width is 750 ns.

4.6.5 Power Supply Control and Protection Systems

Off-the-shelf, commercially available power supplies do not meet the current stability requirements for many of the SPEAR 3 magnet systems. Therefore an additional current-regulating loop is provided for each main magnet. The power supply is located externally to keep it out of the harsh EMI and temperature environments found inside the power supplies. The loop consists of a single or multi-channel power supply controller and two zero-flux current transductors. One transductor forms a part of the current loop and the second transductor is used for monitoring and comparison. The new controllers also integrate the PPS and MPS safety systems into the power supply interlocks.

4.6.5.1 Single Channel Power Supply Controllers

A high-speed, digital, serial-data-link power supply controller and serial communication protocol was recently developed by SLAC for use on the PEP-II project [2]. Communication between the controller and the global computer system is carried on a twisted-pair cable. Analog power-supply

reference inputs and associated analog monitoring functions are done with 20-bit digital-to-analog converters (DACs) and analog-to-digital converters (ADCs). Internal calibration routines, which run while the power supply operates, correct for DAC/ADC offset, drift, gain, and linearity imperfections to produce the required output current stability and resolution. A microprocessor serves as the communications controller and as the intelligence for data I/O, calibration/diagnostic routines, and ramping functions. Several ramping functions (cosine, etc.) are available. Ramp rates can vary from 1 A/sec for some of the sextupole magnets to 15 A/sec for the dipole magnets. Each controller is quite small, physically occupying just one vertical unit of rack space. A signal input/output diagram of the connections between the global control system and the controller and between the controller and the power supply is shown in Figure 4.78. The single channel controllers are used for the unipolar power supplies listed in Table 4.35.

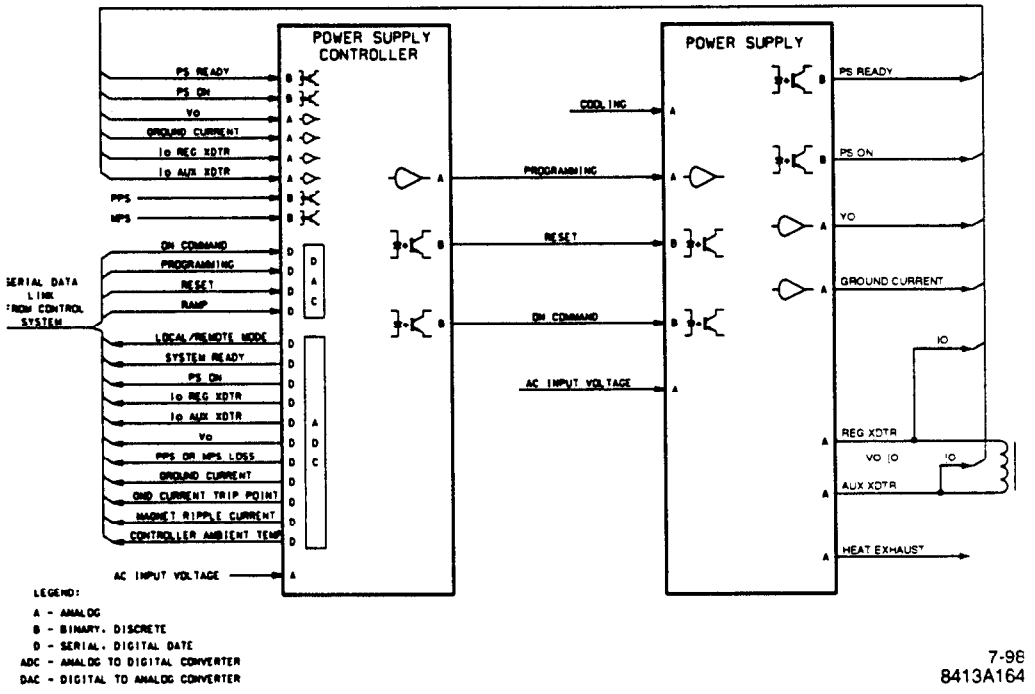

Figure 4.78 Power supply control signal block diagram.

4.6.5.2 Multi-channel Power Supply Controller

Multi-channel controllers will be used to control trim, corrector, and other small power supplies. These controllers will be based on the-PEP II design model [3] but will be developed to handle the high control signal update rates needed for SPEAR 3 corrector supplies (Section 4.8.1.1.1). In principle, the multi-channel controllers are similar to the single-channel controllers previously described, except that six DAC channels are multiplexed on one printed circuit board that mounts into a standard crate. The DAC in the multi-channel controller is multiplexed and accommodates up to eight corrector power supplies on a single PC card. The multi-channel controllers are used for the bipolar power supplies listed in Table 4.35.

4.6.5.3 Personnel Protection System (PPS) Integration

There are almost 80 power supplies that operate with voltages ≥50 V and/or currents ≥50 A. SLAC classifies these voltage and/or current levels as hazardous. This requires covering the magnet terminals, or interlocking the power supplies with the PPS. Covering the magnet terminals is unwieldy and expensive. Interlocking each and every one of the 80 or so power supplies is also

expensive, and there is some concern that due to the large number of power supplies, PPS certification will be difficult, time-consuming and expensive. Therefore instead of interlocking each individual power supply, the upstream AC distribution system is PPS interlocked to reduce the PPS interfaces to a manageable number.

Figure 4.79 shows two AC contactors associated with each 480 V switchgear. The use of two electro-mechanical contactors satisfies the PPS requirements for:

- 2 independent PPS input permit signals per system.
- In addition to receiving close command, each of the 2 contactors receives a separate input PPS permit (designated permit A and permit B). The power supply loads cannot be energized unless both PPS permits are present.
- 2 power breaks between the power source and the load.
- This requirement is satisfied when both of the 2 contactors are open.
- 2 independent read backs, 2 ways.
- Each contactor is furnished with a normally closed (NC) auxiliary contact that monitors the position of the main contacts (i.e., open or closed). Each contactor is also furnished with normally closed circuitry to detect the voltage downstream of the main contacts. This satisfies the requirement for status read back in 2 different ways---position and voltage. The load (power supply) is not considered safe until all read backs (A1, A2, B1 and B2) are all closed.

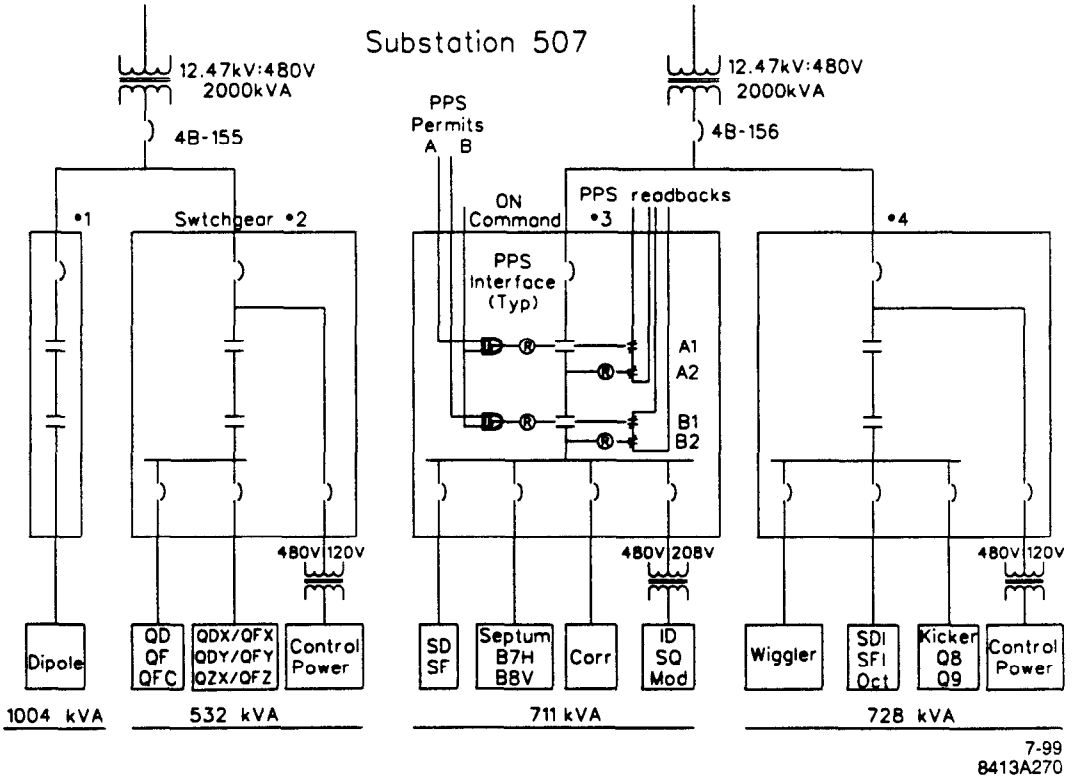

Figure 4.79 PPS control for magnet power systems.

As shown in Figure 4.79, control power for the power supply controllers and the power supplies will be obtained from the source upstream from the switchgear contactors. This will ensure that power supply status and fault information is preserved even when AC power is removed from the power supplies.

4.6.5.4 Machine Protection System (MPS)

The MPS consists of several protection subsystems (Section 4.9.2), one of which is the magnet cooling-water system. As shown in Figures 4.77 and 4.78, one of the several controller interlock ports can be used to turn off the power supply. This is accomplished by inhibiting the SCR or IGBT triggers if the MPS permissive is lost due to a problem with magnet overheating.

4.6.6 Bus and Cabling

In very broad terms, there are two types of DC power leads: reused water-cooled bus and new cable. Each of these is described below. Any DC power cable that is not reused will be removed to reduce heat, avoid cable tray overfill, and create space for new cables.

The cables for the Dipole, QD, QF and QFC strings will be transposed once around the ring to reduce the cumulative ground leakage current vs. distance profile.

A return conductor is run with the supply conductor in all magnet power circuits. This reduces stray field effects on the beam.

4.6.6.1 Reused Cables and Bus

The Dipole string and Wiggler magnets reuse existing aluminum bus since these magnets have the highest operating currents and thus make best use of this rather large conductor. It consists of 1 inch square bar with a 3/8-inch diameter water passage hole passing through its center and an outer rubber insulation. Although the insulation appears to be in good shape, it is conceivable that damage might exist in places not readily visible or apparent. Pre-commissioning hi-pot tests are necessary to ensure that the insulation is free from defects. Damaged insulation is easily repaired or replaced. Conductor damage occurring during the machine installation phase can be cut out and replaced. Replacement conductor can be obtained from the square bus that will be salvaged from SPEAR 2 or from the round, 1-inch diameter, water-cooled bus used on other SLAC projects and available from SLAC Stores. All reused cables are documented and tagged using the CAPTAR database [4]. Any other water-cooled cable that will not be reused will be removed.

4.6.6.2 New Cables

All the other DC magnet power systems not mentioned above employ new, type TC (Tray Cable) cable, as defined by the National Electric Code (NEC) [5], with 600 V, 90 C insulation and stranded copper conductors. Class C, or finer-stranded cable, is used to facilitate installation and to minimize magnet-winding stress. Sunlight-resistant and radiation-resistant insulation and jacket materials such as ethylene-propylene-rubber (EPR) and hypalon are used where appropriate. All new cables are documented and tagged using the SLAC CAPTAR database.

Single conductor cables are used for 1/0 AWG and larger conductor sizes. Multi-conductor cables are used for those circuits where the conductors are smaller than 1/0 AWG. All main magnet strings employ a return conductor for magnetic field cancellation so as not to distort the beam.

Single-conductor, #8 AWG cable was used to connect the old corrector power supplies to the correctors. New twisted-pair cable satisfying the new corrector magnet current needs will be used for SLAC 3. Twisted-pair cable reduces EMI emissions and obviates the need for more costly shielded-pair cable.

Cable capacities and cable-tray fill comply with the requirements of the NEC [5]. Where the requirements of the NEC are impractical to implement, then the guidelines contained in SLAC Safety Bulletin 37 [6] are followed.

4.6.6.3 Kicker Cables

New 5kV shielded cable, suitable for cable tray installation, will be installed for the new SPEAR 3 kickers.

4.6.7 AC Distribution for Power Supplies

AC power for the power supplies emanates from two 2000 kVA transformers as well as circuit breakers 4B-155 and 4B-156 (Section 6.3.5, Figure 6.6). All of these are housed in Substation 507, which is immediately adjacent to Building 118. Branch power is provided via 480V and 208V switchgear and panel boards. These are located inside Building 118, within sight of the power supplies. One 208 V feed is needed for some of the smaller (<5 kW) power supplies. The new Dipole Power Supply is efficient enough so that a 480 V input is adequate for its needs. This allowed removal of the existing 4160 V system. The AC distribution will be PPS interlocked, as described earlier in this section.

4.6.7.1 AC Power Consumption and Substation Requirements

As shown at the bottom of 4.63, the total power required by the SPEAR 3 power supplies amounts to about 3 MVA. Therefore, the existing 480 V power from the two 2 MVA transformers at Substation 507 are more than adequate for power supply needs.

4.6.7.2 Branch Circuits

All free-standing and rack-mounted power supplies have a circuit breaker located in the power supply for protection and turn-on/off purposes. Power supply racks also house branch circuit breakers for the individual rack-mounted power supplies. Figure 4.73 provides a front view of some power supplies and associated equipment, as installed.

AC branch circuits and circuit breakers for power supply feeds conform to the NEC [5]. The circuit breakers are lockable to comply with SLAC's Lock and Tag Program [7] that must be used during equipment installation and maintenance.

4.6.7.3 Transformers

The main AC feeds for the power supplies come from two 2000kVA transformers located in Substation 507, which is adjacent to Building 118. The control circuits are also fed from independent, dedicated transformers rated 480V:208/120V. This arrangement minimizes the conduction of power supply noise to control circuits and other sensitive components. To attenuate common-mode noise propagation among the AC lines, all transformers used for the power supply and control circuits employ electrostatic shielding between the primary and secondary windings.

4.6.8 Grounding

Equipment and circuit grounding addresses the three major issues of 1) personnel safety, 2) equipment protection, and 3) electronic circuit noise reduction. The three issues are addressed below:

4.6.8.1 Safety and Protection

The power supplies are grounded in two ways. First, the incoming AC power supply carries a ground cable. Second, the power supply enclosures are connected solidly to the building's ground grid. The safety grounds must ensure that the voltages among equipment enclosures are kept to safe values (< 50V during normal operation and under fault conditions). Ground conductors are sized in accordance with NEC, thus keeping the ground-circuit impedance low and voltages within safe

limits[5]. Routing the ground conductors with (and alongside) the power conductors minimizes the loop area and keeps the inductances low.

At several places in Building 118, ground pigtails rise from of the concrete floor. These existing ground pigtails will be extended to form a ground bus all the way around the periphery of Building 118. Vertical conductors will be attached to this perimeter system and carried up into the overhead cable trays for final connection to the power supplies or power supply racks.

A 2/0 AWG copper grounding cable currently encircles the ring. New cable will be installed to fill in gaps, thus making the cable contiguous around the entire ring, including the East and West Pits.The ring's ground cable will be connected to the frame of each magnet.

4.6.8.2 Electrical Noise Reduction

Proper grounding also reduces electrical noise. This is accomplished by the use of single-point grounds on circuit boards as well as the reduction of capacitive coupling among circuits through the extensive use of ground planes around traces. Optically coupled circuits are also employed to break ground loops.

4.6.8.3 Ground Fault Detection and Protection

Each unipolar power supply/controller contains ground-fault detection-and-protection circuits. The trip settings of these circuits are adjustable, but they are typically set to turn off the power supply when the ground current exceeds 25 mA. Ground fault detection and protection is achieved at the bulk power supply level for the smaller, more numerous bipolar power supplies.

References

[1] "New 3.3kV, 1200A IGBTs," Eupec advertisement appearing in PCIM Magazine, Page 5, March 1998.

[2] P. Bellomo, L. Genova, T. Jackson, D. Shimer, "Progress on PEP-II Magnet Power Conversion System," UCRL-JC-126951, June 4, 1996.

[3] R. Olsen, "PEP II 16-Channel Corrector Controller Using Bitbus," I.E.E.E. Particle Accelerator Conference, Vancouver, Canada, June 1997.

[4] CAPTAR is the SLAC Cable Plant Tracking Database designed using the commercial Oracle relational database program.

[5] National Electrical Code, Articles 250, 310, 318 and 340, 1997 Edition.

[6] SPEAR/SLAC ES&H Bulletin 37 "Cable Installation."

[7] SLAC Lock And Tag Program For The Control Of Hazardous Energy, Document Number SLAC-I-730-OA10Z-001.

4.7 Beam Stabilizing Systems

SPEAR 3 will incorporate a feedback system to stabilize the beam's closed orbit. The low-level RF control system (Section 4.5.6) will suppress longitudinal common-mode ("Mode Zero") bunch motion. The low impedance of both the vacuum-chamber and the mode-damped RF cavities make a longitudinal, multibunch feedback system unnecessary for operation at 500 mA. Calculations show that the head-tail damping provided with a >0.2 normalized chromaticity will be sufficient to stabilize transverse beam motion driven by the resistive wall impedance or transverse HOMs. Thus, a transverse, multibunch feedback system is also unnecessary (Section 3.6.2.2). Nevertheless, transverse kickers and pick-ups will be installed for diagnostic purposes (Section 4.8.2.3).

- Appendix A.4 presents the specifications for a hypothetical transversal feedback system using these components.

4.7.1 Orbit Feedback System

The orbit feedback system for SPEAR 2 [1] will be expanded to accommodate 92 installed BPMs and 108 orbit correctors (54 horizontal, 54 vertical). The feedback system acts to suppress orbit motion in a bandwidth of approximately 100 Hz. It will handle temperature-related, long-term orbit-drift, and girder-vibration modes. The system also uses vertical photon BPMs (photo emission blade monitors or split-anode ion chambers [2]) installed many meters from the source points in the beam lines. Table 4.16 gives orbit feedback specifications. A functional diagram of the orbit feedback system appears in Figure 4.80, and hardware configuration is depicted in Figures 4.84 and 4.86.

Table 4.37 Orbit feedback system specifications.

Number of electron BPMs	92
Number of photon BPMs	11 (vertical only); 16+ in the future
Number of correctors	54 vertical, 54 horizontal
Correction algorithm	SVD (weighted least squares)
Feedback processor	TI C6X DSP
Feedback filter	PID
Cycle time	0.5 ms
Bandwidth (3 dB closed-loop)	100 Hz
Orbit stabilization goal (dipole/ID)	5/5 mm rms vert, 15/40 mm rms horiz
Attenuation of 5 Hz / 25 Hz noise	20 dB / 6 dB

Most of the new hardware components for the orbit feedback system are associated with the BPM processing system (Section 4.8.2.1) and the corrector magnet power supplies (Section 4.6.3.1). The intermediate frequency (IF) output from each of the 92 RF-IF converters used to detect BPM button signals will be processed digitally by VME-based, 8-channel IF processing modules. Each of four remote BPM processing stations distributed around the ring contains three modules, resulting in a total of 24 processing channels per station. Each BPM station uses a VME digital signal processor (DSP) module (32-bit, floating point TI TMS320C6X) to acquire and process the BPM signals before transmitting them to the central feedback processing VME crate in the SPEAR Control Room. A high-speed reflective-memory data link permits transfers at rates up to 1 Gb/s between central and remote processing crates.

The central-processing DSP executes orbit monitoring and feedback algorithms. It also generates control signals, which are transmitted to the corrector power supplies via new, high-speed fiber-optic links (Section 4.8.1.1.1). Every 0.5 ms, orbits are acquired and corrector control signals are updated (resulting in a 2 kHz update rate). Software development is needed for both the DSP and the SPEAR control system.

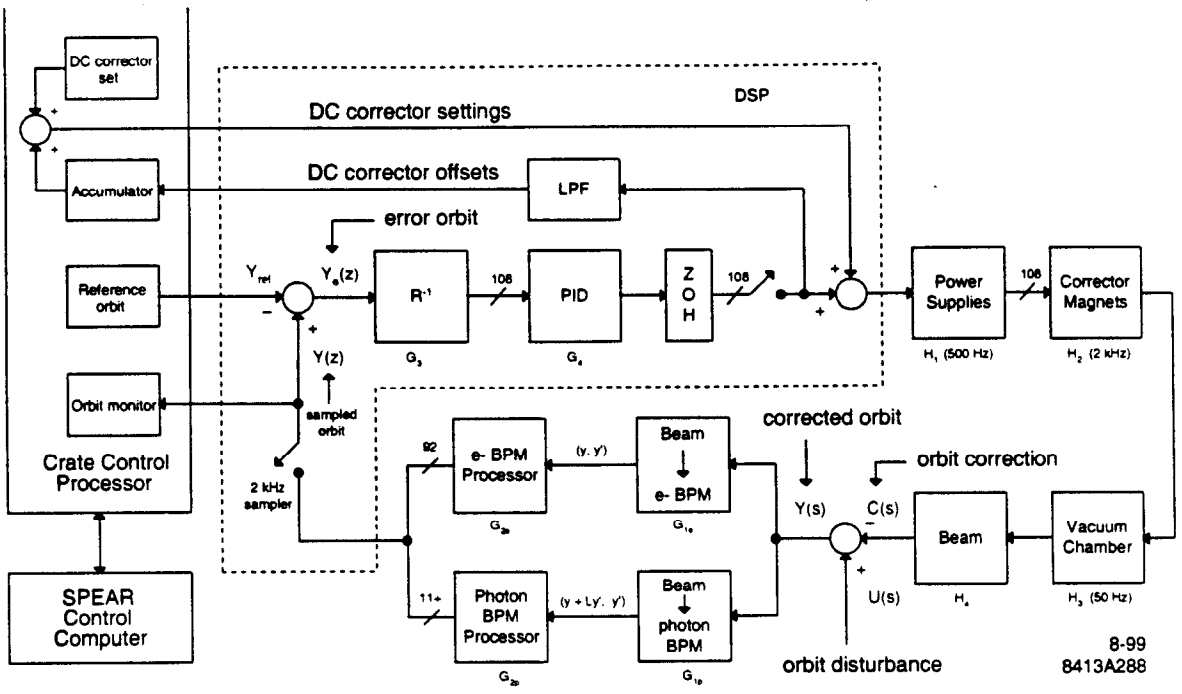

Figure 4.80 Functional diagram of the SPEAR 3 orbit feedback system.

4.7.1.1 Orbit Feedback Algorithms

The orbit feedback correction algorithm uses the measured corrector-to-BPM response matrix to compute orbit corrections as a function of detected orbit error. As Section 3.4.5 details, the detected orbit error vector multiplied by the inverted response matrix produces an orbit correction vector for each feedback cycle. The correction vector passes through a digital PID filter prior to transmission to the orbit correctors. Re-programming the feedback DSP can produce more sophisticated feedback processing, including state-space feedback. Dispersion orbit errors caused by changes in ring circumference (e.g. due to temperature) are corrected by adjusting the RF frequency on a slow timescale with the feedback system.

Control console windows facilitate the selection of BPMs and correctors for inclusion in the feedback system. The console also allows modification of both the system matrix and the digital processing properties.

4.7.1.2 System Bandwidth

Closed-orbit fluctuations caused by girder and magnet motion are anticipated for bandwidths extending from the very low frequency (days), all the way up to the highest significant magnet-girder resonance frequency (<50 Hz). The next significant disturbances are expected to occur at 60 Hz (and its harmonics) arising from power supply ripple. The closed-loop, 3 dB bandwidth of the orbit feedback system will be on the order of 100 Hz, so as to suppress girder-related motion at frequencies below 60 Hz. The system is not intended to respond strongly to 60 Hz orbit noise. Instead, power supply ripple will be reduced so as to attenuate noise at harmonics of 60 Hz.

A feedback cycle rate of the order of 1 kHz is required for a PID feedback filter to produce an open-loop, 0 dB-gain crossover frequency on the order of 100 Hz. The feedback system "plant" consists of 1) corrector power supplies, 2) corrector magnets, 3) the vacuum chamber, 4) the beam itself (for

time scales less than the beam's damping times), and 5) the orbit monitoring system. Table 4.38 lists the 3-dB bandwidth specifications for these components in SPEAR.

Table 4.38 Orbit feedback plant component bandwidths.

Component	3 dB Bandwidth
Corrector magnets	1 kHz
Corrector supplies	500 Hz
BPM processor (2 kHz orbit rate)	500 Hz (ϕ = -45°)
Vacuum chamber	40 Hz horizontal correction 100 Hz vertical correction
Beam (damping τ_x = 4.2 ms, τ_y = 5.1 ms)	>> k Hz

The dominant pole in system response comes from the vacuum chamber, which sustains eddy currents that attenuate the penetration of AC magnetic fields. CuproNickel™ (CuNi) inserts installed at the top and bottom of the copper chamber at corrector sites substantially reduce the attenuation of eddy currents by virtue of their higher resistivity (20 times that of copper). This raises the effective vacuum chamber pole frequencies by a factor of about three. Eddy current attenuation is intrinsically lower for vertical correction, because the vacuum chamber has a relatively low effective surface area for intercepting the horizontal magnetic field.

The next significant pole comes from the 500 Hz corrector magnet power supplies (Section 4.6.3.1) The 50 V, 30 A corrector supplies have sufficient voltage to change corrector strength in steps of 10% (or more) of the full-scale deflection, within the 3.6 ms rise time associated with a 100 Hz bandwidth. Such a step response is induced by a fast orbit transition of the order 100 mm, which represents a relatively extreme disturbance. The expected AC orbit disturbance amplitudes are an order of magnitude less than this, and they are likely to be band-limited to frequencies below 100 Hz.

The bandwidths of plant components have been specified to avoid poles within the feedback system bandwidth of 100 Hz. This eliminates the need for a lead filter, which, despite compensating for poles in the 100 Hz range, would also amplify higher-frequency control signal components and increase noise propagation throughout the system.

Figure 4.26 presents the calculated closed-loop gain and noise-attenuation of the feedback system as a function of frequency, assuming a 2 kHz feedback-cycle rate and the signal sampling times given in Figure 4.39.

As discussed in Section 4.8.2.1, the four button electrodes for each BPM vacuum assembly are multiplexed into a single RF-IF converter module. They cycle through all four buttons every 62.5 μs. It has been shown that the time-skewing of orbit sampling caused by this multiplexing over a 0.5 ms feedback cycle does very little to affect the performance of the digital feedback system at frequencies less than 100 Hz [3]. Sampling frequencies will be adjusted to avoid the aliasing of high-frequency beam signals into the operational bandwidth of the feedback system. This includes noise from the switching power supplies, the 720 Hz SCR-regulated dipole supply, and the synchrotron and betatron oscillations.

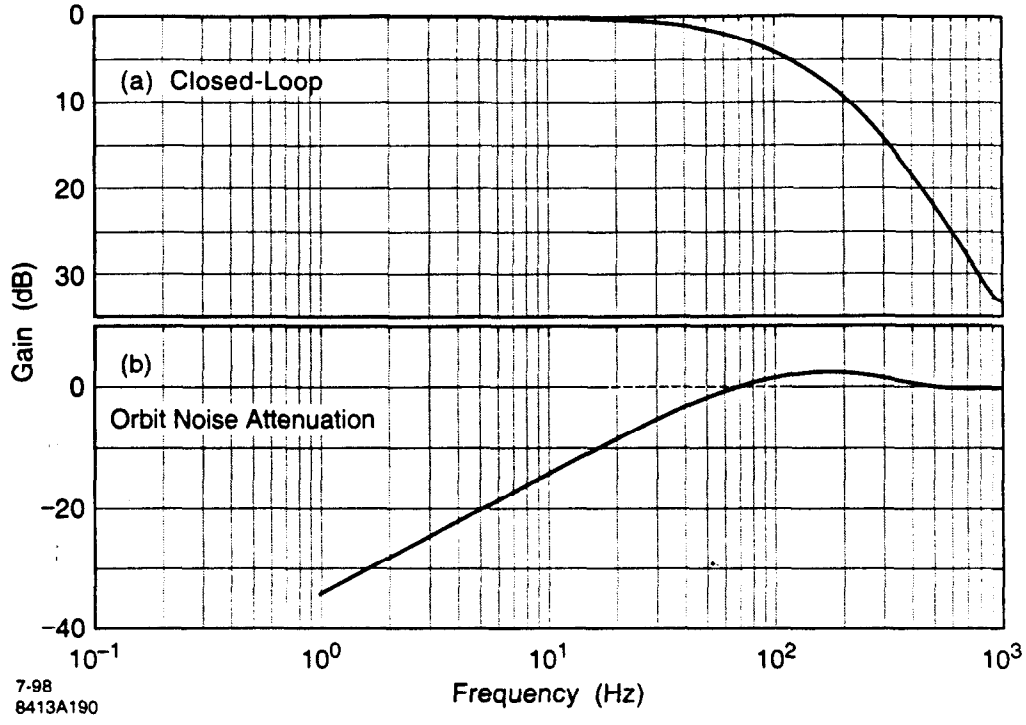

Figure 4.81 Orbit feedback closed-loop frequency response and orbit attenuation with parameters specified in Table 4.39.

Table 4.39 BPM button data acquisition cycle times for an orbit update period of 0.5 ms.

Parameter	# Turns	Time (μs)
data acquisition period / button / cycle	18	14.1
switch transient time / button	2	1.6
4-button cycle period	80	62.5
# cycles / 0.5 ms orbit update period	8	500
# averages / button / 0.5 ms orbit update period	144	112.5

4.7.1.3 Feedback System Performance

The SPEAR 3 orbit-position stability goal is 15 μm rms horizontal and 5 μm rms vertical at the dipole source points, and 40 μm rms horizontal and 5 μm rms vertical at the insertion device source points (Table 3.22). Such stability is achieved if the beam is stabilized in the electron BPMs to levels shown in Table 4.40. With this degree of positional stability at the electron BPMs, angular orbit stability will be maintained to <20 μrad horizontally and <5 μrad vertically. These values fall well within the tolerances for dipole and wiggler source points specified in Section 3.3.1. Vertical angular stability increases to about 1 μrad (the stability needed for future undulator sources) when the beam is stabilized to 10 μm at the photon BPMs (located approximately10 m from the source).

Table 4.40 The orbit stability at BPMs needed to meet the source-point stability requirements specified in Table 3.22.

BPM	Horizontal Stability (rms)	Vertical Stability (rms)
Straight section	<40 μm	<5 μm
Mid-girder	<35 μm	<5 μm
Dipole	<13 μm	<5 μm
Photon monitors	NA	<10 μm

The ability of the orbit feedback system to meet the stabilizing requirements for low-frequency orbit distortion depends primarily on the 1) resolution, 2) stability and 3) noise content of the BPMs and correctors. Other factors include the accuracy of the measured corrector-to-BPM response matrix and the relative weighting of matrix terms that determine the balance between global and local orbit correction. At higher frequencies, feedback performance also depends upon matching the magnetic field frequency response within the vacuum chamber, as determined primarily by the effects of chamber eddy currents. To achieve the intended correction bandwidth and to maintain a stable feedback loop, the frequency response of these components will be matched beyond the system's 100 Hz bandwidth.

The primary limitation upon feedback-system performance in SPEAR 3 is expected to arise from the low-frequency motions of the electron and photon BPMs. Such perturbations emerge when accelerator components change temperature. Electron BPM assemblies tend to shift in response to temperature changes in not just the vacuum chamber, but also the supports upon which the BPMs themselves rest. Thus, supports are being designed to limit motion to the levels specified in Table 4.40.

The intensity-dependence of the electron and photon BPMs also limits feedback performance. The goal for current dependence in the electron BPM processor is <3 μm for a factor of two decay in current. Dipole and wiggler beam line photon monitor intensity dependence is on the order of 10 μm over this current range. For future undulator beam lines, radiation from upstream and downstream dipoles overlaps with the undulator radiation and can cause significant intensity dependence in photon monitors [4]. Highly stable electron BPMs, mounted on supports featuring temperature coefficients low enough to limit their motion to approximately 10 μm horizontally and 3 μm vertically, will be used in the straight sections for these IDs to achieve the required microradian angular orbit stability. New undulator photon monitor technologies will be explored to overcome the dipole radiation problem [5].

The feedback system will suppress the orbit instability caused by girder motion to sub-micron levels. High-frequency orbit noise introduced by the 2 kHz stepping of corrector supplies will also be kept to sub-micron levels by limiting incremental step size with the feedback-compensation filter.

In addition to the orbit feedback system, many of SPEAR 3's focused beam lines will be equipped with mirror-angle feedback systems that stabilize the vertical beam position (at experimental stations to the micron level, as demonstrated on SPEAR 2). These systems will stabilize residual shifts in beam-position that have not already been fully suppressed by the orbit feedback system.

References

[1] R. Hettel et al., Proceedings of the 1996 European Particle Accelerator Conference, Sitges, Spain, June 1996, p. 1931.

[2] R.O. Hettel, Nucl. Instr. and Methods in Physics Research A266, pp. 155-163, 1988.

[3] I. Linscott, internal SSRL note, June 1998.

[4] J.N. Galayda, Y. Chung, R.O. Hettel, "Orbit Stabilizing and Multibunch Feedback Systems," chapter 13 of "Synchrotron Radiation Sources – A Primer," edited by H. Winick, World Scientific Publishing Co., Singapore, 1994, p. 352.

[5] J. Arthur, R. Carr, internal SSRL communication.

[6] T. Rabedeau, internal SSRL communication.

4.7.2 Mode Zero Longitudinal Feedback System

Noise produced by the RF accelerating system can cause longitudinal oscillations in the beam. Noise that occurs at the fundamental frequency of the RF affects all beam bunches equally. The resulting oscillations are common-mode, or rigid-body, oscillations. Taken in consideration of possible higher-order motions, this motion is termed "Mode Zero".

SPEAR 3 will employ an active feedback system to damp the Mode Zero longitudinal oscillation of electron bunches. The system (Figure 4.82) employs a time-domain approach, which measures the energy oscillation of each bunch by measuring each bunch's instantaneous phase with respect to the accelerating frequency. Currently, the system is being commissioned as a multi-mode diagnostic device for SPEAR. The system will be extended by feeding a phase-correction signal to the phase-control loop of the low-level RF (LLRF) electronics for the klystron amplifiers (Section 4.5.6). This system will be completed prior to the SPEAR 3 project.

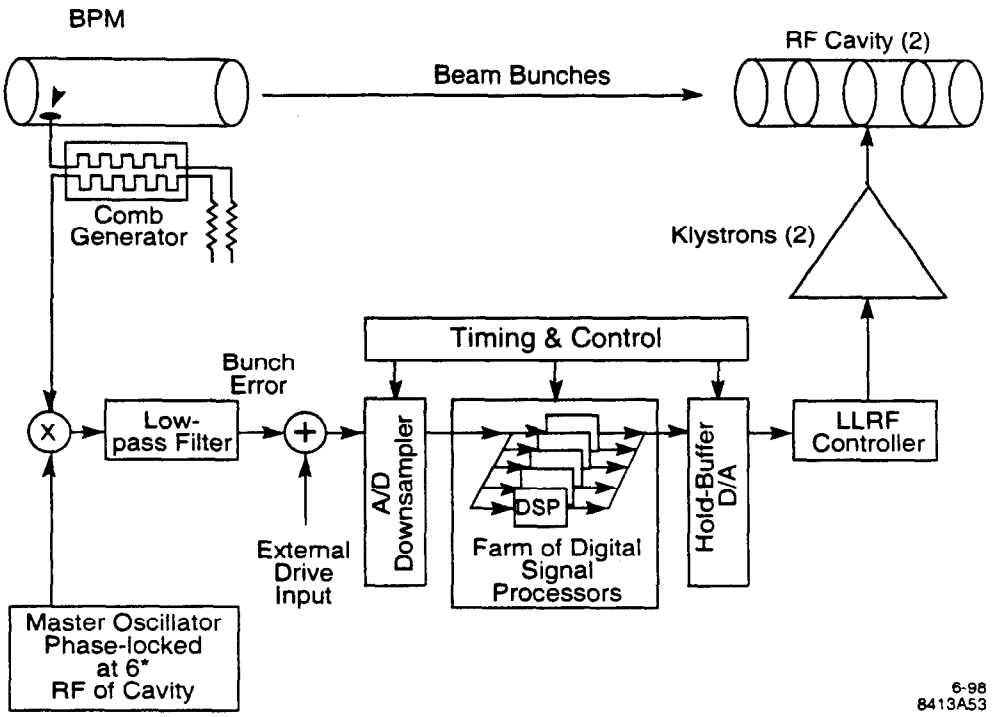

Figure 4.82 Mode Zero longitudinal feedback system, using the PEP-II longitudinal mode processor.

The longitudinal bunch-phase monitor (Section 4.8.2.10) will be used to produce the Mode Zero error signal, which is derived from the beam signal from a four-electrode, 52 mm, stripline detector (Section 4.8.2.3). For each bunch that passes the detector, a comb-generator filter generates a tone-burst at a harmonic of the ring's revolution frequency. The burst is short enough (less than 2.8 ns in SPEAR) to permit unambiguous, individual bunch measurements. The signals are then phase-detected, and the phase error is digitized. The data is directed to the correct DSP channel according to its bucket number and turn number. A hold buffer stores the most recently computed phase value for each bunch. The buffer drives a fast DAC, converting at the bunch's crossing frequency. This signal is available in the control room, and application software exists to display the motion.

The effectiveness of this system was demonstrated experimentally in SPEAR during accelerator physics studies in 1995 and 1997. Together with the mode-damped RF cavities, the system obviates the need for a longitudinal multibunch feedback system for SPEAR 3 operations at 500 mA.

4.8 Instrumentation and Control System

4.8.1 Computer Control System

The SPEAR control system (Figure 4.83) consists of two central computers–one for the storage ring, and the other for the injector. CAMAC and VME crates are used as front-end standards. In each CAMAC and VME crate, intelligent crate controllers manage the interface modules. The X-Window-based operator consoles run on workstations, X-Terminals, and PCs. An EPICS protocol channel-access interface will permit use of high-level EPICS applications and graphics-interface software used by the VMS-based storage ring and injector control systems.

The SPEAR 3 control system will be an expansion of the existing SPEAR control system. This minimizes the time needed to commission the control system itself, as well as the time needed to retrain accelerator physicists and operators. Some areas require the replacement or extension of certain hardware. All existing application software will be reviewed and upgraded to match the new hardware components.

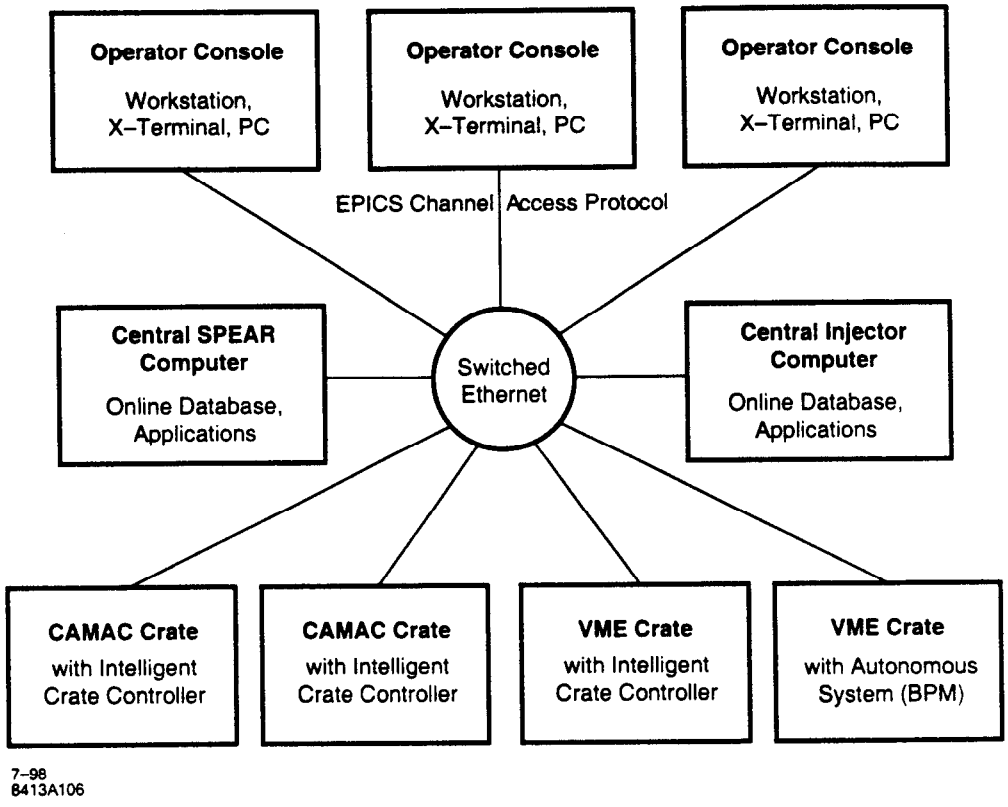

Figure 4.83 SPEAR computer control system architecture.

4.8.1.1 Front-End Hardware and Interfaces

Most of the SPEAR control system's hardware interfaces exist in CAMAC crates, and will be reused for SPEAR 3. New interface components include those for 1) power supplies, 2) the expanded BPM and orbit feedback systems, and 3) the RF system (Section 4.5.6). In addition, SPEAR 3 will use local crate processors extensively to handle many new control and data-logging functions.

4.8.1.1.1 Power Supply Interfaces

New SPEAR 3 power supplies will have intelligent controllers (Section 4.6.5) that communicate digitally with the SPEAR control system, replacing the existing analog interfaces.

The power supply controllers come from the PEP-II design. These BITBUS-based controllers will be modified to replace obsolete microprocessor components.

The 108 horizontal and vertical correctors belonging to the system need to be updated at very short intervals (approximately 0.2 ms) (Section 4.7.1). This corresponds to a data rate of at least 13 Mbit/s (assuming an 8-bit address for each supply and 16-bit setpoint values). Data rates of more than 100 Mbit/s are required to handle this much raw data, plus overhead, which includes framing, error detection, and also the readback data that must be returned from the power supplies for status

monitoring. Such data rates require dedicated, high-speed fiber-optic communication (>100 Mbit/sec) between the VME crate that manages orbit feedback and the power-supply controllers. State-of-the-art fiber-optic connections can be built using either the ATM standard (either 155 Mbit/sec or 622 Mbit/sec) or the Fiber Channel protocol (up to 100 Mbyte/sec). Further studies are necessary to determine the optimal communication-link technology for SPEAR 3.

4.8.1.1.2 BPM processing and orbit feedback interface

The expansion of the orbit feedback system (Section 4.7.1) requires 92 digital IF processors, each of which produces a 32-bit IF-amplitude word every time the beam completes a revolution around the ring (781 ns). To process this much data, DSPs distributed at remote BPM processing crates have to coordinate with the central VME crate that controls orbit feedback (Section 4.8.2.1). The remote data-acquisition DSPs calculate the beam's horizontal and vertical positions from the raw BPM-button information. This data is passed via VME backplanes and high-speed communication links to the central feedback-calculation DSP. Calculated corrector settings are transferred to the corrector power supplies by high-speed, digital controller modules (Section 4.8.1.1). All the DSPs work in a pipelined scheme to achieve an overall feedback cycle time of 0.5 ms. The software for the existing BPM processor, which already performs the basic functions, will be rewritten to accomplish this highly parallel undertaking.

The orbit feedback system also provides highly averaged beam-position data for orbit display and analysis through the interface CPU to the SPEAR control system.

For special beam-diagnostic purposes the BPM-acquisition subsystem within the orbit feedback system can be used to measure and transfer turn-by-turn BPM information to the SPEAR control system.

4.8.1.1.3 Local Processors

The control, monitoring and fast data-logging capabilities of many SPEAR 3 systems, such as those for feedback and power supply regulation, will be implemented in local front-end CPUs and intelligent crate controllers, thereby improving system performance and reducing network and central host utilization. Local memory will be used to store fast records from multiple devices. These records can be block-transferred to the SPEAR control system for post-processing and analysis of component performance.

4.8.1.2 Control System Application Programs

Existing application programs for SPEAR 2 will be adapted to handle the new hardware and machine-lattice configurations. In some cases, new software will be required. Table 4.41 provides an overview of these programs.

Table 4.41 SPEAR control system application programs.

Application	Purpose	Remarks for SPEAR 3
Vgdisp	Vacuum Display	Add vacuum components
Gesa	Get and Save Archives	Define new configuration parameter sets
BPMscan	Collect BPM data	Increase number of configuration of BPMs
Lattice	Perform lattice calculations	Modify for SPEAR 3 lattice
Models	Simulate parameter settings	Modify for new magnets
BMPs	Create local bumps	Adapt to new magnet configuration
MPS	Collect MPS information	Adapt to SPEAR 3 information; define beam position monitoring system limits.
Orbit	Measure and handle orbits	Adapt to new BPM configuration and improve capabilities
Psramp	Ramp/standardize magnets	Adapt to new magnets/power supplies
AKPS	Power supply display	Adapt to new power supply configuration
Monitor	Monitor machine events and generate alarms	Greatly increase the number and acquisition speed of monitored parameters
Orbit Feedback	Orbit stabilization	Development of high speed BPM data acquisition and feedback algorithm in dedicated processors
QMS	Quadrupole modulation for measuring BPM offsets and lattice functions	New application
Orbit and vertical instability interlocks	Configure and monitor Orbit and Instability Interlocks	New applications

4.8.1.3 Databases

All SPEAR 3 design information, hardware configuration and calibration data, and machine optics parameters are stored in databases. A commercial database such as Oracle RDB provides a wide variety of standard applications to access and maintain the data.

The existing SPEAR and booster online databases will be extended to maintain all new parameters and devices.

4.8.1.4 Operator Interface and Consoles

Besides extending the existing graphic capabilities, new graphic applications are needed to better control and monitor SPEAR 3 systems and parameters. Well-developed graphical user interface applications from EPICS or other WEB-based sources as well as in-house applications will be run on X-Windows-based workstations together with PC-based systems and user consoles.

4.8.1.5 Computer Communication

All data communication between front-end systems, central systems, and consoles will be Ethernet-based. Wherever more stations are needed or a higher communication bandwidth is required, the existing network infrastructure will be upgraded (to Fast Ethernet or Gigabit Ethernet).

4.8.2 Beam Monitoring Systems

SPEAR 3's beam-monitoring systems track the following:1) beam position, 2) beam current, 3) ring tune, 4) injection efficiency, 5) synchrotron light, and 6) turn-by-turn bunch-phase space coordinates.

4.8.2.1 Beam Position Monitoring System

The SPEAR 3 Beam Position Monitoring system is composed of a network of 4:1 switched-button RF-IF Converter modules, one for each BPM, and a 92-channel digital intermediate frequency (IF) processing system (Figure 4.84). RF-IF Converter modules and IF Processors are located in four BPM processing stations distributed around the storage ring to reduce the BPM cable lengths. (Figure 4.85). BPM data from the remote stations is transmitted to a central processing station in the SPEAR Control Room. The central processor performs orbit feedback control algorithms (Section 4.7.1). BPM Processing System specifications are summarized in Table 4.42.

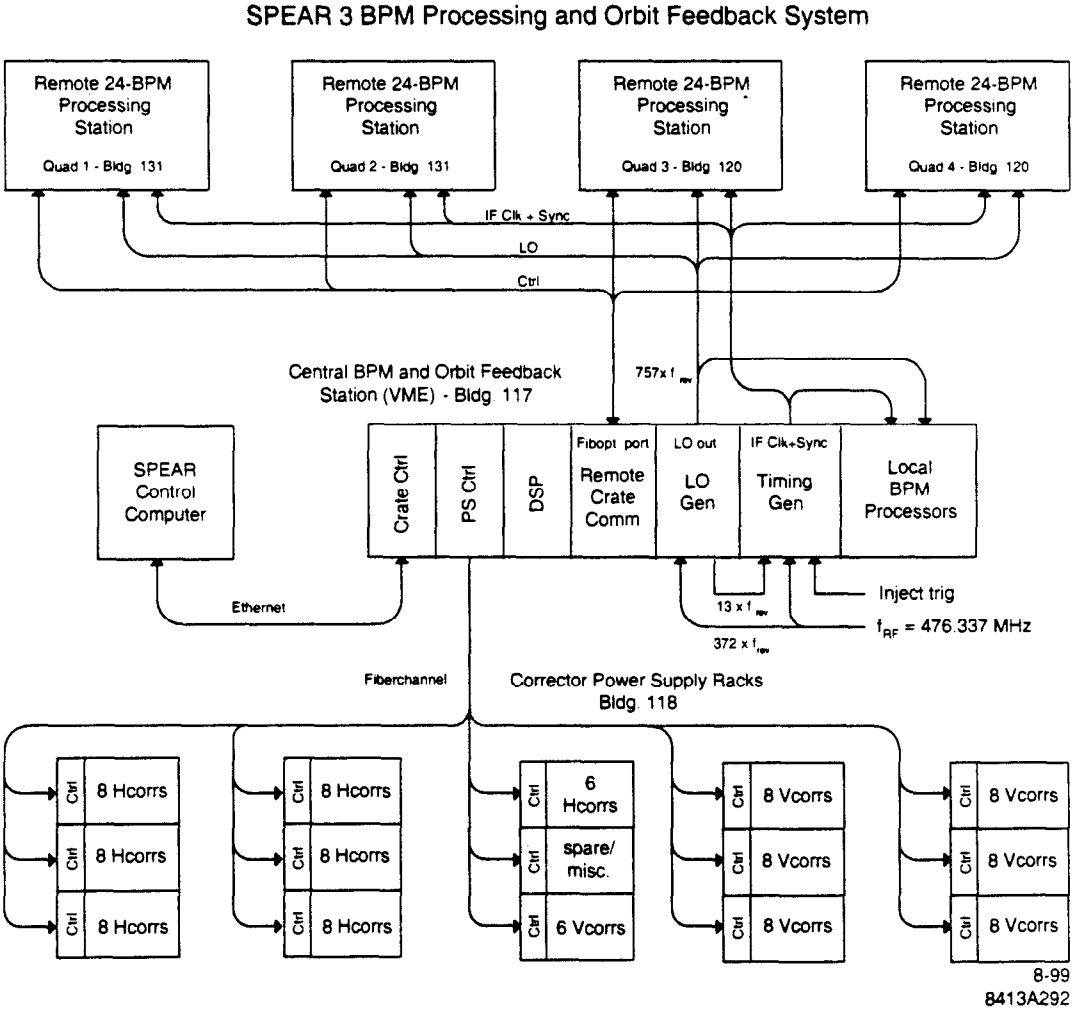

Figure 4.84 SPEAR 3 distributed BPM Processing and Orbit Feedback System.

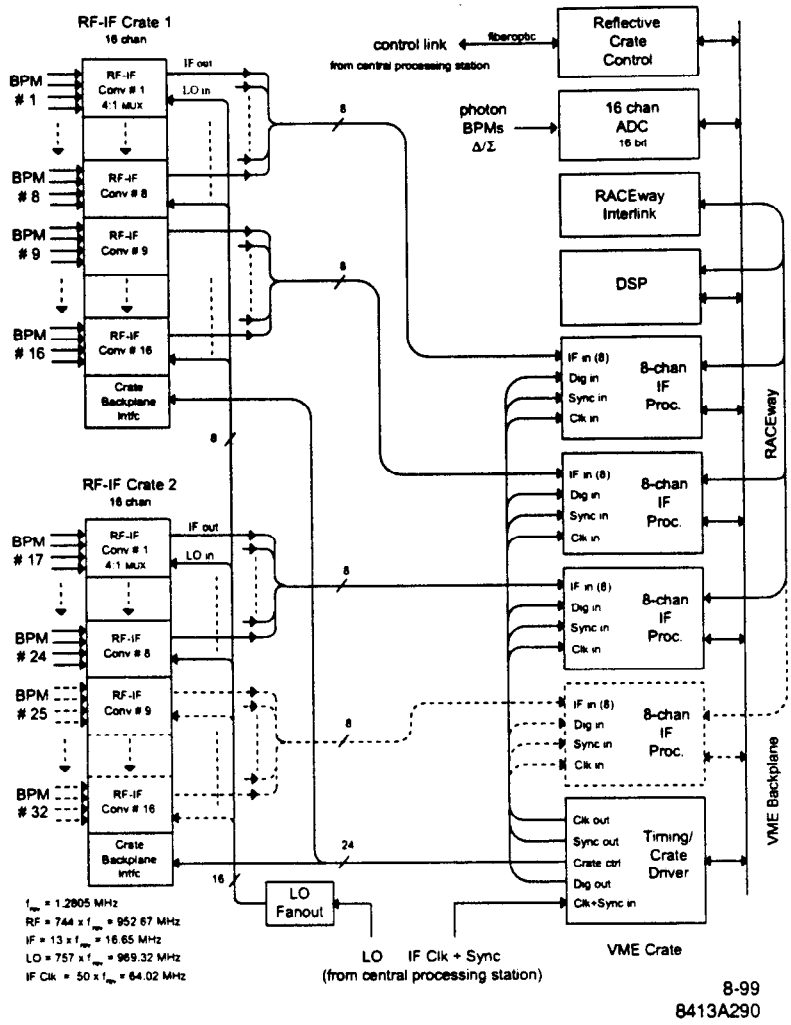

Figure 4.85 One of four remote BPM processing stations supporting up to 32 BPMs. 24 BPMs per station are planned for SPEAR 3.

Table 4.42 SPEAR 3 BPM Processing System specifications.

Number of BPMs	92
RF button multiplexing	4:1
Button mux switch period (min)	2.34 μs / button (3 ring turns)
IF processor multiplexing	none; 1 processor per BPM
Orbit update rate (max)	26 kHz (3 turns/button)
Ring RF frequency (f_{RF})	476.337 MHz
Ring revolution frequency (f_{rev})	1.2805 MHz
Ring harmonic number	372
RF processing frequency	952.674 MHz (2 x f_{RF})
RF-IF processor bandwidth (3 dB)	2.2 MHz
LO Frequency	969.320 MHz (2 x f_{RF} + 13 x f_{rev})
IF frequency	16.646 MHz (13 x f_{rev})
IF processor digitizing frequency	64.02 MHz (50 x f_{rev})
IF processor turn buffer depth (32-bit word)	>128 kWord
Nominal beam current range	1-500 mA
First turn resolution (.025 nC bunch; .03 mA)	1.8 mm
Turn-turn resolution (> 5mA)	12.7 μm
Resolution for orbit feedback (2 kHz orbit update; >5 mA)	1.1 μm (144 turns/button avg)
Resolution for 1 s orbit averaging (>5 mA)	0.045 μm (>5 mA)
Resolution parameter (<5 mA; no multiplexing)	0.056 μm-mA/$\sqrt{Hz}$
Current dependence (for x2 current change); stability over 24 h	<3 μm
Absolute BPM accuracy wrt quad center*	<100 μm
Dynamic current range (for <10 μm turn-turn resolution)	5 mA-500 mA (40 dB)
Position range	± 1 cm vert, ± 2 cm horiz

4.8.2.1.1 Processor Performance Goals and Limitations

Limitations on orbit monitoring resolution and accuracy will be dominated by offsets of the mechanical and electrical centers of each BPM assembly and mechanical instability of those offsets due to mechanical motion caused by temperature variations and girder motion (Section 3.4.1). The quadrupole modulation system (Section 4.8.3) will be used to establish and periodically check BPM electrical centers with respect to nearby quadrupole magnetic centers with an accuracy of <100 μm (Section 3.4.6). The 24-hour stability goal for BPMs near beam line source points is ~5 μm rms vertically and ~20 μm rms horizontally, or better.

Orbit errors due to BPM processing gain drift are minimized by multiplexing the four button signals for each BPM through a single processing channel. Variations in RF cable and input 4:1 multiplex switch attenuation are expected only over long term and will be periodically calibrated. Orbit errors due to processing dependency on beam current and fill pattern will be minimized with careful circuit design. The goal for beam current dependency is <3 μm for a decay from 500 mA to 250 mA.

4.8.2.1.2 BPM Vacuum Chamber Assemblies

Each BPM vacuum chamber assembly has four button-style electrodes - two mounted in the top and two mounted in the bottom of the chamber (Section 4.2.4). Table 4.43 summarizes button and BPM signal parameters.

The 1.5 cm button diameter provides efficient coupling to the 952.7 MHz processing frequency (second harmonic of the ring RF) while the center-to-center button spacing equalizes the horizontal and vertical beam position sensitivities (Figure 4.86). The button vacuum feedthrough design from the 2 A PEP-II Low Energy ring [2] will be used to limit HOM feedthrough losses to safe levels at 500 mA beam current.

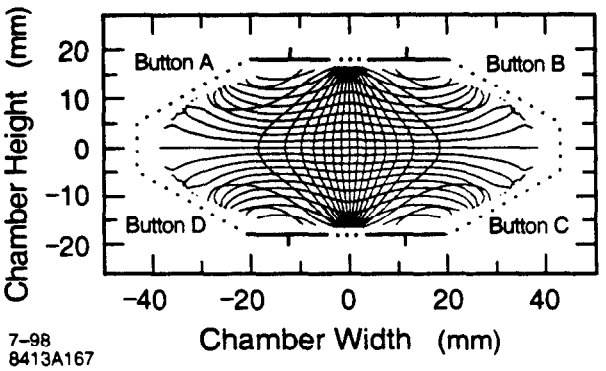

Figure 4.86 BPM spatial response pincushion.

Button impedance and signal power have been estimated both from circuit modeling and from measurements on the PEP-II buttons in a vacuum chamber having dimensions similar to the SPEAR 3 chamber. The resulting button transfer impedance is $|Z_T| = 0.8\ \Omega$ at 952.7 MHz, and the signal power is ~50 $\mu W/mA^2$ (2.0 W @ 200 mA and 12.6 W @ 500 mA) from the button closest to a beam mis-steered horizontally and vertically by 1 cm.

Table 4.43 BPM and button parameters.

Button diameter	15 mm
Button horizontal center spacing	24 mm
Button vertical spacing	36 mm
Total button signal power for centered beam	4.3 $\mu W/mA^2$
Button signal power @ 952.7 MHz, centered beam	0.084 $\mu W/mA^2$
Position sensitivity (near center)	0.5 dB/mm horiz. and vertical
BPM scale factor	Sx = Sy = 16.4 mm

4.8.2.1.3 RF-IF Converters and RF Cables

LMR400 coaxial cable is used to connect the BPM buttons to the RF-IF Converter modules via patch panels located near the Converter modules. Cable lengths range from ~10-50 m, attenuating the 952.67 MHz processing frequency by 1.3 to 6.6 dB; this signal loss also damps out-of-band standing waves in the cable that could act back on the beam. An additional 1 dB loss is introduced by the signal diplexers used for BPMs shared with the Orbit Interlock system (Section 4.9.2.4). The

4 buttons in each BPM are processed sequentially by a common RF-IF Converter to reduce differential processing offsets (Figure 4.87). Differential signal losses in the 4 BPM button cables and RF-IF Converter multiplexing switch are calibrated during system installation, and the information is used to equalize the gains of the 4 processing channels.

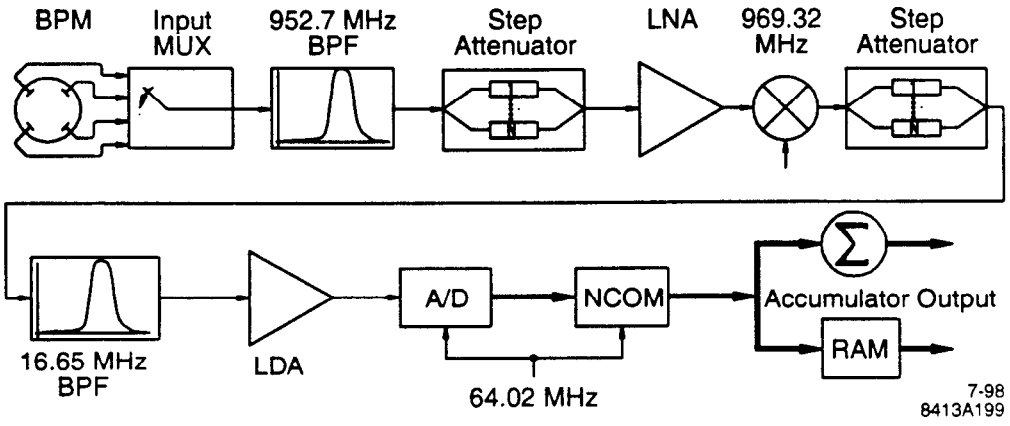

Figure 4.87 RF-IF Converter, followed by digital IF processing components.

The 952.67 MHz signal at the output of the 4:1 switch is filtered by a 1% bandpass filter, attenuated by a programmable attenuator for automatic gain control (AGC), amplified and mixed with a 969.32 MHz Local Oscillator (LO) signal to produce an IF of 16.65 MHz (13 times the 1.2805 MHz ring revolution frequency f_{rev}). The IF is filtered with a 2.2 MHz Bessel bandpass filter and amplified for detection by the IF Processor.

The time-domain responses of the filtered IF output to single-shot and single bunch beam modes are shown in Figure 4.92. A settling time of 2 revolution periods is required after switching buttons before the filtered IF output is ready for digital processing, so the most efficient duty cycle for signal averaging is obtained by processing a button signal for many turns before switching. The 4-button cycle time switching frequency is adjustable down to a minimum of 9.4 μs, or ~2.4 μs per button (3 ring turns). The button switch interval is limited by the 1-turn settling time for the IF output filter, the 1-turn clearing time in the IF processor digital filter, and a 1-turn IF data acquisition time.

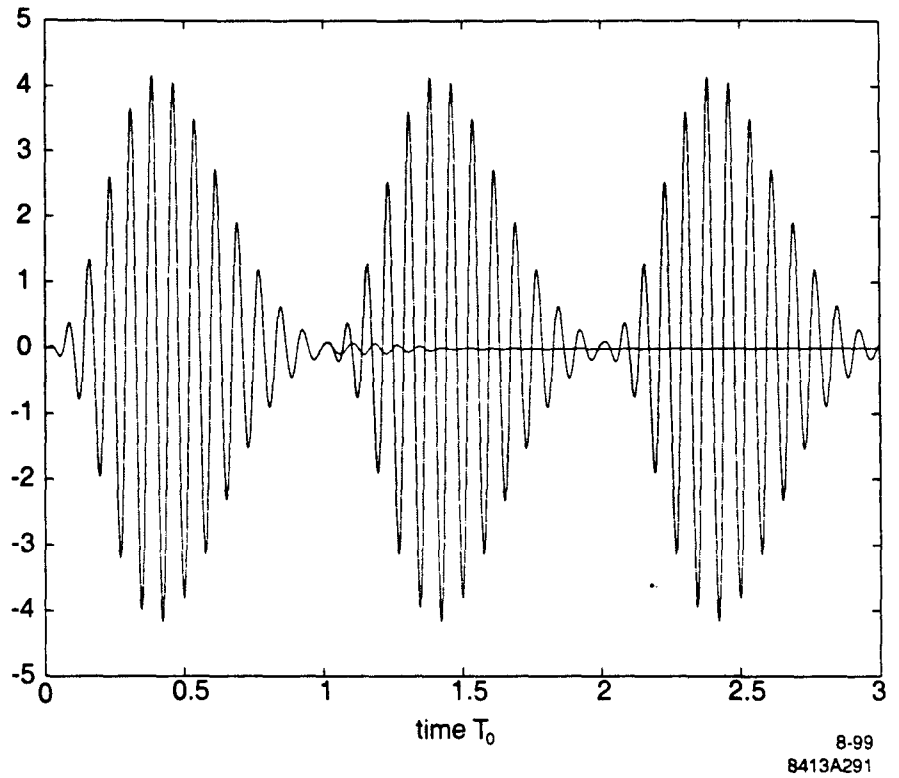

Figure 4.88 First-turn and turn-turn IF (16.65 MHz) output response from RF-IF Converter. T_0 = ring revolution period (781 ms).

Buttons are switched simultaneously for all RF-IF Converters around the ring, with the switch times synchronized to the IF Processor data acquistion cycle. A master synchronizing (Sync) signal is generated from the central BPM processing station and transmitted to the remote processors via the Timing/RF-IF Crate Driver modules, which in turn produce appropriately timed and sychronized button address and IF Processor data acquisition signals (Section 4.2.1.5.).

The turn-by-turn position measurement resolution of the RF-IF Converter as a function of beam current is shown in Figure 4.89. Resistive attenuators having 1 dB step size are used in the RF and IF signal sections of the Converter to regulate RF signal amplitude as a function of beam current at the RF mixer (via the computer-controlled loop) and to establish an optimal IF signal strength of 0.5 V (= 1/2 full scale) at the IF amplifier. For stored beam currents of <5 mA, the attenuators are fully withdrawn and the processing resolution, given by ~0.056 μm-mA/$\sqrt{\text{Hz}}$, decreases with current. For currents >5 mA, the attenuators are inserted, the IF output amplitude is at a constant maximum, and the turn-turn processing resolution remains constant at 12.7 μm. By averaging signals over N turns, processing resolution improves by $N^{-1/2}$. In particular, the processing resolution is 1.1 μm for the 144 turns that each button is averaged for the normal 2 kHz orbit update rate.

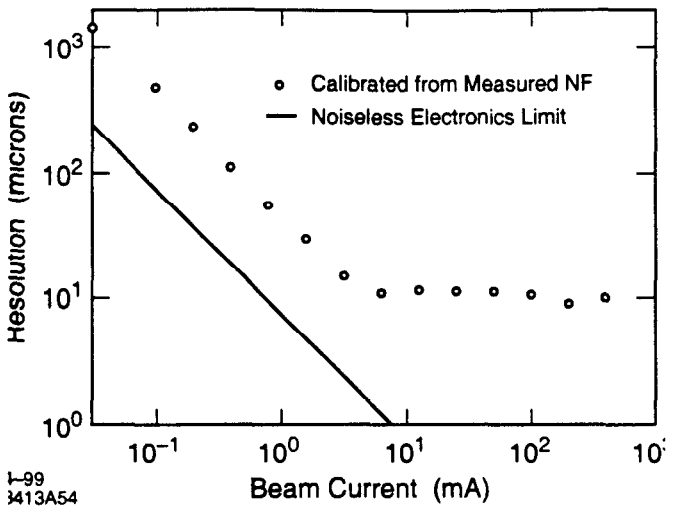

Figure 4.89 SPEAR BPM turn-turn resolution vs. beam current

The 952.7 MHz signal amplitude is proportional to beam current and is independent of bunch fill pattern. The sensitivity of the RF-IF Converter to fill-pattern is minimized by selecting the processing frequency to be a harmonic of the ring accelerating frequency and by careful circuit design.

4.8.2.1.4 IF Processor

Analog IF signals at each processing station are detected by nearby VME-based digital 8-channel IF Processor modules (three modules per crate for 24 BPM channels). A VME DSP module in each station acquires and further processes the data from the IF Processors via a fast mezzanine data bus. The DSP module also supervises the IF Processors and controls RF-IF Converter AGC attenuator settings via the VME backplane.

The 8-Channel IF Processor (Figure 4.90) digitizes the 16.65 MHz IF signal from each of its 8 inputs at a 64.02 MHz (50 x f_{rev}) sampling rate using a 14-bit ADC (12.2 effective bits) for each channel. The ratio of digitizing and sampled frequencies (50/13) is relatively prime, thereby reducing the effect of ADC quantization errors that could accumulate if the IF waveform were repeatedly sampled at the same points. Fifty digitized samples for each channel are processed once per ring revolution period by a numerically controlled oscillator-modulator unit (NCOM) to provide averaged in-phase and quadrature-phase (I&Q) vector component amplitudes of the IF with ~15-bit accuracy. The signal amplitude ($[I^2 + Q^2]^{1/2}$) and phase (16 bits each) can either be calculated every revolution period or the raw I and Q data can be averaged over many turns to increase resolution. The amplitude and phase information can be used to distinguish AM and FM signals arising from transverse and longitudinal beam oscillations, respectively.

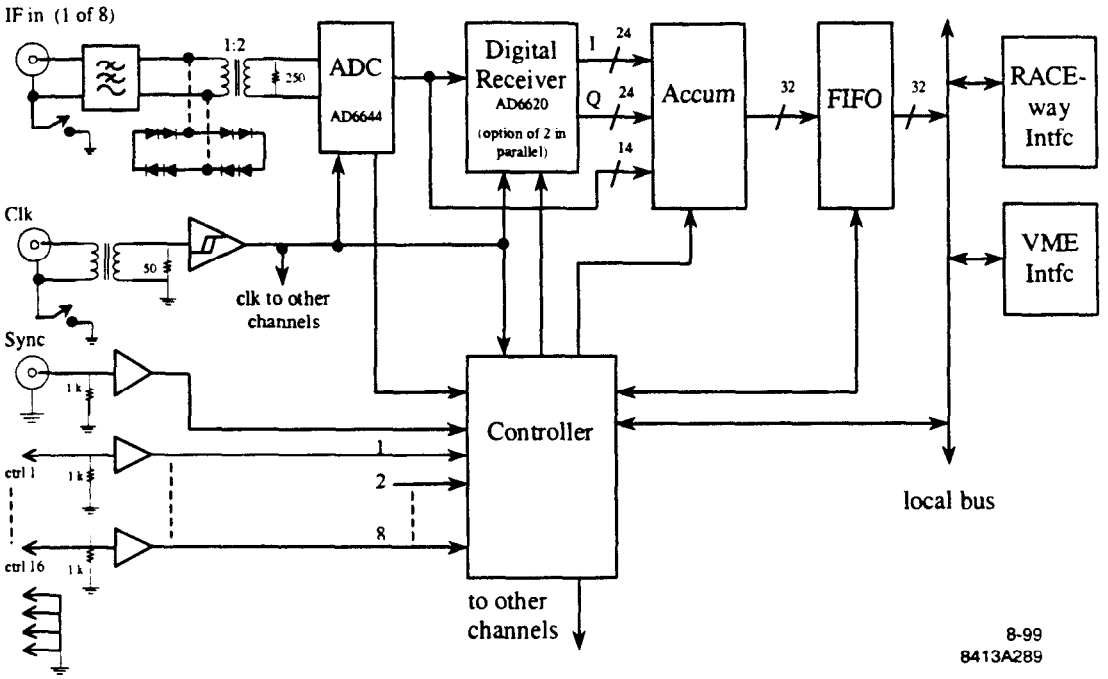

Figure 4.90 VME-based 8-Channel IF Processor.

32-bit button signal words from each of the 8 channels are stored in a FIFO buffer memory (≥128 kWords deep) that is read periodically by the external DSP module. The data, together with system status information, is passed over a high speed RACEway [3] mezzanine bus that can support data rates up to 160 MB/s. The 24-BPM RACEway data rate is ~220 kB/s for normal averaged orbit acquistion at a 2 kHz update rate. The full 160 MB/s data rate would be needed to sustain a turn-by-turn (1.28 MHz) orbit update rate from 24 BPMs, but this acquisition mode is not likely to be used. Instead, turn-by-turn data will be stored in the IF buffer memory and a data record of 128,000 turns will be read out by block transfer at a much lower data rate for post-processing. The DSP module also controls IF processing and readout modes via the VME backplane, and can acquire IF data from the backplane at a limited rate (<30 MB/s for the D32 format) as an alternative to the RACEway bus. The RACEway is a switched bus that requires a RACEway Interlink module in the VME crate to serve as a switching hub.

RF-IF Converter button address switching must be synchronized to the IF Processor data acquisition cycle to avoid ambiguous data. The IF Processor has an external Sync signal input for this purpose, common to the 8 channels. It also has a digital input port from which the current button address can be detected and used to label data records as needed. These timing and address signals are provided at each remote processing station by the VME-based Timing/Crate Driver module (Section 4.8.2.1.5).

The ADC clock ("IF Clock") must have very low jitter to avoid digitizing amplitude errors. The jitter must be <5 ps for a 64 MHz clock and 16.65 MHz IF to achieve full 14-bit (12.2-bit effective) performance from the ADC. The IF Processor contains high-performance circuitry to generate the digitizing clock from a low-jitter sine wave clock input signal.

The 8-Channel IF Processor is being developed jointly by SSRL and a commercial vendor for SPEAR 2. Production units will be available for SPEAR 3 procurement in FY 2000.

4.8.2.1.5 Timing/Crate Driver (T/CD) Module

The Timing/Crate Driver (T/CD) module in each remote VME crate receives and distributes the centrally-generated digitizing IF Clock and Sync signals for the IF Processors. It also receives button switching and attenuator setting information for the RF-IF Converters from the VME backplane and produces control signals to drive the RF-IF Converter crates. The centrally generated ring Revolution Clock (1.2805 MHz) is transmitted on the same cable as the digitizing clock and is used to synchronously clock BPM button address changes. Button address and BPM averaging cycle information is passed to the IF Processors from the T/CD module via front panel digital ports.

The sinusoidal digitizing IF Clock signals for up to four IF Processors in a remote VME crate are derived by amplifying and power-splitting the low-jitter sine wave generated at the central processing station. The cable carrying the centrally generated signal also carries the ring revolution clock sine wave, so a diplexer is required in the T/CD module to separate the two frequencies. The two clock frequencies are detected with Schmitt trigger circuits in the T/CD to produce the digital clock waveforms.

The Sync signals for up to four IF processors and the ring Revolution Clock can be delayed with respect to the centrally-generated Sync signal by programmable increments of the digitizing clock period (~16 ns). The delay function is used to synchronize data acquisition and button switching for all IF Processors distributed in the 4 remote stations. The Sync delay values are programmed via the VME backplane.

The T/CD module generates the BPM button address signals used to drive the RF-IF Converter crates by switching through a four-state look-up table of two-bit button addess codes at a programmable rate. The button address pattern stored in the look-up table is programmable over the VME backplane, as is the switching rate. The normal four-state switch pattern will switch sequentially through button A, B, C and D, but other patterns that permit continuous sampling of a single button or combinations of 2 or more buttons are possible. The switch rate is derived by dividing the IF Processor digitizing clock by a programmable value. The four-state switch sequence is reset to the first state by the Sync signal.

The T/CD module operates in several modes, including

- Measurement mode
  The preloaded button pattern is switched at the programmed rate. RF-IF attenuator settings are updated as necessary for AGC, with the opportunity to change the settings for one Converter module (nine bits attenuator setting + five bits RF-IF Converter address) at each change in button address.

- Configuration mode
  Control words are loaded over the VME backplane to specify button switch rate ($\geq$24-bit divisor for clock divider circuit), button switch pattern (eight bits, two bits for each of four switch cycle states), and IF Sync and Revolution Clock delays (6-bit word for each of four IF Sync delay generators, providing up to one revolution period delay in increments of the ~16 ns IF digitizing clock period).

- Diagnostic mode
  Permits system test and monitoring via the VME backplane.

A 32-bit control word is sufficient to specify mode (three bits) and mode data (27 bits) and to provide strobe and reset signals (one bit each).

4.8.2.1.6 LO, Clock and Sync Generators

Each RF-IF Converter requires a Local Oscillator (LO) mixing signal and BPM button address and attenuator control signals that are synchronized to the IF Processor data acquisition cycle. The IF Processor modules each require a sampling clock (IF Clock) and data acquisition synchronizing signal (Sync) coming from the central processing station. The LO, IF Clock, Sync signal and ring Revolution Clock timing signals will be generated centrally in the SPEAR Control Room and broadcast to the remote processing stations.

The LO signal frequency is 969.32 MHz (= (2 x 372 + 13) x f_{rev}) and will be produced using a phase-locked crystal oscillator having low phase noise. The phase-locking frequency will be synthesized by mixing the 2nd harmonic of the ring RF (952.67 MHz) with the IF frequency, which in turn is produced by multiplying the ring RF by 13/372 using a direct digital synthesizer (DDS) circuit. (An LO generated directly by a DDS would have excessive phase noise and degrade RF-IF Converter performance.) The LO is transmitted by either low-loss RF cable or an optical fiber cable to each remote processing station where it is received and distributed to the RF-IF Converters through power dividers in the LO Fan-Out unit.

The 64.02 MHz sinusoidal IF Clock is also generated from the ring RF frequency by a DDS (f_{dig} = 50/372 x f_{RF}). A crystal oscillator and phase-locked loop (PLL) will be used if necessary to achieve a sufficiently low phase noise for the digitizing clock. The clock signal will be transmitted over coax or fiber optic cable to the remote T/CD modules for distribution to the IF Processors.

The master Sync signal will synchronize the button switching cycles and IF Processor data acquisition at the remote processing stations. A Sync Enable signal is generated under program control from the central processor, and the Sync signal itself generated at the first subsequent rising edge of the ring Revolution Clock. When detecting the first turn of an injected beam bunch, the Sync signal is synchronized with the injection kicker timing signal. The master Sync signal is received and delayed by programmable amounts in the T/CD modules to equalize or intentionally skew the delays between IF processing channels distributed around the ring. The Sync signal also resets the 4-state button pattern generator and switch rate divider circuit so that button switching is synchronized around the ring. The master Sync signal will be transmitted over coax or optical fiber cable, and can be superposed on the cable carrying the IF Clock.

The ring Revolution Clock (1.2805 MHz) is derived by dividing the ring RF frequency by the harmonic number 372. It is transmitted to remote Timing/Crate Driver modules where it is delayed by a programmable amount and used to maintain synchronous BPM button address switching changes. It can also be used to increment ring revolution counters in the remote processing stations. The Revolution Clock is transmitted on the IF Clock cable.

4.8.2.1.7 Distributed Processor Communication Links

BPM data and processing control information is transmitted between the central and remote BPM processing stations over fast fiber optic communication links (up to 1 Gb/s). These communication links could be configured as a reflective memory network, where data must be written to and from central and remote memory locations, or as high speed VME bus extenders, where the central processor can access remote station VME modules as if they were in the central VME crate. A data rate of ~12 Mb/s is required for each of the 4 remote stations for normal orbit acquistion at a 2 kHz update rate.

Data and control information is passed between the central BPM processing station and the SPEAR Control computer via a VME crate controller.

4.8.2.1.8 DSPs

There will be one DSP in each of the four remote locations, loaded with identical software. After the BPM data acquisition configuration is transmitted to the DSP via the communication links, they will configure the IF processor modules and the module in each crate. They will then collect the raw BPM data produced by the IF modules, calculate the simple linear horizontal and vertical positions (Section 4.8.2.1.9) and make this data accessible to the central crate. The remote DSPs will also control the ADC attenuation in the RF/IF modules.

To accomplish the data transfers between the IF modules and the DSP, a high speed switched backplane is used (RACEway). The DSPs will be TMS320C67x floating point processors to perform the required calculation within a cycle time of less than 500 μsec.

The DSP in the central crate will collect the calculated horizontal and vertical beam positions from the remote crates and run the feedback system. The central DSP calculates new 16-bit setpoints for the 108 corrector power supplies during each 500 μsec cycle period and transmits them to the power supply controllers via a fast digitial control link (Section 4.8.1.1).

Different software will be loaded into the DSPs to allow first-turn and turn-by-turn orbit measurements (Section 4.8.2.1.9).

4.8.2.1.9 Orbit Calculation and Monitoring Modes

Beam position is derived from button signals in two ways. A linear method is used by the Orbit Feedback system for fast orbit information:

$$x = \frac{(Vb + Vc) - (Va + Vd)}{Va + Vb + Vc + Vd} Sx \tag{17}$$

$$y = \frac{(Va + Vb) - (Vc + Vd)}{Va + Vb + Vc + Vd} S_y \tag{18}$$

where Va through Vd are the button signal amplitudes (with button orientation shown in Figure 4.86) that have been compensated for BPM electrical offset and differential channel gain information. Sx and Sy are scaling factors dependent on the BPM geometry. A second and more accurate calculation accounts for the spatial "pincushion" distortion with polynomial expressions derived from BPM measurements in the laboratory. This calculation is more time-consuming than the linear one and must be performed by the BPM Processing Interface CPU, which acquires button data from the BPM DSP that has been averaged over many feedback cycles for greater resolution. High resolution orbit measurements are sent to the SPEAR Control computer with an update rate on the order of 1 Hz.

The BPM Processing System can function in the following modes:

- First Turn Mode
  The ~0.025 nC injected bunch charge from the 10 Hz Booster will be detected with a single shot position resolution of 1.8 mm. The processing Sync signal is synchronized with the injection kicker trigger. Four injection pulses are required to sample each BPM button and to calculate an orbit. Pulse-by-pulse button data is stored in the IF Processor memory, the contents of which can be sent on command to the SPEAR Control System in block transfer mode for analysis. By reconfiguring BPM cabling in special circumstances, the four buttons from a single BPM can be processed in parallel by 4 RF-IF converters for first-turn single-shot position monitoring. An alternative method for single shot position mea-

surement is to use hybrid combiners to calculate the difference and sum of RF signals (giving x- and y- proportional signals) prior to detection by the RF-IF Converters.

- Turn-by-Turn Mode
  The turn-by-turn Processor resolution is 12.7 μm for beam currents >5 mA. Turn-by-turn signal amplitudes for a single button at a time can be stored in the IF Processor memory for future transfer to the SPEAR Control computer. One application of this mode is to measure and compare betatron oscillation phase and amplitude at different BPMs to determine lattice properties. As for first turn measurements, the BPM cables can be reconfigured in special circumstances to provide processing of all four BPM buttons in parallel to obtain more accurate turn-by-turn position information.

- Averaged Orbit Mode
  The predominant BPM processing mode for SPEAR 3 will be to average BPM readings over many turns to obtain highly resolved orbit information. Averaging will take place on two time scales: a fast time scale for orbit feedback processing, and a longer time scale for higher resolution monitoring. For orbit feedback, which seeks a closed-loop bandwidth of 100 Hz, the overall orbit sampling rate must be 1 kHz or more. For the 2 kHz orbit sampling rate planned for SPEAR 3, the BPM button multiplexer is switched every ~20 turns (~15.6 μs), which includes ~2 turns of filter settling time and ~18 turns of legitimate data acquisition and averaging. The signal averaging continues for 8 button multiplexing cycles (640 turns) and the resulting data is used to compute the beam orbit having 1.1 μm resolution every 0.5 ms (Figure 4.92). The precise button switching and BPM sampling frequencies must be carefully selected to avoid aliasing of orbit frequencies above the orbit sampling Nyquist frequency (such as the ~10 kHz synchrotron oscillations) into the base bandwidth of the orbit feedback system. Any number of these orbits can be further averaged for higher resolution monitoring. For example, averaging 2000 orbits with orbit updates once every second will yield 0.025 μm processing resolution.

Orbits acquired by the SPEAR Control System are stored in a database where the information is available for display and analysis. Display options included real-time orbit updates, difference orbits from a selected reference orbit, waterfall orbit progressions, regional zoom, and spectral analysis. Orbit history records are archived every 2-5 s.

References

[1] J. Sebek et al., Proc. of the 1996 European Particle Accelerator Conference, Sitges, Spain, June 1996, 1737-39.

[2] N. Kurita et al., Proc. of the 1995 Particle Accelerator Conference, Dallas, May 1995, 2512-14.

[3] RACEWAY Interlink standard, adopted 7/31/95 by ANSI/VITA 5-1994.

4.8.2.2 Current Monitor (DCCT)

The Current Monitor, or Direct Current Transformer (DCCT), measures beam current and is used to calculate beam lifetime. The device works parametrically by sensing asymmetries in the flux of a driven magnetic core. These asymmetries result from the addition of the beam's DC flux component. DCCTs are commercially available, both as "off-the-shelf" models, and as units custom-designed to meet special requirements. Typical performance features include: 1) DC-to-100 kHz bandwidth, 2) dynamic range up to 10^7, and 3) absolute error less than 5×10^{-4} [1].

Based on a comparative study of several options with respect to purchase cost, development cost, and anticipated performance outcome, SPEAR 3 has selected a commercial DCCT system. New, high-quality, shielded cables will connect the sensor to the front-end electronics and also link the front-end electronics to the output chassis. Magnetic shielding for the sensor will also be installed, if required.

References

[1] Bergoz Precision Beam Instruments, 01170 Crozet, France (www.bergoz.com).

4.8.2.3 Tune Monitor

The SPEAR Tune Monitor consists of a single, custom-built, high-frequency electronics chassis and a commercial digital spectrum analyzer (Tektronix 3086DSP). Tunes are driven by a stripline kicker and detected with a stripline pickup assembly.

The transverse kicker for SPEAR 3 has four 50 Ω stripline electrodes (upper, lower, left and right), with each opposing pair driven differentially so as to excite the horizontal and vertical tunes. The maximum electrode length is 1/2 the accelerating RF wavelength, or 0.315 m at 476.337 MHz. The electrode cross-sections are separated adequately to maintain the beam-stay-clear dimensions and to reduce the heating of the electrodes by the beam-image current. The transverse shunt impedance is maximized by adjusting the electrode coverage angle, the electrode separation, and the electrode length. The kickers will produce a maximum impedance of approximately 10 kΩ, and operate in the DC - $f_{RF}/2$ frequency band. A signal generator (either a tracking generator, swept-frequency generator, or pink-noise source) and a small RF amplifier (approximately 10 W) will drive both the horizontal and vertical stripline pairs in tandem through a power splitter.

The detector is a conventional, four-electrode stripline optimized for maximum sensitivity at 1429 MHz, three times the 476.337 MHz accelerating frequency. The stripline length is 1/4 of this 3rd harmonic frequency (52 mm). Striplines are superior to buttons in this respect, as they have two free dimensional parameters (while buttons have only one). The impedance function can thus be tailored to the application. The detector will be carefully manufactured to minimize electrical-center offset, and to provide a smooth transition for the signal currents and beam image current. The electrodes will subtend angles that equalize the intercepted image currents in the elliptical geometry and the downstream ends will be shorted to the chamber. Passive combiners connected to the upstream ends of the electrodes are used to produce horizontal and vertical beam position signals. Those signals are filtered, amplified, and converted to baseband. A low-frequency spectrum is produced, containing the synchrotron tune and the two betatron tunes.

The Tektronix 3086 DSP is used to analyze the signal derived from the beam. The instrument is a "real-time" spectrum analyzer capable of processing the input through a bank of parallel digital filters to create a histogram. At its narrowest frequency span, the instrument's frequency resolution is 1.25 Hz, and it can display and record the time-evolution of the measured tunes. The digital signal processor is controlled via Ethernet by the SPEAR control computer, where a history buffer is maintained.

4.8.2.4 Injection Monitors

The Injection Monitor facilitates beam injection from the booster-to-SPEAR (BTS) line into the SPEAR ring. The equipment suite consists of six BPMs, one current monitor, one Faraday Cup, and six insertable fluorescent screens. Except for the replacement of its long-haul cables (as part of the Cable Plant upgrade, Section 4.10), the system remains unchanged for the SPEAR 3 project.

The BTS BPMs are scheduled for upgrade prior to SPEAR 3. The BPM pickups are 10 cm-long striplines. The readout electronics to be installed are SLAC linac-type baseband BPM modules. The modulesoperate in a 5-50 MHz frequency range.. They use matched Bessel-Thompson low pass filters to limit the bandwidth to 50 MHz. Position differences are taken within the module. A sum signal is produced and used to provide position normalization and a trigger output. This trigger output is timed to occur when the position signal envelope reaches its maximum. The position, sum, and trigger signals appear as outputs at the front of each analog module and are digitized by the Control system. The position resolution is 125 μm.

The BTS current monitor (I4) is a resistive, wall-current detector. It is located upstream of the injection magnet raft, leading to the SPEAR septum magnet. High-quality cable transmits the signal to the control room, where it may be observed on a fast oscilloscope.

The Faraday Cup, an insertable monitor currently used to measure beam current, is located near the I4 current monitor. Its signal is also available for viewing in the control room.

To evaluate beam position and intensity between the booster and SPEAR, fluorescent screens may be inserted into the beam. Screens G49 and G56 are located after the booster ejection septum. Four more screens are situated within the BTS line:17PR2, 17PR2.5, 17PR3, and 17PR4. Screen 17PR3 is located before the SPEAR injection septum. Screen 17PR4 is located after the septum. All six screens are monitored by video cameras. Any three cameras may be displayed simultaneously on video monitors in the control room.

4.8.2.5 Beam Loss Monitors (Operator Display)

A Beam Loss Monitor (BLM) system, using Long Ion Chambers (LIONs), will be installed as part of the SPEAR 3 Beam Containment System (Section 4.9.3.3). In addition to the BLM's role of preventing injection into SPEAR if high losses are detected, BLM analog output signals will be buffered at their source, and made available to a timing and display chassis in the SPEAR Control Room. These electronics will compare the time-of-arrival of the "loss pulse" to the ring-revolution clock, and display where the loss occurred. By localizing beam loss sites to within one meter in the accelerator, this SPEAR 3 enhancement will improve diagnosis of beam-loss problems.

4.8.2.6 Beam Scrapers

SPEAR 3 will incorporate two beam scrapers, one for each plane, located in straight section 10S11. These scrapers will be used to measure beam size and machine aperture, and to diagnose injection behavior.

The motor-actuated scraper beam paddles are operated from a control panel in the SPEAR control room. A separate DC motor and a power supply unit are situated in the same equipment rack. The control panel displays scraper position, as detected by linear potentiometers on the instruments. The devices incorporate microswitch interlocks, preventing excessive travel.

4.8.2.7 Synchrotron Light Monitor

The Synchrotron Light Monitor (SLM) for SPEAR 3 will image visible and near ultraviolet synchrotron radiation. At these wavelengths, the vertical measurement resolution is limited by diffraction. The diffraction-limited resolution (or "diffraction spot size" σ_d) is given by

$$\sigma_d = \frac{\lambda}{4\pi\theta} \tag{19}$$

where λ is the light wavelength, θ is its opening angle:

$$\theta \cong 0.6\left(\frac{3\lambda}{4\pi\rho}\right)^{\frac{1}{3}} \tag{20}$$

and ρ is the bending radius of the light source dipole magnet. The SPEAR 3 SLM will use a wavelength of 210 nm (near ultraviolet) and filtering to obtain a 10% bandwidth (200 nm to 220 nm). This relatively short wavelength permits the use of conventional optical materials (e.g. fused silica) and has a diffraction spot size of 15 μm. The vertical beam size is 5 μm.

A conventional CCD video camera will be used for imaging. However, the camera must be purchased without the standard protective glass over the integrated circuit. A polarizer on the optical bench passes only the horizontally polarized light, which has a nearly Gaussian vertical profile. The image size is the quadrature sum of the electron-beam and diffraction sizes. Table 4.44 lists SLM parameters.

Table 4.44 Synchrotron Light Monitor parameters.

Parameter	Value
Radius of curvature in dipole ρ	7.86 m
Critical energy in dipole E_c	7.62 keV
Critical wavelength in dipole λ_c	0.163 nm
Measurement wavelength λ	210 nm
Opening angle $(1/\gamma)$ at λ_c	0.17 mrad
Opening angle at λ for both polarizations	1.87 mrad
Opening angle at λ for horizontal polarization	1.12 mrad
Diffraction spot size σ_d	15 μm
Electron beam size σ_x	183 μm
Electron beam size σ_y	51 μm
σ_y / σ_d	3.41
Vertical image size σ_{image} (1:1 image)	53 μm
$\sigma_{image} / \sigma_y$	1.04

To withstand the large heat load that results from such high average current, the primary synchrotron light mirror (M1) features extensive water-cooling. To reduce the incident power density, the mirror will be tilted at grazing incidence to the light, and it will stand several meters from the ring. Nevertheless, the hot x-ray fan will cause deformation about the midplane of the mirror. Since the height of the near-ultraviolet fan is much greater than that of the x-rays, the x-ray stripe can be removed by causing it to hit a narrow, cooled, midplane mask. The mask thus shades the center of the mirror. A similar technique is in use at the Advanced Photon Source [1]. When the electron orbit wanders off the midplane, the mirror will not remain flat, but will be cooled sufficiently to remain safely below its yield strength. The electrons may then be steered back to the midplane.

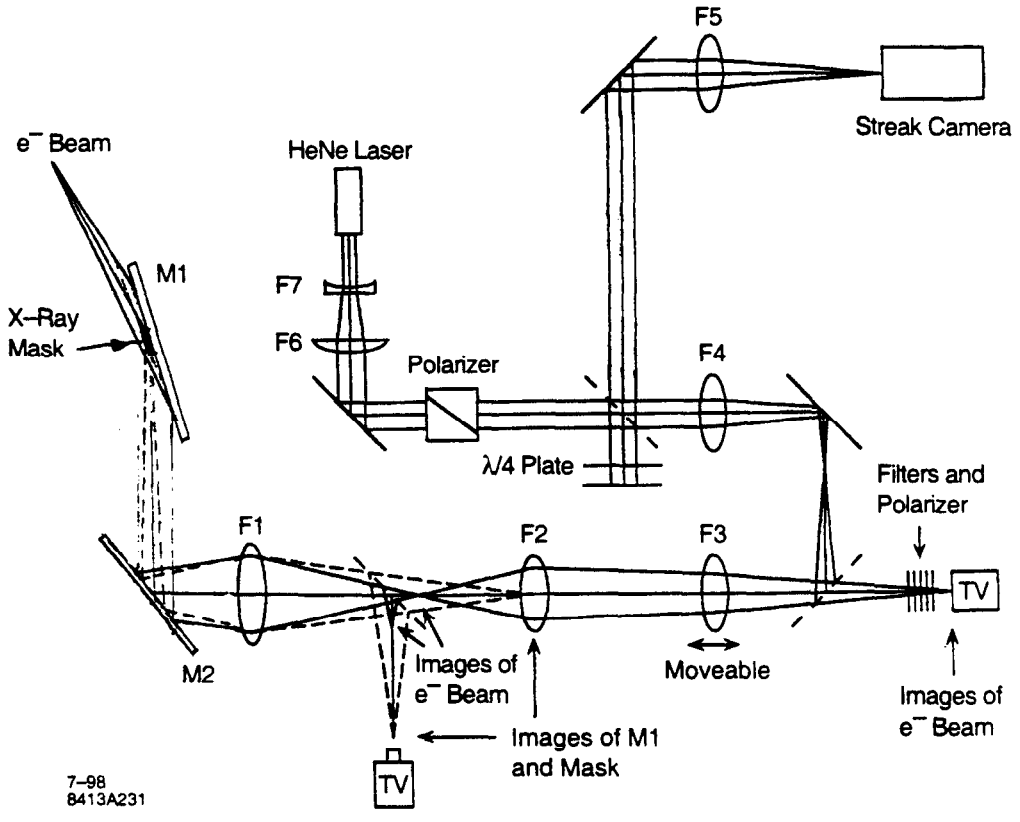

Figure 4.91 Optical configuration for the visible/UV Synchrotron Light Monitor.

As seen in Figure 4.91, the flat mirror (M1) is followed by a turning mirror (M2) at 45° incidence. M2 requires modest cooling due to the deep UV reflected from M1, and by the fused silica window.

At full aperture, the vertical chamber and window must accommodate at least 4σ of the vertical UV beam size. The vertical beam size is dominated by the approximately 1 mrad rms opening angle of the 210 nm light.

Once past the window, the light is brought along an enclosed, evacuated path to an optical table in a hutch that sits atop the roof shielding blocks. The imaging scheme is designed to compensate for the effect of the mask. In geometric optics, a mask or aperture placed in the plane of a lens (like a camera iris) serves only to restrict uniformly the amount of light reaching the image plane. It does not otherwise affect the image. Here, the first focusing mirror (F1) images both the electron beam light and the mask onto the second focusing mirror (F2), which then images the electron light onto the main CCD camera. A second CCD camera images M1, allowing the light to be centered on the mask. A third focusing element (a motorized lens (F3)) adjusts the image focus for different beam orbits. Located ahead of the main CCD, a beam-splitter breaks off an image that can be used simultaneously by additional devices, including 1) a streak camera, 2) a gated CCD, and c) photodiode array (for a photon interlock).

References

[1] B.X. Yang and A.H. Lumpkin, "The Planned Photon Diagnostics Beam Lines at the APS," Beam Instrumentation Workshop, 1994, AIP Conference Proceedings 333, 252-258 (1995).

4.8.2.8 Console Instrumentation

The operator's control area in the SPEAR control room, located in Building 117 inside the ring, contains a wrap-around console, a computer server room, a meeting area, and small offices for the machine operators. The console area consists of 22 full height equipment racks, containing control and monitoring electronics and three computer workstations. Routine machine control is conducted from the computer workstations, served by the central injector and SPEAR computers. Any measured parameter can be displayed, and any control parameter modified, from these workstations. The console instrumentation is mostly unchanged in the SPEAR 3 upgrade

Clustered around the workstation area, a variety of instruments are used by the operators to perform routine monitoring and fault diagnosis. A Tektronix 2467B 400 MHz (micro-channel plate) oscilloscope is connected to a 4-electrode (sum signal) stripline in the booster. The scope is used to display bunch amplitudes and bunch timing prior to SPEAR injection. A Faraday cup, at I4 in the BTS, is instrumented by a Keithley electrometer, and is used occasionally to measure the injected charge. Fluorescent screens (Section 4.8.2.4), used to inject from the BTS into SPEAR, can be easily viewed from three video monitors.

A dedicated video monitor displays a continuously-updated history of the stored-beam current–as measured by the DCCT (Section 4.8.2.2). Betatron tunes are excited by a four-electrode stripline kicker driven by a small power amplifier (approximately 10W). The resulting full betatron spectrum (and its recent history) are displayed by the Tektronix 3086 Digital Spectrum Analyzer (Section 4.8.2.3). Transverse beam profile, as measured with the UV Synchrotron Light Monitor (Section 4.8.2.7) using a CCD camera, is provided on a color monitor by a Spiricon^{TM} Laser Beam Analyzer image-processing instrument. Light focusing in the optical path can be controlled remotely. Horizontal and vertical beam-scraper controls (Section 4.8.2.6) are provided to measure beam size, diagnose injection, and to determine limiting ring apertures.

A variety of portable instrumentation is also available to the operators and accelerator physicists. These include 1) a 2 GS/s Digital Oscilloscope, 2) an RF Spectrum Analyzer, 3) a Vector Voltmeter, and 3) a 300 MHz analog oscilloscope. Also available are two non-dedicated PC's, as well as slots in the NIM, CAMAC, VME, and VXI crates for *in-situ* testing of prototype electronics. Supplies of cables, connectors, and accessories are also readily available.

4.8.2.9 Transverse Bunch Phase Space Monitor

The Transverse Bunch Phase Space Monitor (PSM), developed for SPEAR 2, consists of fast processors for each of two BPMs separated in betatron phase [1]. The PSM acquires turn-by-turn beam-position data from the two BPMs. It can then derive both the turn-by-turn position-angle phase space and the amplitude-dependent tune measurements from this input. The Transverse PSM will be used in SPEAR 3 for beam dynamics studies. Figure 4.92 provides a system diagram.

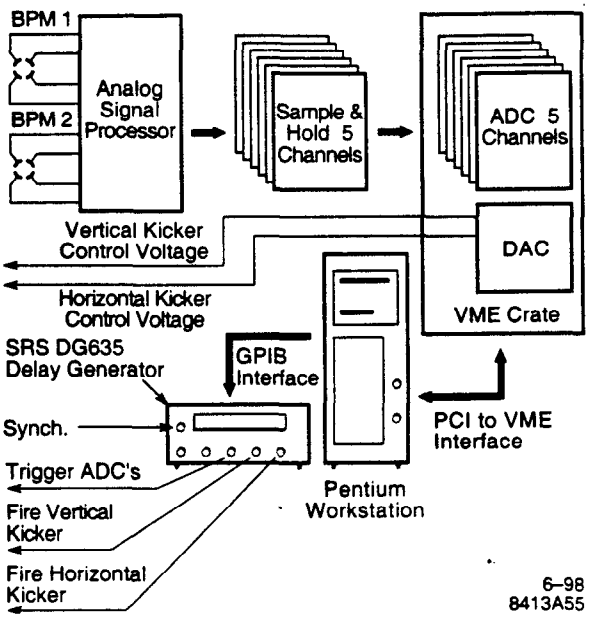

Figure 4.92 Transverse Bunch Phase Space Monitor System.

The system's front-end consists of button sensors and SLAC/Linac-type, baseband BPM modules. Button signals are combined linearly in an analog module using passive, monopulse hybrids. Differences are developed that are proportional to horizontal and vertical beam displacement, as is a sum signal proportional to the total bunch charge. The signals are bandwidth limited to 50 MHz by matched Bessel-Thompson low-pass filters. The sum signal is used to provide position-normalization and a trigger output. This trigger output is set up to occur when the position-signal envelope reaches its maximum. The position, sum, and trigger signals appear as outputs on the front of each analog module.

Two horizontal position signals, two vertical position signals, and one sum signal are detected using high-speed, low-noise, track-and-hold modules, thereby allowing the use of 14-bit analog-to-digital (ADC) converters. The signals are sampled at peak amplitude once-per-turn, and stored in the on-board RAM, for up to 128,000 turns. All the ADCs and related modules are VME-based. System-control has been automated using LabView™ on a PC workstation. This arrangement facilitates highly efficient use of accelerator study time and the post-processing of data.

The system is typically operated in conjunction with the vertical and horizontal kickers. The kicker triggering circuitry allows the data-acquisition cycle to start at a fixed phase with respect to the AC line. This prevents corruption of the data by 60 Hz ripple in the kicker's magnetic field. The current resolution achieved through single-turn measurement is 125 μm, limited principally by the analog electronics. A planned Accelerator Improvement Project (AIP) will replace these electronics with SPEAR-orbit, BPM type modules, thus improving single-turn resolution to 13 μm.

References

[1] A. Terebilo, C. Pellegrini, M. Cornacchia, "Experimental Non-Linear Beam Dynamics Studies at SPEAR", Proc. of Particle Accelerator Conference, 1997, Vancouver, Canada.

4.8.2.10 Longitudinal Bunch Phase Monitor

The digital front-end processing system developed for the PEP-II longitudinal feedback system [1] will be used to monitor the energy (longitudinal phase) oscillations of each bunch (Figure 4.92). The bunch-phase signal is derived from a four-electrode, 210-mm, stripline detector. For each bunch that passes the detector, a comb generator filter produces a tone burst at a harmonic of f_{REV}. The signals are then phase detected, and the phase error is digitized. The data is directed to the correct digital signal processor (DSP) channel for digital filtering, according to its associated bucket number and turn number. The phase oscillation data is orthogonalized into modes, and application software displays the motion.

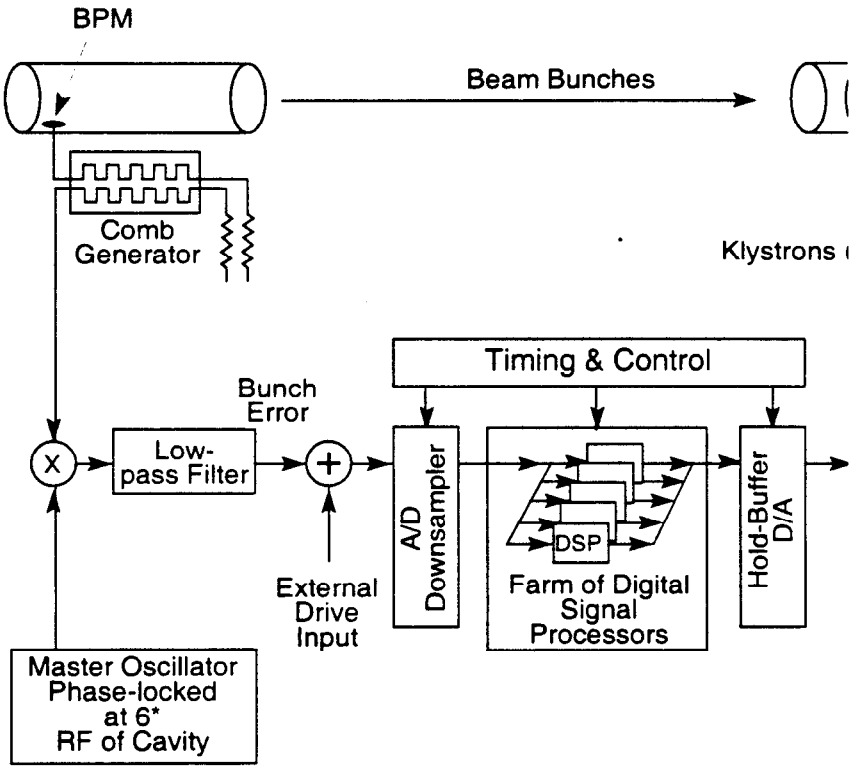

Figure 4.93 Longitudinal bunch phase monitor (PEP II design).

The longitudinal bunch phase monitor will be used to sense common-mode (zero-mode) bunch motion and to stabilize it via the Zero Mode feedback system (Figure 4.83).

References

[1] D. Fox et al., "Observation, Control, and Modal Analysis of Longitudinal Coupled-Bunch Instabilities in the ALS via a Digital Feedback System", 1996 Beam Instrumentation Workshop, AIP Conference Proceedings 390, 207-214 (1997).

4.8.3 Quadrupole Modulation System

The Quadrupole Modulation System (QMS) is a diagnostic tool for determining BPM offsets and measuring ring-lattice functions (Section 3.4.6). The system is capable of introducing low-frequency amplitude modulation in the magnetic flux of any one of the 94 SPEAR 3 quadrupoles. This is accomplished by driving trim windings on the quadrupoles from a bipolar power supply (Section 4.6.3.3). The system excites a selected quadrupole and then observes the resulting orbit

modulation with BPMs. The beam may then be steered through the magnet until the BPM registers minimum motion, thereby locating the quadrupole's magnetic center. Figure 4.94 provides a functional diagram of the system.

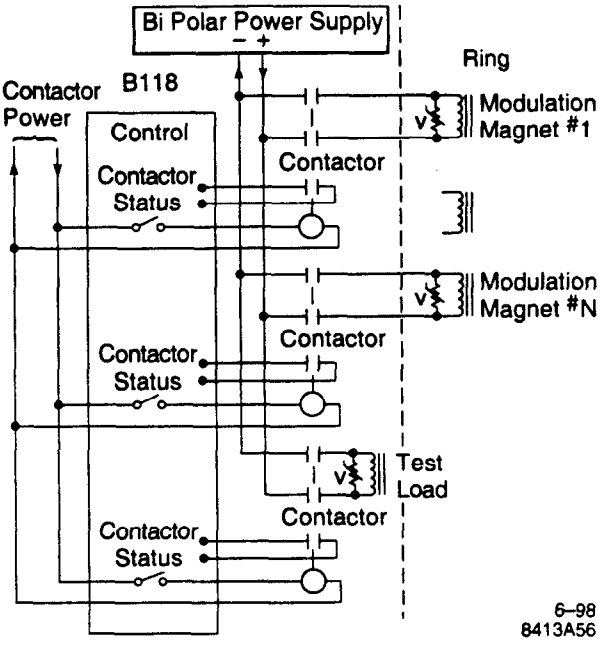

Figure 4.94 Quadrupole Modulation System.

The system incorporates a single bipolar power supply that is switched between magnets. Because the trim currents are small (< 10 A), a light-gauge two-conductor power cable runs to each magnet from the switching network in Building 118. Because the switches operate infrequently, electromechanical relays may be used. The control circuit is designed to open or close the switches only when the power supply is off. Also, switch polling ensures that only one magnet is energized at a time.

Section 3.4.6 gives specifications for quadrupole modulation amplitudes and QMS performance. Trim fields were sized to limit betratron tune shifts to < 0.01, to avoid intercepting a tune resonance during modulation.

4.8.4 Timing System

SPEAR's timing system [1,2] must be modified to accommodate the new RF frequencies for SPEAR (476.337 MHz) and the booster (358.533 MHz). A phase-locked loop between the two frequencies will be implemented to enable accurate, reproducible and stable, on-demand filling of any single SPEAR 3 RF bucket through the timing control system (Figure 4.95). Only single-bunch filling will be supported.

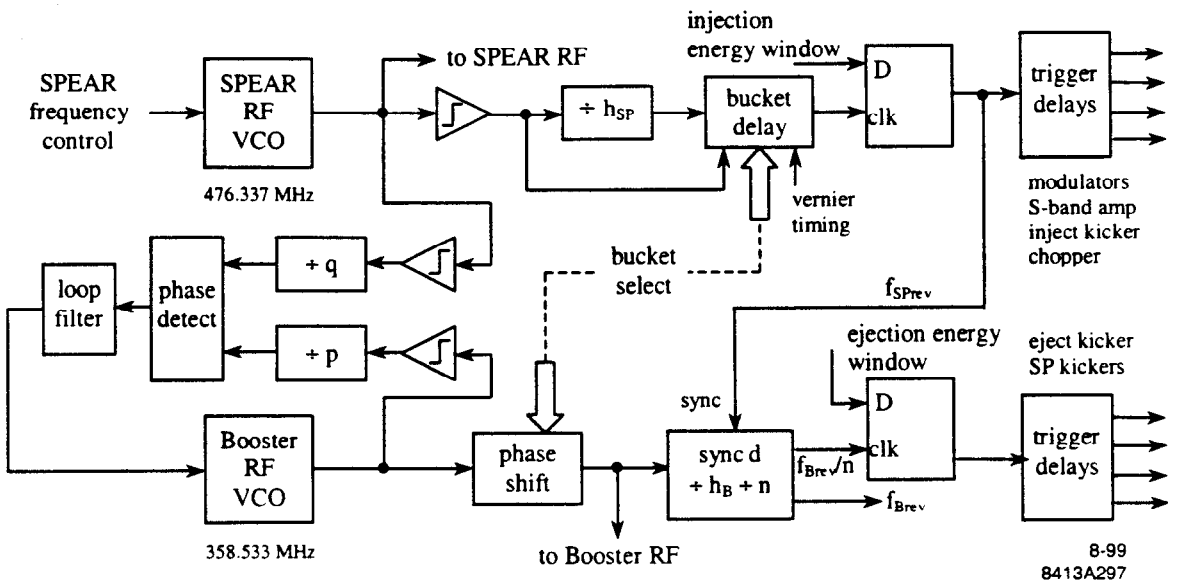

Figure 4.95 RF-synchronized timing system for the injector and SPEAR 3.

The sequence of events needed to inject the beam into a given SPEAR bucket includes:

- Detecting the first SPEAR bucket timing fiducial occurring within the 0.1% injection energy window at 112 MeV.
- Triggering the linac klystron modulator and S-band klystron drive amplifier to produce an electron beam from the gun (and provide power to the linac).
- Triggering the booster injection kicker.
- Triggering the linac beam-chopper to permit 3-5 S-band microbunches to enter the linac and booster.
- Triggering the pulsed power supply for the booster injection septum magnet.
- Triggering the booster extraction kicker after accelerating beam in the booster for approximately 36 ms during a booster revolution period when the bunch is temporally aligned with the target SPEAR bucket.
- Triggering the three SPEAR injection triggers with appropriate inter-kicker delays to account for beam transit time.

The injection timing sequence begins with the receipt of a fiducial timing pulse that corresponds to the target bunch. The timing fiducial is derived by synchronously dividing the SPEAR 3 RF frequency by the SPEAR harmonic number $h_{SP} = 372$. The timing pulse repetition rate is equal to the ring's revolution frequency (1.2805 MHz). The fiducial is delayed in increments of the SPEAR RF period to select different target buckets.

Triggers for the linac and booster injection components listed above are generated with fixed delays from the first bucket timing fiducial that occurs within the 0.1% injection energy window. The injection energy window is detected by a "peaking strip" installed in the gap of a booster dipole magnet. This strip senses when the dipole magnetic field reaches the proper injection value. It consists of a bundle of highly permeable, low coercive-force permalloy wires within a solenoid coil that provides a DC-bias magnetic field that exactly cancels the dipole magnetic field at the proper injection energy. As the net magnetic field passes through zero, the peaking strip induces a pulse in the bias coil, which, in turn, is detected to provide the injection energy timing pulse. The timing pulse width is a few microseconds.

The pulse widths for the S-band klystron-drive amplifier and modulator are approximately 2 μs. The resulting beam macro-pulse produced by the gun is about one μs. It contains approximately 3000 S-band microbunches having an energy of 2 MeV. The stripline beam-chopper sweeps the gun's beam vertically past a slit that permits only 4-5 microbunches to enter the linac. The microbunches are accelerated in the three 3 m linac sections to 112 MeV. They then travel down the linac-to-booster (LTB) transport line to the booster. The trigger timing is adjusted so that the incoming beam arrives at the end of the 260 ns-long "flat-top" of the trapezoidal kicker pulse, (just prior to the 300 ns fall-time). This timing assures that the kicker waveform decays completely before the injected bunch passes the kicker once again (446 ns later).

To ensure successful capture and acceleration, the injected microbunches must arrive at the booster RF cavity within the approximately 1 ns acceptance span of the RF bucket. Since the microbunches are separated by the 350 ps period of the 2856 MHz S-band linac frequency, four microbunches (at most) can be captured in a booster bucket, where they coalesce into a single bunch. To maintain stable beam capture within the booster, the timing between the beam-chopper sweep and the booster RF waveform must be accurate to within 350 ps or better.

To achieve such timing precision, the chopper's timing trigger, and the SPEAR bucket-timing fiducial from which it is derived, must be synchronized to the booster RF waveform. This implies that not only must the master oscillator frequencies of SPEAR and the booster RF be phase-locked, also, the booster RF period must be an exact integer-multiple of the SPEAR revolution period. This ensures recurring synchronism between the SPEAR timing fiducial and the booster's RF waveform. Given the limited ranges of adjustment of the SPEAR and booster circumferences (as defined by accelerator, tunnel and beam line geometries), this condition is met by maintaining the present 4:7 ratio of booster and SPEAR circumferences. Since the circumference C of a storage ring is given by

$$C = h \cdot \lambda = \frac{h \cdot c}{f} \tag{21}$$

where h is the ring harmonic number, c is the speed of light, and λ and are the RF wavelength and frequency, then, for booster harmonic number $h_B = 160$, the number p of booster RF periods in one SPEAR revolution is

$$p = \frac{7}{4} \cdot \frac{C_B}{\lambda_B} = \frac{7}{4} \cdot h_B = 280 \tag{22}$$

where the subscript B indicates booster parameters, and the condition for recurring synchronism is satisfied.

Once captured by the RF, the injected bunch is accelerated in the booster for approximately 36 ms—or until it reaches a 0.1% ejection energy window, as detected by measurement of the booster magnet current. The bunch is extracted from the booster within the energy window by firing the ejection kicker with an RF-synchronized trigger that guarantees the bunch will be injected into the selected SPEAR bucket. Because of the 4/7 booster/SPEAR circumference relationship, there is recurring synchronism between the booster bunch and the target SPEAR bucket every seven booster revolutions. The RF-synchronized ejection trigger is therefore derived by first dividing the master oscillator frequency of SPEAR and the booster RF by $h_B = 160$ to get the booster revolution frequency, and then by 7. The divider must be reset by the linac injection trigger to establish the proper booster bunch-to-SPEAR bucket timing relationship. Throughout the 36 ms booster acceleration cycle, the relative timing stability between the booster and SPEAR RF on the one hand and the timing system frequency sources on the other must be on the order of 200 ps or better. This will result in efficient electron capture within the SPEAR target bucket.

Given the 4/7 booster/SPEAR 3 circumference ratio and Equation 3, the ratio of booster and SPEAR 3 RF frequencies is

$$\frac{f_B}{f_{SP}} = \frac{7 \cdot h_B}{4 \cdot h_{SP}} = \frac{7 \cdot 160}{4 \cdot 372} = \frac{70}{93}. \tag{23}$$

The phase-locked loop (PLL) in Figure 4.95 maintains this harmonic relationship by adjusting the booster RF'S master oscillator to stabilize the phase relationship of the two divided-down frequencies $f_B/70 = f_{SP}/93 = 5.122$ MHz. To obtain the 200 ps relative timing accuracy between the booster and SPEAR master oscillators during the 36 ms booster acceleration period, the integrated phase error of the 5.122 MHz common frequency over this period must remain <0.37°. The loop-filter properties will be optimized to best utilize the inherent short-term stability of the booster's master oscillator and to minimize the phase noise introduced by the PLL. This ensure that the phase-error requirement is met.

The PLL maintains a constant phase relationship between the SPEAR bucket-timing fiducial, which recurs once for every SPEAR revolution period (781 ns), and the booster RF cavity waveform. For a given SPEAR bucket N, this phase relationship must be adjusted by applying a DC phase shift ϕ_N to the booster RF reference frequency to achieve the proper time-of-arrival of the group of 4-5 microbunches from the linac within the booster RF bucket. For bucket N+1, the booster RF phase offset must be shifted by $\Delta\phi$ to re-establish proper synchronism, where

$$\Delta\phi = 360° \cdot \frac{f_B}{f_{SP}} = 360° \cdot \frac{70}{93} \equiv 271° \tag{24}$$

An equivalent phase relationship is reached if the booster RF is shifted by

$$\Delta\phi \equiv 271° - 360° = -89° \tag{25}$$

The booster RF phase shift ϕ_N for bucket N can therefore be expressed as

$$\phi_N = \phi_0 + N \cdot 360° \cdot \frac{70}{93} \tag{26}$$

where ϕ_0 is the phase shift for proper timing of bucket 0. These discrete phase values repeat modulo 2π every 93 buckets. Using Equation 25 for $\phi_N > 180°$, the phase associated with each SPEAR bucket and can thus be mapped into one of 93 values, either in the range 0° to 360°, or in the range -180° to +180°. The 93 discrete values are separated by 3.9° booster phase intervals, equivalent to timing increments of approximately 30 ps. In reality, approximately 100 ps timing resolution is more than adequate for successful SPEAR injection, so, for example, the 93 phase values could be reduced to 32. The SPEAR buckets would have a constant mapping into each of these 32 values. A programmable phase-shifter for the booster RF reference frequency will be controlled by a look-up table containing the 93 (or fewer) phase values associated with the 372 SPEAR buckets.

References

[1] R. Hettel et al., "Triggers and Timing System for the SSRL 3 GeV Injector," Proc. of the 1991 IEEE Particle Accel. Conf., San Francisco, 1478-1480.

[2] R. Hettel, "SPEAR 3 RF: 358 and 476 MHz Frequency and Timing System Options," SPEAR 3 tech note, 4/99.

4.9 Protection Systems

4.9.1 Overview

The existing SPEAR accelerator protection systems, including the Machine Protection System (MPS) and the Personnel Protection System (PPS), will be modified and expanded to accommodate SPEAR 3 requirements. In particular,

- The MPS Vacuum and Magnet Cooling Interlocks will be revised to protect the upgraded accelerator vacuum, magnets, and power conversion systems.
- A Chamber Temperature Monitor system will be implemented to monitor the temperatures of critical vacuum chamber components, including photon absorbers, bellows, etc., and to prevent their overheating.
- An Orbit Interlock system will be implemented to protect the vacuum chamber from mis-steered synchrotron radiation beams.
- The PPS Access Control System (ACS) will be modified to protect against electrical hazards from the new power supply systems and to conform with changes to the tunnel shielding configuration.
- The PPS Beam Containment System (BCS) will be augmented with beam loss monitors (Long Ion Chambers) to protect against excessive beam loss during injection.

The PPS, which includes the Access Control System (ACS) and the Beam Containment System (BCS) will be modified and expanded. The ACS and related transducers will be modified and expanded to accommodate the upgraded accelerator power supply systems and changes to the tunnel shielding configuration. The BCS and related radiation transducers will be modified and expanded to accommodate the modified accelerator lattice and shielding properties together with the 3 GeV injection energy. It will include the design and installation of long ionization chambers in the SPEAR tunnel.

4.9.2 Machine Protection System (MPS)

The SPEAR 2 MPS consists of two separate systems controlled by modular programmable logic controllers (PLCs). One system controls and monitors the ring vacuum system and water flow in the vacuum chamber cooling channels. This system is interfaced to the beam line vacuum control systems to protect the ring vacuum from a vented beam line. The second system monitors the temperature of the water cooled magnets and bus bars.

The MPS PLCs are interfaced to the SPEAR control computer and constantly provide information on the status of the ring vacuum, water flow switches, and thermal switches. This information, as well as the pressure measured by the ion gauges, is kept in a database. Each PLC can control and monitor up to 960 input and output signals [1,2,3]

The MPS must be expanded for SPEAR 3 to include not only vacuum chamber and magnet interlock functions, but also a more extensive vacuum Chamber Temperature Monitor system and an Orbit Interlock system to protect the vacuum chamber from damage from mis-steered synchrotron radiation. The vacuum chamber is passively safe for radiation coming from a beam having an enlarged effective vertical size caused by betatron motion or some other instability mode, and no interlock is required for this situation.

4.9.2.1 Vacuum Interlock System

The SPEAR 3 Vacuum Interlock system will control and monitor the operation of vacuum components including isolation valves, ion gauges, ion pumps and water-cooled photon absorbers,

beam line collimators and masks. A block diagram of the SPEAR 3 Vacuum Interlock system is shown in Figure 4.96.

The existing Vacuum Interlock system (PLC 1) will be modified and extended to monitor the operation of 39 ion gauge controllers, 115 ion pumps (increasing to 162 in 2004), 54 titanium sublimation pumps (TSPs) and approximately 500 water flow switches. It will control the operation of the 6 ring isolation valves and provide permit signals for operation of the ring RF and beam stoppers.

The interlock response to a ring ion gauge or a beam line vacuum fault will be to close all isolation valves. Closing the isolation valves minimizes the propagation of the bad vacuum from some part of the ring or from a beam line. The response to a vacuum chamber water flow switch fault will be to close ring beam stoppers to prevent chamber overheating. All faults will be latched and displayed, including the identification of the faulted interlock transducer. (Figure 4.96).

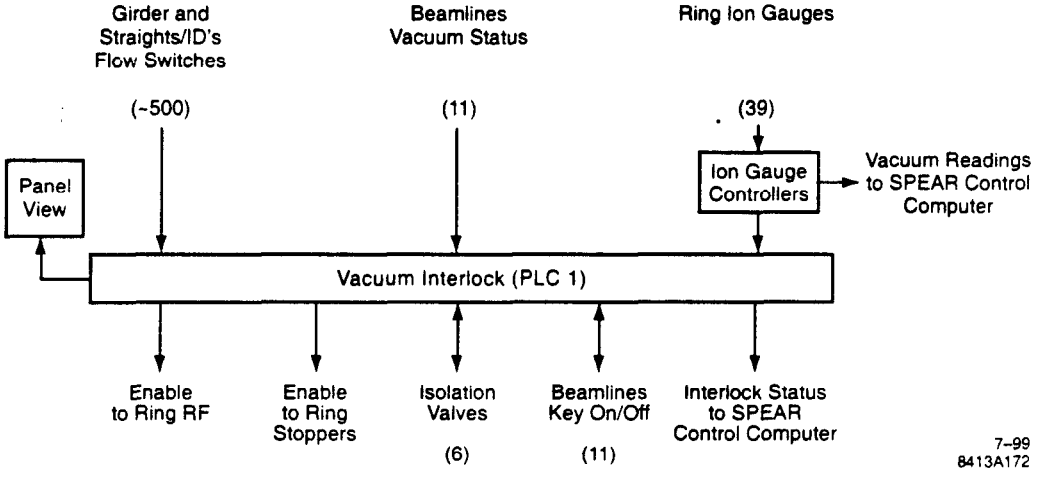

Figure 4.96 Block diagram of the Vacuum Interlock system.

4.9.2.2 Magnet Cooling Interlock System

The SPEAR 3 magnet cooling interlock system will insure the proper cooling of the water-cooled magnets and bus bars. Table 4.45 lists the number of water cooling circuits for the various magnets.

The existing system (PLC 2) will be modified and extended to monitor approximately 1600 thermal switches and approximately 20 water flow switches and to provide enable signals required for the operation of the 76 main magnet power supply systems. The thermal switches for each magnet will be connected in series, providing a single summary signal per magnet. PLC 2 will monitor a total of approximately 325 thermal switch summary signals.

An interlock fault caused by a magnet or a bus bar thermal switch or water flow switch will turn off the appropriate power supply. This will prevent overheating and potential damage to a magnet coil or a bus bar. The faults will be latched and displayed. The display will include the magnet identifiers. Figure 4.97 shows a block diagram of the SPEAR 3 magnet cooling interlock system.

Table 4.45 Thermal switches for SPEAR 3 magnets.

Magnet	thermal switches magnet	magnets /girder	switches /girder
Standard Cell Girder			
Dipole	6	2	12
QF, QD	8	2 of each	32
qfc	8	1	8
SF, SD	7	2 of each	28
H/V corrector	1	2	2
H corrector, V corrector	1	1 of each	2
	total switches/standard girder:		84
Matching Cell Girder			
Dipole	6	2	12
QFX,QFY,QFZ,QDX,QDY,QDZ	8	1 of each	48
SFI, SDI (with skew quad trims)	7	2 of each	28
H/V corrector	1	2	2
H corrector, V corrector	1	2 of each	2
	total switches/matching girder:		92
Total switches for 14 standard and 4 matching girders:			1544

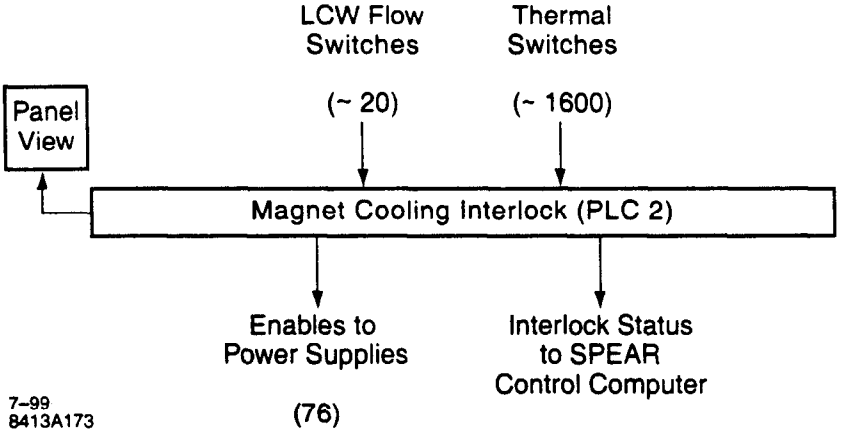

Figure 4.97 Block diagram of the Magnet Cooling Interlock system.

4.9.2.3 Chamber Temperature Monitor System

A Chamber Temperature Monitor system will be implemented to measure the actual temperature of the vacuum chamber water-cooled photon absorbers, chamber bellows, straight sections, scrapers stoppers, and other components that are heated by the stored beam.

Two types of temperature measurement sensors will be accommodated: thermocouples and resistance temperature detectors (RTDs). The SPEAR 3 temperature measurement system specifications are listed in Table 4.46.

Table 4.46 SPEAR 3 temperature measurement system specifications

Thermocouples	
Number	374
Range	30-200°C
Accuracy	± 1°C
Resolution	0.1°C
RTDs	
Number	16
Range	10-70°C
Accuracy	± 1°C
Resolution	0.05°C
Common mode rejection @ 60 Hz	>120 dB
Measurement rate	up to 960 channels/sec
Measurement scan interval	programmable
Digital alarm outputs	32
Control interface	RS-232/422

The signal processing system will be based on PLC modules or on a PC-controlled system. The system will include differential input amplifiers for the thermocouple sensors, excitation circuits for the RTD sensors, multiplexers, A/D converters, a controller, and a control computer interface.

The thermocouple output voltage, at temperatures up to 300 °C, is in the mV range and its sensitivity is approximately 20 uV/°C. With such small signals, special consideration must be given to interference, ground current, and AC line noise. To minimize interference and ground currents, each analog input and output will be floating and isolated from all other channels and ground; and to minimize measurement errors due to the AC line cycle noise, the system will average several measurements of each sensor per line cycle. The system will be interfaced to the SPEAR control computer for logging, analysis, and display. A block diagram of the SPEAR 3 temperature monitor system is shown in Figure 4.98.

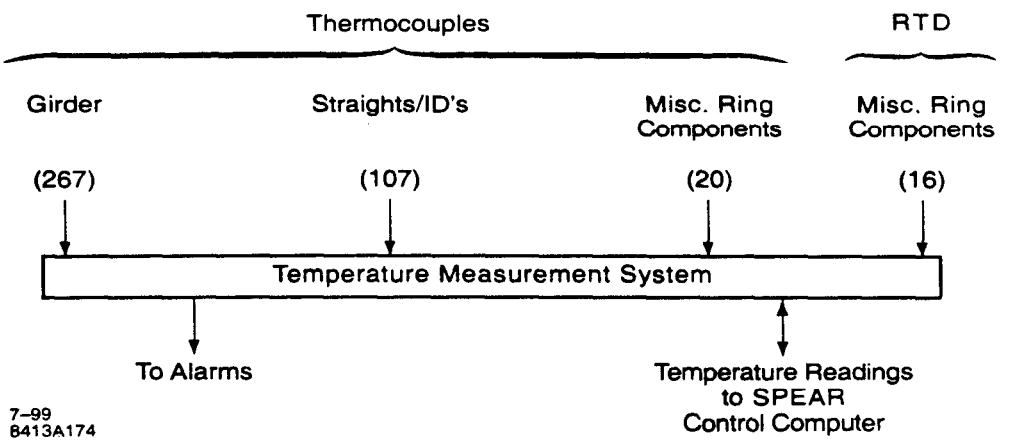

Figure 4.98 Block diagram of the Chamber Temperature Monitor system.

4.9.2.4 Orbit Interlock System

Under normal beam steering conditions, synchrotron radiation either enters the beam lines or is safely absorbed by water-cooled photon stops. However, the intense synchrotron radiation from SPEAR 3 insertion devices will be capable of damaging the copper vacuum chamber if the electron beam in the IDs is sufficiently mis-steered. Vertical mis-steering of the electron beam in an ID can cause the x-ray beam to hit the vacuum chamber above or below the radiation exit slot and severely damage it for currents above a passively safe limit. For example, a vertically mis-steered 500 mA electron beam in the BL 6 54-pole wiggler will begin melting the chamber in approximately 600 ms. An Orbit Interlock is required to protect against such chamber damage from mis-steered ID beams. No interlock is required for mis-steered dipole radiation since the vacuum chamber is passively safe for currents well beyond the 500 mA SPEAR 3 design limit.

The maximum passively safe mis-steered beam current for a given ID is a function of magnetic field strength for that ID and will be approximately 50 mA at the highest field setting of the most powerful ID initially installed in SPEAR 3 (the BL 6 54-pole wiggler). To be conservative, the interlock will become operational for stored beam currents above 20 mA. It is possible to configure the Orbit Interlock to become operational at higher beam currents if the magnetic field strengths for such high power IDs are limited to less than their maximal values.

The Orbit Interlock will detect beam position in BPMs adjacent to IDs and, in its simplest configuration, will abort the beam if the vertical or horizontal position in any one ID BPM exceeds ± 1 mm vertically or ± 5 mm horizontally for currents exceeding 20 mA. These trip levels accommodate BPM offset and vacuum chamber alignment errors (Section 3.1.13). The initial Orbit Interlock requires 14 BPMs to interlock the 7 existing IDs, but the system will be built to accept future ID BPMs, 2 BPMs per ID, as new IDs are installed, for a maximum number not likely to exceed 30. A more complex interlock configuration would permit different field-dependent safe current levels to be assigned to individual IDs, facilitating non-interlocked higher current operation when ID fields are reduced.

The Orbit Interlock BPM processing electronics will be designed to operate at beam currents ranging from 5 mA to 500 mA, with a position resolution of 50 μm or better. The processing electronics will share signals with the processing system used for orbit monitoring and feedback (Section 4.8.2.1) using rf signal diplexers. In addition, the system will monitor the beam average current and insertion device gap settings as sensed with limit switches.

To ensure a high degree of reliability, system component operation will be continuously monitored and system integrity tested at safe beam current levels by the SPEAR operator via the control computer. However, the Orbit Interlock system will operate as a stand-alone system and will not rely on any real-time information from the SPEAR computer. A block diagram of the Orbit Interlock system is shown in Figure 4.99.

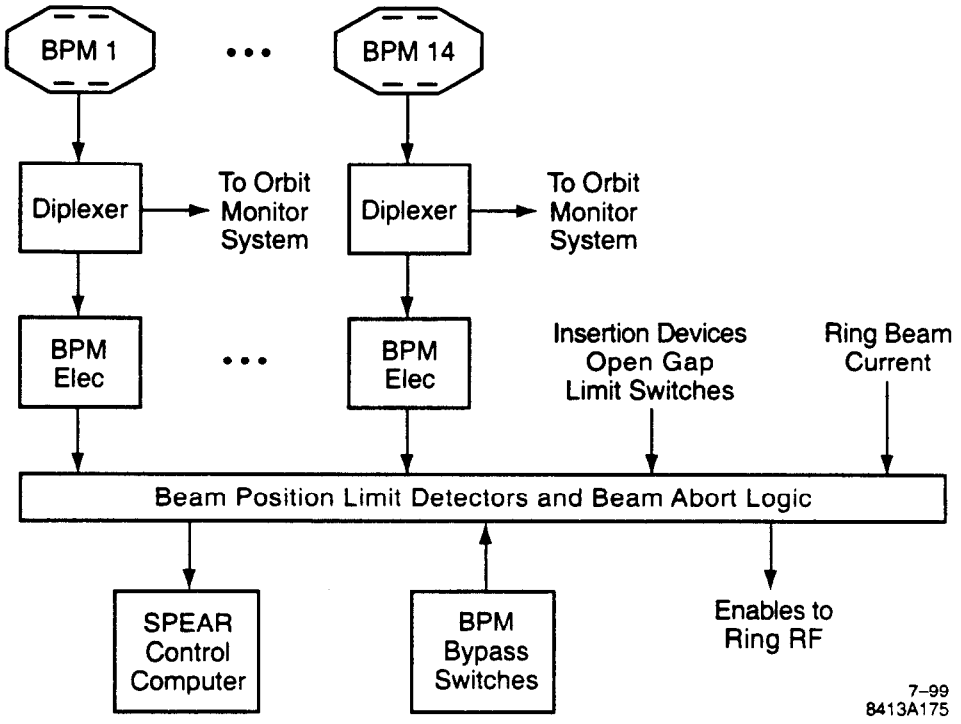

Figure 4.99 Orbit Interlock system.

The Orbit Interlock system will initially consist of:

- 14 each ID BPMs
- 14 each 4-channel diplexers
- BPM processing electronics
- Beam Position Limit Detectors
- Interlock logic and a fast interface to disable the ring RF
- Interface to the SPEAR control computer

These components are discussed below.

4.9.2.4.1 Beam Position Monitors

The ID BPMs used for the orbit interlock are shared with the orbit-monitoring BPM processing system (Figure 4.8.2.1). The BPM processors for the orbit interlock will detect the fundamental RF frequency component (476.34 MHz) of the button signal, while the BPM processing system will detect the first harmonic frequency (952.67 MHz).

The signal power from the 15 mm SPEAR 3 BPM buttons has been determined by calculation and by measurements in SPEAR 2 [5]. The 476.34 MHz button signal power as a function of beam current and vertical distance from the BPM center line (horizontally centered) is shown in Figure 4.100.

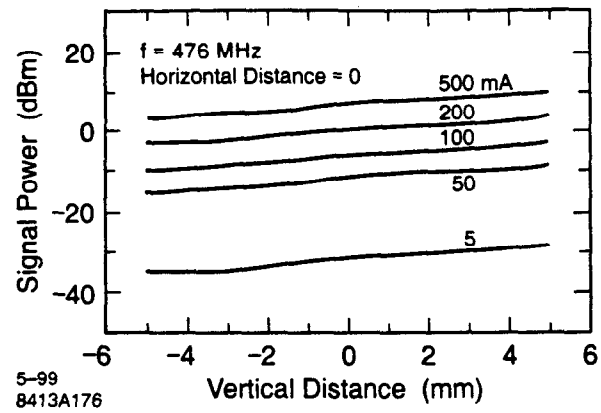

Figure 4.100 476.3 MHz signal power from BPM button.

4.9.2.4.2 Diplexers

A diplexer is a passive high frequency device that divides broadband signal power into two separated frequency bands. Input signal power not transmitted to the diplexer outputs is terminated in an internal dummy load. The power division is accomplished with little power loss in either of the two bands, and with substantial isolation between the output ports.

Table 4.47 BPM signal diplexer specifications.

Input and output ports:	
Impedance	50 ohms
Input power (max)	15 W, DC-10 GHz
VSWR	< 1.2:1, DC-1 GHz
	< 1.5:1, 1-6 GHz
	< 2.4:1, 6-10 GHz
952.6 MHz bandpass filter:	
Center frequency	952.67 MHz ± 2 MHz
Bandwidth (-3dB)	10 % of center frequency
Insertion loss	0.8 dB max
Loss matching	0.05 dB max for 4 channels
Output isolation	> 35 dB, 476.3 ± 25 MHz
476.3 MHz bandpass filter:	
Center frequency	476.34 ± 1 MHz
Bandwidth (-3dB)	10 % of center frequency
Insertion loss	0.8 dB max
Loss matching	0.05 dB max for 4 channels
Output isolation	> 35 dB, 952.6 ± 50 MHz

The SPEAR 3 diplexers will utilize a Butterworth, constant resistance (50 ohm) filter approximation and will provide 952.7 MHz input signals to the orbit monitor BPM Processor system and 476.3 MHz signals to the Orbit Interlock BPM processing system. Each diplexer module will consist of four identical channels connected to the four buttons of a BPM. The diplexers will be installed in the

remote BPM Processor racks distributed around the ring (Section 4.8.2.1). Basic diplexer specifications are listed in Table 4.47[6]

4.9.2.4.3 BPM Electronics

The beam position resolution needed for the Orbit Interlock BPMs is 50 μm or better. The rf processing technologies being considered to achieve this resolution for the BPM electronics include: peak detectors, hybrid junctions, AM demodulators for the difference-over-sum method, and logarithmic amplifiers for the logarithmic ratio method [7,8,9,10,11], all of which can be used to derive normalized, current-independent beam positions from raw button signals. The block diagram of the BPM processing electronics is shown in Figure 4.101.

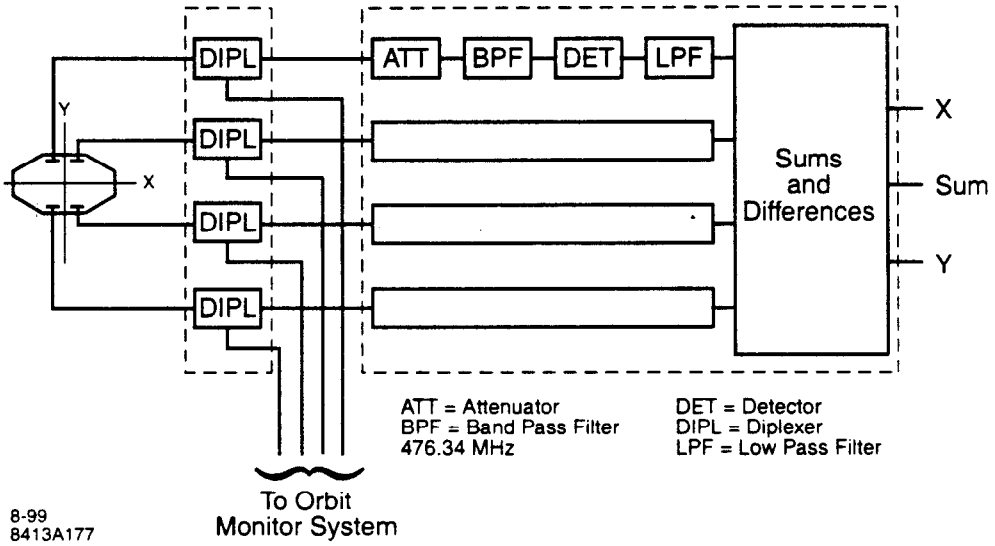

Figure 4.101 Orbit Interlock BPM processing system.

The main characteristics considered in the design of a BPM signal processing system are: linearity error, dynamic range, noise figure, resolution, burst response, stability, channel matching, and temperature drift. New, inexpensive, components like a complete 500 MHz receiver on a chip for AM demodulation, and a demodulating logarithmic amplifier with a 86 dB dynamic range and a DC-500 MHz bandwidth are being considered for the BPM processor. BPM processing parameters for the Orbit Interlock are listed in Table 4.48.

Table 4.48 BPM processing parameters for the Orbit Interlock system.

Number of BPMs	14
RF frequency	476.34 MHz
Revolution frequency	1.2805 MHz
Harmonic number	372
Ring circumference	234.126 m
Revolution period	781 ns
Bunch separation	2.1 ns - 781 ns
Nominal beam current	5 -500 mA
Resolution @ I_b > 5 mA	< 50 μm
Accuracy @ I_b > 5 mA	< 100 μm
Dynamic range, intensity	> 60 dB
Channel isolation	>60 dB

The BPM electronics will be packaged in modules to be installed in the remote BPM Processor racks. Each module will process the position of one BPM and provide analog output voltages proportional to beam horizontal and vertical positions and average beam current. Each BPM module will be equipped with diagnostic signal inputs.

4.9.2.4.4 Beam Position Limit Detector (BPLD)

The BPLDs will monitor the analog output voltages of the 14 Orbit Interlock BPMs and will disable the ring RF if the beam position exceeds its trip limits. The difference between the mechanical and electrical centers of each BPM will be measured by using the orbit monitor system and stored in the SPEAR control computer database. These offset values will be subtracted form the desired trip limits to provide a table of position limits for the BPLDs. The position limits will be downloaded to the microcontrollers. The BPLDs will be packaged in modules and installed in crates in the four remote BPM processor stations located outside the ring. A BPLD crate will accommodate four BPLD modules.

A BPLD module will support four BPMs and will provide four enable signals to the system summary interlock. This will allow the summary interlock to detect which of the four channels generated a beam abort. The BPLD will digitize the processed BPM position signals and compare them to the limit values. At power-up the BPLD microcontroller will enter an initialization mode where it will load its RAM with position limits from the microcontroller EEPROM. When completed, the microcontroller will begin limit-checking operation. In order to avoid aborting the beam from noise or spurious signals, the microcontroller will be programmed to turn off the ring RF only if mis-steered beams are detected continuously for 500 μs.

The BPLD module will have a 16-bit microcontroller to manage interlock logic, status display, and diagnostic functions. A typical microcontroller for this application has the following features:

- 16-bit CPU operating at 40 MHz
- up to 512 kBytes of ROM/flash
- 512 bytes of EEPROM
- up to 512 kBytes of SRAM
- 8 channels of 12-bit A/D, 10 ksample/s
- 2 channels of 12-bit D/A, 10 ksample/s
- 32 I/O pins

- 3 each 12-bit timers
- 1 watchdog timer
- 2 each RS232 and 1 each RS485 communication ports

A functional layout of a BPLD module is shown in Figure 4.102.

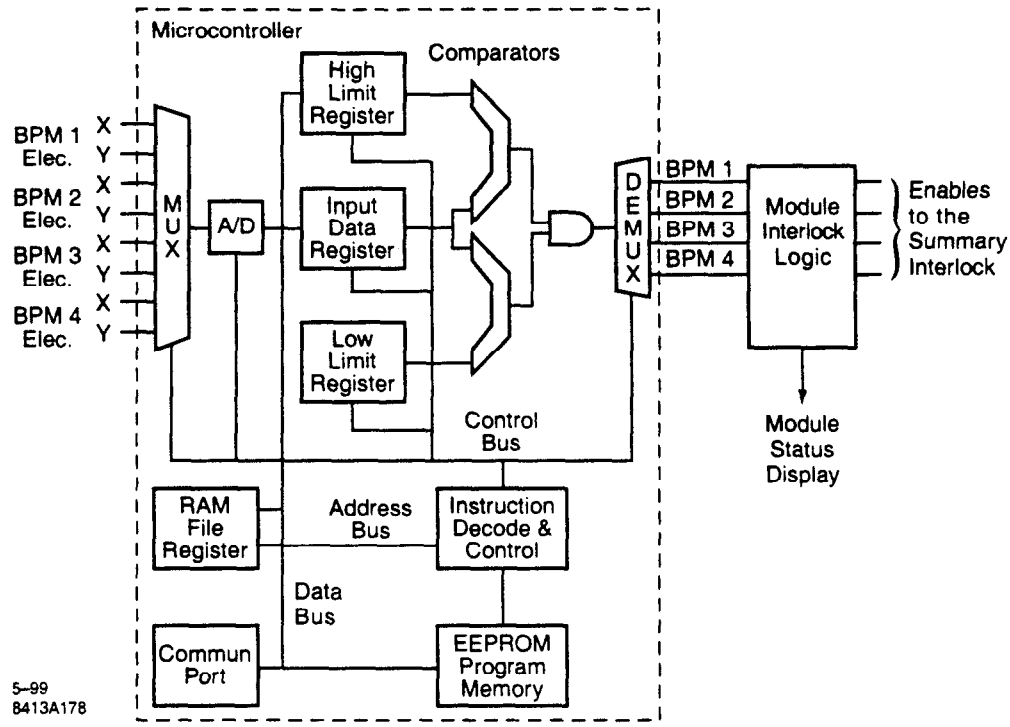

Figure 4.102 Beam position Limit detector Module (BPLD).

The BPLD master controller will communicate with the SPEAR control computer. Its main functions will be to download position limits to the BPLDs and to transfer BPLD status information to the SPEAR computer. The master controller will consist of a microcontroller, EEPROM, and communication ports.

4.9.2.4.5 Summary Interlock and RF Interrupt

The summary interlock logic will be designed to monitor the BPLD enable signals, insertion device gap limit switches, average beam current, and status of switches that bypass unused BPMs. BPLD faults will be latched and displayed. The summary interlock outputs will have a fast interface to the ring RF system, capable of aborting stored beam in less than 200 μs.

4.9.2.4.6 Orbit Interlock Control Interface and Integrity Test

The four remote BPLD crate controllers will be interfaced to the SPEAR computer through an RS-232/485 network. This interface will allow the SPEAR computer to:

- download the BPMs position limits to nonvolatile memory (EEPROM) in the micro-controllers
- monitor and display the status of the Orbit Interlock system
- keep a running record of the orbit over the most recent 100 ms for after-fault orbit analysis
- control the overall system integrity test

The Orbit Interlock system will operate as a stand-alone system and will not rely on any real-time information generated by the SPEAR control computer.

System integrity tests will be performed routinely prior to normal machine fills. These tests will be fully controlled by the SPEAR control computer. Application software will be written to automatically generate local orbit perturbations and move the beam at each BPM until a trip limit is reached, with a passively safe beam current (<20 mA). The software will check measured trip values against stored data to determine whether all criteria have been satisfied.

4.9.3 Personnel Protection System (PPS)

Several hazards will be present in the SPEAR 3 accelerator enclosure during operation, including:

- ionizing radiation dose rates in the order of kRad/hr caused by beam loss
- ionizing radiation dose rates in the order of Rad/hr caused by field emission in the RF cavities
- non-ionizing radiation dose rates in the order of mW/cm^2 caused by open or missing RF waveguide
- exposed electrical leads on magnets that operate at voltages up to 425 V and currents up to 900 A

The first line measures used to prevent personnel exposure to the hazards include:

- adequate shielding
- locked gates or doors to keep personnel away from hazardous devices
- administrative procedures for the proper operation of hazardous devices
- employee awareness training on the hazards present during beam operations

The Personnel Protection System (PPS) is intended to prevent unauthorized or accidental entry to areas having the potential for radiation or electrical hazards. It is also intended to shield personnel working outside the accelerator enclosures and the experimental stations from potential radiation generated during the accelerator operation.

The PPS includes shielding, an Access Control System (ACS), and a Beam Containment System (BCS). The ACS and BCS are active protection systems designed to ensure personnel safety if one or more of the first line measures fail.

Elements of the PPS include physical barriers, beam stoppers, entry stations, beam shut-off ion chambers, status signs and warning indicators, audio/visual warning devices, and a body of administrative procedures that define safe shielding entry conditions.

PPS systems are in place for the linac vault and diagnostics room, the booster synchrotron, the SPEAR storage ring, and the x-ray experimental stations.

4.9.3.1 Shielding

Beam losses are the main source of radiation produced in particle accelerators. The beam losses occurring in the SPEAR 2 storage ring can be divided into three categories:

- losses during injection and energy ramping
- loss of stored beam during users mode
- losses when beam is dumped prior to a new beam injection

It has been estimated that, on average, 40% of the SPEAR 2 beam is lost during injection and ramping from 2.35 GeV to 3 GeV; 50% of the stored beam is lost during the 24 hours of users mode; and 50% is lost when the beam is dumped.

Injection into SPEAR 3 will be at the operating energy of 3 GeV. Two of the loss scenarios described above can thus be avoided: dumping of the stored beam prior to injection and energy ramping after injection. It is expected that the SPEAR 3 injection efficiency will be better than for SPEAR 2, and that only 25% of the beam will be lost during injection. In spite of this improvement in injection efficiency, the cumulative radiation dose behind shielding for SPEAR 3 will increase by a factor of approximately 1.6 at 200 mA, and a factor of approximately 4 at 500 mA, as a result of the increase in current and injection energy.

The SPEAR 3 shielding and the BCS are designed to prevent excessive radiation dose or dose rates outside the accelerator enclosures and experimental stations [15,16].

4.9.3.2 Access Control System (ACS)

The Access Control System protects against the following hazards:

- entry to a shielding exclusion area
- beam transport from an exclusion area to an occupied area
- operation of radiation-producing devices while a shielding area is occupied
- electrical shock from powered magnets

In addition the ACS controls or provides administrative assistance for the following functions:

- search and secure sequence
- transfer of the access modes
- entry to an area
- emergency crash
- audio/visual warning

Elements of the system include gates and doors, a search and secure system, keybanks, emergency crash system, beam stoppers, status signs and warning indicators, closed circuit TV, audio/visual warning devices, interlock logic, and a body of administrative procedures that define safe entry conditions.

The basic principles used in the design of the SPEAR ring ACS are:

- all circuits are designed to be fail-safe
- the system fault logic is implemented using two independent chains, each capable of aborting the beam
- all inputs are sensed independently by two parallel systems
- the system uses three methods to shut off the electron beam
- the system uses three methods to prevent beam transport from an exclusion area to an occupied area

Redundancy in the ACS interlock circuitry ensures that an undetected failure of one interlock chain will not compromise the ability of the other to maintain safety. The redundancy is maintained from sensors (e.g., two switches on every door) to the final shutdown mechanism [17,18,19,20].

The SPEAR ring ACS operates in the modes listed in Table 4.50

Table 4.49 SPEAR ring access modes.

Permitted Access:	Unrestricted access to the ring.
Controlled Access:	Entry and exit from the ring is done under the control of an operator. It requires keys release and logging of the entries.
Restricted Access:	Prior to the transfer of the ring to Restricted Access mode, the ring must be searched and secured. Electrical hazards may be turned on, but the ring RF is kept off, stoppers are kept closed, and beam can not be injected into the ring.
No Access:	Prior to the transfer of the ring to No Access mode, the ring must be searched and secured. All systems can be turned on, stoppers can be opened and beam can be injected into the ring.

The ACS allows the transfer of the ring to an access state only if there is no potential for radiation or electrical hazards. This requires that the booster-to-SPEAR (BTS) and ring stoppers be closed and that the ring RF and all electrical hazards be off. The system allows beam to be injected into the storage ring only after the ring has been searched and secured and is in the No Access state.

A block diagram of the SPEAR ACS and BCS is shown in Figure 4.103.

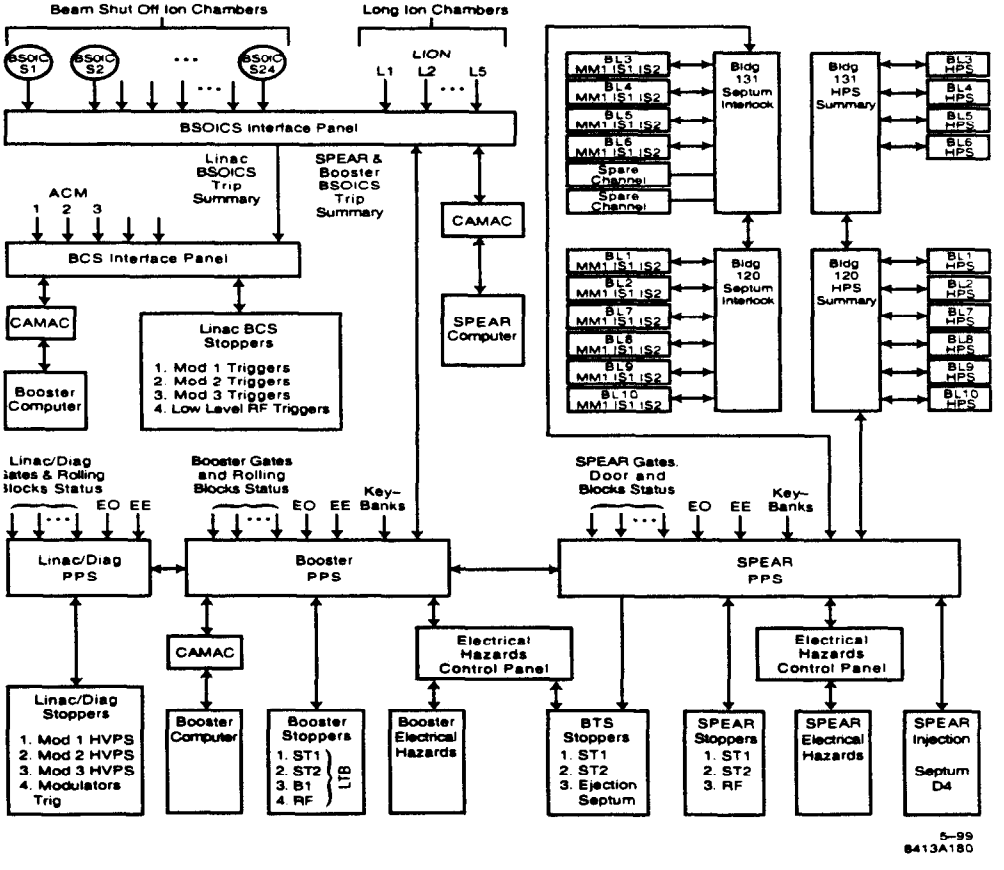

Figure 4.103 SPEAR ACS and BCS.

The linac, booster, SPEAR storage ring, and the x-ray experimental stations have independent ACS systems. By switching the linac beam into the diagnostics room and closing the linac-to-booster (LTB) stoppers, the booster tunnel may be entered while the linac is on. The SPEAR tunnel can be

accessed while the booster is operating by inserting the BTS stoppers and experimental stations can be accessed with beam in SPEAR by inserting the photon stoppers. Table 4.22 lists the requirements for access to each part of the SPEAR facility.

Table 4.50 Requirements for access to the SPEAR facility.

REQUIRES THAT / ACCESS TO	HUTCH STOPPERS 1. HS1 2. HS2	SPEAR RING STOPPERS 1. ST1 2. ST2 3. SPEAR RF	BTS STOPPERS 1. ST1 2. ST2 3. ES MAG PS	BOOSTER STOPPERS 1. LTB ST1 2. LTB ST2 3. LTB MAG B1 PS 4. BOOSTER RF	LINAC STOPPERS 1. MOD 1 HVPS 2. MOD 2 HVPS 3. MOD 3 HVPS 4. TRIG TO MOD	ADDITIONAL REQUIREMENTS
X-RAY EXPERIMENTAL STATION	IN	N/R	N/R	N/R	N/R	
SPEAR RING	N/A	IN/OFF	IN/OFF	N/R	N/R	SPEAR ELECTRICAL HAZARDS OFF
BOOSTER RING	N/A	N/A	N/A	IN/OFF	N/R	BOOSTER ELECTRICAL HAZARDS OFF
LINAC / DIAGNOSTICS ROOMS	N/A	N/A	N/A	N/A	OFF	

BTS = BOOSTER - TO - STORAGE RING
ES = EJECTION SEPTUM
HVPS = HIGH VOLTAGE POWER SUPPLY
LTB = LINAC - TO - BOOSTER
MAG = MAGNET
MOD = MODULATOR
N/A = NOT APPLICABLE
N/R = NOT REQUIRED
PS = POWER SUPPLY
ST = STOPPER

7-98
8413A183

Beam stoppers separating two adjacent areas are always controlled by the ACS for the area down-beam of the stoppers. LTB beam stoppers are controlled by the booster ACS and the BTS beam stoppers are controlled by the SPEAR ring ACS. Beam line photon and injection stoppers are controlled by the Hutch Protection Systems (HPS), which functions as the access control system for the beam line experimental stations.

Operation of the SPEAR storage ring ACS requires a "handshaking" with the booster ACS and the photon beam line HPS. A security fault on a beam line dumps the SPEAR beam and, if injecting, closes the BTS stoppers and shuts off the SPEAR septum magnet (via the Septum Interlock), required to be on for injection. A security fault in the SPEAR takes the same action. Table 4.51 lists possible PPS violations and system responses for various areas of the SPEAR facility.

Table 4.51 Possible PPS violations and their corresponding responses.

RESPONSE / PPS VIOLATION	HUTCH STOPPERS	SPEAR INJECTION SEPTUM MAG PS	SPEAR RING STOPPERS	BTS STOPPERS	BOOSTER STOPPERS	LINAC STOPPERS	ADDITIONAL RESPONSE
			1. BT1 2. BT2 3. SPEAR RF	1. BT1 2. BT2 3. ES MAG PS	1. LTB BT1 2. LTB BT2 3. LTB MAG B1 PS 4. BOOSTER RF	1. MOD 1 HVPS 2. MOD 2 HVPS 3. MOD 3 HVPS 4. TRIG TO MOD	
PHOTON BEAM LINE HPS	IN	N/A	IN / OFF	N/R	N/R	N/R	
PHOTON BEAM LINES SEPTUM MAG PS INTERLOCK	N/A	OFF	N/R	IN / OFF IF SEPTUM MAGNET PS IS NOT OFF	N/R	N/R	
SPEAR RING	N/A	OFF	IN / OFF	IN / OFF	IN / OFF IF THE BTS STOPPERS ARE NOT IN / OFF	OFF IF THE BTS STOPPERS ARE NOT IN / OFF	1. DUMP SPEAR ELEC HAZARDS
BOOSTER RING	N/A	N/A	N/A	OFF 1. EJEC SEPT PS	IN / OFF	OFF IF THE LTB STOPPERS ARE NOT IN	1. DUMP BOOSTER ELEC HAZARDS
LINAC / DIAGNOSTICS ROOMS	N/A	N/A	N/A	N/A	N/A	OFF	

BTS = BOOSTER - TO - STORAGE RING
ES = EJECTION SEPTUM
HPS = HUTCH PROTECTION SYSTEM
HVPS = HIGH VOLTAGE POWER SUPPLY
LTB = LINAC - TO - BOOSTER
MAG = MAGNET
MOD = MODULATOR
N / A = NOT APPLICABLE
N / R = NOT REQUIRED
PS = POWER SUPPLY
ST = STOPPER

7-98
8413A184

4.9.3.3 Beam Containment System (BCS)

The Beam Containment System (BCS) prevents the accelerated beams from diverging from the desired beam channel and from exceeding safe levels of energy and intensity, both which may cause excessive radiation in occupied areas.

Elements of the SPEAR 3 BCS include slits and collimators, electron beam stoppers, and beam shut-off ion chambers (BSOICs) installed outside the ring. The existing SPEAR BCS will be augmented for SPEAR 3 with a Beam Loss Monitor (BLM) system that uses long ion chambers (LIONs) installed in the BTS and SPEAR tunnels. The Linac BCS, which also employs Average Current Monitors, will remain unchanged for SPEAR 3.

The SPEAR 3 BLM system will:

- help limit the localized beam losses during injection
- prevent excessive radiation, resulting from incorrectly steered beam, in areas that might be occupied by people
- provide a relative measurement of beam loss rates and the approximate location of the beam loss events throughout the ring
- provide data on potential radiation hot spots
- provide beam loss histories that will allow to keep an account of the total electron losses over the year
- provide diagnostic information that can be used to improve beam steering and control during commissioning and operation

4.9.3.3.1 Long Ionization Chamber (LION)

The LION is a distributed ion chamber used to monitor and localize radiation losses along a beam line resulting from mis-steering. The sensitivity of this type of monitor depends on a number of factors, including the diameter of the cable, the distance of the cable from the beam line, the amount of shielding between the beam line and the cable, the ion chamber gas and pressure, and the DC voltage applied to the center conductor [21,22,23,24,25].

The SPEAR 3 BLM system will use 7/8-inch air dielectric coaxial cables for ionization chambers. The LION cables will be filled with a gas consisting of 90% Ar and 10% CF4 that will be kept at 20 psi. To maximize the system sensitivity, the LION cables will be installed parallel and as close as feasible to the vacuum chamber. To minimize exposure of the cables to synchrotron radiation, they will be installed out of the plane of radiation.

The ionization current generated in a LION cable can be the result of a single point beam loss or of a distributed beam loss. The maximum length of the LION cables will be determined by the expected linear beam loss (W/m) and the maximum allowed single point loss (W). Short length cables make it easier to isolate beam losses for turn-by-turn diagnostic measurements.

A voltage of 250 VDC will be applied to the center conductor of each LION cable and the cable shield will be kept at ground potential. The signal from each LION cable will be connected with a coaxial extension cable to processing electronics. The electronics include: a current to voltage converter, an integrator, an interface to the SPEAR control computer, level comparators to generate shut-off commands, and a logic interface to the BCS. The LION electronics will also include continuous automatic checking (house-keeping) to verify the integrity of the ion chamber cable plant. If the integrated beam loss is above the preset level the system logic will abort injection to the SPEAR ring. The beam losses measured by the LIONs will be constantly sent to the SPEAR control computer and stored in a database. This data will be used for further beam loss analysis. Figure 4.104 shows a schematic layout for the LION detector.

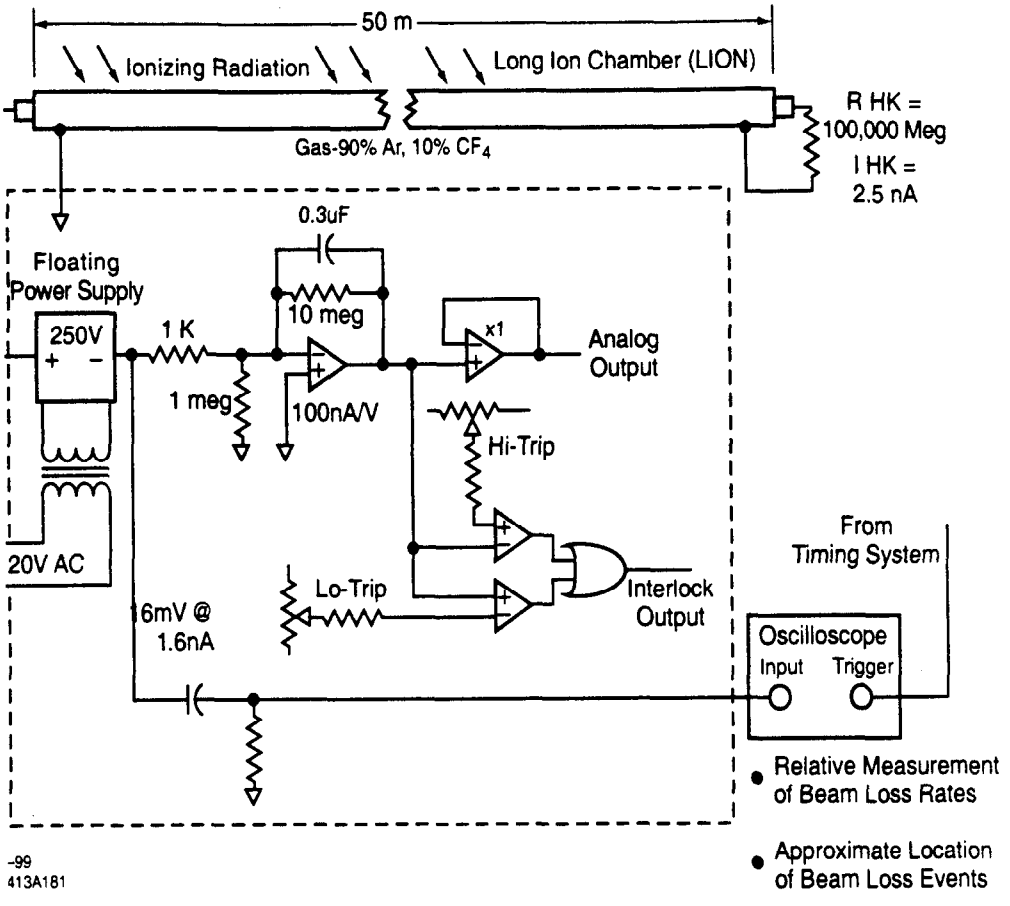

Figure 4.104 Long Ion Chamber (LION) detector electronics.

The minimum detectable charge in a LION is determined by the leakage currents in the loss monitor electronics, gas-filled cables, and signal cables. For the SLAC FFTB tunnel the leakage is approximately 10 pA. Maintaining pressure in the cables has kept the leakage within specifications. It is estimated that the sensitivity of the system, with the cables placed 0.3 m away from the vacuum chamber and using a 100 nA/V current-to-voltage converter, will be about 2 mV for a loss of 10^7 electrons [26]. This is a beam loss of about 2.5% of the injected current to SPEAR 3. The sensitivity may vary by more than a factor of 10 depending of the location of the loss. This is because losses at some locations see relatively little shielding between the loss point and the loss monitor cable, while losses at other locations may see several feet of shielding (steel and copper in large magnets).

In addition to its primary function as part of the SPEAR 3 BCS, the LION system will be used as a beam loss diagnostics tool. The system will provide information on the approximate location of beam losses for accelerator operators and can be used to determine beam loss causes to improve beam steering and control.

4.9.3.4 SPEAR Operational Safety Protocol

An administrative protocol developed by the SSRL Operations group and approved by the SLAC Radiation Physics and SSRL Safety Offices guarantees that the SPEAR ACS and BCS interlocks and devices function properly and that all necessary shielding and locking panels are in place before SPEAR ring operation is permitted [27]. This protocol includes performing system check-outs and

inspections and completing "Beam Authorization Sheets" according to written instructions. It also addresses the training and certification of personnel who will become "SPEAR PPS Operators" and/or Searchers. A SPEAR PPS operations logbook is provided in which relevant information is entered according to the established protocol.

References

[1] R. Yotam, "SPEAR MPS", PLC program listing, October 1996.

[2] R. Yotam, "SPEAR magnet & bus LCW MPS", PLC program listing, October 1996.

[3] Allen-Bradley Co., "SLC 500 Modular Hardware Style", publication 1747-6.2, July 1994.

[4] B. Scott, "Vacuum System", SPEAR 3 Upgrade Project CDR, June 1988.

[5] J. Sebek, "Flux on 15mm Button vs. Vertical Distance from SPEAR 3 Chamber Axis, private communication.

[6] D. Martin, "Diplexers for the Orbit Interlock System", private communication.

[7] K.B. Unser, "New Generation Electronics Applied to Beam Position Monitors", Beam Instrumentation: Proceedings of Seventh Workshop, May 1996.

[8] E. Medvedko, S. Smith, and A. Fisher, "A Machine Protection Beam Position Monitor System", Proceedings of the Eighth Beam Instrumentation Workshop, May 1998.

[9] Analog Devices Inc., "Low Power Mixer/AGC/RSSI 3V Receiver IF Subsystem", AD607, 1995.

[10] G. R. Aiello and M. R. Milles, "Preliminary Evaluation of AD640 Logamp Detector for BPM Electronics", SSCL-N-787, February 1992.

[11] Analog Devices Inc., "DC-500 MHz/86 dB Dynamic Range Logarithmic Amplifier", AD8307, 1977.

[12] J. Safranek, "Photon Beam Steering Envelope", SPEAR 3 Upgrade Project CDR, July 1998.

[13] R. Merl and G. Decker, "Design of Digitizing Beam Position Limit Detector", Proceedings of the Eighth Beam Instrumentation Workshop, May 1998.

[14] R.J Nawrocky and G. Decker, "An Active Interlock System for the NSLS X-Ray Ring Insertion Devices", Proceedings of the Sixth Beam Instrumentation Workshop, May 1995.

[15] J. Corbett, E. Guerra, and N. Ipe, "Electron Beam Loss for SPEAR 3, October 1997.

[16] Vashek Vylet and Alberto Fasso, "Shielding and Radiation Considerations for the SPEAR 3 Upgrade, SLAC Radiation Physics note RP-98-8, June 1998.

[17] R. Yotam, "Description of the SSRL SPEAR Personnel Protection System", SSRL note code: 1565 serial M233, August 1994.

[18] SLAC, "Health Physics Manual of Good Practices for Accelerator Facilities", SLAC report 327, April 1984.

[19] DOE, "Safety of Accelerator Facilities", DOE 5480.25.

[20] DOE, "Guidance for an Accelerator Facility Safety Program", DOE 5480.25.

[21] J. Rolfe et al., "Long Ion Chamber Systems for the SLC", SLAC-PUB-4925, March 1989.

[22] R.W. Zdarko, "LIONs at the Stanford Linear Accelerator Center", January 1998.

[23] D.R. Patterson, "Design and Performance of the Beam Loss Monitor System for the Advanced Photon Source", Proceedings of the Fifth Beam Instrumentation Workshop, October 1994.

[24] D.R. Patterson, "Initial Commissioning Results from the APS Loss Monitor System", Proceedings of the Seventh Beam Instrumentation Workshop, May 1996.

[25] A.S. Fisher et al., "Commissioning the Beam Diagnostics for the PEP-II B Factory", Proceedings of the workshop on Diagnostics and Instrumentation for Particle Accelerators (DIPAC, Frascati, Italy), October 1997.

[26] D. McCormick, "SPEAR 3 Loss Monitor System," private communication, March 1998.

[27] SLAC-I-720-0A05Z-002, SLAC ES&H Dept., 1998.

4.10 Cable Plant

The cable plant upgrade stands as an essential element of the SPEAR 3 project, because cabling influences the performance and reliability of every system in the facility. Cables must be selected and installed as carefully as any other accelerator component, since the technical requirements of all those other components influence the specification of all cable hardware. Cable system design encompasses every aspect of an engineering project, including: 1) technical performance; 2) material, assembly, and installation costs; 3) reliability and maintainability; and also 4) adherence to civil codes, resource conservation, and safety practices.

The SPEAR 3 technical systems employ a large number of cables. Some of the cables now in use are relatively new and in good condition, while others date to the early years of SPEAR. Several factors—including technical feasibility, cost, schedule, and the ultimate performance of the completed machine—contributed to the decision to raze the existing cable plant. The advantages of this plan are significant. Removal of the tunnel's aisle-side cable tray and cable load will facilitate the unimpeded installation of new girders, magnets, and related facility improvements. Additionally, damage to these existing cables during heavy installation will be eliminated as a concern. An entirely new cable plant will ensure compliance with the most up-to-date construction code and safety requirements. Upon completion of the project, the properly designed cable plant will enhance the reliability, performance, and appearance of SPEAR 3.

Considerable documentation is necessary to implement the project. Each family of cables must be described by a layout drawing that provides information on: 1) cable endpoints, 2) cable numbers, 3) vertical travel, 4) routing, 5) connector type, and 6) dressing. Some of the information will only become available through physical inspection of the site. This drawing package is necessary for both the bidding and installation phases of the project. The CAPTAR database† will handle the labelling and documenting of all new cables, as well as whatever existing cables will be reused in SPEAR 3.

A single aisle-side cable tray is used for routing and supporting the majority of cables inside the ring. Also located within the tunnel, a second wire-way holds cables for the high-current series-connected devices: i.e., the Dipole, QFC, SF, and SD magnets. The current aisle-side cable tray, which is in poor condition overall, needs replacement. New external trays running above and outside the machine enclosure will feed the replacement aisle-side tray. Connections to the external trays will be made through six new shielding penetrations. A wire-way now used to enclose high-voltage ion-pump (HIP) cables will be removed but not replaced. New HIP cables will be installed in the aisle-side cable tray using a tray separator.

†CAPTAR is the SLAC Cable Plant Tracking Database developed from the commercially available Oracle relational database program.

As a system, the cable tray, cables, and associated connectors will meet the performance requirements of each technical system, along with all safety requirements established by the National Electrical Code, Stanford Linear Accelerator Center, and the Department of Energy.

4.10.1 NEC Compliance

Pursuant to Bulletin 37 of the SLAC Environment, Safety and Health Division (ES&H), all cables installed in a new facility—or installed as a major modification to an existing facility—must be installed according to applicable National Electrical Code (NEC) regulations. Therefore, all SPEAR 3 cables and associated cable-plant upgrades must conform to the requirements of Bulletin 37.

Compliance to the requirements of Bulletin 37 and NEC will be achieved primarily through proper engineering design and review of these designs by the SLAC Electrical Safety and Fire Prevention Safety Committees. Additionally, engineering oversight of qualified electrical contractors at each stage of construction will be provided to ensure regulatory compliance.

Several aspects of the National Electrical Code are of particular relevance to the SPEAR 3 cable plant. Engineering design and planning early in the project will ensure the following:

- Cable tray shall be a contiguous, grounded, engineered system (NEC 318-2).
- Cable tray shall meet cable-fill requirements (NEC 318-9).
- Cables shall be tray-rated (Type TC), whenever possible (NEC 340-1).
- Cables shall be rated Low-Smoke Non-Halogen, whenever possible.
- Radiation resistant material shall be specified, whenever possible.
- Special-purpose cables (e.g. RF) shall be installed according to NEC 725-820.
- The Laboratory Director shall approve situations outside the cited codes.

Detailed issues related to NEC compliance are addressed in Section 4.10.2 through Section 4.10.6

4.10.2 Cable Tray and Wire Way

Cable tray is used for routing, supporting, and protecting instrumentation and power cables. The existing SPEAR 2 aisle-side ring tray is overfilled, not contiguous, and is generally in poor condition. The tray will therefore be replaced. Heavy-duty 6" x 12" hot-dipped galvanized tray meets the capacity requirement, resists corrosion, and withstands occasional—but inevitable—use as a climbing support. In four short areas adjacent to the East and West pits (Matching Cells), the cable tray width increases to 18." The new aisle-side tray will fit in the space vacated by the existing tray. The NEC 318.9 limit on the maximum number of cables shall be met, as shown in Figure 4.105. This is accomplished by carefully balancing the cable load through the available penetrations, so that no tray carries more than the cable allocation for a single girder. Exceptions are made for the four Matching Cells, where the wider tray carries cables for two girders. The existing floor-level cable tray in the East and West pit areas is 6" x 18" ladder type, in good condition, and will be reused, subject to the details of civil engineering modifications. Additional overhead trays must be added in the pit areas to feed the Matching Cell girders as well as each girder adjacent to a Matching Cell (girders 1,2,8,9,10,11,17,18). New trays will also be required to service the RF cavities in the West pit, and the special devices (e.g. the transverse kicker) in the East pit. Total power dissipation (at operating currents) for the 12" aisle-side tray configuration has been estimated at 80W/m of tray.

The enclosure trays are fed through shielding wall penetrations (three penetrations in each arc, and one penetration in each pit area) by a three-tier tray system running above and outside the enclosure, as shown in Figure 4.106. These new trays connect to an existing cable tray highway

serving Buildings 117 and 118. The fill factors of the three cable trays, shown in Figure 4.107, meet the requirements for power and instrumentation cable tray (NEC 318.9a(2) and NEC 318.9b, respectively). Additional entry to the equipment buildings is provided by four 10" diameter underground conduits, extending east and west toward Building 118. An overall goal of the cable tray plan is to allow SPEAR 3 cables to be installed unencumbered by the existing cable plant. This parallel effort 1) allows for the cleanest possible installation of the new system; 2) it is not disruptive to present operation; and 3) it simplifies the decommissioning of SPEAR 2.

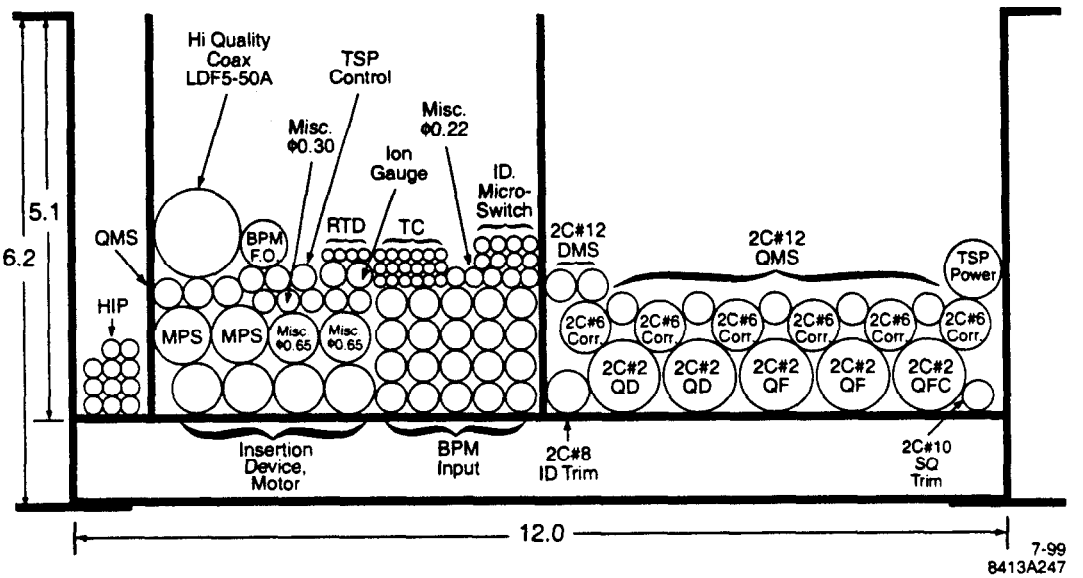

Figure 4.105 Aisle-side cable tray cross-section.

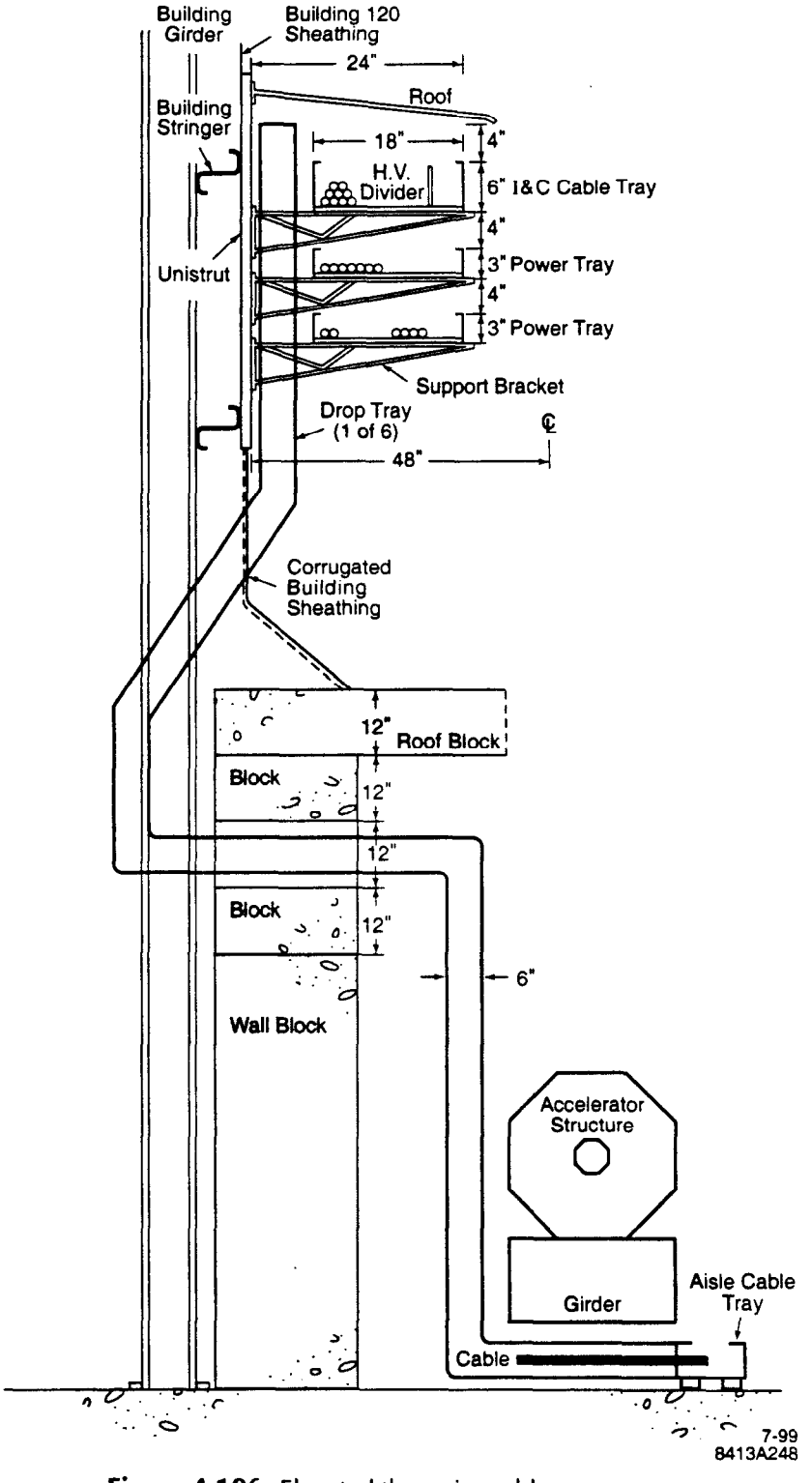

Figure 4.106 Elevated three-tier cable tray system.

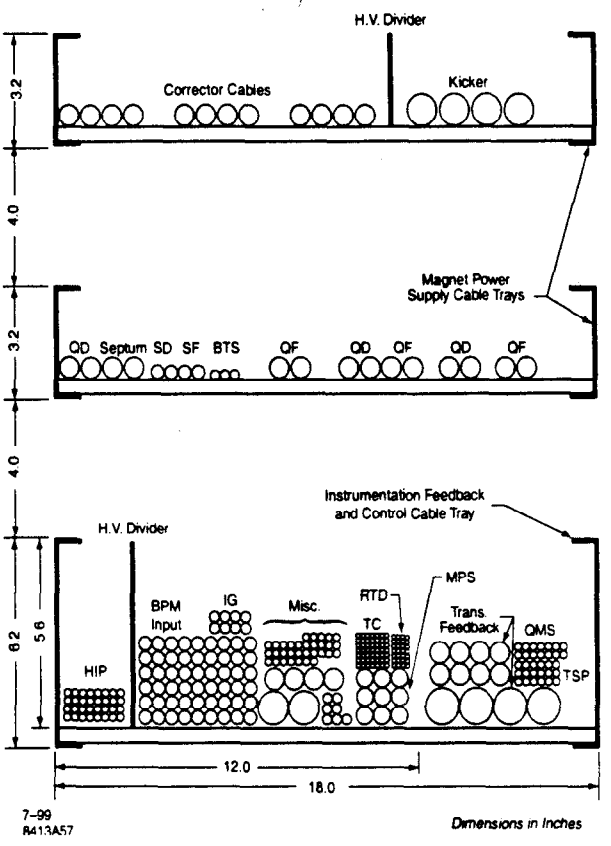

Figure 4.107 Three-tier cable tray cross-section

Mounted on aluminum blocks 2" above the enclosure floor, the enclosure cable tray runs the entire aisle-side circumference of the ring (except for breaks at the RF cavities). Tray loading is not a concern, as the spacing between blocks can be made as small as necessary. To meet future contingencies, the blocks are designed to support a smaller, second-tier tray as well. Cables extend in the air, taking the shortest possible route from the cable tray to the devices served. The power cables, which are least likely to require attention during the facility's life-span, will be placed closest to the girder. To prevent an inadvertent cable snag from damaging a connected device, each cable will be strain-relieved where it connects to a device. The "dressing-in" of each cable will also include a service loop to facilitate connector replacement.

At the insertion devices (IDs), the tray must be rotated 90°, in order to maintain maximum aisle clearance. As such a component is not commercially available, a suitably "twisted" tray section will be designed and installed, two at each ID. These specially designed tray sections will maintain the performance characteristics of the standard tray. Radiation-resistant cable ties will secure cables crossing these tray sections.

Type MV (NEC 326-1) or suitably rated cables will be utilized to power high-voltage ion pumps (HIP's) in SPEAR 3. This cable will be run in the aisle tray, separated by a solid, fixed, metal tray barrier (NEC 318-6f). An exemption (waiver) to the single-layer requirement of NEC 318-12 will be requested, since the ion-pump cables produce negligible heat (< 1 μW/m of cable tray).

Construction of the SPEAR 3 cable tray system will be coordinated with the various stages of civil modifications. Construction of the tray penetrations will occur during the FY2000 SPEAR 2

maintenance period. Concurrently and thereafter, all external trays can be assembled on the experimental hall buildings, and connections to the existing cable highways can be completed. A significant portion of the new cable plant can be completed during the prior year's, "normal" machine operation. Cables can be pulled into these trays, and connections made to equipment racks. The enclosure ends of the cables will be coiled for final installation during the FY2002 shutdown. In most cases, it will be feasible to pre-terminate the cables outside the enclosure, thereby saving critical final installation time.

4.10.3 Cable Tray Grounding

Cable-tray grounding addresses the issues of personnel safety, equipment protection, and electronic noise reduction. NEC 318.6 requires that cable tray shall be contiguous, grounded, and installed as a complete system. The tray thus constitutes an equipment-grounding conductor capable of carrying fault currents back to the ring ground and bonded neutral. This prevents the exposed metal surface from being energized. Grounded cable tray also serves as a ground plane for low level instrumentation signals.

Grounding will be made to the buried ring-wide ground bus (Section 4.6.8) through 4/0 bare copper cable at established intervals. Galvanized tie plates between tray sections will provide mechanical connection as well as electrical bonding.

4.10.4 Cable Removal

The SPEAR facility contains a significant burden of now-unused cable. Removal of these cables is desirable in several respects: cable tray space is freed, the cooling of operating cables is increased, and system maintenance is enhanced. Additionally, the combustible load decreases, and the finished appearance of the facility improves.

Unused cable in the enclosure aisle-side cable tray will be removed when this cable tray is dismantled in FY2002. Other unused cable, not in the tray, but still slated for removal, will be identified and cleared out on a case-by-case basis. An ongoing campaign to remove old and unused cables during SPEAR maintenance periods further benefits the SPEAR 3 project.

Cable removal begins with the identification and removal of cables whose functions are uncertain. These cables are then examined by SSRL system managers for correlation to their respective systems. Final identification is made by determining that at least one end is not connected. Cables tagged for removal are cut into suitable lengths and pulled from the trays. This material is loaded into scrap bins and transferred to the SLAC Salvage Yard, where it is checked for radioactivity and its final disposition is determined. Typically, this material can join the commercial scrap metal stream.

The scope of cable removal work includes clearing of: 1) the existing 4" x 12" ring instrumentation tray, 2) the cable trays in both the East pit and West pit, and 3) the four 10" diameter underground steel conduits connecting the ring tray in two places to Building 118. The East and West pit trays are presently filled to 80% and 95% capacity, respectively. The conduits are at 20% of capacity. Unused cable will also be removed from the overhead trays running to Buildings 117 and 118, as well as from under the computer floor in Building 118.

Working cables may be removed during the FY2002 installation shutdown on a case-by-case basis, when doing so simplifies the entire project. These cables will be replaced during the new-cable installation phase.

4.10.5 Reused Cable

A significant number of installed cables shall be retained for use in SPEAR 3. The ID cables fall in this category. Cables for the IDs run from the ring enclosure, through shielding penetrations, and to the beam-line areas. During the project installation phase, these cables will be folded back against the outer enclosure wall. Because some ID cables may be damaged, the project cost estimate includes a fractional replacement cost as a line item. Only those cables damaged during the installation phase will be replaced.

All reused cables will be inspected for connector integrity and tested according to operating requirements or governing specifications. Connectors found to be damaged, corroded, out of tolerance, or otherwise unsatisfactory will be replaced.

Many other cables in SSRL are unaffected by the upgrade project. Cables that do not enter the ring enclosure, nor carry beam-related signals, nor carry power to magnets, fall into this category. Largely unaffected by the upgrade project are: 1) the control cables running between SPEAR control room (Building 117) and the SPEAR power supply building (Building 118), 2) computer cables, and 3) conventional AC distribution cables.

4.10.6 New Cable Installation

Numerous new cables will be installed in the SPEAR 3 upgrade. These cables are identified by family and function in Table 4.52.

Type TC (Tray Cable) control cable with braided shield is specified for all applications, except in cases where Type TC is unavailable. In these situations, specified cable will adhere to SLAC Bulletin 37. Cables that run through tray into overhead outdoor trays to Building 117 and Building 118 will have "sunlight resistant" jacket material, such as ethylene-propylene rubber (EPR). After all superseding requirements are satisfied, cables within the shielding enclosure will be selected for radiation resistance and for Low Smoke Non-Halogen (LSNH) jacket material. Where practical, cables will be pre-assembled with connectors to reduce installation time. In most cases, cable connectors will be installed in the field. Safe high-voltage (SHV) connectors will be utilized for high-voltage ion pump cables.

BPM jumpers will be employed from the button sensors to N/SMA bulkhead-adapter fittings, mounted on the girders, and bringing all BPM connections to a common girder flange. The flexible jumpers protect the button from accidental movement of the LMR-400 trunk cable, and allow for easier connection at the button. A similar system is in place at the Advanced Photon Source, and it has worked well. The jumpers will be routed through the interior of the girder. The jumpers incorporate a radiation resistant dielectric. TEFLON™ is not suitable, but TEFZEL™, REXOLITE™, PE, PEK, and PEEK polymers are radiation resistant and available at reasonable cost, with PE (polyethylene) the most likely choice. Extreme radiation resistance, to 5 x 10^9 rads, can be achieved using PEEK, but it is not required. SiO_2 cable is virtually impervious to radiation but also relatively expensive, and usually it must be formed into place.

Electrical noise around accelerators covers a wide range of amplitudes and frequencies, often creating interference with sensitive instrumentation. Long cables are the principle means by which noise is introduced into the electronics. The shielding requirements of each system shall be considered when I&C cables are specified. Table 4.52[1,2] identifies several cable types and their relative shielding effectiveness.

SPEAR 3 uses many coaxial cables, particularly for the BPM system. While it is clear that a semi-rigid coaxial cable fully covered by metal offers the highest shielding and lowest attenuation, the cost of the cable must be considered. For the BPM system, a composite braid/foil cable has been

selected. The foil improves the shielding and decreases the inter-modulation distortion (IMD) produced by a braided shield. This type of cable offers performance similar to a premium-cost semi-rigid cable.

Table 4.52 SPEAR 3 cables by function

Cable Function	Cable Type	No.	Avg. Length (feet)	O.D. (inches)	Weight (lbs./ft.)	Jacket Material	Temp. Rating	Notes
BPM Buttons	LMR-400	360	190	0.405	0.068	PE (UV)	+85°C	ES&H Bulletin #37 NEC 820-53(c)
BPM Process, output	Fiber Optic	4	365	0.600	0.055	NSR-PVC	+80°C	ES&H Bulletin #37 NEC 820-53(c)
Transverse stripline, out	LDF5-50A	8	200	1.09	0.33	Halogen, Fire Retardant	+100°C	ES&H Bulletin #37 NEC 820-53(c)
Transverse stripline, in	LDF5-50A	4	200	1.09	0.33	Halogen, Fire Retardant	+100°C	ES&H Bulletin #37 NEC 820-53(c)
Transverse feedback correlator	LDF5-50A	1	780	1.09	0.33	Halogen, Fire Retardant	+100°C	ES&H Bulletin #37 NEC 820-53(c)
Transverse stripline terminal monitor	LDF4-50A	4	200	0.63	0.15	Halogen, Fire Retardant	+100°C	ES&H Bulletin #37 NEC 820-53(c)
Transverse stripline load	LDF4-50A	4	100	0.63	0.15	Halogen, Fire Retardant	+100°C	ES&H Bulletin #37 NEC 820-53(c)
Transverse feedback local oscillator	LDF4-50A	2	350	0.63	0.15	Halogen, Fire Retardant	+100°C	ES&H Bulletin #37 NEC 820-53(c)
Transverse feedback control	16C#22	4	250	0.34	0.046	PVC (UV)	+80°C	Type TC
ID motor	6C#8	40	247	0.65	0.38	PVC (UV)	+80°C	Type TC
ID switch	2C#22	80	247	0.20	0.011	PVC (UV)	+80°C	Type TC
SR monitor								
Analog signal	LDF4-50A	2	400	0.63	0.15	Halogen, Fire Retardant	+100°C	ES&H Bulletin #37 NEC 820-53(c)
SR monitor control	26C#22	2	300	0.387	0.078	PVC (UV)	+80°C	Type TC
Vacuum pump HV coaxial	SLAC #61-329-007-10	180	110	0.22	0.036		+80°C	HIP Cable, Type MV or RG-58C/U Red
Vacuum TSP power	3C#6	4	400	0.7	0.35	PVC (UV)	+90°C	Type TC
Vacuum TSP control	2C#18	72	350	0.20	0.05	PVC (UV)	+90°C	Type TC
Vacuum ion gauge	CWPT6686	32	350	0.3	0.06			Perkin-Elmer special
DCCT, analog	LDF2-50A	1	350	0.44	0.08	Halogen, Fire Retardant	+100°C	ES&H Bulletin #37 NEC 820-53(c)
DCCT, control and power	LMR-400	2	350	0.405	0.068	PE (UV)	+85°C	ES&H Bulletin #37 NEC 820-53(c)
RF cavity, jumper	LDF2-50A	12	10	0.44	0.08	Halogen, Fire Retardant	+100°C	Not located in ring IC&P cable tray.
RF cavity, replacement	LDF4-50A	2	350	0.63	0.15	Halogen, Fire Retardant	+100°C	Not located in ring IC&P tray.
Injection monitor	LMR-400	2	350	0.405	0.068	PE (UV)	+85°C	ES&H Bulletin. 37 NEC 820-53(c)

Table 4.52 SPEAR 3 cables by function

Cable Function	Cable Type	No.	Avg. Length (feet)	O.D. (inches)	Weight (lbs./ft.)	Jacket Material	Temp. Rating	Notes
Injection monitor	6C#16	4	350	0.27	0.07	PE (UV)	+80°C	Type TC
Injection monitor	RG-223/U	4	350	0.216	0.036	NSR-PVC	+80°C	ES&H Bulletin #37 NEC 820-53(c)
Tune monitor	RFS 7/8RG-333/U	4	250	1.0	0.4	pe	+80°C	Existing
Phase space monitor	RFS 7/8RG-333/U	4	250	1.0	0.4	pe	+80°C	Existing
Thermocouples	2C#20	324	350	0.145	0.05	PVC (UV)	+80°C	Type TC
rtd	2C#20	60	350	0.145	0.05	PVC (UV)	+80°C	Type TC
QD magnet	2C#2	36	350	0.95	0.6	EPR	+90°C	Type TC, 600V
QF magnet	2C#2	36	350	0.95	0.6	EPR	+90°C	Type TC, 600V
QFC magnet	2C#2	14	350	0.95	0.6	EPR	+90°C	Type TC, 600V
Corrector magnet	2C#6	108	350	0.65	0.25	EPR	+90°C	Type TC, 600V
ID trims	2C#8	18	350	0.57	0.20	EPR	+90°C	Type TC, 600V
Dipole trims	2C#12	36	350	0.47	0.13	EPR	+90°C	Type TC, 600V
Quad mod sys	2C#12	90	350	0.38	0.13	PE (UV)	+90°C	Type TC, 600V
SQ trims	2C#10	18	350	0.42	0.16	EPR	+90°C	Type TC, 600V
Hi-quality coaxial, misc.	LDF5-50A	6	350	1.09	0.33	PVC (UV) Type II	+80°C	ES&H Bulletin. #37 NEC 820-53(c)
Multicond. misc. function	25C#18	36	300	0.65	0.17	PVC (UV) Type II	+80°C	Type TC, 300V
Multicond. misc. function	15C#22	90	300	0.30	0.05	PVC (UV) Type II	+80°C	Type TC, 300V
Multicond. misc. function	8C#22	90	300	0.22	0.03	PVC (UV) Type II	+80°C	Type TC, 300V
Kickers	LDF4-50A	16	300	0.63	0.15	Halogen, Fire Retardant	+100°C	ES&H Bulletin #37 NEC 820-53(c)

Table 4.53 Shielding effectiveness of various cable types.

Cable/Connector Type	Shielding @100 MHz
Single braided shield twisted pair, Burndy Trim-Trio™ connector	60 dB
Single braided shield twisted pair, Burndy Trim-Trio™ connector, with cylindrical shield termination.	70 dB
Double shielded coaxial (RG-223), N connector	85 dB
Semi-rigid coaxial, (LDF4-50), N connector	105 dB
Semi-rigid coaxial, (LDF4-50), N connector, solder backshell	120 dB
Test methods: MIL-C-39012, MIL-C-17	

References

[1] Vance, Edward F., "Coupling To Shielded Cables", John Wiley & Sons, 1978, pg. 127 – 147

[2] Martin, D., private communication.